SCIENCE CHINA
Chemistry

•REVIEWS•

June 2023 Vol.66 No.6: 1553–1633
https://doi.org/10.1007/s11426-023-1578-y

Biomimetic asymmetric catalysis

Xiao Xiao[2], Kaini Xu[3], Zhong-Hua Gao[4,5], Zhou-Hao Zhu[6], Changqing Ye[5,9], Baoguo Zhao[2*], Sanzhong Luo[3*], Song Ye[4,5*], Yong-Gui Zhou[6*], Senmiao Xu[5,7*], Shou-Fei Zhu[8*], Hongli Bao[5,9*], Wei Sun[5,7*], Xiaoming Wang[1*] & Kuiling Ding[1*]

[1]*State Key Laboratory of Organometallic Chemistry, Center for Excellence in Molecular Synthesis, Shanghai Institute of Organic Chemistry, Chinese Academy of Sciences, Shanghai 200032, China;*
[2]*The Education Ministry Key Laboratory of Resource Chemistry, Shanghai Key Laboratory of Rare Earth Functional Materials, and Shanghai Frontiers Science Center of Biomimetic Catalysis, Shanghai Normal University, Shanghai 200234, China;*
[3]*Center of Basic Molecular Science, Department of Chemistry, Tsinghua University, Beijing 100084, China;*
[4]*Beijing National Laboratory for Molecular Sciences, CAS Key Laboratory of Molecular Recognition and Function, Institute of Chemistry, Chinese Academy of Sciences, Beijing 100190, China;*
[5]*University of Chinese Academy of Sciences, Beijing 100049, China;*
[6]*State Key Laboratory of Catalysis, Dalian Institute of Chemical Physics, Chinese Academy of Sciences, Dalian 116023, China;*
[7]*State Key Laboratory for Oxo Synthesis and Selective Oxidation, Lanzhou Institute of Chemical Physics, Chinese Academy of Sciences, Lanzhou 730000, China;*
[8]*State Key Laboratory and Institute of Elemento-Organic Chemistry, College of Chemistry, Nankai University, Tianjin 300071, China;*
[9]*Key Laboratory of Coal to Ethylene Glycol and Its Related Technology, State Key Laboratory of Structural Chemistry, Center for Excellence in Molecular Synthesis, Fujian Institute of Research on the Structure of Matter, Chinese Academy of Sciences, Fuzhou 350002, China*

Received February 10, 2023; accepted March 22, 2023; published online April 25, 2023

Enzymes are the core for biological transformations in nature. Their structures and functions have drawn enormous attention from biologists as well as chemists since last century. The large demand of bioactive molecules and the pursuit of efficiency and greenness of synthesis have spurred the rapid development of biomimetic chemistry in the past several decades. Biomimetic asymmetric catalysis, mimicking the structures and functions of enzymes, has been recognized as one of the most promising synthetic strategies for the synthesis of valuable chiral compounds. This review summarizes the evolution of asymmetric catalysis inspired by aldolases, vitamin B_1/B_6-dependent enzymes, NAD(P)H, flavin, hydrogenases, heme oxygenases, non-heme oxygenases, and dinuclear/multinuclear metalloenzymes in aspects of biomimetic design, catalyst development and related catalytic transformations. Those well-established synthetic approaches originating from biological reactions have demonstrated the unique prowess of biomimetic asymmetric catalysis in bridging the gap between bio-catalysis and chemical synthesis.

biomimetic catalysis, amine catalysis, carbene catalysis, vitamin B_1, carbonyl catalysis, vitamin B_6, NAD(P)H, flavin, biomimetic oxidation, dinuclear/multinuclear metal catalysis, asymmetric hydrogenation

Citation: Xiao X, Xu K, Gao ZH, Zhu ZH, Ye C, Zhao B, Luo S, Ye S, Zhou YG, Xu S, Zhu SF, Bao H, Sun W, Wang X, Ding K. Biomimetic asymmetric catalysis. *Sci China Chem*, 2023, 66: 1553–1633, https://doi.org/10.1007/s11426-023-1578-y

*Corresponding authors (email: zhaobg2006@shnu.edu.cn; luosz@tsinghua.edu.cn; songye@iccas.ac.cn; ygzhou@dicp.ac.cn; senmiaoxu@licp.cas.cn; sfzhu@nankai.edu.cn; hlbao@fjirsm.ac.cn; wsun@licp.cas.cn; xiaoming@sioc.ac.cn; kding@mail.sioc.ac.cn)

© Science China Press 2023

CONTENTS

1 Introduction 1555
2 Aldolase-based biomimetic asymmetric catalysis 1555
2.1 Early days in mimicking aldolase 1555
2.2 Aminocatalysis in the golden era of organocatalysis 1556
2.2.1 Activation mode 1556
2.2.2 Developed aminocatalysts 1556
2.2.3 Synthetic applications 1557
2.2.4 Current developing trends 1557
2.3 Recent advances in bio-inspired chiral primary amine catalysis 1557
2.3.1 Tuning secondary enamine intermediate 1558
2.3.2 Synergistic catalysis with chiral primary amine 1559
2.4 Summary and perspectives of aldolase-based biomimetic asymmetric catalysis 1560
3 Vitamin B_1-related *N*-heterocyclic carbene catalysis 1560
3.1 Vitamin B_1 and *N*-heterocyclic carbene 1560
3.1.1 Vitamin B_1 1560
3.1.2 *N*-heterocyclic carbene 1561
3.2 NHC catalysis *via* Breslow intermediate 1561
3.2.1 Benzoin reaction 1562
3.2.2 Aza-benzoin reaction 1562
3.2.3 Stetter reaction 1563
3.2.4 Hydroacylation reaction 1563
3.2.5 Umpolung of aldimine 1564
3.3 NHC catalysis *via* acylazolium intermediate 1564
3.4 NHC catalysis *via* azolium enolate intermediate 1564
3.5 NHC catalysis *via* homoenolate intermediate 1566
3.6 NHC catalysis *via* α,β-unsaturated acylazolium intermediate 1567
3.7 NHC catalysis *via* azolium dienolate intermediate 1570
3.8 NHC catalysis *via* α,β-γ,δ-bisunsaturated acyl azolium intermediate 1571
3.9 NHC catalysis *via* *p*-quinodimethane intermediate 1572
3.10 Cooperative NHC/photo catalysis 1572
3.11 Cooperative NHC/transition-metal catalysis 1573
3.12 NHC catalysis *via* other modes 1574
3.13 Summary and perspectives of vitamin B_1-related N-heterocyclic carbene catalysis 1575
4 Vitamin B_6-based asymmetric catalysis 1575
4.1 Vitamin B_6-dependent enzymatic transformations 1575
4.2 Bio-inspired enantioselective reactions enabled by stoichiometric chiral pyridoxamines and pyridoxals 1576
4.3 Vitamin B_6-based catalytic asymmetric biomimetic transamination 1577
4.4 Vitamin B_6-based biomimetic asymmetric carbonyl catalysis 1578
4.5 Summary and perspectives of vitamin B_6-based asymmetric catalysis 1581
5 NAD(P)H-based biomimetic asymmetric catalysis 1581
5.1 BMAR participated by stoichiometric NAD(P)H models 1582
5.1.1 Stoichiometric achiral NAD(P)H models 1582
5.1.2 Stoichiometric chiral NAD(P)H models 1583
5.2 BMAR catalyzed by achiral NAD(P)H models 1584
5.3 BMAR catalyzed by chiral NAD(P)H models 1585
5.4 Summary and perspectives of NAD(P)H-based biomimetic asymmetric catalysis 1586
6 Flavin-based biomimetic asymmetric oxidation 1587
6.1 Asymmetric oxidation of thioethers 1588
6.2 Asymmetric Baeyer-Villiger oxidation 1590
6.3 Asymmetric oxidative esterification, thioesterification, and amidation 1591
6.4 Summary and perspectives of flavin-based biomimetic asymmetric oxidation 1592
7 Hydrogenase-based biomimetic asymmetric catalysis 1592
7.1 Biomimetic hydrogenation catalysts based on [FeFe]-hydrogenases 1593
7.2 Biomimetic hydrogenation catalysts based on [Fe]-hydrogenases 1597
7.3 Biomimetic hydrogenation catalysts based on [NiFe]-hydrogenases 1597
7.4 Summary and perspctives of hydrogenase-based biomimetic asymmetric catalysis 1599
8 Heme oxygenase-based biomimetic asymmetric catalysis 1600
8.1 Metalloporphyrin-catalyzed asymmetric cyclization of alkenes 1600
8.1.1 Asymmetric epoxidation of alkenes 1600
8.1.2 Asymmetric cyclopropanation of alkenes 1604
8.1.3 Asymmetric aziridination of alkenes 1607
8.2 Metalloporphyrin-catalyzed asymmetric C–H bond activation 1608
8.2.1 Asymmetric hydroxylation of C–H bonds 1608
8.2.2 Asymmetric carbon-hydrogen bond alkylation 1608
8.2.3 Asymmetric amination of C–H bonds 1609
8.3 Metalloporphyrin-catalyzed asymmetric sulfoxidation 1610
8.4 Summary and perspectives of heme-oxygenase-based biomimetic asymmetric catalysis 1611
9 Nonheme oxygenase-based biomimetic asymmetric catalysis 1612
9.1 Asymmetric epoxidation of olefins with nonheme metal complexes 1612
9.2 Asymmetric *cis*-dihydroxylation of olefins with nonheme metal complexes 1615
9.3 Asymmetric C–H oxidation catalyzed by nonheme metal complexes 1616
9.4 Summary and perspectives of nonheme oxygenase-based biomimetic asymmetric catalysis 1617
10 Biomimetic asymmetric catalysis mediated by dinuclear & multinuclear metal complexes 1618
10.1 Chiral multimetallic self-assembled complexes developed by Shibasaki group 1618
10.2 Chiral metallosalen-type bimetallic systems 1618
10.3 Chiral dinuclear ProPhenol/Zn catalysts 1619
10.4 Other selected chiral dinuclear metal catalysts 1621
10.5 Chiral binuclear complexes containing metal-metal bonds 1622
10.6 Summary and perspectives of biomimetic asymmetric catalysis mediated by dinuclear & multinuclear metal complexes 1623
11 Conclusions and outlooks 1623

1 Introduction

Asymmetric catalysis, maintaining an irreplaceable role in construction of enantioenriched compounds for chemistry, pharmaceuticals, biology, and material science over the past half-century, has become one of the most widely utilized synthetic protocols in academia [1] as well as in industry [2]. The catalysts principally cover enzymes [3] and chemical catalysts [4–6]. In recent times, global concerns on sustainable development and environmental issues require modern asymmetric catalysis to address more challenges facing cost, pollution, renewability, *etc*. Indeed, enzymatic asymmetric synthesis, featured with high efficiency and mild conditions, represents an intriguing approach to single-enantiomers and it has been frequently employed in medicinal chemistry, food science, and fine chemical industry [7]. However, fragile stability, substrate specificity together with the complicatedness of protein modification makes enzymatic catalysis still problematic in the synthsis of unnatural or customized chiral compounds. Conversely, despite generally being less efficient, conventional chemical catalysts also possess notable advantages such as small molecular weight, well-designed structure, high stability, and wide substrate scope [8]. And up to now chemical catalysis still dominates the synthesis of various optically active compounds. Biomimetic asymmetric catalysis aims to develop more efficient and more powerful chemical catalysis based on the concept of the imitation of the structures and functions of enzymes [9]. It may merge the advantages of biological catalysis and chemical catalysis, to achieve asymmetric transformations with high efficiency and precise control under environmentally benign conditions [10], which meets the requirements of sustainable chemistry [11] and has become an increasingly significant area of catalysis science.

Enzymes perform functions at catalytic centers (*i.e*., coenzymes for most of the cases) with the assistance and cooperation of the surrounding proteins. The catalytic centers usually carry out the basic catalytic function of the enzymes, which are directly relevant to the structure of biomimetic catalysts as well as the reactions promoted. The surrounding proteins build a chiral cavity for the enzymatic catalysis. An ideal biomimetic catalyst should incorporate the two aspects, however, currently biomimetic catalysis still mainly focused on the imitation of the catalytic centers. It is much more challenging to chemically construct an analog to mimick the three-dimensional catalytic cavity of enzymes. Molecular imprinting technique represents a relatively effective method for this imitation [12a]. But only inspiring performances were observed for most of the cases. Additionly, although the peptide catalysts which mimick the amino acid residues of enzymes have been well-developed recently [12b], it is out of the scope of this review. The above two aspects will not be discussed herein.

Biomimetic catalysis has attracted considerable endeavors of chemists. As early as 1930s, chemists started to simulate aldolases for organic synthesis [13]. Breslow, the pioneer of biomimetic catalysis, firstly proposed the concept of "biomimetic chemistry" in 1958 [14]. He has made many significant contributions to this field, such as demonstrating the active carbene species for vitamin B_1 catalysis for the first time [15] and the development of vitamin B_1/B_6-based artificial enzymes for the imitation of biological transformations [16]. Innumerous other research groups from around the world have also dedicated substantial efforts to the development of biomimetic asymmetric catalysis. Many areas have already been developed into powerful synthetic tools for construction of bioactive chiral molecules.

Chiral biomimetic catalysts can be divided into organo and metallic categories [17,18], respectively mimicking nonmetalloenzymes and metalloenzymes. Representative biomimetic organocatalysts developed include aldolase-inspired chiral amines [19], vitamin B_1-based chiral *N*-heterocyclic carbenes [16,20], vitamin B_6-based chiral pyridoxals/pyridoxamines [16,21], biomimetic chiral NAD(P)H catalysts [22], flavin-based oxidation catalysts [23]. The widely-used biomimetic metallic catalysts are those developed based on hydrogenases [24], heme oxygenases [25], non-heme oxygenases [26], and dinuclear/multinuclear metalloenzymes [27]. This review attempts to give an overview on the development of biomimetic asymmetric catalysis. The structure and function of the original enzymes, the design and development of the biomimetic catalysts, as well as the corresponding catalytic transformations are all discussed herein. And the main challenges along with the future perspective of biomimetic asymmetric catalysis are also described at the end of the review.

2 Aldolase-based biomimetic asymmetric catalysis

2.1 Early days in mimicking aldolase

Aldol reaction is a fundamental C–C bond construction strategy in chemical and biological processes [28]. In nature, aldolases are ubiquitous enzymes that are responsible for metabolism and storage of carbohydrates *via* C–C bond cleavage and formation [29–31]. In eukaryotes, this type of enzymes, classified as type I aldolase, functions through lysine residue primary amine (Figure 1) [32,33]. There have been enduring efforts over last century in the pursuit of understanding and mimicking the catalysis of aldolase for synthetic purpose. In 1934, Pederson [13a] reported arguably the first example of aminocatalysis (named amine catalysis then) for enamine-based decarboxylation. Four years later, Westheimer reported an aminocatalysis for retro-aldol reaction [13b]. In 1970s, Hine [34] had extensively studied enamine formation using a variety of bifunctional primary

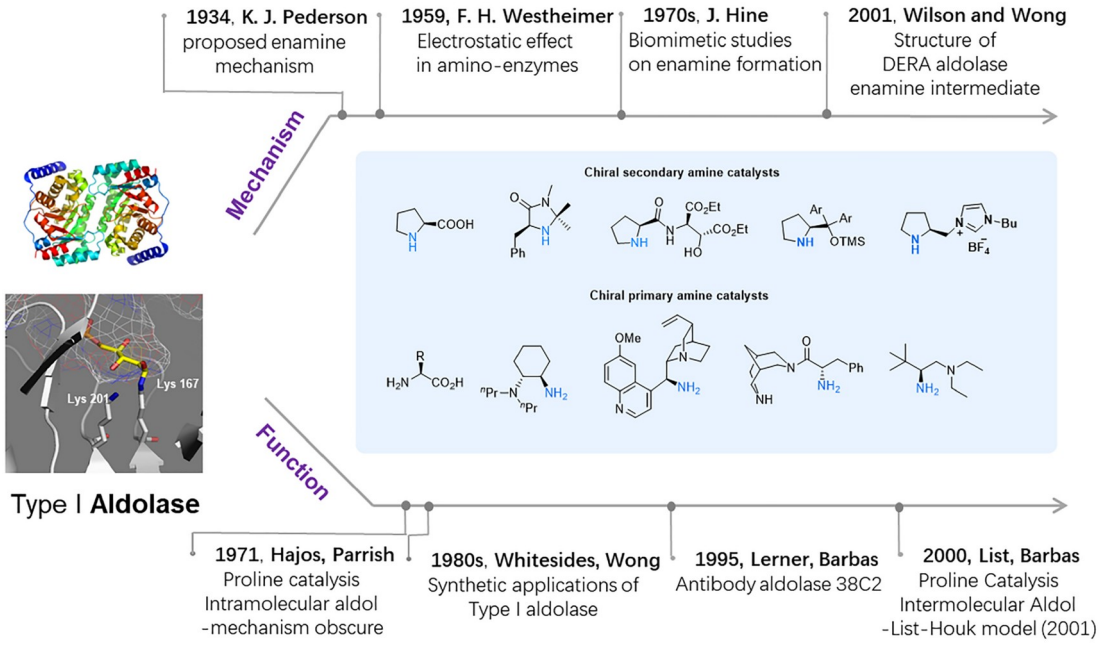

Figure 1 Cornerstones of bio-mimetic studies of Type I aldolase and the representative aminocatalysts developed since 2000 (inside) (color online).

amines. Besides chemists' model studies, biochemists have also gained in-depth understanding of aldolase. For example, Westheimer *et al*. [35] disclosed the prevalent electrostatic effect in aminocatalytic enzymes in 1959. The first structural evidence to covalent enamine intermediates in Type I aldolase was not achieved until 2001 by the work of Wilson and Wong *et al*. [36].

Parallel to the model studies, the synthetic applications of aminocatalysis was slowly caught up particularly in asymmetric catalysis. In 1971, two independent works [37,38], one by Hajos and Parrish and the other by Weichert, Sauer and Eder, reported *L*-proline catalysed intramolecular aldol reaction with remarkable stereoselectivity. This is sometime referred as Hajos-Parrish-Weichert-Sauer-Eder reaction, probably the longest-named reaction. In 1980s, aldolases were investigated in organic synthesis mostly by the work of Whitesides and Wong [39], and one landmark achievement along this line is the scalable synthesis of statins derivatives as cholesterol-lowering blockbuster drugs [40]. In 1995, Lerner and Barbas [41] developed a simplified aldolase, catalytic antibody 38C2, using transition-state-induced immunological approach, that showed significant application in asymmetric synthesis. Related studies on antibody aldolases also set basis for *de novo* computational design of retro-aldolase [42].

In retrospect, type I aldolase provides chemists initial impetus to explore amine catalysis in a much earlier time, provided with its metal-free and pure organic working mode as well as the readily accessibility of small molecular amine compounds. However, it was not until 2000 when List, Barbas and Lerner [43] reported the first example on proline catalysed intermolecular direct aldol reaction (Scheme 1, above), that enamine catalysis has started to receive recognition as a viable and general catalytic mode and eventually becomes a mainstay in asymmetric catalysis.

2.2 Aminocatalysis in the golden era of organocatalysis

2.2.1 Activation mode

The year of 2000 is iconic for the renaissance of organocatalysis. The work by List, Barbas and Lerner represented a general enamine-activation mode (HOMO raising), closely resembling its nature counterpart. In the same year, MacMillan *et al*. [44] designed a new chiral amine catalyst and successfully realized the first enantioselective organocatalytic Diels-Alder reaction. The reaction proceeds *via* an iminium ion activation (LUMO lowering) process (Scheme 1, below). These two seminal works disclosed two fundamental, yet complementary activation modes of aminocatalysis, which later on were proved to be generally applicable.

2.2.2 Developed aminocatalysts

Chiral secondary amines are most frequently explored in the early developing stage of aminocatalysis. Besides proline and MacMillan's imidazolinone catalyst, diphenylprolinol derivatives were first utilized as aminocatalysts by Hayashi *et al*. [45] and Jørgensen *et al*. [46] independently. H-bonding type pyrrolidines were first introduced by Gong *et al*. [47] and ionic-liquid type pyrrolidines [48] are some of the representative secondary amine catalysts. Chiral primary amine catalysts, the truly structural mimic to Type I aldolase, did not receive attention at the very beginning, mostly due to

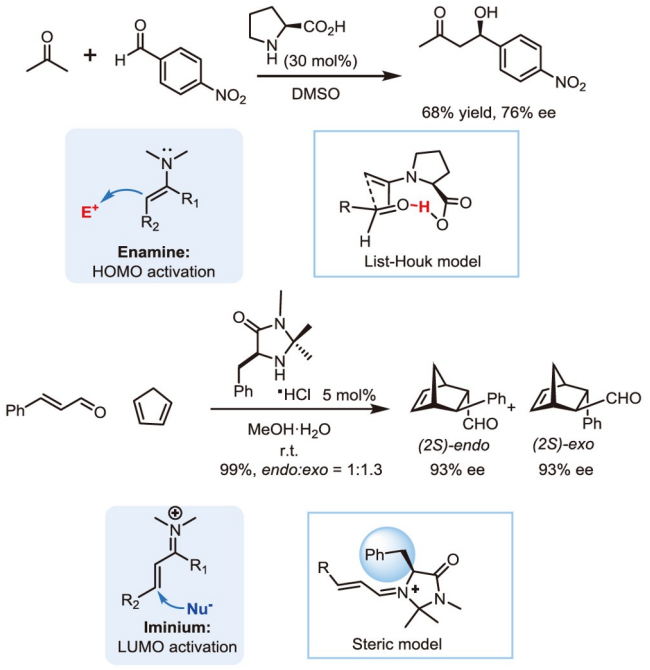

Scheme 1 Seminal works in aminocatalyis and the general activation modes (color online).

the known fact that primary amine tends to form imine instead of enamine [49]. Some of the prevalent chiral primary amine catalysts include amino acid derivatives [50], primary amine-urea/thioureas [51], cinchona-derived primary amines [52], and vicinal primary-tertiary diamine catalysts [53] (Figure 1, inside).

2.2.3 *Synthetic applications*

Aminocatalysis provides an enabling tool in the direct functionalization of ketones and aldehydes *via* C–C [54] and C–X [55] bond formation. Over 20 years, the scopes have been significantly expanded as witnessed by the increasing complexity of substrates as well as the target products. The sites of functionalization can be extended from the typical α- or β-position of carbonyls to the remote γ-, δ-, or ε-position *via* new types of intermediates such as dienamine [56] or trienamine intermediates [57,58]. The mild conditions as well as functional group tolerability are well demonstrated in multi-component reactions and cascade processes [59]. There have been increasing numbers of successful applications of advanced aminocatalysis in the constructions of pharmaceuticals and natural products as featured in Figure 2 [60–68].

2.2.4 *Current developing trends*

As a mature field, there are still notable advances that significantly expand the reaction spaces of aminocatalysis. One of the major advances is external tuning of enamine that enables the incorporation of nucleophiles as coupling partners (Figure 3). In this strategy, enamine could be polarity-reversed by single-electron-transfer *via* chemical [69], photochemical [70] or electrochemical processes [71] to give enamine radical cation or its associated species as electrophilic intermediates [72,73]. Enamines could also be tuned by photo-energy transfer to enable transformations through an excited species [74,75]. Another viable strategy is synergistic aminocatalysis by combining with other catalytic approaches (Figure 4). In this regard, the possible combinations are enormous including other chemical catalysis such as transition metal catalysts [76–85], organocatalysts [86–88], photocatalytic systems [89] or electrochemical processes [90,91].

2.3 Recent advances in bio-inspired chiral primary amine catalysis

Though born with a biological origin traced to Type I aldolase, aminocatalyst has been evolved mainly with a focus on synthetic methodology. Chiral primary amines bear structural resemblance to the enzymatic lysine residue catalysis, and their catalysis has largely complemented those secondary aminocatalysis by their conformational flexibility, hence space tolerance of sterically hindered ketones and aldehydes. Luo *et al*. have developed primary-tertiary vicinal diamines as both structural and mechanistic mimics of its natural counterpart, not only mimicking six natural aldol processes [92], but also demonstrating broad applicability in a number of different transformations. Mechanistically, this type of bio-inspired primary aminocatalysis proceeds *via* anion-proton shuttle for iminium-enamine tautomerization, a feature closely resembling the natural water-proton shuttle observed in DERA-type I aldolase [93] (Figure 5). The cavity

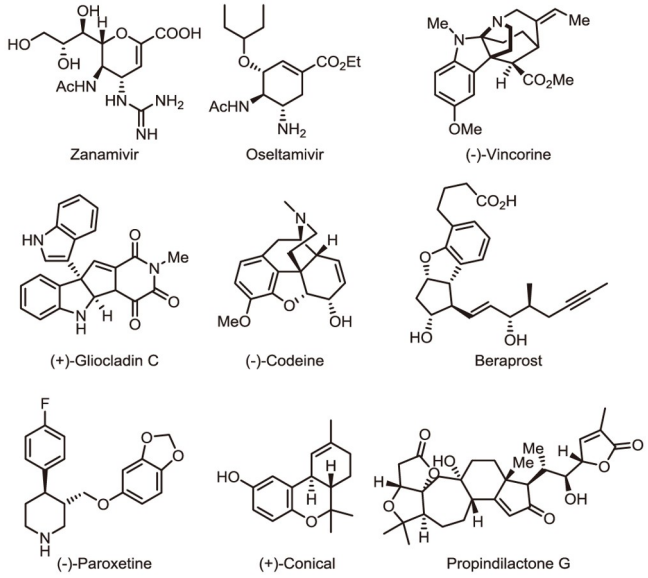

Figure 2 Representative drugs and natural products enabled by aminocatalysis.

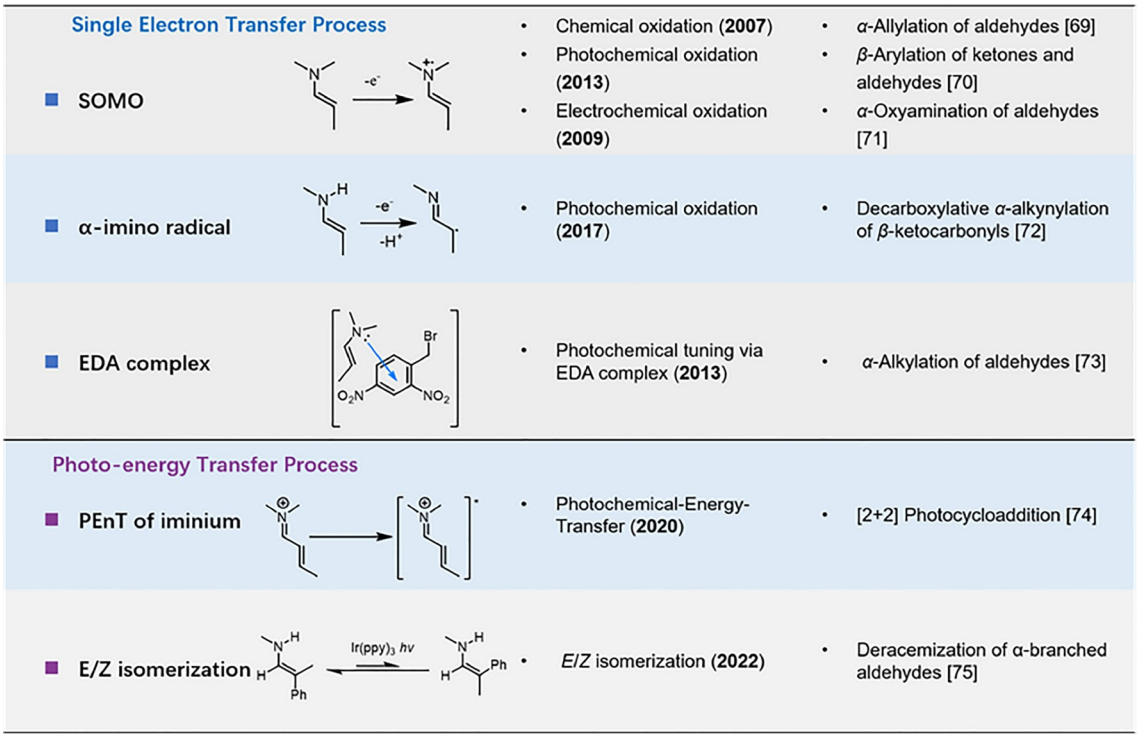

Figure 3 External tuning of aminocatalytic intermediates (color online).

effect on primary aminocatalysis was also investigated in a supramolecular primary amine catalyst [94]. Representative advances with this type of primary aminocatalysts were illustrated herein.

2.3.1 *Tuning secondary enamine intermediate*

α-imino radical. Unlike its tertiary counterpart in singly occupied molecular orbital (SOMO) type catalysis, radical cation of secondary enamine has an acidic enaminyl N–H (pK_a<10) and tends to lose a proton to form α-imino radical intermediate (Figure 3). In 2017, Luo *et al*. [77] reported an α-imino radical catalysis with chiral primary aminocatalyst in a photocatalytic decarboxylative alkynylation reaction. Recently, they further advanced the α-imino radical catalysis to a dehydrogenative allylic alkyla tion reaction using a triple catalytic system involving chiral primary amine, cobalt metal catalyst and Ir-based photosensitizer. Mechanism studies disclosed a cooperative radical addition process *via* a sandwich-type TS (Scheme 2, TS-1) involving a chiral α-imino radical and Co(II)-metalloradical.

E/Z isomerization of enamine. Besides photoinduced electron transfer, energy transfer was also found to modulate the reactvity of enamine intermediate. Very recently, Luo and coworkers [75] developed a photochemical E/Z isomerization of enamine intermediate *via* energy transfer strategy (EnT), enabling the deracemization of α-branched aldehydes by merging chiral primary aminocatalyst and a photosensitizer. Enantioenriched α-aryl aldehydes were obtained with high efficiency and enantioselectivity. Enamine E/Z isomerization *via* EnT facilicates the conversion of the matched (*S*)-aldehyde into mismatched (*R*)-aldehyde (Scheme 3), leading to deracemization. The stereospecific iminium/enamine tautomerization *via* anion-proton shuttle is

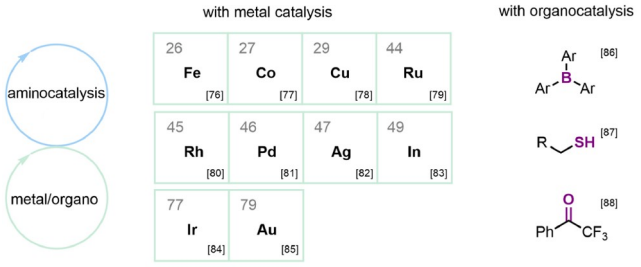

Figure 4 Synergistic aminocatalysis with other catalytic system (color online).

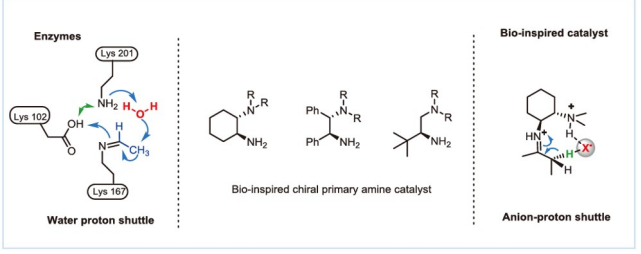

Figure 5 Bio-inspired chiral primary amine catalyst and the underlying mechanism (color online).

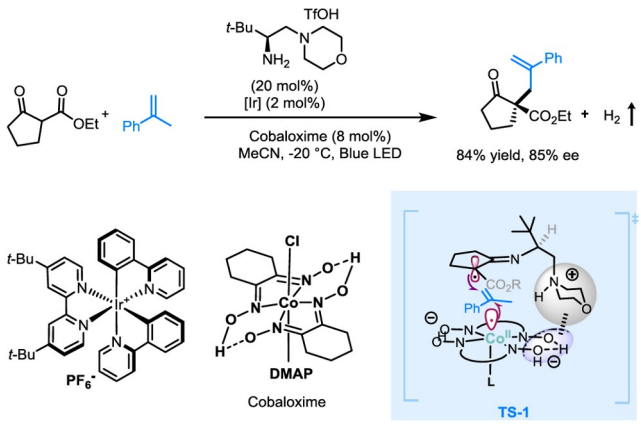

Scheme 2 Activation of SOMO by photocatalysis and cobalt catalysis (color online).

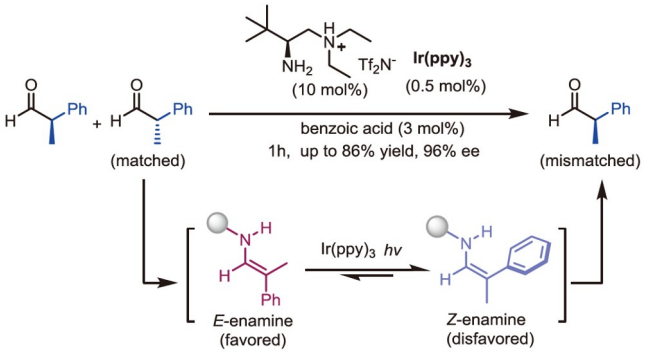

Scheme 3 Deracemization through photochemical E/Z isomerization of enamines (color online).

also a key factor that underlines the stereocontrol in the whole process.

2.3.2 *Synergistic catalysis with chiral primary amine*

Amine/ketone cooperative catalysis. Amine and ketone are yin and yang in organocatalysis that are known to mutually transform each other. A cooperative activation between this pair is rare and has not been reported in asymmetric catalysis. In 2021, Luo's group [88] reported the first example of cooperative amine/ketone catalysis for asymmetric α-hydroxylation of β-ketocarbonyls with hydrogen peroxide. It was found that the addition of catalytic amount of trifluoroacetophenone ($PhCOCF_3$) could enhance the reaction rate by eight times. Mechanistic studies revealed that aminocatalyst and ketone work cooperatively to activate hydrogen peroxide in the form of oxaziridine. The reaction proceeds *via* an enamine-oxidaziridine coupling to afford the desired hydroxylation adducts in high enantioselectivity (Scheme 4).

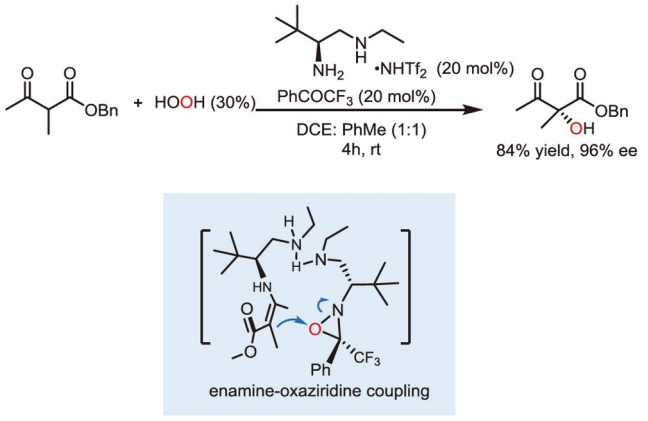

Scheme 4 Asymmetric hydroxylation catalyzed by cooperative amine-ketone catalysis (color online).

Amine/Pd synergistic catalysis. Though amine/metal synergistic catalysis is quite established, to develop aminocatalyst endowed with distinctive coordinating feature remains elusive. In 2020, Luo's group [95] developed a chiral primary amine catalyst bearing arene as π-ligand. The asymmetric allyl alkylation of β-ketocarbonyl group can be successfully achieved by this catalytic system (Scheme 5). Compared with the typical sterically bulky aminocatalyst, π-coordinating aminocatalyst can not only greatly enhance the reaction rate, but also guide facial selectivity of enamine attack, leading to the reversal of chiral induction.

Amine/photoredox synergetic catalysis. In 2017, Luo and Wu *et al.* [89] developed asymmetric cross-dehydrogenative coupling (CDC) of tertiary amines with ketones using a triple catalytic system involving a photoredox catalyst, a chiral primary amine catalyst, and a cobaloxime co-catalyst. The cooperative photoredox/Co catalysis leads to the generation of an iminium cation intermediate, which is

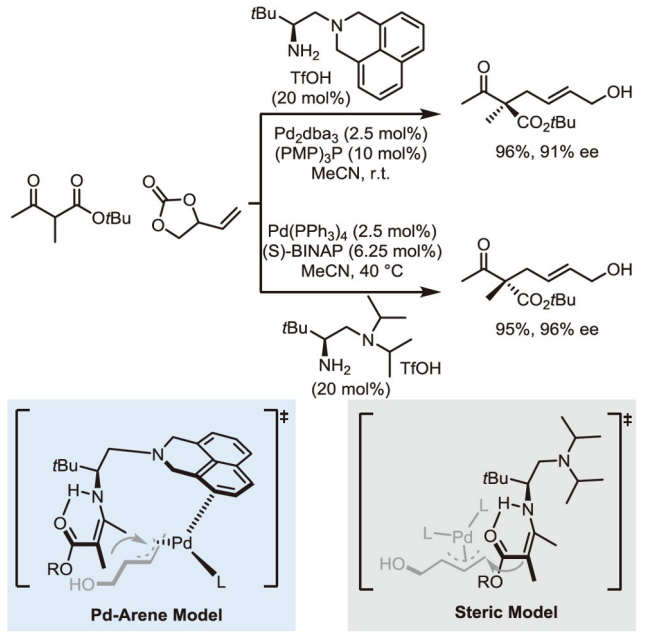

Scheme 5 Chiral primary amine/Pd co-catalyzed allyl alkylation (color online).

intercepted by *in-situ* generated enamine intermediate to provide CDC products with high enantioselectivities. A repulsion model with mixed steric and charge effects were proposed to account for the high stereocontrol (Scheme 6).

Aminocatalysis in electrochemical cell. Primary aminocatalysis also works well in an electrochemical setting, further adding their green credentials by avoiding the use of chemical oxidants, meanwhile enabling novel reactivity. In 2017, Luo's group [90] reported an electrochemical version of the asymmetric cross dehydrogenative coupling of ketones and tertiary amines. In 2020, they developed an electrochemical protocol for *in-situ* oxidative generation of benzyne or cyclohexyne from 1-aminobenzotriazole and realized a catalytic asymmetric α-arylation of cyclic β-ketocarbonyls with benzynes by chiral primary aminocatalysis (Scheme 7) [91].

2.4 Summary and perspectives of aldolase-based biomimetic asymmetric catalysis

Over a centennial exploitation, chemists have excelled in mimicking natural aminocatalytic enzyme, *e.g.*, Type I aldolase, and developing privileged chiral aminocatalysts with strong biological features. Now, aminocatalysis, once an icon for the renaissance of organocatalysis, has become an established and enabling strategy in asymmetric catalysis. As illustrated in this short summary, the potentials of aminocatalysis, particularly those bio-inspired chiral primary amines, can be significantly expanded by judiciously combining with light, electricity or another catalytic system. We see no limits in the explorations along this line.

3 Vitamin B_1-related *N*-heterocyclic carbene catalysis

3.1 Vitamin B_1 and *N*-heterocyclic carbene

3.1.1 Vitamin B_1

Vitamin B_1 (thiamine, **1**) is one of the 13 vitamins that are

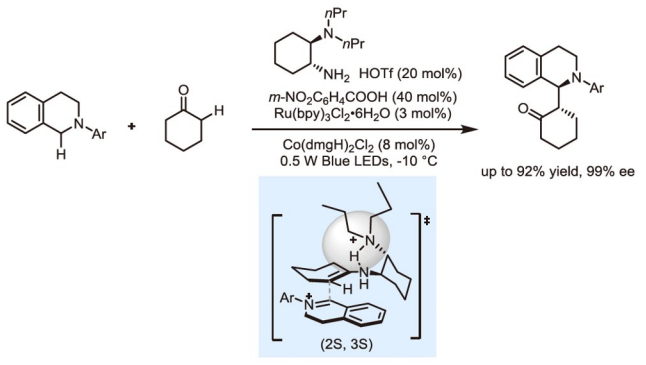

Scheme 6 Asymmetric cross dehydrogenation coupling catalyzed by synergistic photoredox, cobalt catalysis and aminocatalysis (color online).

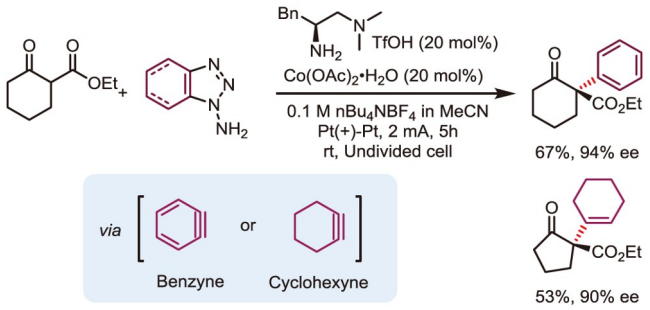

Scheme 7 Electrocatalytic asymmetric α-arylation of cyclic β-ketocarbonyls by chiral primary amine (color online).

essential for human beings. As determined by Williams and Waterman [96] in the middle of 1930s, the structure of thiamine contains a pyrimidine substituted thiazolium motif, bearing a free amino and hydroxy group (Figure 6, left). Thiamine pyrophosphate (TPP, **2**) (Figure 6, right) is the most common active species of thiamine in promoting biochemical transformations. TPP is the cofactor of many important enzymes, such as transketolase, pyruvate decarboxylase, dihydroxyacetone synthase, and 1-deoxyxylulose-5-phosphate synthase. Figure 7 shows the structure of two thiamine-dependent enzymes (transketolase and pyruvate decarboxylase), in which thiamine is embedded in a narrow channel. The crowded space, together with possible H-bonding effect and cooperative interaction of metals, is crucial for highly selective catalytic reactions.

Although the role of TPP **2** as a coenzyme in pyruvate decarboxylase was established by Lohmann and Schuster [97] in 1937, the mechanism of thiamine promoted biosynthetic process was unclear, which lasted for a long time. In 1943, Ukai *et al*. [98] reported that thiamine and other thiazolium salts could catalyze benzoin condensation of aldehydes under basic conditions, while Mizuhara *et al*. [99] recognized that in this benzoin reaction the role of thiazolium salt was the same as thiamine in catalyzing biochemical reactions, both involved the formation of an acetyl C1-carbanion intermediate or its equivalent.

A rational mechanism for thiamine catalysis was proposed by Breslow in 1958 (Scheme 8) [100]. He noticed that C2-H on thiazolium ring could undergo fast H-D exchange with deuterium oxide, indicating easy formation of C2-carbanion from thiazolium salt. Based on Lapworth's theory of cyanide catalyzed benzoin reaction [101], Breslow proposed that thiazolino-2-ylidene **4** (originally written as a C2-carbanion), a heterocyclic carbene, was the actual catalyst in thiamine promoted benzoin reactions. First, the addition of *in situ* formed thiazolino-2-ylidene **4** with aldehyde **5a** after 1,2-H shift generates an enaminol intermediate **7**, now known as the Breslow intermediate, which acts as a nucleophile to attack another aldehyde molecule. Then, the newly formed intermediate **8** provides a benzoin product **9** and regenerates

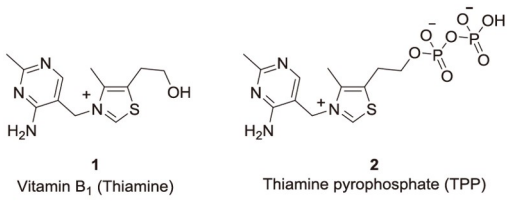

Figure 6 Structure of vitamin B_1 (thiamine) and thiamine pyrophosphate (TPP).

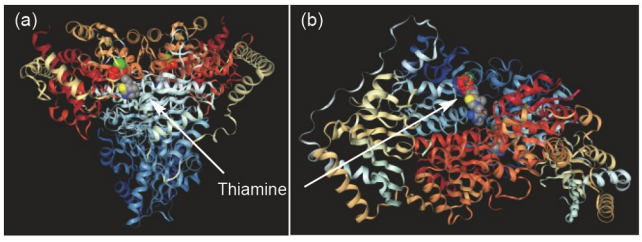

Figure 7 Structures of thiamine-dependent enzymes: (a) transketolase; (b) pyruvate decarboxylase (color online).

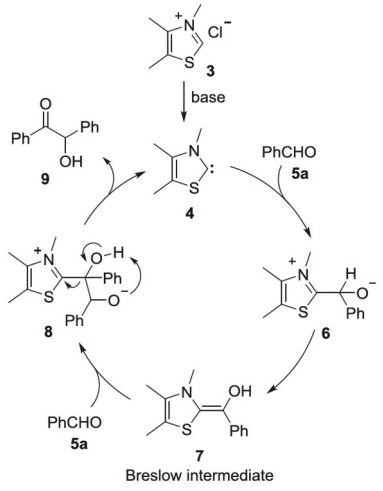

Scheme 8 Mechanism of thiamine catalysis proposed by Breslow.

the carbene catalyst. Breslow's proposal that thiazolium salts served as carbene precursors to promote transformations without the need of complex enzyme proteins indicated the feasibility of small molecules to mimic thiamine as a catalyst.

3.1.2 N-heterocyclic carbene

Carbenes are neutral species with a divalent carbon atom. Due to their incomplete electron octet, carbenes are often regarded as highly reactive species in organic chemistry, and could not be isolated until the late 1980s and early 1990s when Bertrand *et al.* [102] and Arduengo *et al.* [103] respectively reported the preparation of stable carbenes, phosphinocarbene **10** and *N*,*N*'-di(adamantyl)imidazolin-2-ylidene (IAd, **11**) (Figure 8). Since then, the development of *N*-heterocyclic carbene (NHC) catalysis in organic synthesis has been widely explored.

Early reports of vitamin B_1-based biomimetic catalysis were dominated by the thiazolium derivatives, while with the development in this field imidazolium and triazolium derived NHC catalysts became popular (Figure 9). The origin of vitamin B_1-based biomimetic asymmetric catalysis could be dated back to 1966 when Sheehan and Hunneman [104] investigated the asymmetric benzoin reaction by utilizing chiral thiazolium salts as NHC precursors. After that, a variety of chiral thiazolium-based NHC catalysts were synthesized with the introduction of chiral centers on either *N*-alkyl substituents or the thiazolium backbones (Scheme 9a). Similarly, chiral amines were the main chirality sources for imidazole or imidazoline-based NHC catalysts (Scheme 9b). As first reported by Enders and coworkers [105], chiral triazolium-based NHC catalysts became popular in catalytic asymmetric transformations because of their wide variety and easy access. Versatile chiral triazoliums were prepared from aminoalcohols, natural amino acids, and lactams, *etc.* (Scheme 9c, d). Overall, the vast number of chiral thiazolium-, imidazolium- and triazolium-based catalysts constituted an inclusive toolbox for asymmetric NHC catalysis [20].

3.2 NHC catalysis *via* Breslow intermediate

The addition of NHC to aldehyde generates the corresponding Breslow intermediate, which serves as a nucleophile *via* the umpolung of aldehyde. The Breslow intermediate is very reactive, and early research on the characterization of it encountered difficulties. Berkessel and Teles *et al.* [106] reported a keto tautomer of the Breslow intermediate (**32**), and Rovis *et al.* [107] reported its aza-analogues (*e.g.*, **33**) and measured their oxidation potentials (Figure 10). The *O*-methylated Breslow intermediates (*e.g.*, **34**) and their nucleophilicity were investigated by Maji and Mayr (Figure 10) [108]. It was until very recently that Berkessel and coworkers [109] fulfilled the characterization of the solution and X-ray crystal structure of Breslow inter-

Figure 8 Structures of stable carbenes.

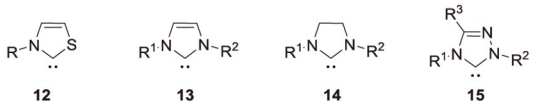

Figure 9 General types of carbene catalysts.

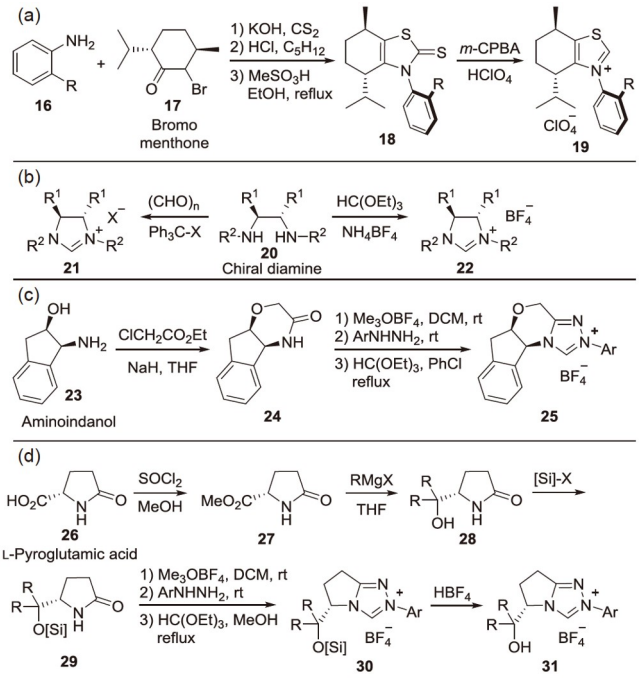

Scheme 9 Typical synthetic procedures of chiral NHC precursors.

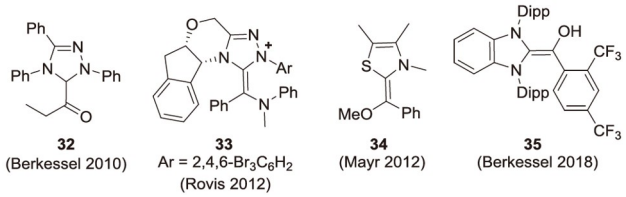

Figure 10 Structure of the Breslow intermediate and its analogues.

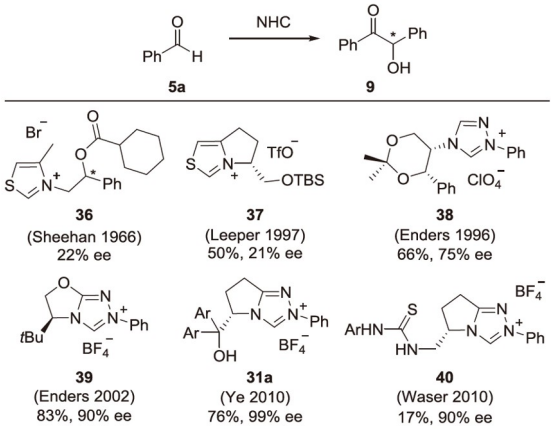

Scheme 10 Representative NHCs in asymmetric benzoin reactions.

mediate (**35**) and confirmed its role as an acyl anion equivalent in catalytic reactions (Figure 10).

3.2.1 *Benzoin reaction*

Among NHC-catalyzed various transformations, the benzoin reaction is widely investigated, and asymmetric benzoin reaction has become a benchmark reaction to test the activities of novel chiral NHC catalysts. The results of several representative NHC catalysts on asymmetric benzoin reactions are summarized in Scheme 10 [104,110]. Firstly reported by Sheehan and Hunneman [104], chiral thiazolium **36** worked as the preNHC catalyst to give the benzoin product **9** with 22% ee [110a]. Bicyclic thiazolium salt **37** by Leeper and coworkers [110b] could elevate the benzoin reaction efficiency but still with low ee values. A breakthrough of this asymmetric reaction was realized by Enders and coworkers who employed triazolium **39** as the NHC precursor to deliver the corresponding product in 83% yield with 90% ee [110c]. The bifunctional NHC **31a** with a free hydroxyl group, developed by Ye's group [111], promoted the benzoin reaction with 99% ee. The bifunctional NHC **40** bearing a thiourea moiety was employed by Waser and coworkers [110e].

Asymmetric intramolecular benzoin reactions *via* NHC catalysis also have been well established. Tetracyclic triazolium **43** were evaluated by Enders and coworkers [112] to achieve intramolecular benzoin reactions with moderate to good enantioselectivities (Scheme 11a). Suzuki and coworkers [113] disclosed that an aminoindanol-derived NHC precursor **44**, first reported by Rovis *et al.* [114], showed excellent enantioinduction effect in most cases (Scheme 11b). You and Jia [115] developed a method for the asymmetric synthesis of dihydroisoquinolones *via* intramolecular benzoin reactions, with the employment of a camphor-derived preNHC **45** (Scheme 11c).

3.2.2 *Aza-benzoin reaction*

An asymmetric aza-benzoin reaction was disclosed by Miller and coworkers [116] in 2005 (Scheme 12a). A chiral peptide thiazolium **48** was utilized to deliver the corresponding α-aminoketones in good yields with up to 87% ee. Rovis and DiRocco [117] demonstrated the highly enantioselective reactions between aliphatic aldehydes and *N*-Boc aldimines by using an aminoindanol-based NHC precursor **25a** (Scheme 12b). Reactions of straight-chain aldehydes proceeded well, while branched aldehydes gave the products with excellent enantioselectivities but in low yields.

Taking into account the potential H-bonding effect in enzyme catalysis, Ye and coworkers [118] designed a novel type of bifunctional carbene catalyst (**31**) with an H-bond donor, derived from L-pyroglutamic acid [20h]. A highly enantioselective aza-benzoin reaction of enals with ketimines was established with the employment of hydroxy-carbene catalyst **31b** (Scheme 13). In comparison, *t*-butyldimethylsilyl (TBS) protected NHC **30a** with the same backbone was proved to be ineffective, indicating the significance of hydrogen-bonding effect between the catalyst and imine substrate. It is interesting that possible competing

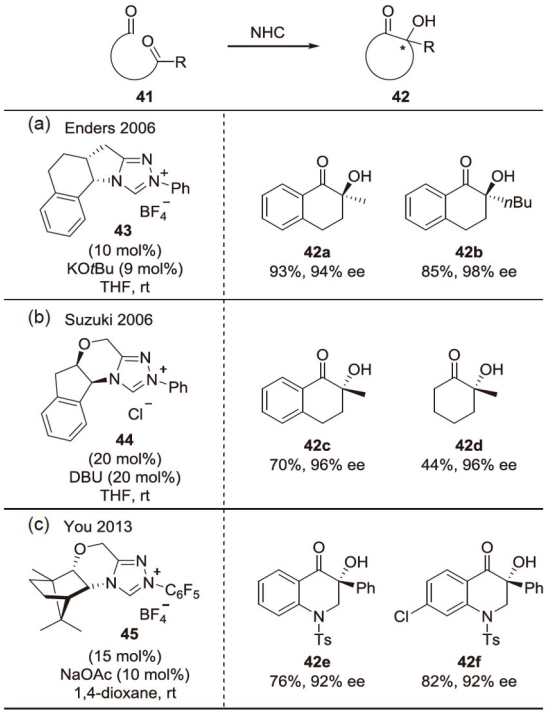

Scheme 11 Selected examples of intramolecular benzoin reactions.

reactions *via* either enolate or homoenolate intermediates were suppressed.

3.2.3 *Stetter reaction*

In 1976, Stetter [119] reported a thiazolium catalyzed 1,4-addition of aldehydes to Michael acceptors to access 1,4-difunctionalized molecules, which provided a new synthetic approach for NHC catalysis. Such kind of transformation was named after Stetter. Enders and coworkers [120] first realized the enantioselective intermolecular Stetter reaction of *n*-butanal and chalcone with moderate enantioselectivity by utilizing a chiral thiazolium catalyst. An improved ee value was obtained when they introduced a bicyclic triazolium carbene precursor **57** for the reaction of aromatic aldehyde with chalcone **56** (Scheme 14a) [121]. The Rovis's group [122] reported the Stetter reactions of glyoxamide **59** with α,β-unsaturated esters **60** in good yields with excellent enantioselectivities (Scheme 14b).

Intramolecular Stetter reaction *via* NHC catalysis was disclosed by Ciganek [123] in 1995. Enders and coworkers [124] first reported an enantioselective variant of such kind of reaction. Triazolium preNHC **38** was utilized to deliver 4-chromanones in moderate to good yields with 41%–74% ee. Since then, asymmetric Stetter reaction has become an arena with the introduction of novel NHC catalysts, and substrates bearing different linkers between the aldehyde group and versatile Michael acceptors. Selected examples of NHC catalysts for enantioselective intramolecular Stetter reactions were listed in Scheme 15 [114,125].

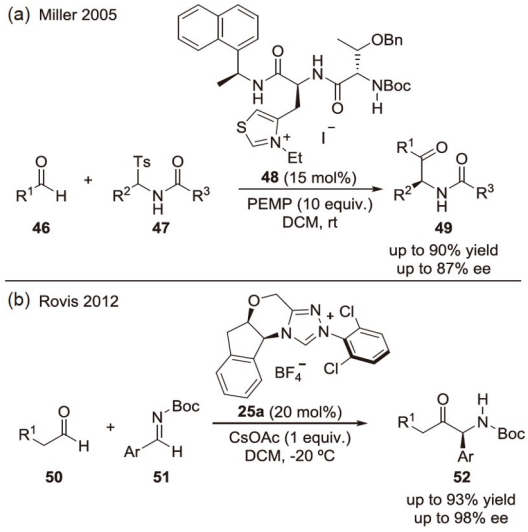

Scheme 12 Enantioselective intramolecular aza-benzoin reaction by Miller *et al.* [116] and Rovis *et al.* [117].

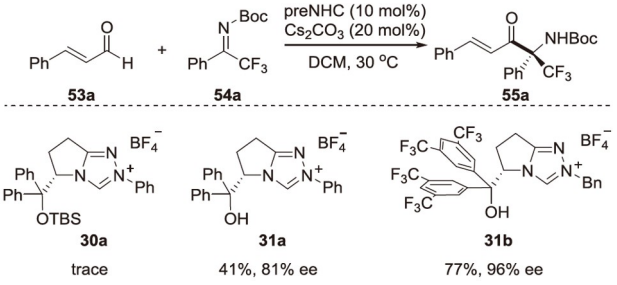

Scheme 13 Enantioselective aza-benzoin reaction of enals with ketimines *via* bifunctional NHC catalysis.

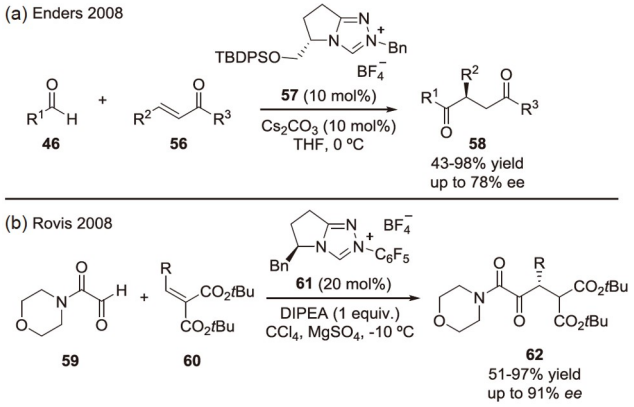

Scheme 14 Enantioselective intermolecular Stetter reaction by Enders *et al.* [121] and Rovis *et al.* [122].

3.2.4 *Hydroacylation reaction*

While the Stetter reaction generally refers to acylation of activated alkene that is conjugated to an electron-withdrawing group, She and coworkers [126] developed an NHC catalyzed direct hydroacylation of enol ethers generated *in situ* from tethered alkyl tosylates. Glorius and coworkers

[127] disclosed the enantioselective intramolecular hydroacylation of unactivated alkenes (Scheme 16). A morpholine-based bicyclic carbene precursor **69** was employed to give the corresponding chromanones **70** in good yields with excellent enantioselectivities. Soon after, they accomplished the enantioselective intermolecular hydroacylation of cyclopropenes **71** with the use of an *N*-(2,6-dimethoxyphenyl) substituted preNHC **72**, affording the products **73** with high levels of stereocontrol [128].

3.2.5 *Umpolung of aldimine*

Aldimines often serve as good electrophiles in the field of NHC catalysis [129]. During the research of aldimines involved cycloaddition and aza-benzoin reactions, adducts of NHC catalysts with aldimines were detected by several groups [117,130], possessing a structure similar to the Breslow intermediate (*e.g.*, **77**). From another perspective, by using this kind of intermediate to realize the umpolung of aldimines seems to be an interesting topic. In 2017, Biju *et al.* and Suresh *et al.* [131], respectively reported the intramolecular aza-Stetter reaction *via* NHC catalysis, affording the corresponding substituted indole products in moderate to good yields. In these two examples, umpolung of the aldimine to attack the Michael acceptor is the key step. Two years later, Lupton and coworkers [132] demonstrated an enantioselective intermolecular aza-Stetter reaction by utilizing a morpholine-based NHC catalyst **76**, giving the desired dihydrocoumarins **78** with excellent levels of stereocontrol (Scheme 17a). Almost at the same time, Biju *et al.* [133] disclosed an NHC catalyzed highly enantioselective cycloaddition of bisimine **79**, providing an approach to access dihydroquinoxalines **81** (Scheme 17b). Density functional theory (DFT) calculations revealed that the initially generated aza-Breslow intermediate was stabilized by the hydroxy group of the substrate due to the hydrogen-bonding effect.

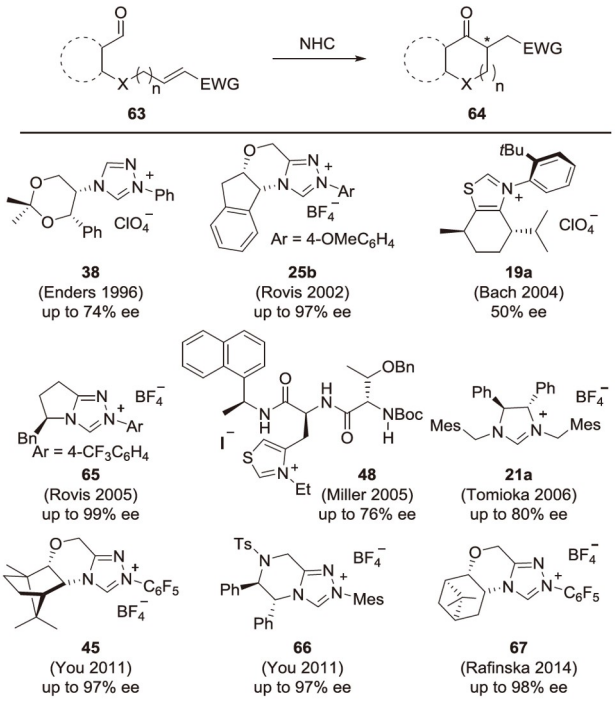

Scheme 15 Representative chiral NHCs for intramolecular Stetter reaction.

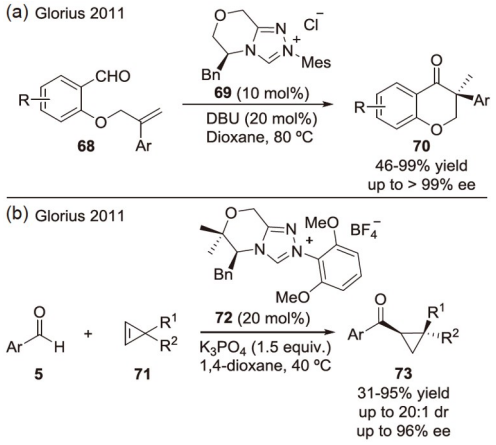

Scheme 16 Enantioselective hydroacylation reactions of alkene by Glorius *et al.* [127].

3.3 NHC catalysis *via* acylazolium intermediate

The addition of NHC to carboxylic acid derivatives or the oxidation of Breslow intermediate would form an acylazolium intermediate **84**, which is of strong electrophilicity (Scheme 18). By utilizing transesterification reaction *via* acylazolium intermediate, Suzuki and coworkers [134] fulfilled asymmetric transformations of vinyl acetate **85a** with secondary alcohols. Kinetic resolution of racemic alcohols was initially realized but with comparatively low enantioselectivities (Scheme 19a). Better results were achieved by Maruoka and coworkers [135] when a bulky vinyl ester was used (Scheme 19b).

The kinetic resolution of racemic 1,2-diol **89** was demonstrated by Yamada, Takasu and coworkers [136] *via* an NHC catalyzed redox esterification reaction (Scheme 20). Aldehydes bearing a leaving group (**82a**) at the α-position were selected as the substrate to generate acylazolium intermediate *via* internal oxidation. In this study, a series of aminoindanol-derived NHC catalysts with the introduction of functional groups, such as bromo and nitro groups, on the indane-ring were reported, which presented opportunities for further transformations to increase the diversity of NHC catalysts to a great extent.

3.4 NHC catalysis *via* azolium enolate intermediate

Azolium enolate (**92**) is an important intermediate in NHC

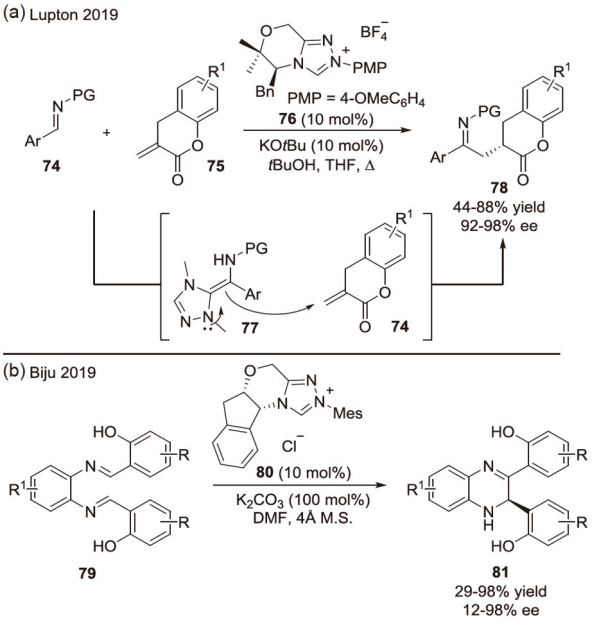

Scheme 17 Enantioselective NHC catalysis for umpolung of aldimine.

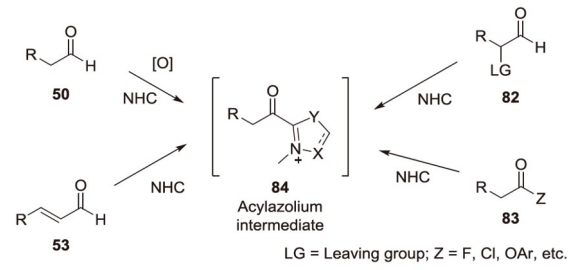

Scheme 18 Generation of acylazolium intermediate.

catalysis to achieve α-functionalization or serve as C2 synthon in [2+*n*] cycloaddition reactions. A variety of substrates could be used to generate NHC-bounded enolate intermediate, such as ketenes, acyl fluorides, anhydrides and other aliphatic acylazolium precursors (Scheme 21). In 2006, Bode and coworkers [137] presented an NHC catalyzed enantioselective [2+4] cycloaddition reaction of enals with unsaturated imines, giving the corresponding dihydropyridinones in good yields with excellent diastereo- and enantioselectivities (Scheme 22). Mechanistically, addition of NHC to the enal substrate generates a vinyl Breslow intermediate, which undergoes fast β-protonation to form the key enolate intermediate. In the same year, they reported a highly enantioselective oxodiene Diels-Alder reaction *via* NHC catalysis with α-chloroaldehyde **96** as the azolium enolate precursor (Scheme 22) [138]. Noteworthy was that a very low catalyst loading (0.5 mol%) was sufficient for excellent stereocontrol.

In 2008, Ye and Smith's groups [139] independently reported the asymmetric Staudinger reactions *via* NHC catalysis (Scheme 23). In Ye's work, L-pyroglutamic acid derived carbene catalyst **30a** was used to deliver β-lactams in

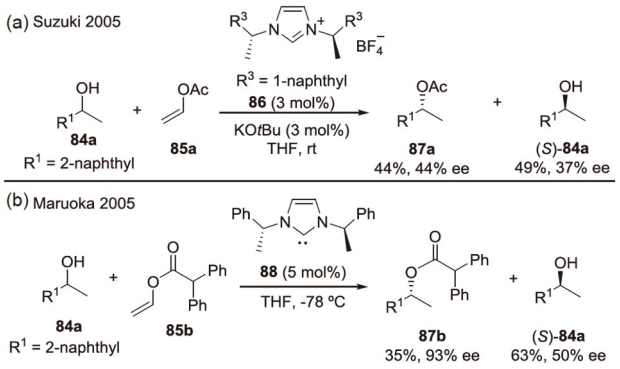

Scheme 19 Kinetic resolution of secondary alcohols *via* NHC catalysis.

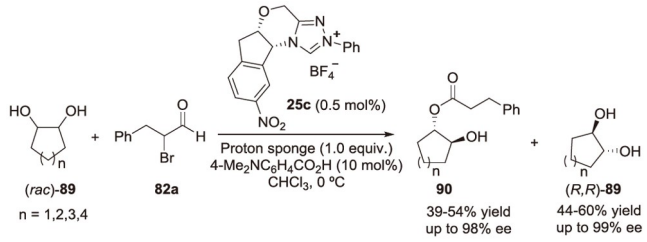

Scheme 20 Kinetic resolution of 1,2-diols *via* NHC catalysis.

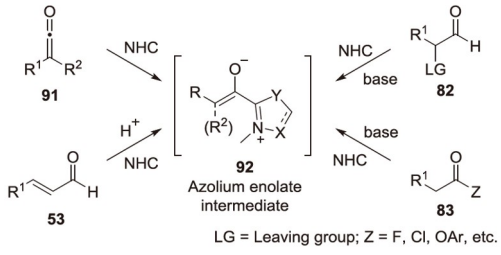

Scheme 21 Generation of azolium enolate intermediate.

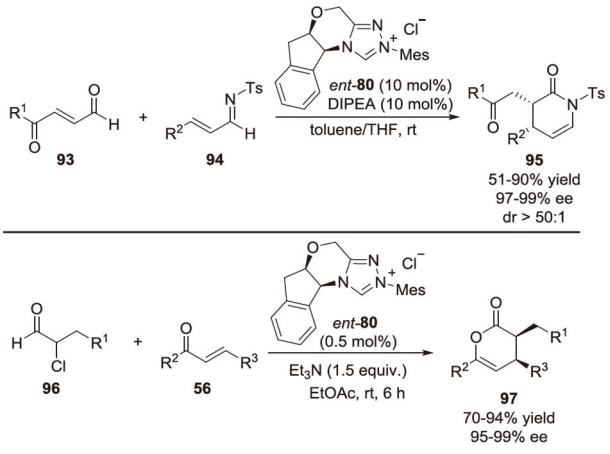

Scheme 22 Enantioselective [2+4] cycloaddition reactions of unsaturated imines/ketones by Bode *et al.* [137,138].

good yields with moderate to good diastereoselectivities and excellent enantioselectivities (Scheme 23a). Two possible catalytic cycles were proposed. One initiated from the addition of carbene to ketene with the generation of an enolate intermediate, while the other started from the NHC-imine adduct, which was isolated from the reaction. Smith *et al.* employed an aminoindanol-based preNHC **25d** as the catalyst and the reaction proceeded well to obtain the β-lactams in good yields, with moderate to good enantioselectivities (Scheme 23b).

In 2012, Chi and coworkers [140] demonstrated the use of stable aliphatic carboxylic esters as azolium enolate precursors to accomplish an asymmetric azadiene Diels-Alder reaction, with a bicyclic carbene as the catalyst (Scheme 24).

Arylacetic esters **104** and aryl substituted unsaturated imines **105** were tolerable substrates to deliver the corresponding dihydropyridones **106** in high yields, with good stereoselectivities. In the carboxylic ester, electron-deficient aryl phenoxide served as a good leaving group after addition of carbene catalyst, generating the key azolium enolate intermediate after deprotonation.

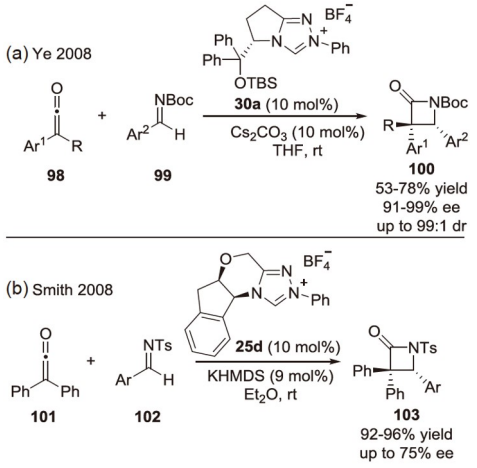

Scheme 23 Asymmetric [2+2] cycloaddition of ketenes with aldimines *via* NHC catalysis.

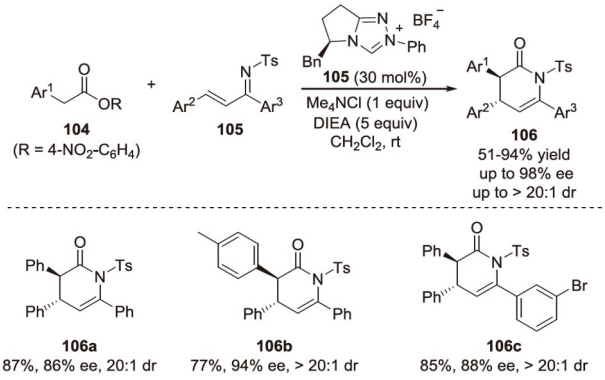

Scheme 24 Asymmetric azadiene Diels-Alder reaction of aliphatic carboxylic esters.

3.5 NHC catalysis *via* homoenolate intermediate

The polarity of aldehyde could be changed *via* its interaction with carbene catalyst, generating an acylanion equivalent to react in an a^1 to d^1 umpolung. When enals **53** were employed as the substrate, the corresponding vinyl Breslow intermediate **107** would be formed. In 2004, Glorius and Bode's groups [141] independently demonstrated that extended Breslow intermediate selectively reacted with carbonyl compounds at the β-position *via* an a^3 to d^3 umpolung, and these elegant seminal reports opened a new chapter of NHC catalysis. The extended Breslow intermediate is often viewed as a homoenolate equivalent **108** (Scheme 25) to accomplish β-functionalization, or as a C3 synthon to participate in [3+*n*] cycloaddition reactions [142].

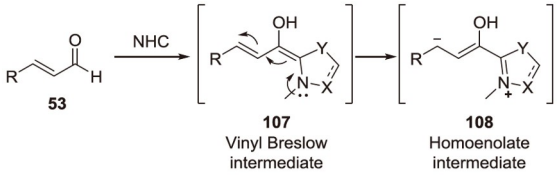

Scheme 25 Generation of homoenolate intermediate.

Bode and coworkers [143] disclosed a highly enantioselective cascade annulation of enals **53** with 4-oxoenoates **109** by employing the aminoindanol-derived carbene precursor **25e**, affording substituted *cis*-cyclopentenes **111** in moderate to good yields, with excellent diastereo- and enantioselectivities (Scheme 26a). A bicyclic lactone **110** was initially formed, which released a CO_2 to deliver the corresponding cyclopentenes. Similar to Bode's work, Scheidt and coworkers [144] developed a novel concept of dual carbene/Lewis acid catalysis to realize the asymmetric annulation of enals **53** with chalcones **56**, providing *cis*-cyclopentenes **112** with high levels of stereocontrol *via* the employment of a Lewis acid, titanium isopropoxide, as the cocatalyst (Scheme 26b).

Asymmetric [3+2] annulations of enals **53** *via* homoenolate intermediate with isatins **113** were reported by Ye and coworkers (Scheme 27) [145]. Bifunctional carbene catalyst **31c** with a hydrogen-bond donor was efficient to deliver the desired spirolactones **114** in excellent yields and stereoselectivities. As a comparison, TBS-protected carbene catalysts **30a**/**b** were ineffective for this annulation reaction, which indicated the special properties of bifunctional NHC catalysts. A possible transition-state (**TS-A**) was proposed to elucidate the enantioselectivity. The H-bonding effect enhances the reactivity and induces the addition of homoenolate to the *Si* face of isatin.

A novel ferrocene-based planar chiral carbene catalyst **116** was reported by Scheidt and coworkers [146]. In the synthetic process, a chiral aminoalcohol moiety was introduced

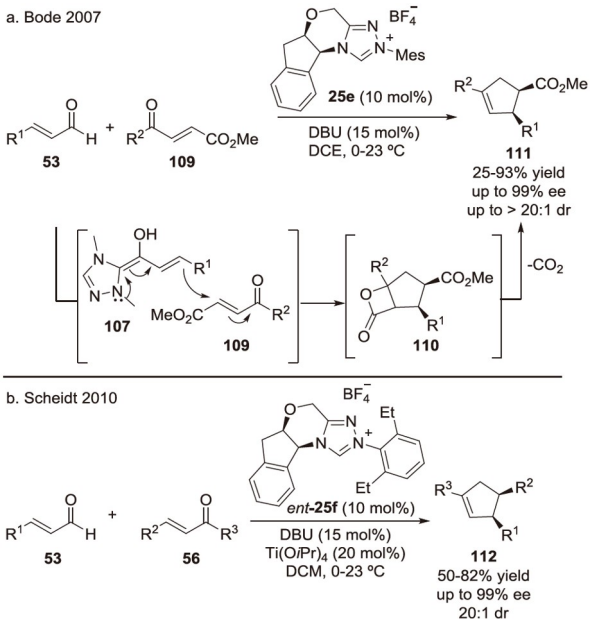

Scheme 26 NHC catalyzed cascade annulation of enals with unsaturated ketones.

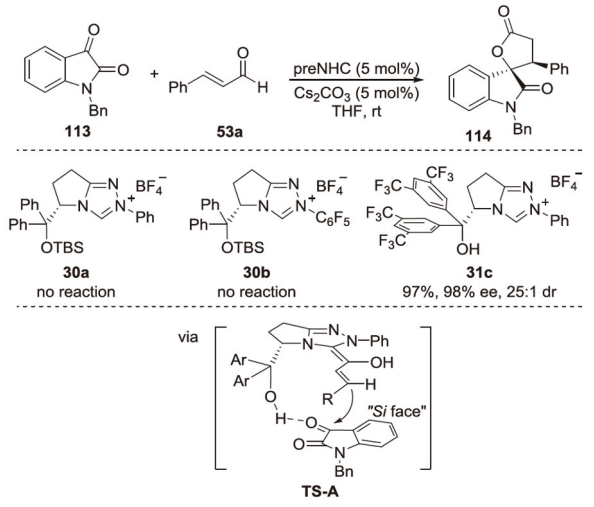

Scheme 27 Comparison of normal and bifunctional carbenes in [3+2] annulations.

for fast resolution *via* column chromatography, allowing for scalable preparation. Application of this planar catalyst **116** was demonstrated to promote asymmetric [3+2] annulations of enal **53a** with α-ketoester **115** (Scheme 28). The corresponding γ-lactone **117** could be afforded in 62% yield with 70% ee (*cis*) and 50% ee (*trans*), but the diastereoselectivity was only 1:1. Additionally, this kind of novel carbene was good ligand for transition-metal catalyzed asymmetric transformations.

In 2008, Scheidt *et al*. [147] disclosed a carbene catalyzed enantioselective [3+3] cycloaddition of enals **53** with nitrones **118** (Scheme 29). Nucleophilic addition of NHC-bound homoenolate intermediate to the 1,3-dipole followed

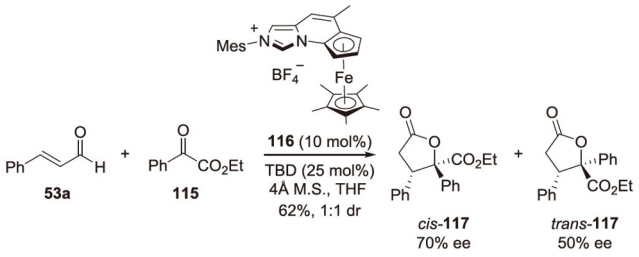

Scheme 28 Enantioselective [3+2] annulation of enal with ketoester *via* ferrocene-based planar chiral carbene catalysis.

by intramolecular lactonization afforded the heterocyclic compounds **119**, which underwent a subsequent ring-opening process *via* alcoholysis. Both β-alkyl and β-aryl substituted enals were well tolerated to give the corresponding linear esters **120** in good yields, with high stereroselectivities.

Medium-sized ring could also be accessed *via* NHC catalysis. In 2013, Scheidt and Ye's groups [148] independently disclosed the enantioselective [3+4] annulations of enals with *o*-quinone methides (*o*-QMs) to furnish ε-lactone products (Scheme 30). In Scheidt's work (Scheme 30a), the reactive *o*-QMs were generated *in situ* from silyl protected precursors **121** through a desilylation/elimination process, while Ye and coworkers directly used dioxolane-fused *o*-QMs **123** as the substrate (Scheme 30b). Mechanistically, carbene adds to enal to form a vinyl Breslow intermediate, which undergoes a subsequent Michael addition to *o*-QM to give a phenoxide intermediate. Further intramolecular lactonization affords the final product and releases the carbene catalyst. The rearomatization process is proposed to be a driving force and also a key step to suppress the possible competing [3+2] annulations.

Enals were not the only precursor of homoenolate in carbene catalysis. Bode *et al*. [149] reported that α′-hydroxyenones **125** were feasible surrogates for enals to undergo versatile annulation reactions *via* NHC-bound homoenolate intermediate. However, steric substitution of the substrate restricted its application in asymmetric catalysis with the employment of a bulky chiral carbene catalyst **127** (Scheme 31a). Chi and coworkers [150] demonstrated that saturated carboxylic esters were efficient precursors of homoenolate intermediate. Cascade annulations of aliphatic esters **129** with chalcones **56** *via* NHC catalysis furnished the corresponding cyclopentenes **112** in good yields, with excellent stereoselectivities (Scheme 31b). The homoenolate intermediate was proposed to be generated after β-proton shift to the azolium enolate oxygen.

3.6 NHC catalysis *via* α,β-unsaturated acylazolium intermediate

Similar to the Breslow intermediate, the α,β-unsaturated

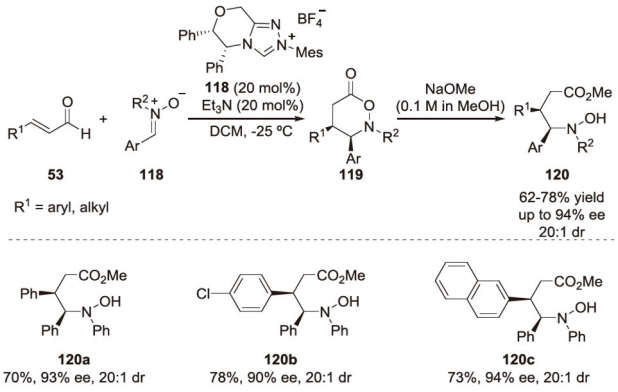

Scheme 29 Enantioselective [3+3] cycloaddition of enals with nitrones.

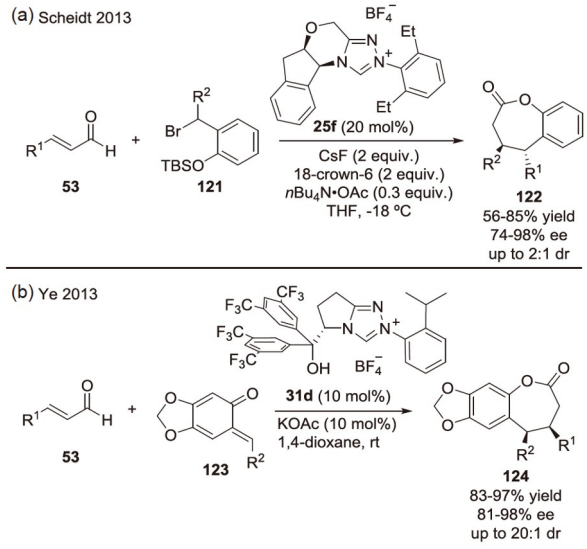

Scheme 30 Enantioselective [3+4] annulation *via* homoenolate intermediate.

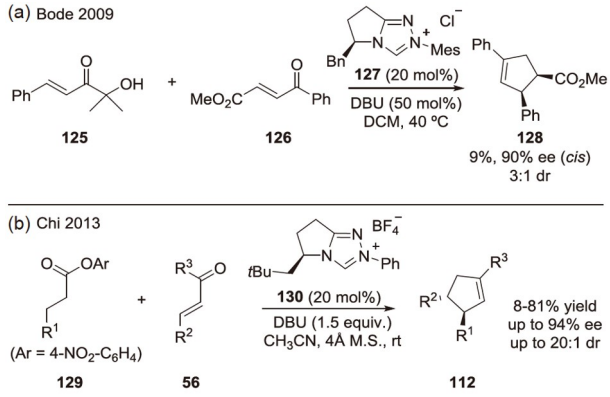

Scheme 31 α′-Hydroxyenone and aliphatic ester as homoenolate precursors in NHC catalysis.

acylazolium is an important intermediate in biochemical transformations, serving as a potential biselectrophile. In efforts towards biosynthesis of clavulanic acid **135** (Scheme 32), a potent β-lactamase inhibitor, Townsend and coworkers [151] revealed that TPP-derived α,β-unsaturated acylazolium **134** was proved to be a key intermediate, which promoted the fast development of such intermediate in the field of thiamine biomimetic catalysis. A variety of substrates were demonstrated for the generation of α,β-unsaturated acylazolium intermediate (Scheme 33).

Zeitler reported the carbene catalyzed esterification of ynals with alcohols, which involved the formation of α,β-unsaturated acylazolium *via* β-protonation of alkynyl Breslow intermediate [152]. Later, Bode *et al*. [153] disclosed the asymmetric β-addition reactions of ynals **136** with Kojic acids **140** (Scheme 34a). Both aromatic and aliphatic ynals were tolerated to furnish the desired acyclic esters **141** in good yields, with excellent enantioselectivities. Xiao and colleagues [154] reported the enantioselective [3+3] annulations of ynals with 1,3-dicarbonyl compounds (Scheme 34b). The corresponding 3,4-dihydropyranones **145** were afforded stereoselectively. Compared with the aromatic ynals, the alkyl substituted ones provided the products with a slightly decreased enantioselectivity. Interestingly, both of the two enantioselective reactions were free of base, possibly due to the easy generation of carbene catalyst from its precursor.

Lupton *et al*. [155] demonstrated the use of unsaturated acyl fluorides **146** as α,β-unsaturated acylazolium precursors. A highly enantioselective Ireland-Coates-Claisen rearrangement of unsaturated acyl fluorides **146** with strained silylated cyclopropanes **147** was achieved, giving the functionalized bicyclic β-lactones **149** in moderate to good yields (Scheme 35). The addition of NHC to unsaturated acyl fluoride generated the α,β-unsaturated acylazolium intermediate, and a fluoride anion to promote the desilylation, which was helpful for the subsequent ring-opening of strained cyclopropanes *via* a retro-aldol process. Both β-alkenyl and β-alkyl substituted unsaturated acyl fluorides were tolerable, albeit alkyl substituted β-lactones being afforded in slightly decreased yields and enantioselectivities.

In 2011, Ye and colleagues [156] introduced α-bromo enals **137** as effective α,β-unsaturated acylazolium precursors. Enantioselective [3+3] annulations of α-bromo enals with 1,3-dicarbonyl compounds were reported to access 3,4-dihydropyranones in high efficiency (Scheme 36). In this reaction, addition of carbene to α-bromo enal and subsequent debromination generated the corresponding α,β-unsaturated acylazolium intermediate. Noteworthy was that L-pyroglutamic acid derived carbene catalysts bearing a free or silyl protected hydroxy group furnished the cycloadducts with opposite configurations, respectively. The existence of hydrogen-bonding effect between the α,β-unsaturated acylazolium intermediate and carbonyl substrate, or not, was accountable for the differentiation of stereoselectivity.

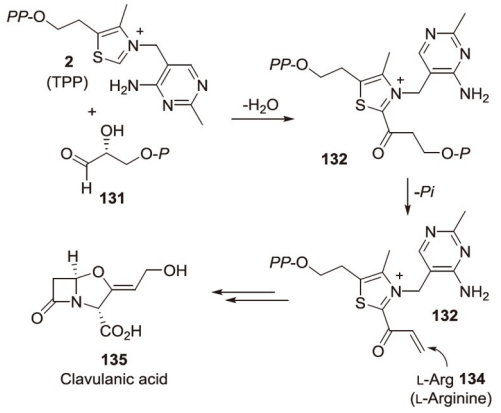

Scheme 32 Biosynthesis of clavulanic acid.

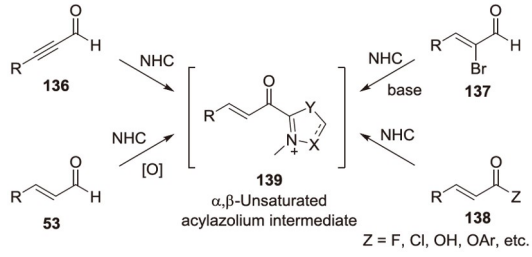

Scheme 33 Generation of α,β-unsaturated acylazolium intermediate.

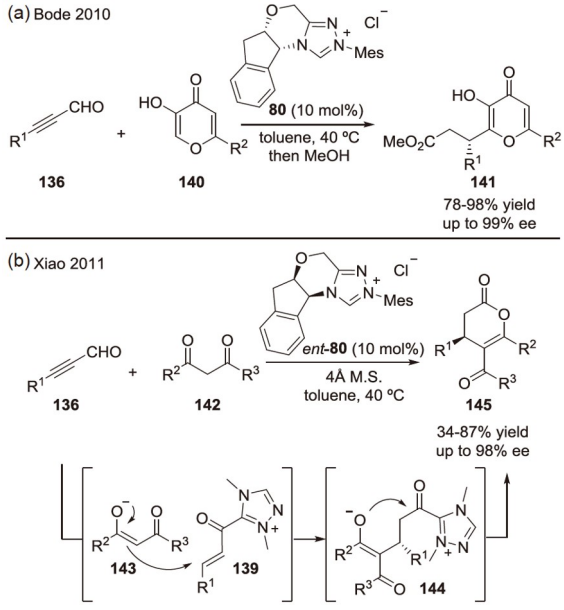

Scheme 34 Enantioselective addition reactions of ynals *via* NHC catalysis.

Electron-deficient unsaturated esters **150** were employed by Chi and coworkers [157] to participate in carbene catalyzed asymmetric annulations with ketimines **151** (Scheme 37). The key α,β-unsaturated acylazolium intermediate was formed upon carbene addition to the ester and elimination of the substituted phenoxide. Ketimines with either electron-withdrawing or -donating groups on the aryl ring were well tolerated to give the dihydropyridones in high yields, with excellent enantioselectivities. A less bulky carbene precursor **154** was used for the reactions of β,β-disubstituted unsaturated esters **153**, and the desired products **155** with a quaternary stereocenter were afforded in good yields with high ee values.

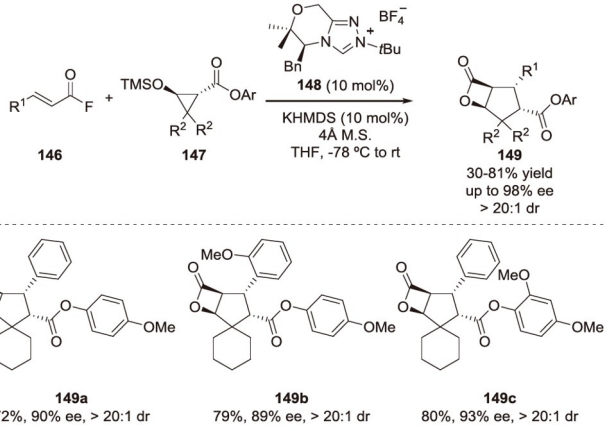

Scheme 35 Enantioselective Ireland–Coates–Claisen rearrangement of unsaturated acyl fluorides with silylated cyclopropanes.

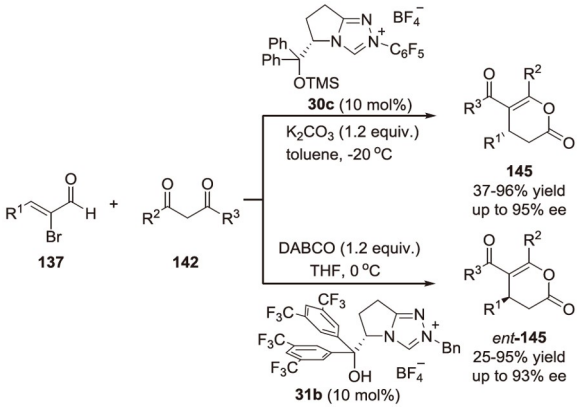

Scheme 36 Enantioselective [3+3] annulation of α-bromoenals with 1,3-dicarbonyl compounds.

As discussed before, addition of carbene to enal **53** would generate a vinyl Breslow intermediate **107**, a homoenolate equivalent. Studer and coworkers [158] reported that oxidation of the extended Breslow intermediate with external oxidant **156** gave access to the α,β-unsaturated acylazolium intermediate. [3+3] Cycloaddition reactions of enals with 1,3-dicarbonyl compounds *via* oxidative NHC catalysis were disclosed by Studer *et al*. [159]. An asymmetric variant of this annulation reaction was demonstrated by You and colleagues [160] with the employment of the camphor-derived carbene catalyst **45** (Scheme 38). A series of 3,4-dihydropyranones **145** were obtained in moderate to good yields, with high enantioselectivities.

Carboxylic acids are abundant, low-cost and readily

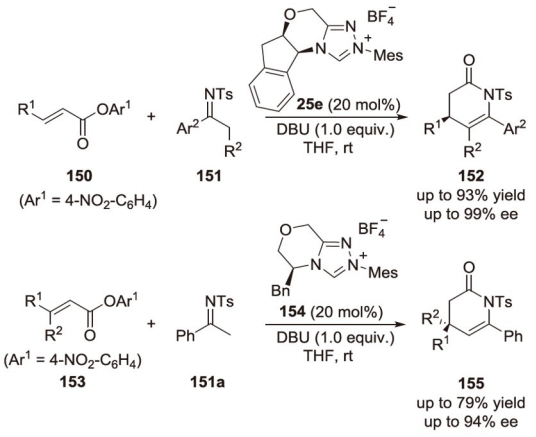

Scheme 37 Enantioselective [3+3] annulation of α,β-unsaturated ester with ketimines.

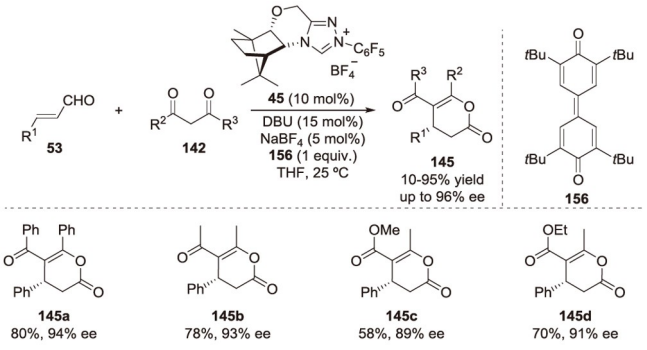

Scheme 38 Asymmetric [3+3] annulation of enals with 1,3-dicarbonyl compounds *via* oxidative NHC catalysis.

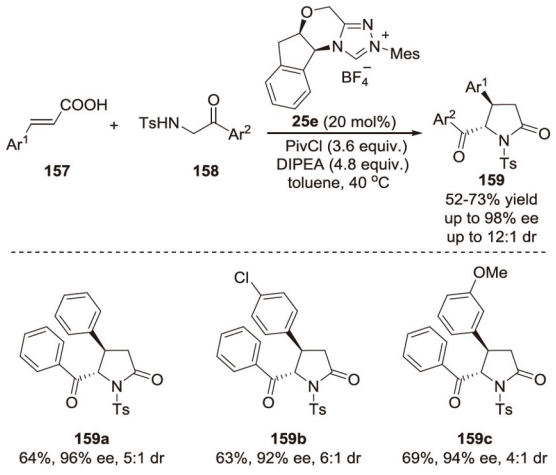

Scheme 39 Asymmetric annulation of α,β-unsaturated carboxylic acid with α-amino acetophenone.

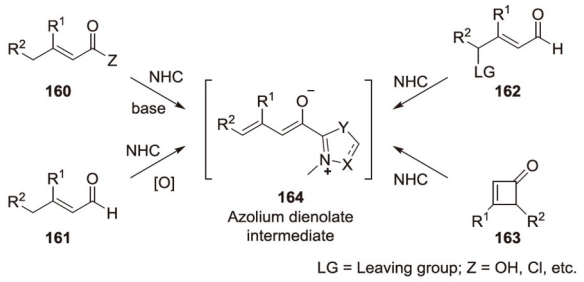

Scheme 40 Generation of azolium dienolate intermediate.

available compounds. The direct use of carboxylic acids, without the preparation and separation of their derivatives, in carbene catalysis is of great value. Ye and coworkers [161] reported an interesting asymmetric [2+3] annulation reaction with the employment of α,β-unsaturated carboxylic acids **157** as the starting material (Scheme 39). A two-step one-pot process was involved. Mixed anhydride was initially formed from acids in the presence of base and acyl chloride. Then, carbene addition to the mixed anhydride after elimination generated the α,β-unsaturated acylazolium intermediate. Deprotonation of α-amino acetophenone **158** formed an enolate, which underwent Michael addition to the α,β-unsaturated acylazolium. Subsequent lactamization afforded the desired γ-lactam **159** and released the carbene catalyst. Curiously, fused lactones instead of γ-lactams were obtained by Chi *et al*. [162] when they conducted the reactions of enals with alkyl substituted α-amino ketones *via* oxidative NHC catalysis.

3.7 NHC catalysis *via* azolium dienolate intermediate

Deprotonation of β-alkyl substituted α,β-unsaturated acylazolium would afford a nucleophilic azolium dienolate intermediate to realize γ-functionalization (Scheme 40). Ye and coworkers [163] demonstrated the carbene catalyzed asymmetric [4+2] annulations of unsaturated acyl chlorides **165** with activated ketones **166** to furnish a series of δ-lactones **169** bearing a tetrasubstituted stereocenter in good yields, with good enantioselectivities, which involved the formation of a NHC-bound dienolate intermediate (Scheme 41a). Shortly afterward, Chi *et al*. [164] employed the strategy of oxidative carbene catalysis to complete cycloaddition reactions of β-alkyl enals **170** with trifluoromethyl ketones **166** (Scheme 41b). The addition of Sc/Mg Lewis acids as cocatalysts was crucial for high levels of enantioinduction.

Ye and coworkers [165] reported that enals bearing a γ-leaving group could be employed as efficient dienolate precursors. The highly enantioselective [4+2] annulations of γ-oxidized enals **171** with azodicarboxylates **172** were developed, representing a good example of asymmetric formal γ-amination (Scheme 42). Both γ-aryl and γ-alkyl substituted enals were tolerable to give the corresponding dihydropyridazinones **173** in good yields with excellent enantioselectivities. Valuable γ-amino acids (*e.g.*, **174**) could be easily accessed from the cycloadducts without apparent erosion of the enantioselectivity.

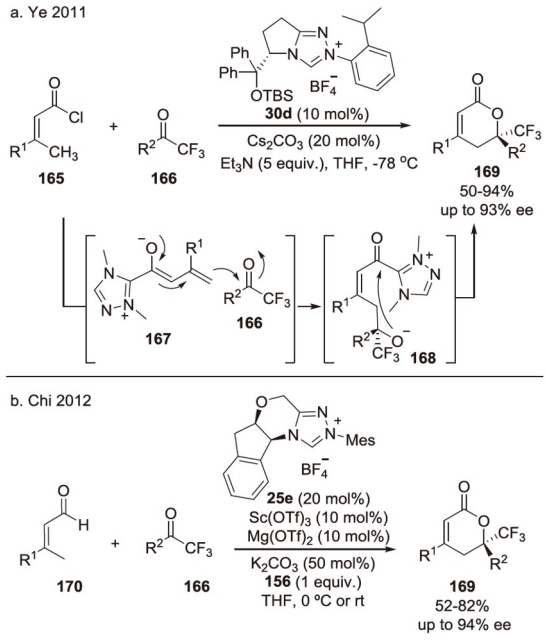

Scheme 41 Enantioselective [4+2] annulation of activated ketones *via* NHC catalysis.

Small strained-rings are widely utilized in organic synthesis due to their unique properties, while the direct activation of small rings *via* carbene catalysis has not been established. To address this issue, Chi and coworkers [166] selected cyclobutanone **175** as the substrate, and fulfilled its activation through carbene addition and subsequent ring-opening process, generating an azolium dienolate intermediate.

Then, the [4+2] cycloaddition reaction of cyclobutenones with either saccharin- or isatin-derived imines under carbene catalysis proceeded efficiently (Scheme 43). Aminoindanol-based carbene catalysts **25e**/**g** were proved to be effective to furnish lactam products **177** with excellent enantioselectivities and in good yields.

3.8 NHC catalysis *via* α,β-γ,δ-bisunsaturated acyl azolium intermediate

Introduction of additional conjugated C=C bonds to the carbonyl substrates provides possibilities for carbene catalyzed remote-site activation (Scheme 44). Chi and coworkers [167] first disclosed the generation of α,β-γ,δ-bisunsaturated acyl azolium intermediate *via* oxidative carbene catalysis with the employment of α,β-γ,δ-bisunsaturated aldehyde **178** as the substrate. The addition of 1,3-dicarbonyl compounds to this type of intermediate occurred selectively at the δ-position. A new benzene ring was formed after cascade annulation and decarboxylation steps. Further application of this strategy by Zhu *et al*. [168] fulfilled the construction of axially chiral biaryl compounds (Scheme 45). A series of *ortho*-substituted benzyl ketones **181** and bisunsaturated aldehydes **178** were selected as the substrates, affording the

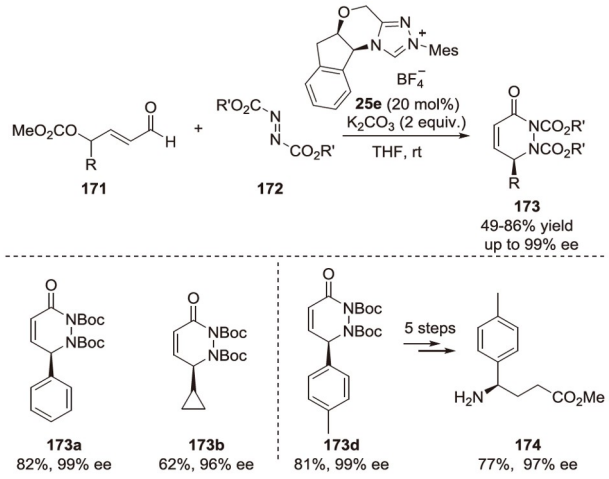

Scheme 42 Enantioselective [4+2] annulations of γ-oxidized enals with azodicarboxylates.

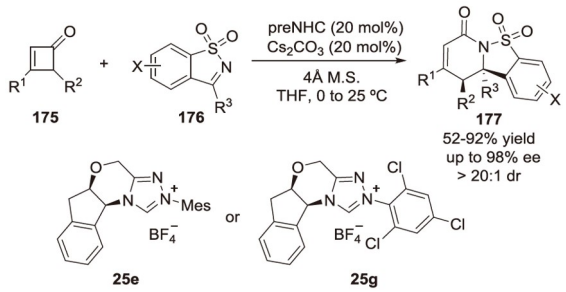

Scheme 43 Enantioselective [4+2] annulation of cyclobutenones with imines.

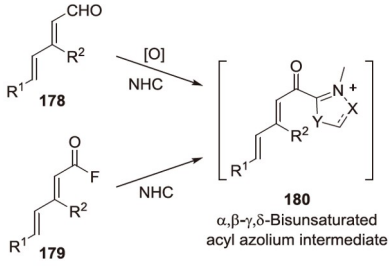

Scheme 44 Generation of α,β-γ,δ-bisunsaturated acyl azolium intermediate.

corresponding atropisomeric biaryls **184** in good yields with excellent enantioselectivities. The formation of axial chirality was proposed through a formal central-to-axial chirality conversion.

Lupton and coworkers [169] presented another protocol for δ-carbon activation *via* NHC catalysis. Substituted α,β-γ,δ-bisunsaturated acyl fluorides **186** were utilized as the precursor of α,β-γ,δ-bisunsaturated acyl azolium intermediate. Annulation reactions of the substrates with TMS enol ether of 1,3-dicarbonyl compounds (**185**) proceeded efficiently to deliver the corresponding fused-β-lactones **188**

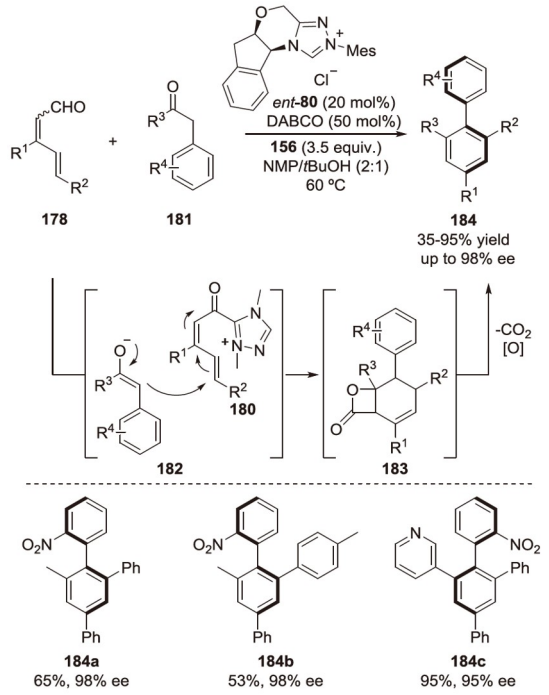

Scheme 45 Asymmetric cascade reaction of α,β-γ,δ-bisunsaturated aldehyde with ketone.

in moderate to good yields, with high levels of stereocontrol (>20:1 dr for all cases, up to >98% ee) (Scheme 46).

3.9 NHC catalysis *via p*-quinodimethane intermediate

Activation of remote positions of carbonyl compounds *via* carbene catalysis is attractive for organic chemists, but the enantioselective control at remote site is challenging due to its long distance from the chiral catalyst backbone. Very recently, Ye's group [170] demonstrated a novel protocol for carbene catalyzed ε-functionalization transformation. ε-Umpolung of aldehyde *via* a *p*-quinodimethane intermediate (*p*-QDM, **189**) and its nucleophilic addition to ketones were reported, giving the corresponding tertiary alcohols in good yields under mild conditions (Scheme 47). An attempt for asymmetric catalysis by using chiral triazolium **25e** led to the product **190** in 60% yields with 11% ee, indicating the challenge of enantioinduction at the remote site.

3.10 Cooperative NHC/photo catalysis

Photocatalysis has emerged as an efficient tool in synthetic chemistry for easy generation of highly reactive radical intermediate. Cooperative NHC/photo catalysis provides an important platform for interesting chemical transformations. In 2012, Rovis and coworkers [171] first demonstrated this protocol, realizing enantioselective aza-benzoin reactions of *N*-aryl tetrahydroisoquinolines **191** by using an aminoindanol-based NHC precursor **25h** as the catalyst and $Ru(bpy)_3Cl_2$ as

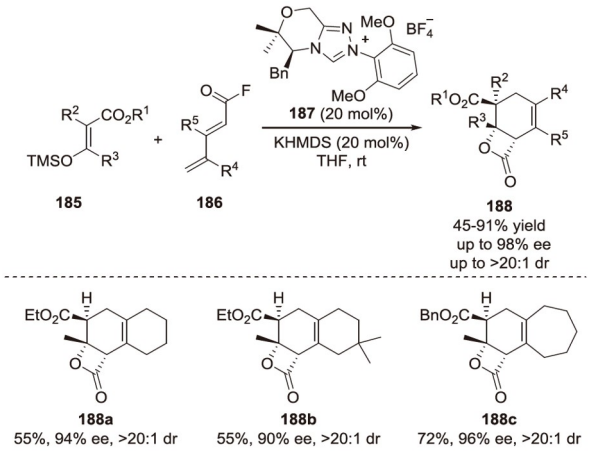

Scheme 46 Asymmetric cascade reaction of α,β-γ,δ-bisunsaturated acyl fluorides with TMS enol ethers.

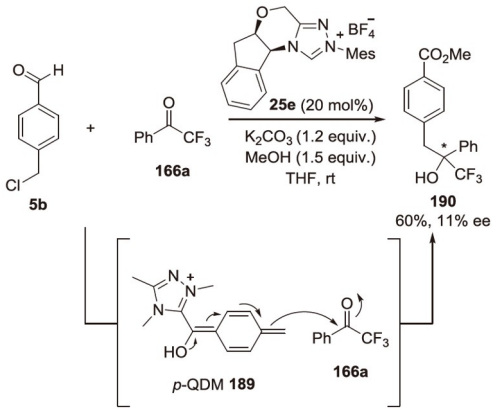

Scheme 47 Primitive enantioselective ε-addition of 4-(chloromethyl)-benzaldehyde to ketone.

the photocatalyst (Scheme 48). The corresponding α-amino ketones **196** could be afforded in good yields with excellent enantioselectivities. Mechanistically, Ru(III) is generated upon oxidation of photoexcited Ru(II)* by a mild oxidant *meta*-dinitrobenzene (*m*-DNB). Tertiary amine is then oxidized by Ru(III) into a radical cation, which further undergoes 1,2-H shift and deprotonation to afford an iminium ion **194**. Addition of Breslow intermediate **193** to iminium ion followed by elimination affords the final product **196** and regenerates the carbene catalyst **192**.

Scheidt and coworkers [172] disclosed a radical alkylation reaction of carboxylic acid derivatives with the strategy of dual carbene/photoredox catalysis. 4-Alkyl substituted Hantzsch ester was proved to be an effective alkyl radical precursor and its reaction with acyl imidazole proceeded efficiently by using a simple triazolium as the catalyst and an iridium complex as the photocatalyst under blue LED irradiation. An example of enantioselective catalysis was presented with the use of an aminoindanol-derived carbene catalyst **25d**, affording the corresponding ketone product **200**

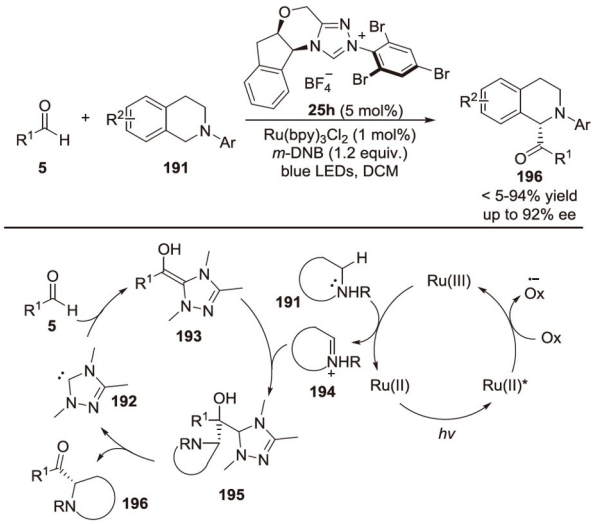

Scheme 48 Enantioselective aza-benzoin reaction *via* dual NHC/photoredox catalysis and the proposed catalytic cycle.

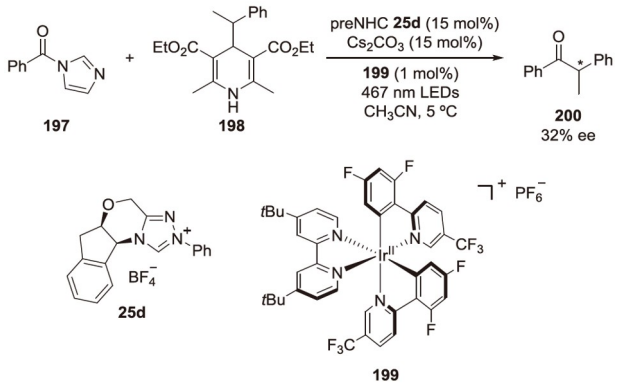

Scheme 49 Radical alkylation of acyl imidazole *via* cooperative NHC/photoredox catalysis.

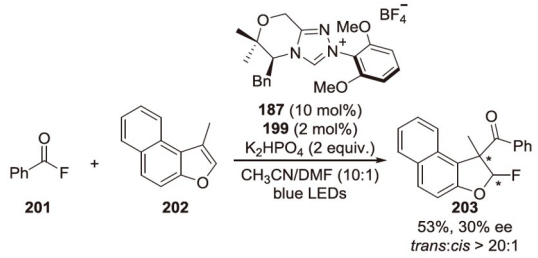

Scheme 50 Fluoroaroylation of benzofurans *via* dual NHC/photoredox catalysis.

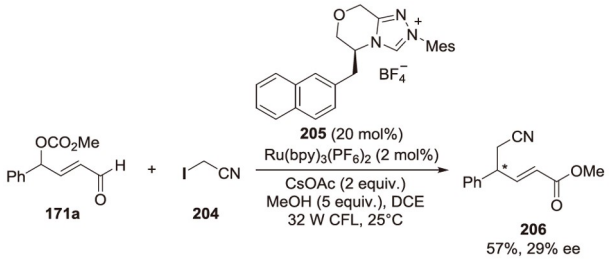

Scheme 51 Remote alkylation of γ-oxidized enals *via* dual NHC/photoredox catalysis.

with 32% ee (Scheme 49). Similar to Scheidt's work, Chi *et al*. [173] realized an alkylation reaction of esters with the same kind of radical precursor. Interestingly, this visible-light promoted reaction proceeded well without the use of any photosensitizer.

Very recently, Studer and coworkers [174] reported the fluoroaroylation of benzofurans *via* cooperative carbene/photoredox catalysis with aroyl fluorides serving as bifunctional agents. The desired functionalized 2,3-dihydrobenzofurans could be afforded in good yields with good regio- and diastereoselectivities. An asymmetric variant was demonstrated to furnish the product **203** in 53% yield, 30% ee and >20:1 dr, with the employment of morpholine-based NHC catalyst **187** and the photosensitizer **199** (Scheme 50).

Remote radical reaction *via* cooperative NHC/photo catalysis was also developed. In 2016, Sun's group [175] reported one example of visible light induced NHC catalyzed γ-dichloromethylenation with trichloromethyl radical. Later, Ye and coworkers [176] disclosed an interesting γ- and ε-alkylation of γ-oxidized enals by combination of carbene catalysis and photocatalysis. Attempt for asymmetric catalysis was also carried out, furnishing the γ-alkylated product **206** in 57% yield with 29% ee by using morpholine-based carbene catalyst **205** (Scheme 51). Noteworthy was that when γ-vinyl substituted γ-oxidized enals were employed, alkyl radical addition occurred selectively at the ε-position rather than the γ-position as previously observed, implying the involvement of an azolium trienolate intermediate.

3.11 Cooperative NHC/transition-metal catalysis

NHCs are good ligands for transition-metal catalysis and the complexes of metal-NHC are effective catalysts for various organic reactions. However, coordination of NHC with transition-metal might be detrimental for cooperative catalysis by inhibiting the reactivity of carbene as an organocatalyst. To address this issue, several groups employed an additional ligand for metal catalyst and regulated the steric and electron effects of NHC to alleviate and even avoid its coordination to transition-metal center.

Glorius *et al*. [177] first demonstrated the asymmetric NHC/Pd dual catalysis, realizing [3+4] annulation of enals **53** with vinyl benzoxazinanones **207** to access azepine derivatives **209** with up to 99% ee (Scheme 52). Detailed mechanistic investigation reveals that NHC both serves as an organocatalyst and a ligand to form a Pd/NHC/phosphine complex, and that the phosphine ligand is crucial for this annulation reaction. The asymmetric [5+2] cycloaddition reaction of enals with vinylethylene carbonates *via* cooperative NHC/Pd catalysis has also been developed by

Glorius and coworkers [178].

In 2020, the Glorius's group [179] reported an example of dual NHC/Ir asymmetric catalysis, accomplishing the annulation reaction *via* NHC-bound enolate intermediate with Ir-allyl complex (Scheme 53). The corresponding lactones and lactams were afforded in good yields, with good diastereoselectivities and excellent enantioselectivities. Soon afterward, Deng and coworkers [180] demonstrated an alternative protocol of NHC/Ir cooperative catalysis to promote regiodivergent [3+2] and [3+3] annulations of enals with allyl indoles, furnishing fused lactams with high levels of stereocontrol. Interestingly, base plays an important role in regulating the regioselectivy of this reaction. Recently, an enantioselective [4+3] annulation of anthranilaldehydes or salicylaldehydes with vinyl aziridines to access benzodiazepinones and benzoxazepinones *via* cooperative NHC/Ir/urea catalysis was well developed by Gong, Song and coworkers [181].

A cooperative NHC/Cu catalysis was disclosed by Gong, Song and coworkers [182]. Enantioselective annulation reactions of isatin-derived enals **213** with ethynyl substituted carbonates/benzoxazinanones (**216**/**214**) proceeded efficiently with the employment of chiral NHC precursor and copper catalyst (Scheme 54). A Cu-NHC complex was identified *via* ESI-MS spectroscopy. The key copper-allenylidene intermediate **219** was proposed to be generated after sequential deprotonation and decarboxylation of ethynyl-copper complex. Nucleophilic addition of homoenolate **218** to copperallenylidene **219** formed a C–C bond, followed by intramolecular lactonization/lactamization and protonation to provide the corresponding cycloadduct and release the carbene catalyst.

Just recently, Ye and coworkers [183] demonstrated the compatibility of cooperative NHC and Ni catalysis. Hydroacylation of 1,3-dienes with aldehydes was achieved with water as the sole solvent. Mechanistic studies excluded the common process of Ni-promoted aldehyde-to-alkene hydrogen transfer and thus estimated the dual catalysis mechanism. Soon after, Gong, Song and coworkers [184] disclosed a highly enantioselective β-allylation reaction of isatin-derived enals **213** with vinyl epoxides **222** and allylic carbonates **225** (Scheme 55). The corresponding allylic products could be afforded in good yields, with excellent stereoselectivities. A Ni(0)/Ni(II) catalytic cycle was proposed with Ni-allyl complex as the key intermediate to react with the NHC-bound homoenolate.

Asymmetric relay catalysis of NHC with other transition-metals, such as Cu [185], and Au [186] was also well established.

3.12 NHC catalysis *via* other modes

The scope of asymmetric carbene catalysis is not restricted to carbonyl substrates with the formation of NHC-bound acyl anion or azolium intermediates. Carbene as a Lewis base can also add to Michael acceptor to generate a zwitterionic intermediate, subsequent nucleophilic addition of which to other electrophiles offers approaches for the Morita-Baylis-Hillman (MBH) and Rauhut-Currier (RC) reactions.

In 2007, Ye and colleagues [187] first disclosed the car-

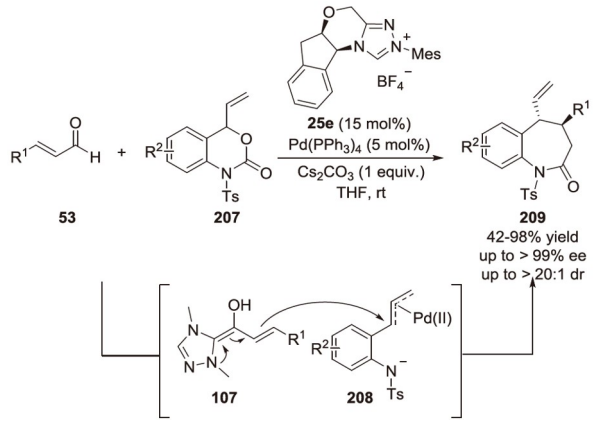

Scheme 52 Enantioselective [3+4] annulation of enals with vinyl benzoxazinanones *via* NHC/Pd cocatalysis.

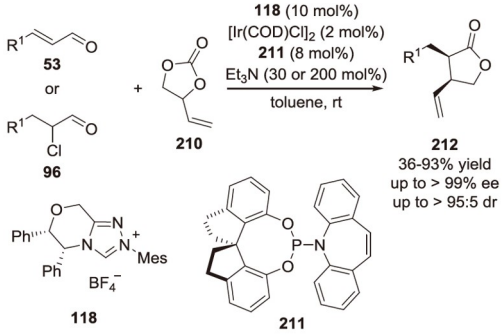

Scheme 53 Asymmetric annulation of enals or α-chloroaldehydes with vinylethylene carbonates *via* dual NHC/Ir catalysis.

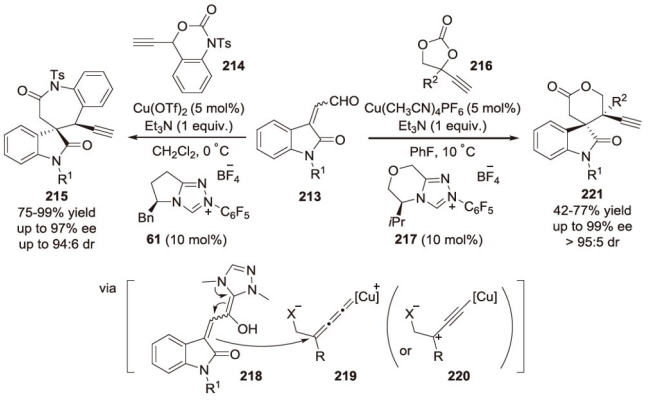

Scheme 54 Enantioselective annulation of isatin-derived enals with ethynyl substituted carbonates/benzoxazinanones *via* cooperative NHC/Cu catalysis.

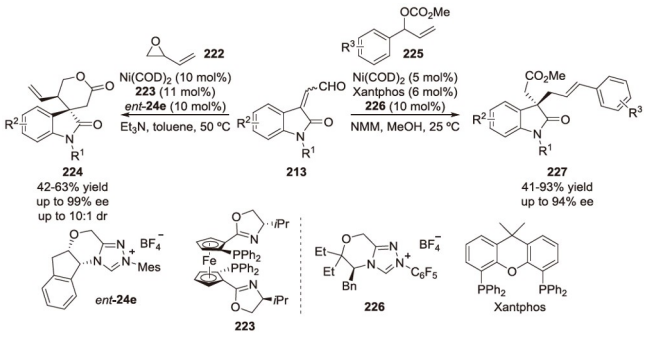

Scheme 55 Enantioselective β-allylation of isatin-derived enals with allylic carbonates and vinyl epoxides *via* dual NHC/Ni catalysis.

bene catalyzed MBH-reactions by employing cyclic enones and *N*-Ts aldimines as the substrates [130b]. An asymmetric variant was reported with the use of bifunctional carbene **31c**, affording the adduct **229** with a promising enantioselectivity (44% ee) (Scheme 56a). Later, a RC-type [4+2] annulation of nitroolefins with cyano-chalcones was reported by the same group [188]. The desired dihydrolpyranes could be obtained in good yields with moderate to good diastereoselectivities. An enantioselective variant was also presented with the employment of bifunctional carbene **31b**, giving the cycloadduct **232** in 24% yield, 5:1 dr and 29% ee (Scheme 56b).

A highly enantioselective RC-reaction *via* carbene catalysis was reported by Lupton and coworkers [189] in 2019. The morpholine-based carbene catalyst **187** with an *N*-(2,6-dimethoxyphenyl) group was effective to promote intramolecular reactions of less electrophilic bis(enoate) **233**, affording lactone products **234** in moderate to good yields with >20:1 dr for all cases and up to 96% ee (Scheme 57). Intermolecular reactions by employing α,β-unsaturated acyl fluorides and TBS protected naphthols *via* a cascade esterification/RC-reaction process were also achieved in an enantioselective manner.

3.13 Summary and perspectives of vitamin B_1-related N-heterocyclic carbene catalysis

The past decades have witnessed the enormous capacity of N-heterocyclic carbenes to mimic vitamin B_1 in catalytic asymmetric transformations. Broad scope of substrates has been well established, ranging from aldehydes to ketenes, carboxylic acids, and their derivatives, *etc*. Carbene catalysis, with the generation of various nucleophilic and electrophilic intermediates, has accomplished selective functionalization at different position of the substrate. Despite the great advances, defects of carbene catalysis at current stage are also apparent. Carbene catalyst loading is still very high, about 10 mol%–20 mol% for most cases. Enantioselective control of carbene catalyzed radical reactions and remote functionalizations is still challenging. Thus,

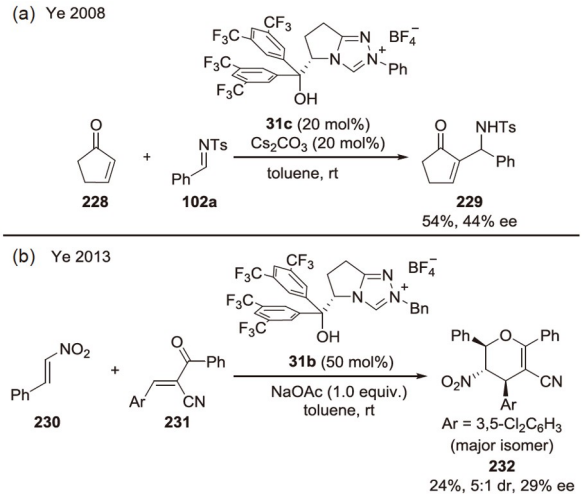

Scheme 56 Asymmetric MBH and RC reactions *via* bifunctional NHC catalysis.

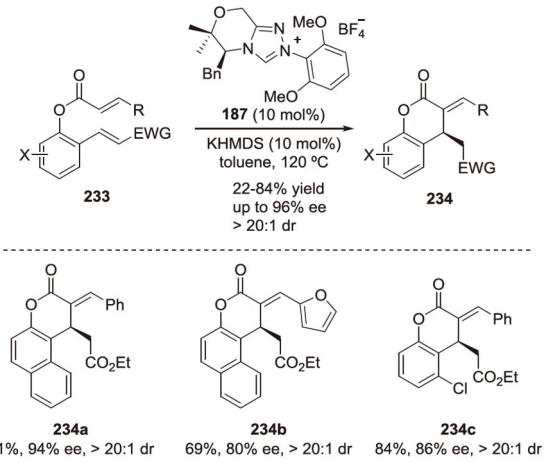

Scheme 57 Enantioselective intramolecular R-C reaction of bis(enoate).

the design and application of novel reactive and selective carbene catalysts, especially the bifunctional ones, are highly desirable. Cooperative carbene catalysis with other catalytic strategies, to expand the scope to "inert" substrates, would undoubtedly lead to the discoveries of novel activation modes and interesting chemical transformations.

4 Vitamin B_6-based asymmetric catalysis

4.1 Vitamin B_6-dependent enzymatic transformations

Vitamin B_6 (VB_6), containing pyridoxal (PL), pyridoxamine (PM) and the related phosphorylated derivatives (PLP and PMP), is an essential coenzyme in living organism [190]. The VB_6-dependent enzymes are an enormous family containing hundreds of members (around 4% of the all enzyme activities) [191]. Typically, pyridoxal/pyridoxamine serves as the catalytic active site while proteins provide chiral

surrounding for enzymatic reactions, wherein the amino acid residues of the proteins are able to accelerate the rate of biological conversion *via* cooperative catalysis. It is discovered that these enzymes catalyze numerous transformations mainly involving the synthesis and metabolism of amino acids and amines, such as transamination, aldol reaction of glycine, retro aldol reaction of β-hydroxy-α-amino acids, decarboxylation and racemization of α-amino acids, β-substitution of serine and derivatives (Figure 11), supplying diversified chiral bio-based amines [192].

Among these VB_6-dependent enzymes, aminotransferases and threonine aldolases were the most investigated ones. In the process of transamination, the 1,3-proton shift of imines **235**/**237** prompts the amino group transferring from an amino acid toward a keto acid, wherein pyridoxal and pyridoxamine are interconvertible *via* two half-transaminations (Scheme 58) [193,194]. Regarding the threonine aldolase enabled aldol reaction of glycine, instead of 1,3-proton shift, intermediate **238** proceeds addition toward aldehyde to afford β-hydroxy-α-amino acids (Scheme 59) [195]. In these biological transformations, the Lys residue not only promotes the 1,3-proton shift or the electrophilic addition to aldehyde as an intramolecular base but aslo assists the product release *via* forming internal aldimine as well [196]. This cooperative effect of the Lys has been proven by the evidence that changing the lysine with a different amino acid or totally removing it *via* mutagenesis resulted in up to 10^6-fold deceleration of transamination [197]. Due to the synthetic importance of these products (chiral α-amino acids and β-hydroxy-α-amino acids), VB_6-based biomimetic asymmetric catalysis primarily includes the simulation of transaminases and threonine aldolases.

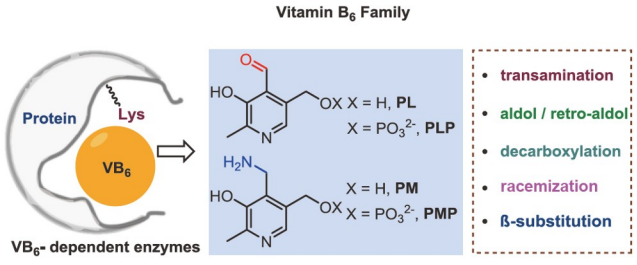

Figure 11 Vitamin B_6 and related enzymatic transformations (color online).

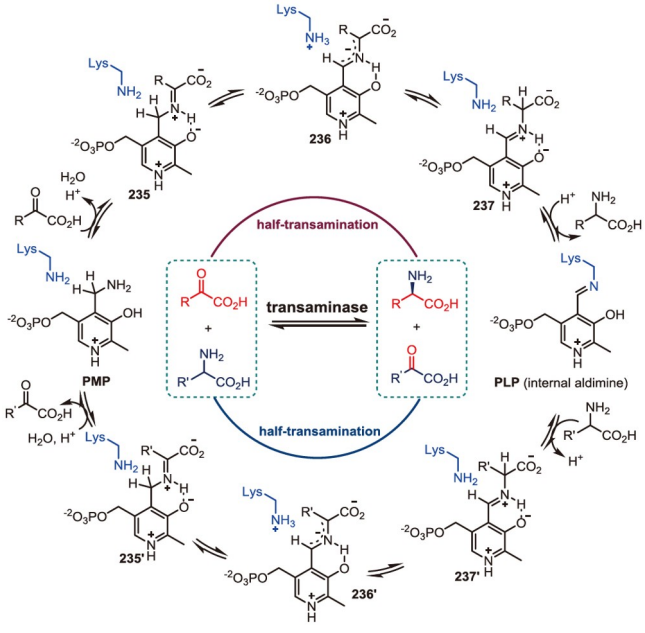

Scheme 58 Biological transamination (color online).

Given the VB_6 possesses powerful catalytic ability and enables a wide range of reactions to deliver chiral amines that have been vastly utilized in pharmaceuticals, fine chemicals as well as materials, the development of VB_6-dependent biomimetic catalysis is of central importance and thus have drawn considerable attention from chemists since 1940s [21,198]. Precedent studies have demonstrated that the 3-OH, 4-CHO/CH_2NH_2, and the pyridine ring of PLP and PMP are indispensable for catalytic function (Figure 12). The 5-phosphate is not catalytically necessary, and it is adjacent to the catalytic center (4-CHO/CH_2NH_2). Accordingly, the 5-position of the pyridine ring is an ideal place to introduce an appropriate moiety to construct chiral biomimetic pyridoxal/pyridoxamine catalysts, which are capable to imitate the corresponding enzymes in varied transformations. In the course of biomimetic catalyst design, it has been found that the functional side chain tethered to the 5-position as well as the electronic property of the pyridine ring impact catalytic activity and selectivity. The side chain is expected to mimick the amino acid residues of enzymes to perform cooperative catalysis.

4.2 Bio-inspired enantioselective reactions enabled by stoichiometric chiral pyridoxamines and pyridoxals

In 1978, Kuzuhara's group [199] reported the first biomimetic asymmetric transamination using stoichiometric chiral pyridoxamine **241** to imitate aminotransferase. Compound **241** acted as amino source to transfer its NH_2 to α-keto acids, delivering the corresponding pyridoxal **242** and enantioenriched α-amino acids. Further studies demonstrated the ratio of Zn^{2+}/**241** affected the enantioselectivity. Pyridoxamine **241b** (1 equiv.) together with and $Zn(ClO_4)_2 \cdot 6H_2O$ (0.5 equiv.) enabled the asymmetric transamination to provide chiral amino acids with up to 96% ee (Scheme 60) [200]. Breslow and his coworkers [201] also investigated stoichiometric bio-inspired transamination of α-keto acids using a series of pyridoxamines with a chiral sulfur-containing side chain. Pyridoxamine **244** delivered optically active α-amino acids with up to 92% ee [201b]. The side arm was assumed to has an analogous cooperative effect as the Lys residue of transaminases, accelerating the process of the

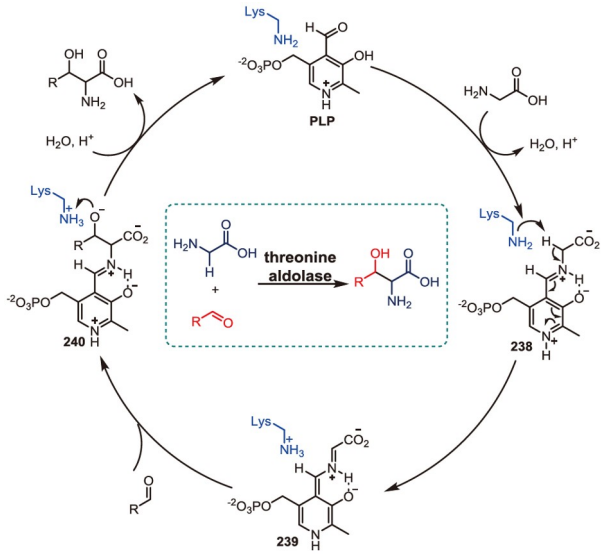

Scheme 59 Biological aldol reaction (color online).

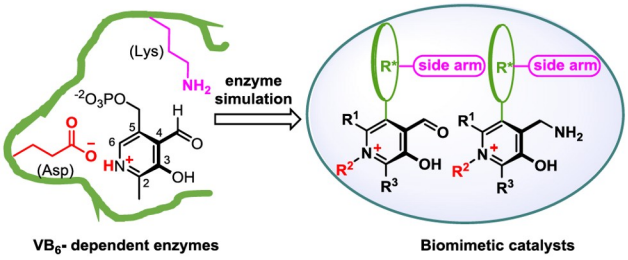

Figure 12 VB_6-based biomimetic catalyst design (color online).

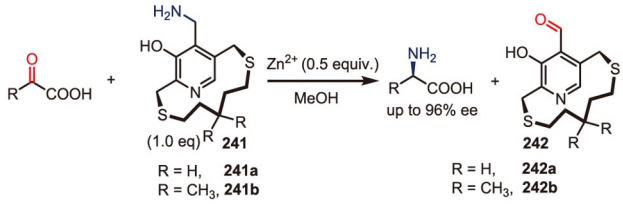

Scheme 60 Asymmetric transamination promoted by pyridoxamines **241** (color online).

transamination (Scheme 61). In addition, chiral pyridoxals **245** (Kuzuhara) [202] and **246** (Breslow) [203] were employed for imitation of biological aldol reaction of glycine, wherein complex **247** consisting of pyridoxal, glycine, and metal was formed initially and then underwent nucleophilic addition to aldehyde to furnish optically active threonine with up to 74% ee and allo-threonine with up to 88% ee, respectively (Scheme 62). Although beyond the scope of this review, the studies of VB_6-related artificial enzymes developed by Breslow are still worth mentioning, which described β-cyclodextrin-derived [204] or chiral-polymer-attached [205] pyridoxamines (**248** and **249**) enabled biomimetic enantioselective transamination (Figure 13).

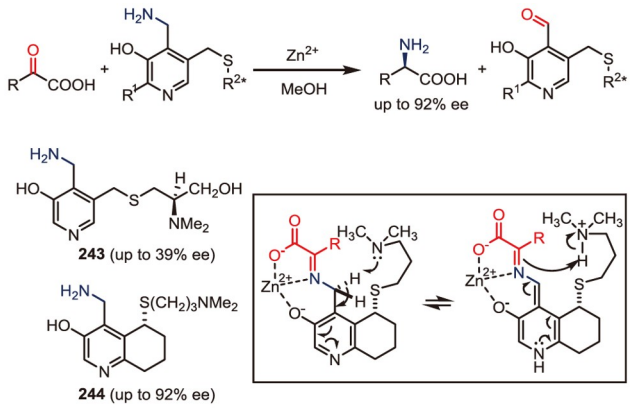

Scheme 61 Asymmetric transamination promoted by pyridoxamines **243** and **244** (color online).

4.3 Vitamin B_6-based catalytic asymmetric biomimetic transamination

The first chiral pyridoxal/pyridoxamine catalyzed asymmetric transamination was reported by Zhao's group. They found chiral pyridoxal **250** [206] and chiral pyridoxamine **251** [207] were both capable to catalyze asymmetric biomimetic transamination of α-keto acids with diphenylglycine as a sacrificial amine source (Scheme 63). Previous catalytic asymmetric protocols mainly involved artificial enzymes [208] as well as chiral base/acid [209,210] catalyzed asymmetric 1,3-proton shift of Schiff bases. Zhao *et al.* [211] later discovered axially chiral biaryl pyridoxamine **252a** owned the competence to enable highly enantioselective amino transfer reaction, delivering a variety of α-amino acids with excellent activity and enantioselectivity (up to 99% yield and 94% ee) (Scheme 64). Catalyst comparison revealed that the NHMe lateral chain was crucial for the obviously high activity and enantioselectivity. It was supposed to mimick the Lys residue of transaminases to accelerate the asymmetric transamination *via* cooperative catalysis (Scheme 64 below) [196]. A proposed reaction pathway illustrates this enzyme-like process (Scheme 65). Chiral pyridoxamine captured α-keto acid to form ketimine **253**, which consequently proceeded 1,3-proton shift, promoted by the amine group of the side chain, forming aldimine **255**. Under the assistance of the amine side chain, amino acid product was released along with the formation of internal iminium **252a′**. Iminium **252a′** underwent decarboxylative transamination with diphenylglycine to regenerate pyridoxamine **252a**, completing a catalytic cycle. Chiral induction occurs during the step of the asymmetric 1,3-proton shift, forming chiral aldimine **255** from ketimine **253**. As delineated in transition state model **259**, the amine fastens the carboxylic group of α-keto acid by acid-base and/or hydrogen bonding interactions and also serves as an intramolecular base to deprotonate the benzylic C–H of ketimine **253** from beneath, producing the deloca-

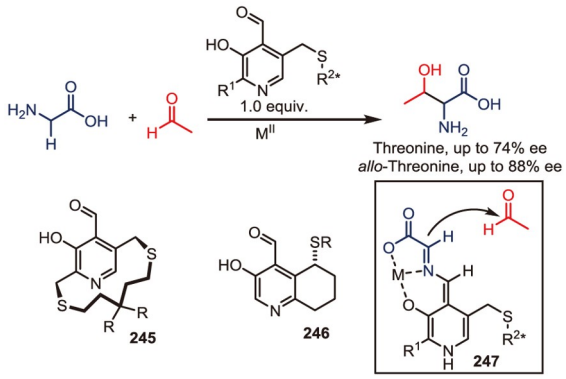

Scheme 62 Asymmetric aldol reaction promoted by pyridoxals **245** and **246** (color online).

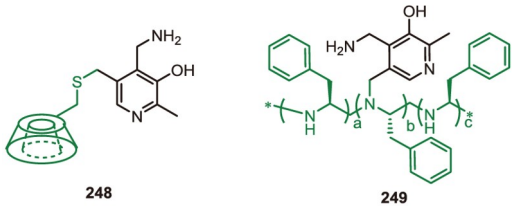

Figure 13 VB_6-based artificial enzymes developed by Breslow (color online).

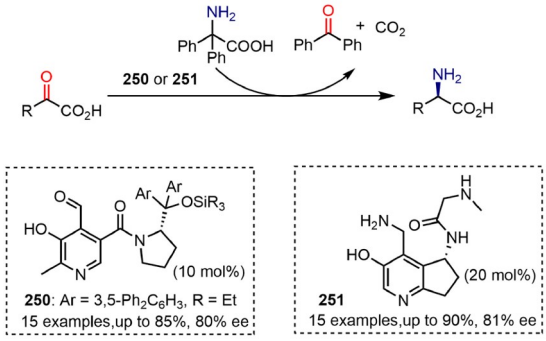

Scheme 63 Asymmetric transamination of α-keto acids catalyzed by **250**/**251** (color online).

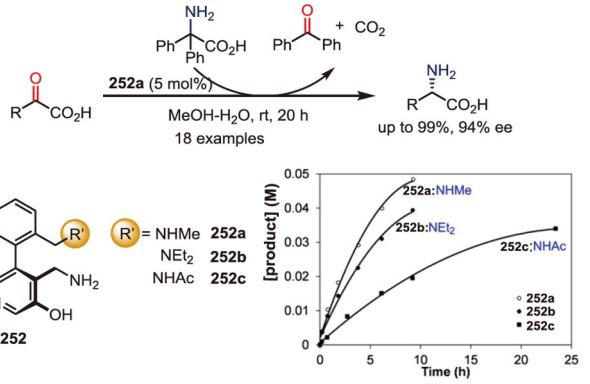

Scheme 64 Pyridoxamine **252a** enabled catalytic asymmetric transamination of α-keto acids (color online).

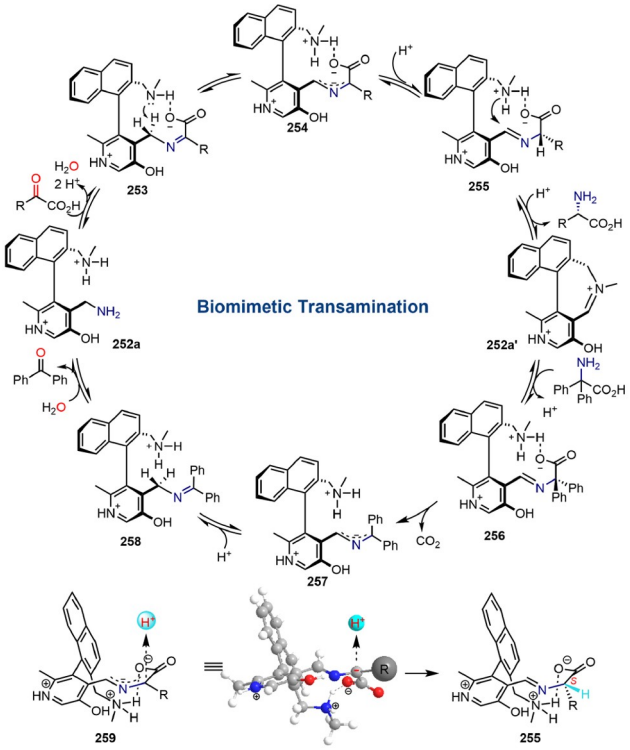

Scheme 65 The proposed transamination mechanism and transition state for chiral induction (color online).

lized azaallylanion. Conversely, protonation of the azaallylanion occurs from the top, generating (*S*)-α-amino acid from (*R*)-pyridoxamine catalyst **252a**. Altogether, this study not only initiates a new avenue to optically active α-amino acids, but also demonstrates that multiple imitation of enzymes is a promising strategy to develop highly efficient biomimetic catalysts.

Encouraged by the outstanding performance of chiral pyridoxamine **252a** in biomimetic transamination of α-keto acids, Zhao's group [212] recently reported their studies on the stereo-divergent transamination of α-keto amides to peptides (Scheme 66). To address the challenge of low reactivity of α-keto amides, N-quaternized chiral pyridoxamines **260** [213] were designed to make the pyridine ring more electron-deficient for facilitating deprotonation of the ketimine formed between α-keto amide and pyridoxamine [214]. By this catalyst, a wide array of α-keto amides underwent asymmetric transamination to offer pharmaceutically and biologically crucial peptides with up to 90% yield, 98% ee or 99:1 dr. The peptides could be obtained as diastereomers respectively by using configurationally reverse catalysts. Intriguingly, a successive "condension-transamination" strategy was employed to make hexapep tide **262** from tetrapeptide **261**, the methyl ester of DPP-IV inhibitor Diprotin A [215], exemplifying an efficient approach for peptide extension (Scheme 66).

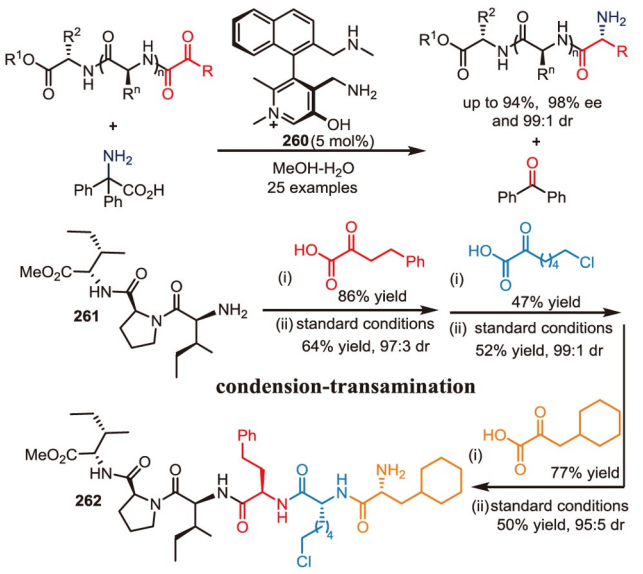

Scheme 66 Pyridoxamine **260** enabled catalytic asymmetric transamination of α-keto amides (color online).

4.4 Vitamin B_6-based biomimetic asymmetric carbonyl catalysis

As a novel catalysis mode, carbonyl catalysis utilizes an appropriate aldehyde or ketone to catalyze α-C−H functionalization of primary amines without protecting group manipulations towards the NH_2 group, providing a new attractive strategy to make α-substituted chiral amines [216]. Threonine aldolase enabled aldol reaction of glycine actually is a typical biological carbonyl catalysis process [195], wherein pyridoxal 5′-phosphate temporarily protects glycine by forming imine **238** to increase its α-C–H acidity, promoting the succeeding nucleophilic addition to aldehydes (Scheme 59). Inspired by this enzymatic transformation, in 2018, Zhao and his coworkers [217] reported their efforts on VB_6-based biomimetic carbonyl catalysis (Scheme 67). Chiral pyridoxal **263** has proven highly effective in enantioselective Mannich reaction of glycinate and imines. Under 0.2–1 mol% catalyst loading, a great range of *N*-diphenylphosphinyl aromatic imines went through asymmetric Mannich reaction with NH_2-unprotected glycinate to deliver structurally attractive and pharmaceutically relevant α,β-diamino acid esters with up to 94% yield, 99% ee and >20:1 dr. The reaction proceeds *via* a mechanistic pathway similar to that of enzymatic aldol of glycine (Scheme 67). Condensation of glycinate with pyridoxal catalyst **263** forms imine **264**. Deprotonation of aldimine **264** leads to delocalized carbanion **265** which is stabilized by *N*-quaternized pyridine [218]. Asymmetric addition of carbanion **266** to *N*-diphenylphosphinyl imine followed by the hydrolysis of compound **267** produces chiral α,β-diamino acid ester and regenerates pyridoxal **263**. As shown in transition state **Ts-266**, the amide lateral arm participates in activation of *N*-

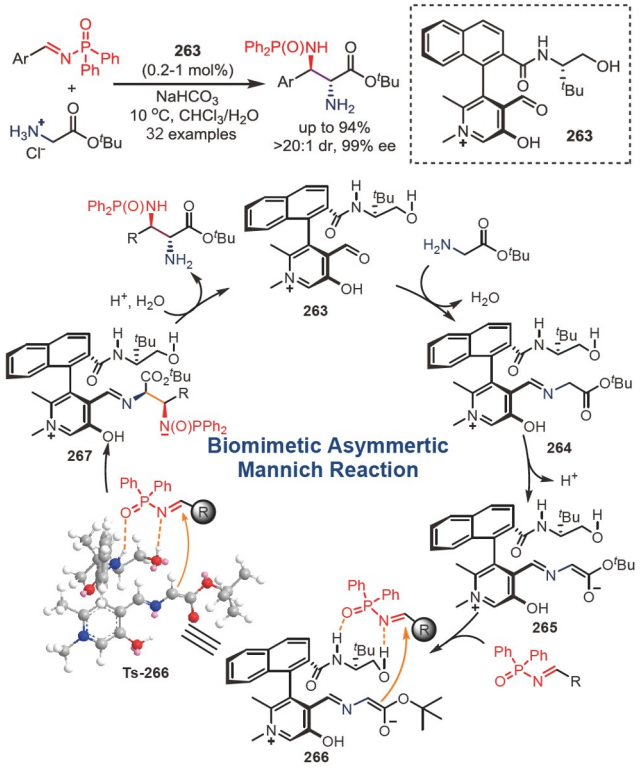

Scheme 67 Pyridoxal **263** catalyzed biomimetic asymmetric Mannich reaction and its mechanism (color online).

diphenylphosphinyl imine by double hydrogen bonds. The enzyme-like cooperative catalysis accounts for the astonishingly high activity and stereoselectivity of pyridoxal catalyst **263**.

Taking advantage of carbonyl catalysis strategy [219], Zhao *et al.* [220] further achieved catalytic asymmetric biomimetic aldol reaction between glycine and trifluoromethyl ketones by employing chiral pyridoxal catalyst **268** (Scheme 68). By using only 0.1 mol% catalyst loading, diverse alkyl trifluoromethyl ketones were effective for this transformation and furnished enantiomerically enriched β-trifluoromethyl-β-hydroxy-α-amino acids (up to 82% yield, 99% ee, and >20:1 dr), which are frequently found in biologically active molecules. The incredible high efficiency of biomimetic catalyst was revealed by the fact that 0.0033 mol% pyridoxal **268** still enabled this aldol reaction to deliver product **269** with 59% yield, 97% ee and 13:1 dr, which has reached (even surpassed) the efficiency of related enzymes. Mechanistic investigation disclosed that N-methylation of the pyridine ring and the N–H group on the side chain combined with the additive Tf_2NH all contributed to the fantastic activity and stereoselectivity of this transformation (**Ts-270**).

In addition to biomimetic Mannich and aldol reactions, Zhao and his coworkers continuously explored new α-C−H transformations of glycinates. In 2020, they applied chiral pyridoxal **271** into the 1,4-conjugated addition of glycinate

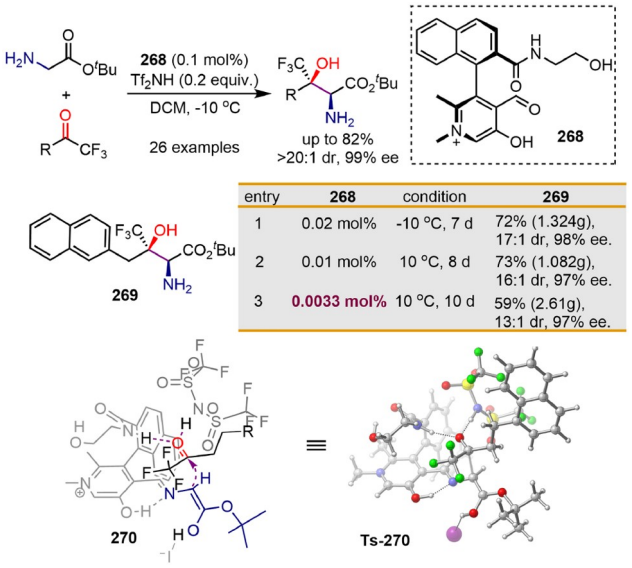

entry	268	condition	269
1	0.02 mol%	-10 °C, 7 d	72% (1.324g), 17:1 dr, 98% ee.
2	0.01 mol%	10 °C, 8 d	73% (1.082g), 16:1 dr, 97% ee.
3	**0.0033 mol%**	10 °C, 10 d	59% (2.61g), 13:1 dr, 97% ee.

Scheme 68 Pyridoxal **268** catalyzed biomimetic asymmetric aldol reaction (color online).

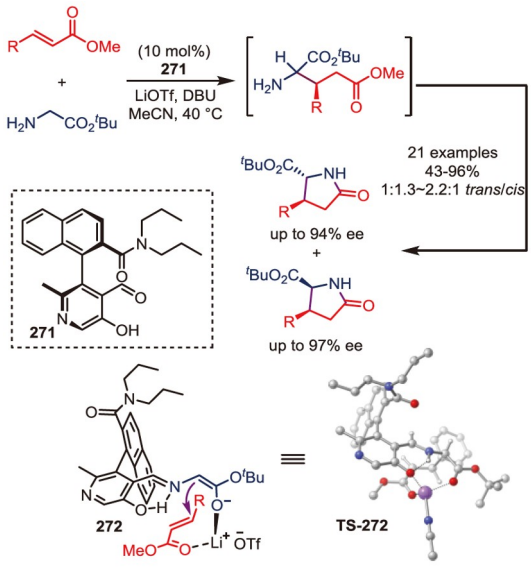

Scheme 69 Pyridoxal **271** catalyzed asymmetric 1,4-conjugated addition of glycinate (color online).

towards α,β-unsaturated esters, to afford a variety of biologically significant chiral pyroglutamic acid esters with up to 96% yield and 97% ee albeit with low *trans*/*cis* ratios caused by rapid epimerization under the basic reaction conditions (Scheme 69) [221]. Surprisingly, *N*-methyl pyridoxal catalyst was inactive for this reaction, probably because the well-stabilized carbanion was not nucleophilic enough for the addition to α,β-unsaturated esters. Besides the catalyst, additive LiOTf was also crucial for the reaction, which was supposed to activate the α,β-unsaturated ester as well as stabilize the enolated anion (**Ts-272**). Very recently, they reported asymmetric α-allylation of glycinate with Morita-Baylis-Hillman (MBH) adducts (Scheme 70) [222]. Given the activating site of MBH acetate is relatively far from its reactive center, pyridoxal **273** featured with larger chiral cavity by attaching side chain at C3 position of the naphthyl ring was designed and utilized in this S_N2'-S_N2' transformation. Under carbonyl catalysis strategy, NH_2-unprotected glycinate directly engaged α-allylation reaction to deliver enantioenriched glutamic acid esters (up to 86% yield, 97% ee and >20:1 dr). Simple transformations of the α-allylation product **275** furnished biologically active lactam **276** and chiral glutamic acid analogue **277** without any loss of enantiopurity, demonstrating the potential of this protocol in synthetic utilization.

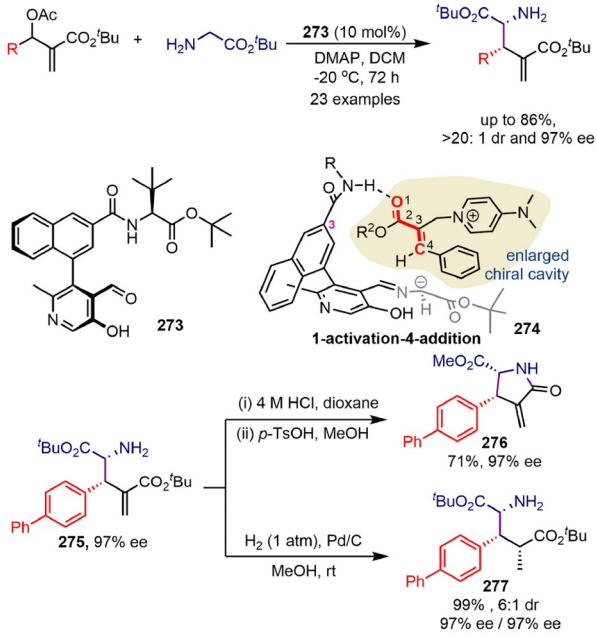

Scheme 70 Pyridoxal **273** catalyzed asymmetric α-allylation of glycinate with MBH acetates (color online).

Direct functionalization of inert C(sp^3)–H bond is a fundamental but tremendous challenge for modern organic chemistry [223]. In order to pursue their interest in development of biomimetic carbonyl catalysis, Zhao's group [224] extended the exploration of primary amines from activated glycinates to inert substrates. Primary propargylamines are challenging substrates for direct α-C−H functionalization, due to the very low acidity of the α C−H bonds (calculated pK_a~42.6). Astonishingly, propargylamines can be greatly activated by chiral pyridoxal catalysts **278** *via* the formation of imines, resulting in dramatic increase of the acidity of the α-C−H bonds by up to 10^{22} times (Scheme 71) [225]. Asymmetric α-addition of propargylamines to alkyl trifluoromethyl ketones produced a broad array of structurally intriguing and medicinally significant chiral β-hydroxy-β-trifluoromethyl propargylamines in high yields (up to 84%) and excellent stereoselectivities (up to 99% ee and >20:1 dr). Undoubtedly, the remarkable co-

operative effect of lateral arm was also identified in this reaction. Furthermore, primary benzylamines bearing inert α-C−H bonds (calculated pK_a~42.7) was also targeted for straightforward enantioselective α-addition to aldehydes (Scheme 72) [226]. A new sort of chiral pyridoxal **279** featured with a squaramide side chain, of which the double N–H bonds were proven essential for activity and stereoslectivity, was developed for realizing this challenge transformation. Various synthetically useful *syn*-β-aminoalcohols were delivered from diversified benzylamines and benzaldehydes with up to 92% yield, >20:1 dr and 99% ee. The efficiency of this method was demonstrated by the quick synthesis of AM-8735 (**282**) [227], a morpholinone inhibitor of MDM2-p53 protein-protein interaction, and antagonist MGluR5 PAM (**285**) [228], wherein pyridoxal **279** catalyzed asymmetric α-addition of benzylamines **280** and **283** to aldehydes were the principal step for these streamlined routes.

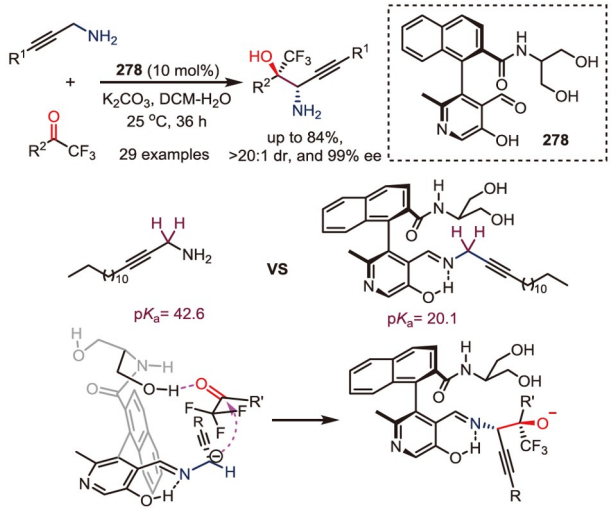

Scheme 71 Pyridoxal **278** catalyzed asymmetric α-addition of propargylamines to alkyl trifluoromethyl ketones (color online).

4.5 Summary and perspectives of vitamin B_6-based asymmetric catalysis

In short, VB_6-based biomimetic asymmetric chemistry has been developed from stoichiometric simulation into catalytic imitation during the past several decades. A variety of novel and efficient pyridoxal/pyridoxamine catalysts have been invented based on the inspiration of the structures and functions of VB_6-dependent enzymes. These pyridoxals/pyridoxamines have displayed extraordinary performances in catalytic biomimetic transamination and α-C−H functionalization of primary amines. With an axially chiral biaryl pyridoxamine as the catalyst, biomimetic transamination of α-keto acids and α-keto amides were both successfully achieved, respectively producing various bioactive α-amino acids and peptides with excellent enantiopurities. Enzymatic aldol reaction of glycine brought to carbonyl catalysis, a new catalytic mode for direct α-C−H functionalization of NH_2-unprotected primary amines with electrophiles. By utilizing chiral pyridoxals as carbonyl catalysts, the strategy has already been applied to the reactions of glycinates and inert primary amines, *i.e.*, propargylamines and benzylamines, with various electrophiles including aldehydes, imines, trifluoromethyl ketones, α,β-unsaturated esters, and Morita-Baylis-Hillman (MBH) adducts. These studies have exhibited the robust and unique catalytic competence of VB_6 for constructing optically active amine compounds, and would further spur the development of VB_6-based biomimetic catalysts for asymmetric catalysis and organic synthesis. Despite the forementioned achievements, VB_6-based biomimetic asymmetric catalysis still remains in its early stage of development and some challenges still await to be addressed, which are (1) transamination of inactivated carbonyl compounds, such as alkyl aldehydes and ketones, (2) direct asymmetric α-C−H functionalization of alkyl amines enabled by carbonyl catalysis, (3) further development of more efficient chiral pyridoxamine/pyridoxal catalysts, and (4) biomimetic chemistry based on the simulation of other VB_6-dependent enzymatic transformations, such as decarboxylation of α-amino acids and β-substitution of serine and derivatives. It is believed that continuous development of this field will eventually unlock a powerful platform for green synthesis of complicated organic compounds.

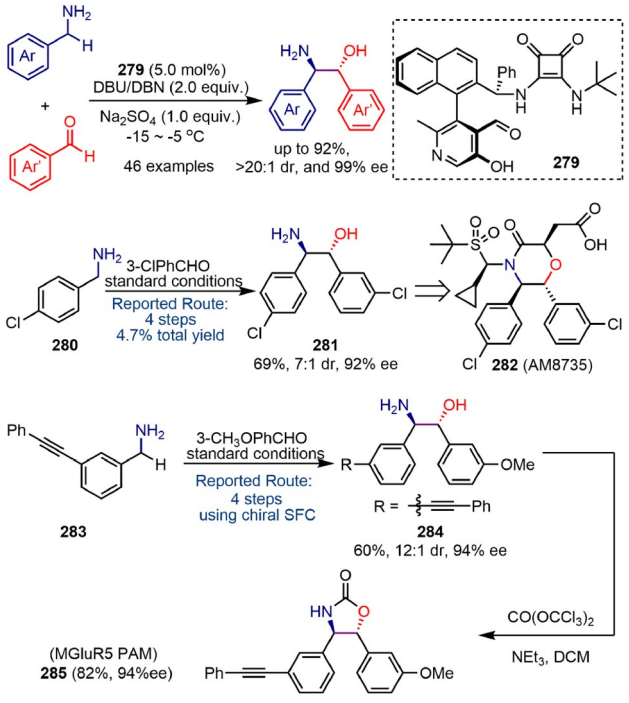

Scheme 72 Pyridoxal **279** catalyzed asymmetric α-addition of benzylamine to aldehydes (color online).

5 NAD(P)H-based biomimetic asymmetric catalysis

In the cell, the reduced nicotinamide adenine dinucleotide (NADH) and nicotinamide adenine dinucleotide phosphate (NADPH) are recognized as a couple of crucial enzymes, and over 400 enzyme redox reactions, such as the citric acid cycle, glycolysis, and amino-acid decomposition, depend on the interconversion of NAD(P)H and $NAD(P)^+$ (Figure 14a). NADH and NADPH contain the 1,4-dihydropyridine rings, which can be used as the hydrogen sources to reduce unsaturated double bonds owing to its driving force of aromatization (Figure 14b) [22,229,230].

Inspired by the reduction mechanism of NAD(P)H, a series of efficient methods to realize biomimetic asymmetric reductions (BMAR) have been studied intensively, accompanying the development of novel NAD(P)H models. According to the type of the NAD(P)H models, it is divided into the following three aspects: (1) BMAR participated by stoichiometric amount of NAD(P)H models; (2) BMAR catalyzed by achiral NAD(P)H models; (3) BMAR catalyzed by chiral NAD(P)H models (Figure 14c).

5.1 BMAR participated by stoichiometric NAD(P)H models

In earlier studies, some scientists modified niacinamide, the core structure of coenzyme NAD(P)H, to satisfy the fact that the NAD(P)H models could have a drive to restore aromatization similar with the coenzyme NAD(P)H. Thus, the BMAR *via* stoichiometric amount of achiral NAD(P)H model were successfully realized with chiral transfer catalyst (Scheme 73).

5.1.1 Stoichiometric achiral NAD(P)H models

Stoichiometric achiral NAD(P)H models mainly include Hantzsch ester (HEH) **285** and benzothiazoline **286** (Scheme 74). In 1985, Gelbard's group [231] first realized the BMAR of methyl benzoylformate by using stoichiometric HEH **285** as the NAD(P)H model and the chiral shift reagent (+)-$Eu(tfc)_3$ as the Lewis acid. However, the yield and enantioselectivity of the reduction were not satisfactory. Until 2004, List's group [232] achieved BMAR of α,β-unsaturated aldehyde using the stoichiometric HEH and the chiral amine salt as the catalyst in good yield and enantioselectivity (Scheme 75).

Later, Rueping *et al.* [233] and List *et al.* [234] used the combination of catalytic chiral phosphoric acid (CPA) and HEH **285** to achieve the BMAR of ketoimines respectively, resulting in high activities and enantioselectivities (Scheme 76).

Subsequently, in the presence of HEH, the BMAR of some unsaturated substrates containing C=C, C=O or C=N was achieved with the participation of chiral organic catalysts or metal complexes. Under mild conditions, a great number of important chiral organic synthetic blocks could be obtained with superior yields and enantioselectivities [235–241].

In addition to the Hantzsch ester **285**, benzothiazoline **286** could also be used as the NAD(P)H model, which converted to the more stable benzothiazole after dehydrogenation. In

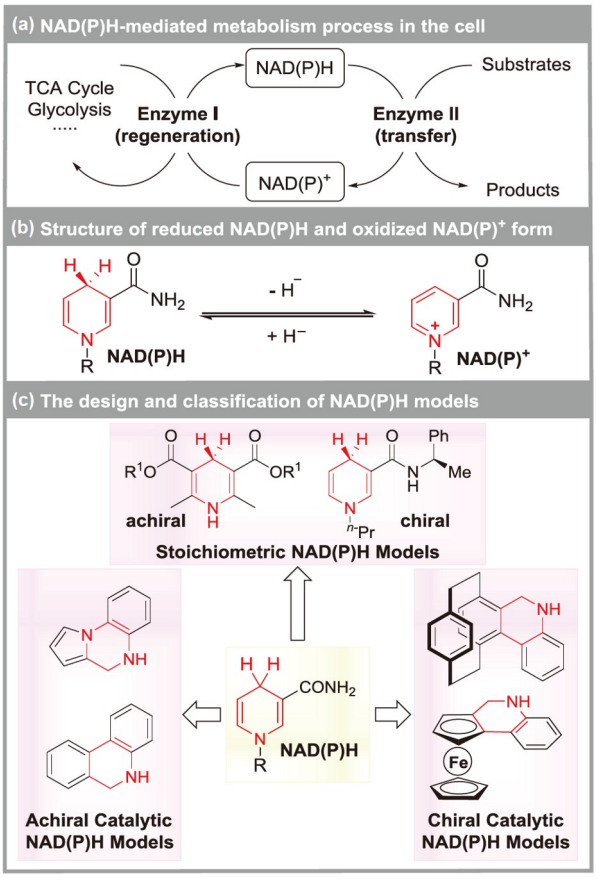

Figure 14 (a) NAD(P)H-mediated metabolism process in the cell. (b) Structure of the reduced NAD(P)H and oxidized $NAD(P)^+$ form. (c) The design and classification of NAD(P)H models (color online).

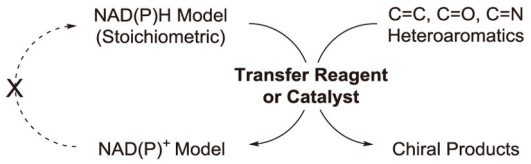

Scheme 73 BMAR participated by stoichiometric NAD(P)H models.

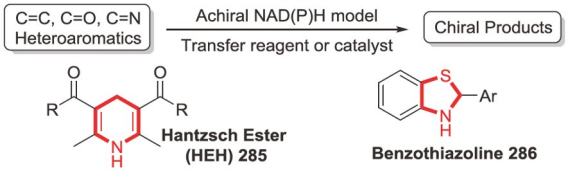

Scheme 74 Stoichiometric achiral NAD(P)H models (color online) .

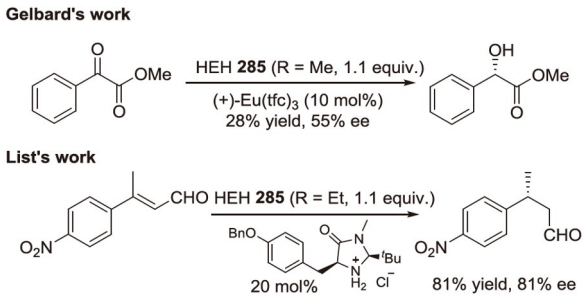

Scheme 75 BMAR of methyl benzoylformate and α,β-unsaturated aldehyde.

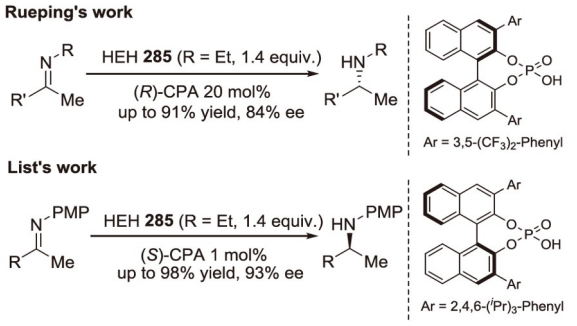

Scheme 76 BMAR of ketoimines by the combination of HEH and CPA.

2009, utilizing benzothiazoline **286** and CPA, Akiyama and coworkers [242] achieved the BMAR of ketoimines with excellent activities and enantioselectivities (Scheme 77). Since then, benzothiazoline **286** was mainly used as a NAD(P)H model in the BMAR of C=N bond.

5.1.2 Stoichiometric chiral NAD(P)H models

Compared with the achiral NAD(P)H model, the BMAR involved the chiral NAD(P)H models could be achieved without additional chiral catalysts or reagents. At present, the stoichiometric chiral NAD(P)H models mainly focused on the chiral niacinamide derivatives. The spatial effect on the molecular structure of the NAD(P)H model is generated by each substituent on its active group dihydropyridine, or through its own specific spatial configuration, to achieve stereoselective reactions. According to the symmetry of the NAD(P)H models, it is divided into the following aspects: (1) C_1-symmetrical chiral NAD(P)H models and (2) C_2-symmetrical chiral NAD(P)H models.

(1) C_1-symmetrical chiral NAD(P)H models

The design of the C_1-symmetrical chiral NAD(P)H models is mainly based on the core skeleton of niacinamide, which can be introduced into chiral groups at the N-1, C-3 or C-4 positions, and designed as different types of stoichiometric chiral NAD(P)H models for BMAR.

As early as 1975, Ohnishi's group [243] first applied the NAD(P)H model **287** containing chiral groups at the C-3 position to the BMAR of ethyl benzoylformate. In the presence of stoichiometric $Mg(ClO_4)_2$, the desired hydrogenated product could be obtained with poor 20% ee. The chiral organometallic NAD(P)H model **288** was designed through introducing a chiral iron-containing complex at the C-3 position of nicotinamide by Davies's group [244]. The reduction of ethyl benzoylformate could achieve excellent enantioselectivity (98% ee) because the hydroxyl and carbonyl group of NAD(P)H model jointly involved in the coordination with the Mg^{2+} cation. Due to the similar structure of sulfinyl groups and amides, Iwata's group [245] described the synthesis of the novel NAD(P)H model **289** and their use in effective BMAR of methyl benzoylformate (75% yield, 97% ee). Inspired by this, Levacher's group [246] prepared the 1,4-dihydroquinolines bearing a chiral sulfinyl group, the novel NAD(P)H model **290**, which was applied to the asymmetric reduction of methyl benzoylformate with 70% yield and 95% ee. In 2009, the strongly rigidified β-lactam peptidomimetic NAD(P)H model **291** has been synthesized by Aizpurua's group [247] and used to the BMAR of methyl benzoylformate (>99% yield, 90% ee). The chelation of NAD(P)H model with Mg^{2+} cation to form a seven-membered ring was found to be the actual reason of the excellent stereodiscrimination (Scheme 78).

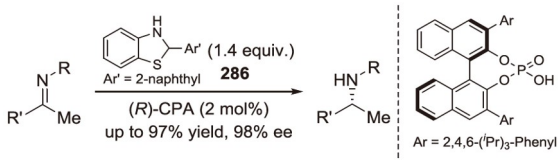

Scheme 77 BMAR of ketoimines by benzothiazoline **286** and CPA.

Inouye's group [248] attempted to introduce the L-prolinamide at the *N*-1 position of the niacinamide, and successfully synthesized the NAD(P)H model **292**. In the presence of $Mg(ClO_4)_2$, the chiral alcohol was obtained with 90% ee and 39% yield (Scheme 79).

In order to better control the enantioselectivity of the reaction, a series of NAD(P)H models with a chiral center at the C-4 position were synthesized which had reaction and stereocenters at the same position. Ohno's group [249] improved the stereoselectivity in the process of BMAR of methyl benzoylformate by additional introduction of methyl group at the C-4 position in the NAD(P)H model **293**. Subsequently, Vekemans and coworkers [250] replaced the chiral amide group with an achiral *N*,*N*-dimethylamide group at the C-3 position. The BMAR of ethyl benzoylformate could get 95% ee at −25 °C which indicated that the C-4-substituent played an important role in the control of stereoselectivity. In order that the reaction could proceed smoothly at room temperature, Mikata's group [251] described the more stable quinoline-type NAD(P)H model **295** which had the high enantioselectivity (up to >99% ee). In 1986, Meyers's group [252] synthesized the chiral NAD(P)H

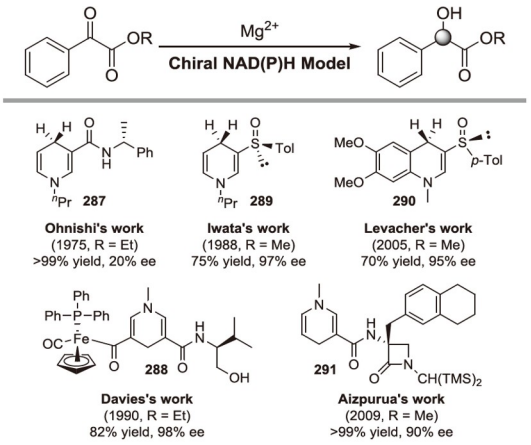

Scheme 78 BMAR of benzoylformates by NAD(P)H model containing chiral groups at the C-3 position.

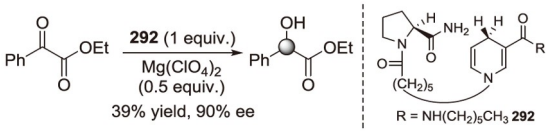

Scheme 79 BMAR of ethyl benzoylformate by NAD(P)H model **292** containing chiral groups at the N-1 position.

model **296a** without amide group at the C-3 position, and the reduction of methyl benzoylformate could afford 95% ee. When the C-5-substituent was the amide group (**296b**), the amide group competed favorably with the hydroxy group, resulting in a reversal of stereochemistry (Scheme 80).

Besides introducing chiral groups at the N-1, C-3 or C-4 positions, NAD(P)H models with other chiral modifications were also developed. Bourguignon and Levacher *et al.* [253,254] reported the synthesis of NAD(P)H models **297** with cyclic amide group successively. In the reduction of methyl benzoylformate, it was found that the out-of-plane C=O amide orientation may have important implications in the stereospecific hydrogen transfer. In order to avoid the side reaction of the enamine in the NAD(P)H models, Levacher's group [255] subsequently designed new axially chiral NAD(P)H model **298**. On the one hand, the introduction of a benzene improved the stability of the NAD(P)H model, and on the other hand, the axial chirality and central chirality of the seven-membered cyclic lactam realized the good control of enantioselectivity. The synthesis of difunctional NAD(P)H model **299** in the pyrrolo[2,3-*b*]pyridine series was described by Levacher *et al.* [256]. The methyl mandelate was obtained in good enantioselectivity with either (*S*) or (*R*) configuration simply by changing the Mg^{2+} cation concentration. Kanomata's group [257] reported the chiral bridged NAD(P)H model **300** by cyclizing the C-2 and C-5 positions of the 1,4-dihydropyridine. The presence of bridge increased the steric hindrance of NAD(P)H models, and 99% ee could be obtained in the reduction of methyl

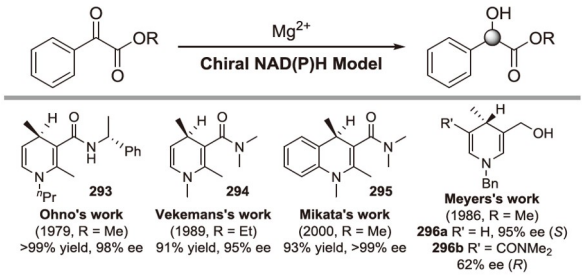

Scheme 80 BMAR of benzoylformates by NAD(P)H model containing chiral groups at the C-4 position.

benzoylformate (Scheme 81).

(2) C_2-symmetrical chiral NAD(P)H models

Starting from optically pure *L*-amino acid esters, Kellogg's group [258] synthesized a series of C_2-symmetrical NAD(P)H models **301** with various bridges. These NAD(P)H models have achieved the BMAR of ethyl benzoylformate with up to 90% ee. The enantiomeric excesses decreased with the increasing of the bridge length, which possibly affected the coordination between the bridged 1,4-dihydropyridine, Mg^{2+} cation, and carbonyl component (Scheme 82).

5.2 BMAR catalyzed by achiral NAD(P)H models

The BMAR participated by stoichiometric NAD(P)H models has achieved good results, but the harsh regeneration conditions of NAD(P)H models resulted in the poor atom economy, which limited the development of the BMAR. Through the simulation of the cyclic regeneration of coenzymes in biological processes, the scientists developed a series of renewable chiral NAD(P)H models, realizing the asymmetric reduction of carbonyl compounds, imines and so on, as shown in Scheme 83.

In 2002, Fish's group [259] successfully reduced the NAD(P)H model **302** into its corresponding 1,4-dihydroanalogue using rhodium as the catalyst precursor, and sodium formate as the hydride source. Subsequently, the highly enantioselective BMAR of ketone was realized with horse liver alcohol dehydrogenase. The first class of thiourea- and nicotinamide-based bifunctional organocatalyst **303** has been developed in 2007 by Connon's group [260]. In the BMAR of 1,2-diketone, the thiourea could activate the substrate by forming an intermolecular hydrogen bond avoiding the addition of stoichiometric Lewis acid, and the nicotinamide, as the NAD(P)H model, could regenerate in the presence of sodium dithionite. Unfortunately, the stereoselectivity of the reaction was poor albeit high activity (Scheme 84).

The regeneration of Hantzsch ester *in-situ* has been achieved by Ru complexes under hydrogen gas through the efforts of Zhou and coworkers [261]. In the presence of chiral phosphoric acid, the BMAR of benzoxazinones was realized with up to 99% ee. Although the use of hydrogen gas

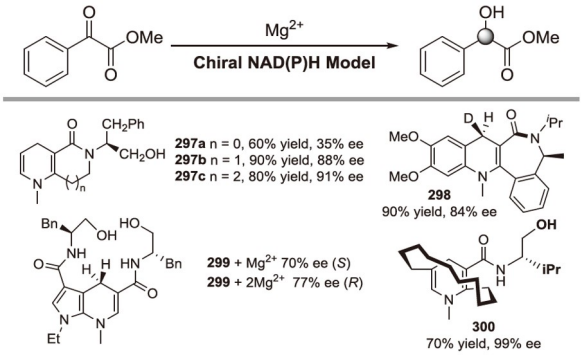

Scheme 81 BMAR of methyl benzoylformate by NAD(P)H models with other chiral modifications.

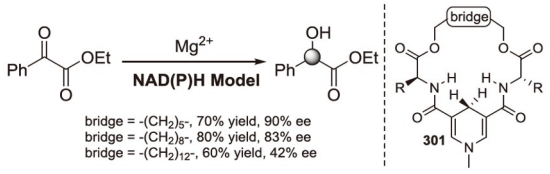

Scheme 82 BMAR of ethyl benzoylformate by NAD(P)H model **301**.

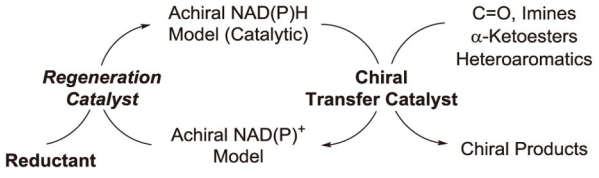

Scheme 83 BMAR catalyzed by achiral NAD(P)H models.

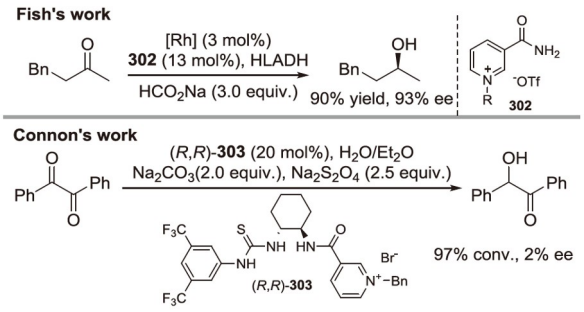

Scheme 84 BMAR of C=O by regenerable NAD(P)H models **302** and **303**.

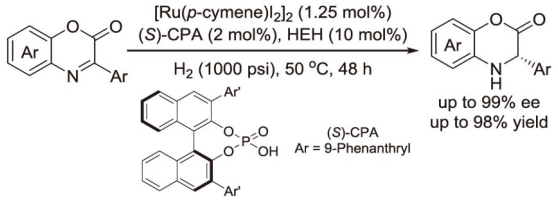

Scheme 85 BMAR of benzoxazinones by catalytic HEH.

as a reductant made this hydrogenation to be an ideal atom economic process, the harsh regeneration conditions of HEH and the presence of background reactions limited the scope of substrate. Therefore, it was necessary to explore NAD(P)H models which were easily regenerated *in-situ* under mild conditions (Scheme 85).

Most of the currently successful NAD(P)H models, such as HEH and 1-benzyl-1,4-dihydronicotinamide (BNAH), usually contained a dihydropyridine skeleton which played an important role in the hydride transfer process. Based on the dihydropyridine skeleton, a new and easily regenerable NAD(P)H model 9,10-dihydrophenanthridine (DHPD) was reported by Zhou and coworkers [262]. At room temperature, the DHPD could regenerate from phenanthridine by Ru complexes under hydrogen gas. Compared with 1,4-hydride transfer of the current NAD(P)H models, the 1,2-hydride transfer pathway occurring in DHPD-mediated reduction was better for controlling the enantioselectivity owing to the decrease in steric distance between substrate and catalyst. Besides benzoxazinones, the benzoxazines, quinoxalines, quinolines and alkynyl ketimines could also be hydrogenated with excellent activities and enantioselectivities using a catalytic amount of chiral phosphoric acid (Scheme 86).

Encouraged by the successful application of DHPD, 4,5-dihydropyrrolo[1,2-a]quinoxalines (DHPQ), a series of tunable and regenerable NAD(P)H models, have been synthesized easily through the mild partial hydrogenation of corresponding pyrrolo[1,2-a]quinoxalines (PQ) by Zhou's group [263]. Subsequently, the biomimetic asymmetric hydrogenation of benzoxazines proceeded well with excellent yields and enantioselectivities when the chiral phosphoric acid was used as the transfer catalyst (Scheme 87).

Besides transition metal ruthenium complexes, inexpensive metal complexes could also enable *in-situ* regeneration of NAD(P)H models. In 2003, Beller and coworkers [264] demonstrated that iron catalysts were not only responsible for the regeneration of NAD(P)H model phenanthridine, but also acted as the Lewis acid to promote the transfer hydrogenation of methyl benzoylformate. The desired product could be obtained in excellent yield and moderate enantioselectivity. When Lewis acid was replaced by chiral phosphoric acid, the BMAR of benzoxazinones has been accomplished in high yields and enantioselectivities (up to 96% yield, 96% ee) [265] (Scheme 88).

5.3 BMAR catalyzed by chiral NAD(P)H models

Through the simulation of the coenzyme circulation process *in vivo*, the *in-situ* regeneration of coenzyme NAD(P)H models was successfully achieved. With the continuous deepening of people's research, various achiral regenerable NAD(P)H models have been designed and synthesized, and widely used in the reduction of diverse substrates. However,

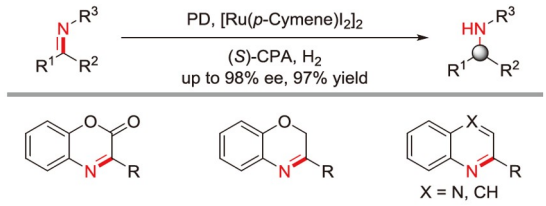

Scheme 86 BMAR of C=N by catalytic phenanthridine (color online).

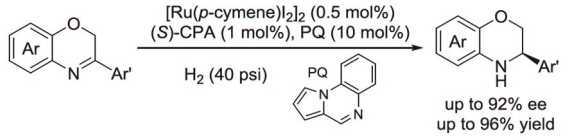

Scheme 87 BMAR of benzoxazines by catalytic pyrrolo[1,2-a]quinoxaline.

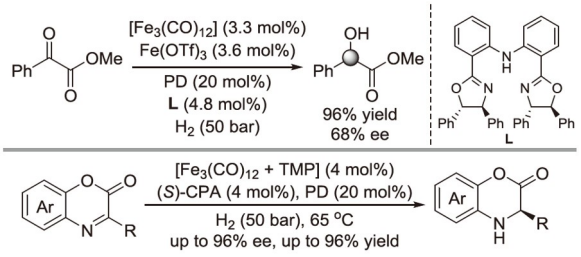

Scheme 88 The regeneration of phenanthridine by iron catalysts.

with the change of substrates, chiral transfer catalysts must be re-screened. Thus, the further application of this method is limited by the kind of chiral transfer catalysts. To solve the above challenges, in the new generation of BMAR system, the chiral environment of the transfer catalyst is transferred to the NAD(P)H model. Therefore, only commercially available achiral transfer catalysts need to be screened, and the substrate range of BMAR should be further expanded (Scheme 89).

In 2019, Zhou's group [266] introduced the chirality of the ferrocene skeleton into the NAD(P)H model, and synthesized the new chiral regenerable NAD(P)H model FENAM, which was easy to regenerate under hydrogen gas using a ruthenium catalyst. The BMAR of nitrogen-containing aromatic heterocyclic compounds and tetra-substituted electron-deficient olefins could be achieved in excellent yields and diastereo- and enantioselectivities by using hydrogen as the terminal reducing agent, ruthenium complex as the regeneration catalyst, and simple Lewis acid ($Sm(OTf)_3$ or $Yb(OTf)_3$) as the transfer catalyst (Scheme 90).

Subsequently, Zhou's group [267,268] changed the transfer catalyst from Lewis acid to simple Brønsted acid, which achieved the asymmetric reduction of imines and nitrogen-containing heteroaromatics with excellent results. A series of chiral amines could be synthesized (Scheme 91).

Besides Lewis acid and Brønsted acid, the organic catalyst

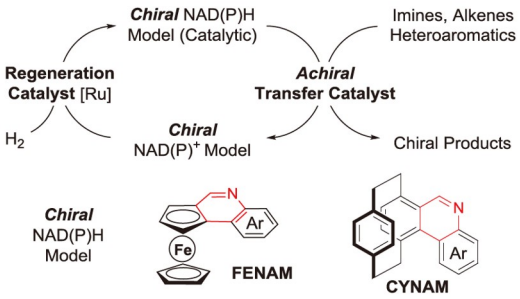

Scheme 89 BMAR catalyzed by chiral regenerable NAD(P)H models (color online).

urea could be also used as the transfer catalyst. In 2020, Zhou's group [269] found that the organic catalyst urea could activate the substrate through hydrogen bonding interaction, and the BMAR of benzoxazinones and quinoxalineones was achieved with up to 98% ee (Scheme 92).

Considering that the ferrocene skeleton is unstable under strong acid or oxidation conditions, Zhou's group [270] introduced a more rigid and stable [2.2]paracyclophane skeleton into the NAD(P)H model, and synthesized the new chiral regenerable NAD(P)H model CYNAM. The catalytic efficiency and stability have been improved to a certain extent compared with FENAM. Using ruthenium as the regeneration catalyst and simple Brønsted acid as the transfer catalyst, the BMAR of imines and nitrogen-containing heteroaromatics was realized with high activities and enantioselectivities (Scheme 93).

Similarly, using ruthenium as a regeneration catalyst and simple Brønsted acid or Lewis acid as the transfer catalyst, the BMAR of electron-deficient tetra-substituted olefins could be successfully completed. The *in-situ* alkylation with allyl group delivered highly enantioenriched stable products with two continuous stereocenters and one quaternary carbon center (up to 99% yield, 99% ee, >20:1 dr). Pleasingly, the chiral bioactive podophyllotoxin analogue could be concisely synthesized for the first time using the hydrogenated product as the key intermediate. Furthermore, Zhou's group [271–273] also found that the BMAR of 3-sulfonylcoumarin substrates could be directly realized, without transfer catalyst by regulating the reaction temperature. A broad range of highly diastereo- and enantiomerically enriched 3-sulfonyl dihydrocoumarins could be conveniently prepared with up to 99% yield, >20:1 dr and 99% ee (Scheme 94).

5.4 Summary and perspectives of NAD(P)H-based biomimetic asymmetric catalysis

The biomimetic asymmetric reduction (BMAR) catalyzed by NAD(P)H has made some progress, from the early stoichiometric simulation to the current regenerable simulation, which showed excellent hydrogen transfer ability and high stereoselectivity in asymmetric reduction of carbon-carbon

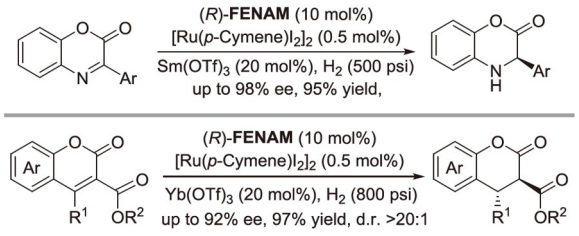

Scheme 90 BMAR catalyzed by FENAM and Lewis acid.

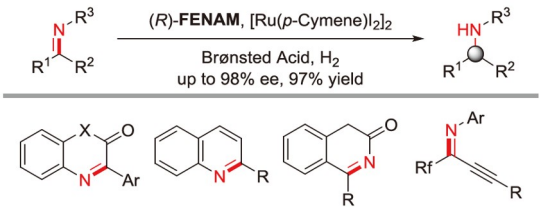

Scheme 91 BMAR of C=N catalyzed by FENAM and Brønsted acid (color online).

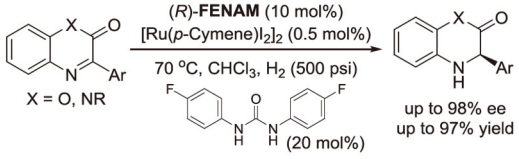

Scheme 92 BMAR of C=N catalyzed by FENAM and organic catalyst urea.

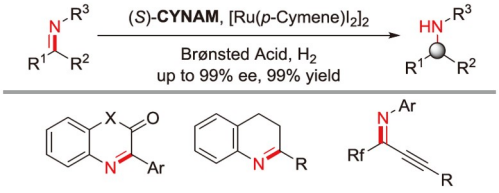

Scheme 93 BMAR of C=N catalyzed by CYNAM and Brønsted acid (color online).

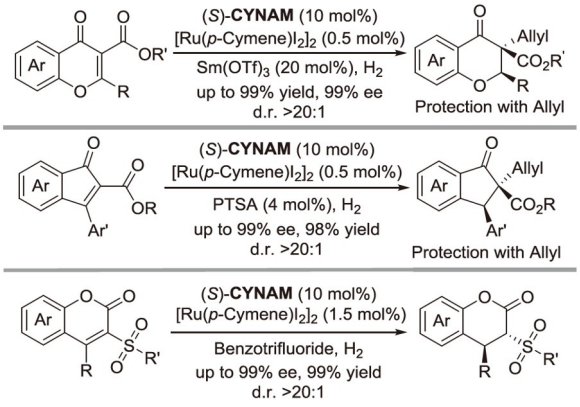

Scheme 94 BMAR of tetra-substituted olefins catalyzed by CYNAM.

double bond, carbon-nitrogen double bond and carbon-oxygen double bond. However, the research field is still in the early stage of development. At this stage, a prominent problem is that the efficiency of this biomimetic catalytic system is not high, and the amount of biomimetic catalyst usually needs to be 10 mol%–20 mol%. Thus, the more efficient NAD(P)H chiral biomimetic catalytic systems need to be developed. In addition, owing to the couple of NAD(P)H and $NAD(P)^+$, the stereoselective dehydrogenative oxidation based on coenzyme NAD(P)H should be explored in the future. With the further development of this field, BMAR based on coenzyme NAD(P)H will become a new method for synthesis of the chiral molecules.

6 Flavin-based biomimetic asymmetric oxidation

The discovery of simple and efficient catalyst systems for asymmetric oxidations of organic substrates is a challenging task of catalytic chemistry [274]. Simulation of the functions of enzymes such as flavoenzymes cytochrome P-450 using simple organocatalysts and transition metal catalysts have led to the discovery of biomimetic catalytic oxidation reactions [275–277]. In particular, flavin-catalyzed oxidation is one of the attractive approaches for designing environmentally benign catalytic oxidation reactions with organocatalysts [23,275]. There are three important flavins with unique functions in nature, which are riboflavin, flavin mononucleotide (FMN), and flavin adenine dinucleotide (FAD) [278–284]. Flavin-containing enzymes have three major functions: monooxygenase family, as a member of oxidase family, and as a member of the electron-transferase family (Figure 15). In this regard, flavin-dependent monooxygenases are biological agents responsible for the oxidation of substrates by activation of molecular oxygen to transfer oxygen atoms to the substrates [285], while oxidases are dehydrogenating agents. Given emerging focus on biomimetic catalysis, this review summarizes advances of biomimetic flavin catalysts in asymmetric oxidation [278].

The catalytic cycle of the FAD-containing monooxygenase (FADMO) has been well elucidated using its simple analogue 5-ethyl-3-methyllumiflavin as shown in Scheme 95. FlEtH (**A**) reacts with molecule oxygen to generate hydroperoxyl species FlEtOOH (**B**) [286]. Subsequent oxygen transfer from **B** to substrate S provides oxidized product SO with the concurrent formation of hydroxyl species FlEtOH **C** [287]. Acid promoted dehydroxylation of **C** gives the oxidized flavin $FlEt^+$ (**D**). Reduction of **D** by hydrogen donor NAD(P)H could regenerate FlEtH (**A**) for the next catalytic cycle. Alternatively, the highly electrophilic FIEt+ (**D**) could be also attacked by H_2O_2 from active species FlEtOOH (**B**) which was isolated for the first time by Bruice and coworkers [288] in 1976. It should be noted that oxidation ability of FlEtOOH is very powerful and 104 times stronger than H_2O_2 [289]. Interestingly, FlEtOH could be readily transformed

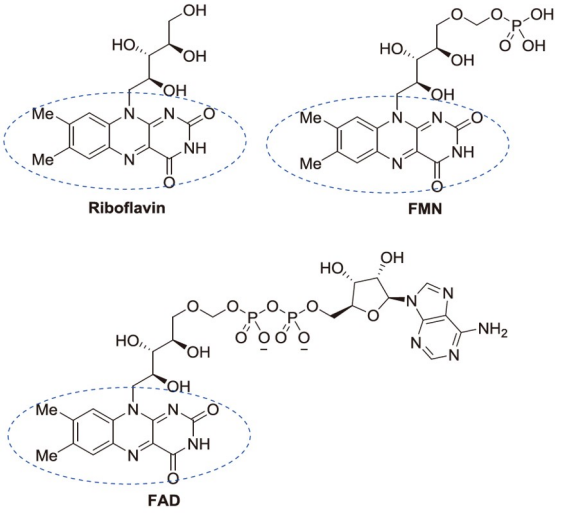

Figure 15 Flavin-cofactors (color online).

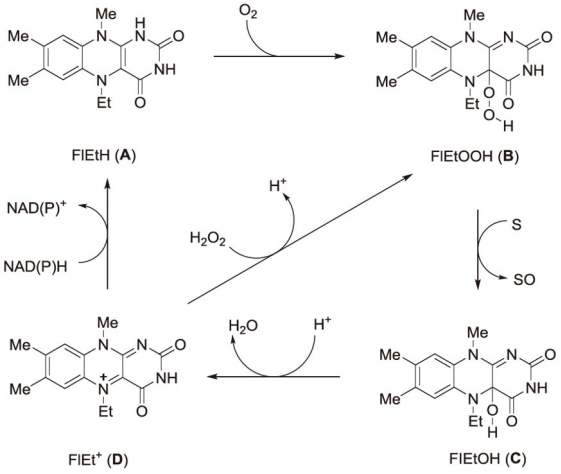

Scheme 95 Catalytic cycle for simple analogue 5-ethyl-3-methyllumiflavin.

into FlEtOOH upon treatment with H_2O_2. Thus, the oxidation of a substrate with H_2O_2 in the presence of catalytic amount of FlEtOH should also occur. From the viewpoint of practicality, the catalytic cycle **D-B-C-D** is more practical by avoiding the involvement of NAD(P)H. On the other hand, the robustness of $FlEt^+$ (**D**) makes flavinium salts benchstable organocatalysts.

It has been reported that the interaction of a substrate with a particular flavoprotein involved the interaction with the *Si*- and *Re*-face of the flavin. The reason is to fix the chiral reaction site by hydrogen bonding and π-π stacking interaction. Thus, asymmetric catalytic oxidations could be performed using a proper chiral flavin organocatalyst. In this aspect, two important classes of asymmetric oxidations, sulfoxidations and Baeyer-Villiger oxidations, were systematically studied. A variety of flavin-based chiral organocatalysts were synthesized and the representative examples are listed in Figure 16.

6.1 Asymmetric oxidation of thioethers

Chiral sulfoxides are of great importance in both synthetic and medicinal chemistry. In this vein, Esomeprasol [(*S*)-omeprazil, NEXIUM®] [290], psychostimulant armodafinil [(*R*)-modafinil, NUVGILTM] [291], (*R*)-lanoprazole, and (*R*)-sulindac are examples of enantiomerically pure sulfoxides used as pharmaceutical substrates. Although numerous asymmetric methods have been developed for construction of these flameworks [292], the use of flavin-based organocatalysts is able to provide environmentally benign and attractive alternatives.

The enantioselective sulfoxidation could be traced back to 1988 when Shinakai and coworkers [293] reported a planar chirality featured *N*(5)-ethylated flavinophane (+)-**304** as an asymmetric autorecycling catalyst for mono-oxygenation of methyl aryl sulfides in the presence of an excessive amount of 35% aqueous H_2O_2 (Scheme 96). The corresponding chiral sulfoxides were obtained with up to 65% ee value in CH_3OH/H_2O. They found that both the chemical and optical yield increased with increasing water concentration in the solvent. These asymmetric sulfoxidations are highly useful examples catalyzed by a non-acid and non-base organocatalyst albeit with only moderate enantioselectivities. A plausible reaction mechanism was proposed as elucidated in Scheme 96. Electrophilic flavinophane **(+)-304** is attached by H_2O_2 to form the hydroperoxy species **304-OOH.** Delivery of oxygen from **304-OOH** to sulfide furnishes sulfoxide with the concurrent formation of hydroxy species **304-OH**. Dehydroxylation of **304-OH** regenerates (+)-**304** for the next catalytic cycle.

Cibulka and coworkers [294] developed a novel planar chiral flavinium salt **(−)-305**, which bears a phenyl cap that covers one side of the isoalloxainium skeleton plane (Scheme 97). The racemic form of **305** showed high turnover number with 870 for oxidation of thioanisole using 30% aqueous H_2O_2. Up to 54% enantioselectivity was observed when the reaction was carried out with enantiomer of **(−)-305**. The covalently bonded phenyl "cap" in **(−)-305** covers one side of the isoalloxainium skeleton, allowing the access of H_2O_2 and the substrate only from the uncovered face of the flavin moiety [295]. Comparison of the enantioselectivity of the oxidation of thioanisole and cyclohexyl methyl sulfide showed that π-π stacking between **305-OOH** and substrate is crucial to achieve high chiral induction.

In 2012, Yashima and coworkers [296] introduced a main-chain optically active riboflavin polymer for asymmetric catalysis. Polymer **306** was prepared from naturally occurring riboflavin (vitamin B_2) with supermolecularly twisted helical structure. Asymmetric sulfoxidation of sulfides using H_2O_2 yielded sulfoxides with up to 60% ee, whose enantioselectivity is higher than that delivered by the mono-

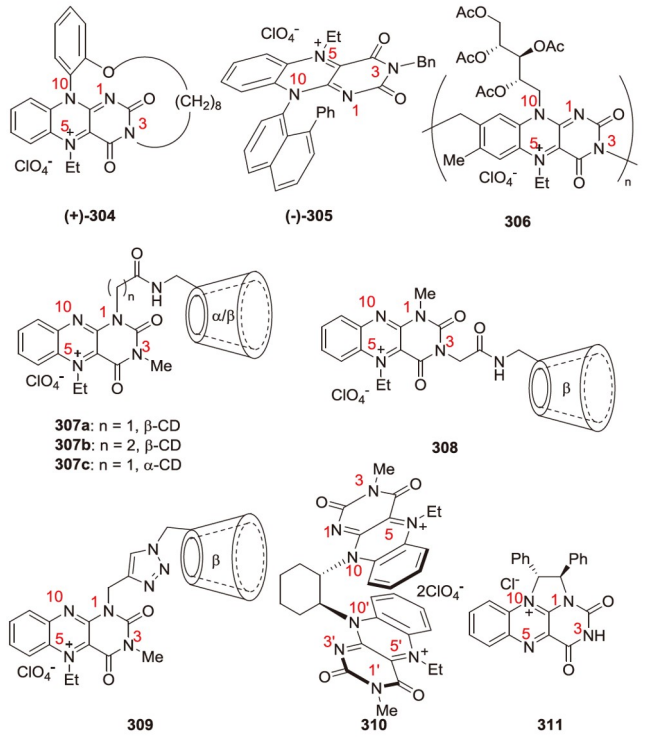

Figure 16 Representative chiral flavin-based organocatalysts for asymmetric oxidations (color online).

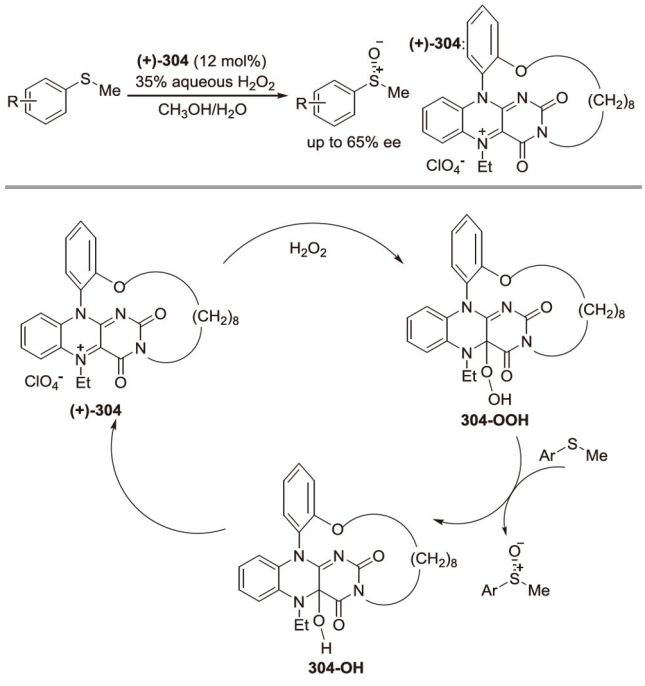

Scheme 96 Flavinophane **304**-catalyzed enantioselective sulfoxidations.

meric catalyst (30% ee). This result revealed that the supermolecular chirality induced in the riobofalvin-containing polymers seemed to play a significant role in the enantio-determining step. To further understand the origin of the enantioselectivity, they proposed a transition state model

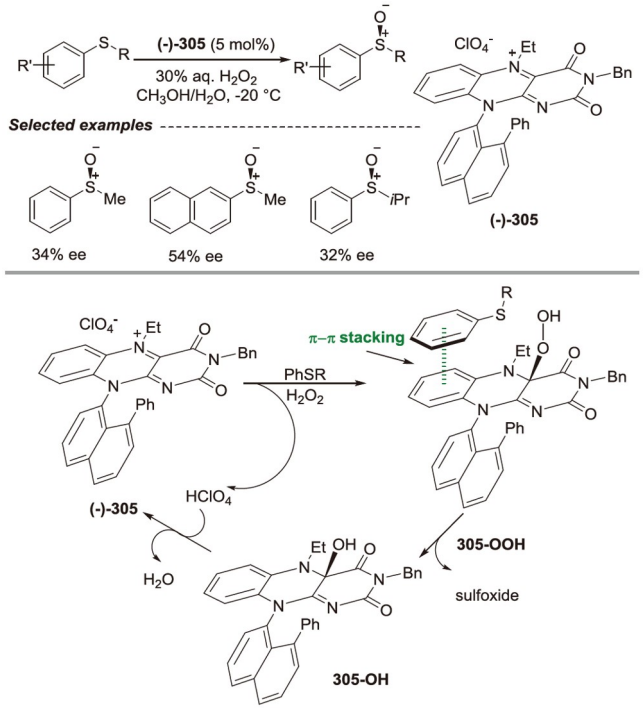

Scheme 97 Flavin **(–)-305**-catalyzed enantioselective sulfoxidations (color online).

as shown in Scheme 98. They assumed that polymer **306** may predominantly form a *Re-Re* stacked duplex, to which the nucleophilic addition of H_2O_2 occurs from the opposite site of *Si* face, generating the hydroperoxy adduct. The sulfide approaches the hydroperoxy species in such a way that the phenyl ring of the substrate preferentially interacts with the aromatic group of the poly *via* hydrophobic π-stacking to provide (*S*)-sulfoxide.

The stereodiscrimination in above sulfoxidations is predominantly controlled by weak π-π interaction between the flavin hydroperoxide and the aromatic ring of sulfide. It could be expected that catalytic performance could be further improved by an approach inspired by enzyme-like catalysis which takes advantage of a chiral substrate-binding site to control the stereoselectivity. To this end, Cibulka, Kraus, and coworkers [297] designed flavin-cyclodetrin conjugates as enzyme mimics capable of significant improvement of reaction rate in neat aqueous media as well as providing a chiral environment by cyclodextrin cavities. They found that *N*(1)-β-cyclodextrin-flavin conjugate **307a** with a linkage of an amide bond could oxidize aryl methyl sulfide in aqueousmedia in high efficiency (0.2 mol% catalyst loading) using hydrogen peroxide as the oxidant. This reaction tolerated a broad spectrum of substrate scope and corresponding sulfoxides were obtained with up to 80% ee value (Scheme 99). As a comparison, the use of a mixture of β-cyclodextrin and 5-ethyl-1,3-dimethylalloxazinium salt in lieu of conjugate **307a** under otherwise identical reaction conditions showed lower efficiency and provided no de-

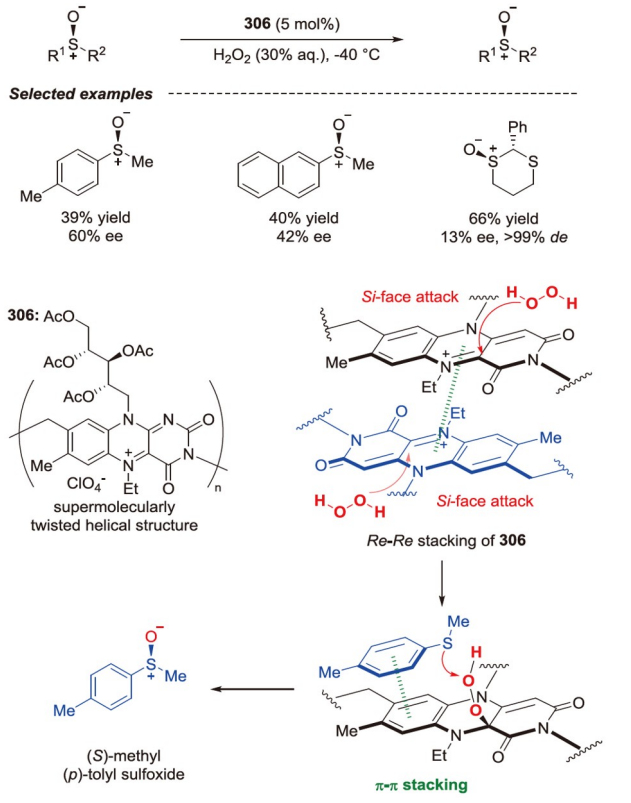

Scheme 98 Polymer **306**-catalyzed enantioselective sulfoxidations (color online).

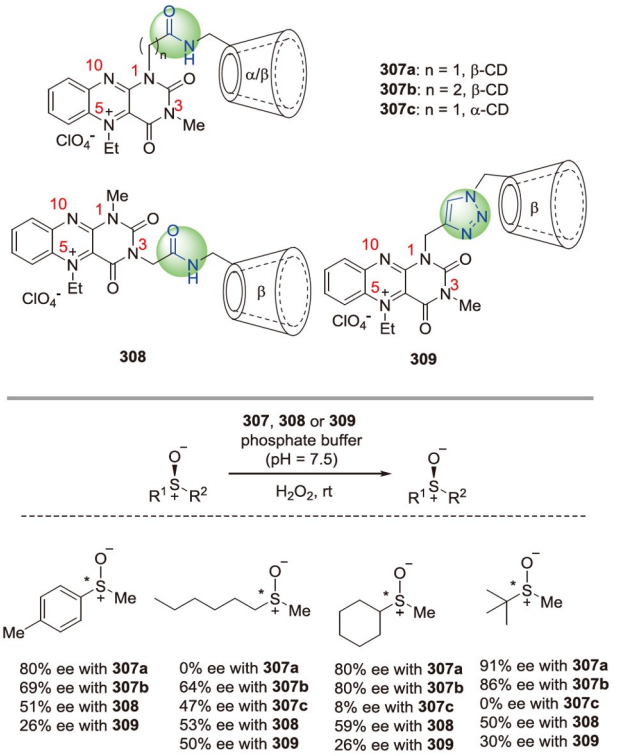

Scheme 99 Flavin-cyclodextrin conjugates-catalyzed enantioselective sulfoxidations (color online).

tectable enantioselectivities, indicating that covalent linking of flavin and β-cyclodextrin components is essential [297]. The use of amide-linked *N*(1)-β-cyclodextrin-flavin conjugate **307b** and *N*(3)-β-cyclodextrin-flavin conjugate **308** in oxidation of *p*-tolyl methyl sulfide provided sulfoxide with inferior enantioselectivity (Scheme 99) [298,299]. Interestingly, *N*(1)-β-cyclodextrin-flavin conjugates **307a** and **307b** showed excellent chiral induction (80%–91% ee) in sulfoxidation of hindered dialkyl sulfides such as cyclohexyl methyl sulfide and *tert*-butyl methyl sulfide (Scheme 99) [298]. In particular, 91% ee was achieved for the oxidation of *tert*-butyl methyl sulfide, which represented the highest value at that time for this substrate using synthetic (non-enzymatic) catalysts. Recently, they developed cyclodextrin-flavin conjugates by click chemistry to further extend scope of flavin-based organocatalysts as represented by *N*(1)-β-cyclodextrin-flavin conjugate **309** [300]. Unfortunately, only low ee values were observed for sulfoxidations of various of sulfides (Scheme 99).

6.2 Asymmetric Baeyer-Villiger oxidation

Asymmetric Baeyer-Villiger (B-V) oxidation of prochiral cyclic ketones is one of the most straightforward manners to access optically active lactones. Due to the moisture- and air-sensitivity, transition metal catalysis in this field encounters problematic issues including incompatibility of aqueous H_2O_2 or requirement of stoichiometric additives. Therefore, the development of highly efficient methods with environmentally benign oxidants is a goal in this area [301,302].

Murahashi, Imada and coworkers [303] elegantly developed a novel planar-chiral bisflavinium percholorate **310** with a backbone of (*S*,*S*)-1,2-diaminocyclohexane. With aqueous H_2O_2 as the oxidant, **310** could efficiently catalyze B-V rearrangement of 3-arylcyclobutanones in an enantioselective manner. The corresponding γ-lactones were obtained with 61%–74% ee values (Scheme 100). This method requires low temperature and long reaction time (6 days), which has lower efficiency in terms of both reactivity and enantioselectivity than chiral phosphoric acid catalyzed systems [304,305]. They proposed a plausible catalytic cycle as shown in Scheme 100. The enantioselectivity is induced by face selectivity in the formation of Criegee adduct. Since one face of the catalyst is completely blocked, the substrate would be attached by the opposite site of the other flavin group. The asymmetric induction is likely induced by hydrophobic π-π stacking between the phenyl ring of the substrate and that of the catalyst to fix the direction of the substrate. Nucleophilic attack of the hydroperoxylflavin at the carbonyl carbon of the substrate takes place from the opposite side of the phenyl group of the substrate. Thus, a subsequent 1,2-rearrangement occurs antiperiplanar to the

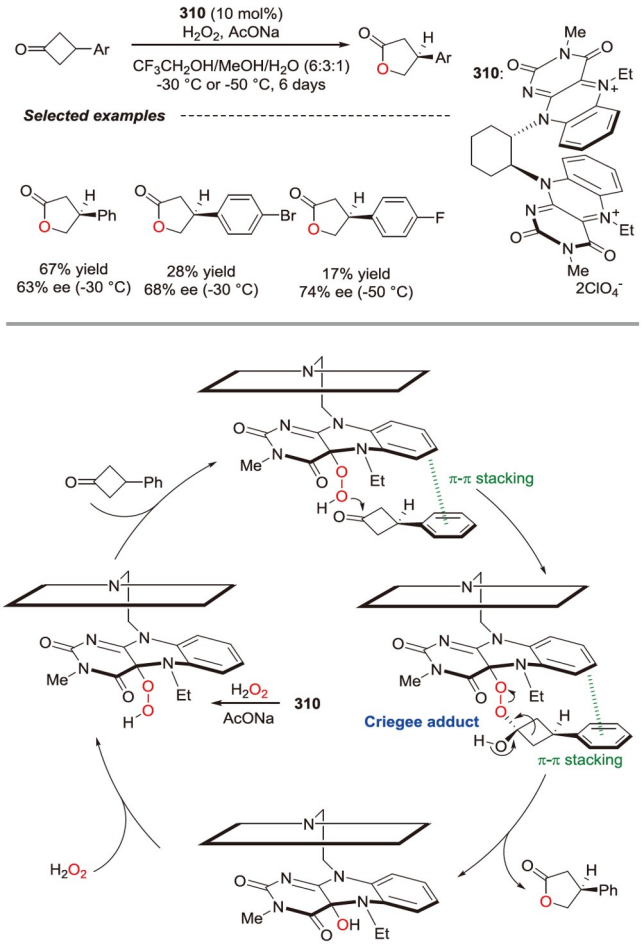

Scheme 100 Bisflavinium **310**-catalyzed enantioselective B-V reaction of 3-substituted cyclobutanones (color online).

leaving group to give the desired (*S*)-γ-lactone.

The difficulty in attaining chiral induction using flavin-based organocatalysts stems from their conformational changes [306–308]. They cycle between a "bent (hydroperoxide)" form and a "planar (flavinium)" form during the redox cycle. The catalyst designed by Murahashi and coworkers [307] is to block one face of the flavin with a covalently bound chiral cap. The substrate therefore approaches and reacts on the opposite site of the chiral cap, leading to low efficiency of chirality transfer. To this end, Yamamoto and coworkers [309] developed a self-assembled ion-pair organocatalysis for asymmetric B-V oxidation of 3-substituted cyclobutanones using 30% aqueous H_2O_2 as the oxidant. The combination of (*R*,*R*)-1,2-diphenylethylenediamine-based flavinium chloride **311** with dihydroquinine dimer $(DHQ)_2PHAL$ is responsible for enhancing catalytic efficiency and stereoselectivity.

The protocol is applicable to structurally diverse 3-substituted cyclobutanones, delivering good to excellent enantioselectivities. To explain the importance of ion-pair formation in chiral induction, they proposed a plausible mode of the transition state for enantio-determining step, as illustrated in Scheme 101. Flavinium binds to either side of the $(DHQ)_2PHAL$ with a selective orientation set by π-π stacking and ionic interaction. Subsequently, H_2O_2 attacks iminium moiety of **311** to form hydroperoxyl species. The hydroperoxyl group then attacks the less hindered side of the carbonyl carbon of 3-phenylcyclobutanone to form a Creigee intermediate that undergoes H-bonding facilitated 1,2-rearrangement.

6.3 Asymmetric oxidative esterification, thioesterification, and amidation

The cooperative catalysis involving flavin could provide new platforms for asymmetric oxidation. Oxidative chiral *N*-heterocyclic carbene (NHC) catalysis open a new avenue in NHC chemistry [310]. However, the requirement of hazardous oxidants as well as stoichiometric waste is the main hurdle. To this end, Yashima, Iida, and coworkers [311] employed redox-active riboflavin by uptake of molecule oxygen as the terminal green oxidant, realizing cooperative oxidative NHC-catalyzed esterification, *via* kinetic resolution, giving unreacted alcohols with moderate to excellent ee values (Scheme 102). In addition, the present method could also be applied to the oxidative thioesterification of thiols and amidation of amines, although the selectivity for the enantioselective processes (as well as the efficiency) is still modest or low at this stage. A proposed mechanism is elucidated in Scheme 102. Reaction of thiazolium-based chiral NHC **312** with aldehyde forms Breslow intermediate **E**. Immediate oxidation of **E** by flavin catalyst **313** provides chiral acylation reagent **F** along with the formation of reduced flavin $\mathbf{313}_{red}$ which could regenerate **313** through the

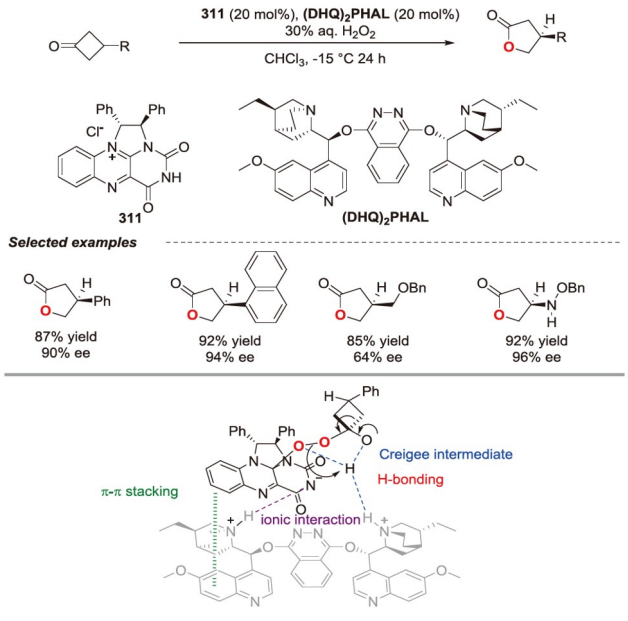

Scheme 101 Flavin **311**/$(DHQ)_2PHAL$-catalyzed enantioselective B-V reaction of 3-substituted cyclobutanones (color online).

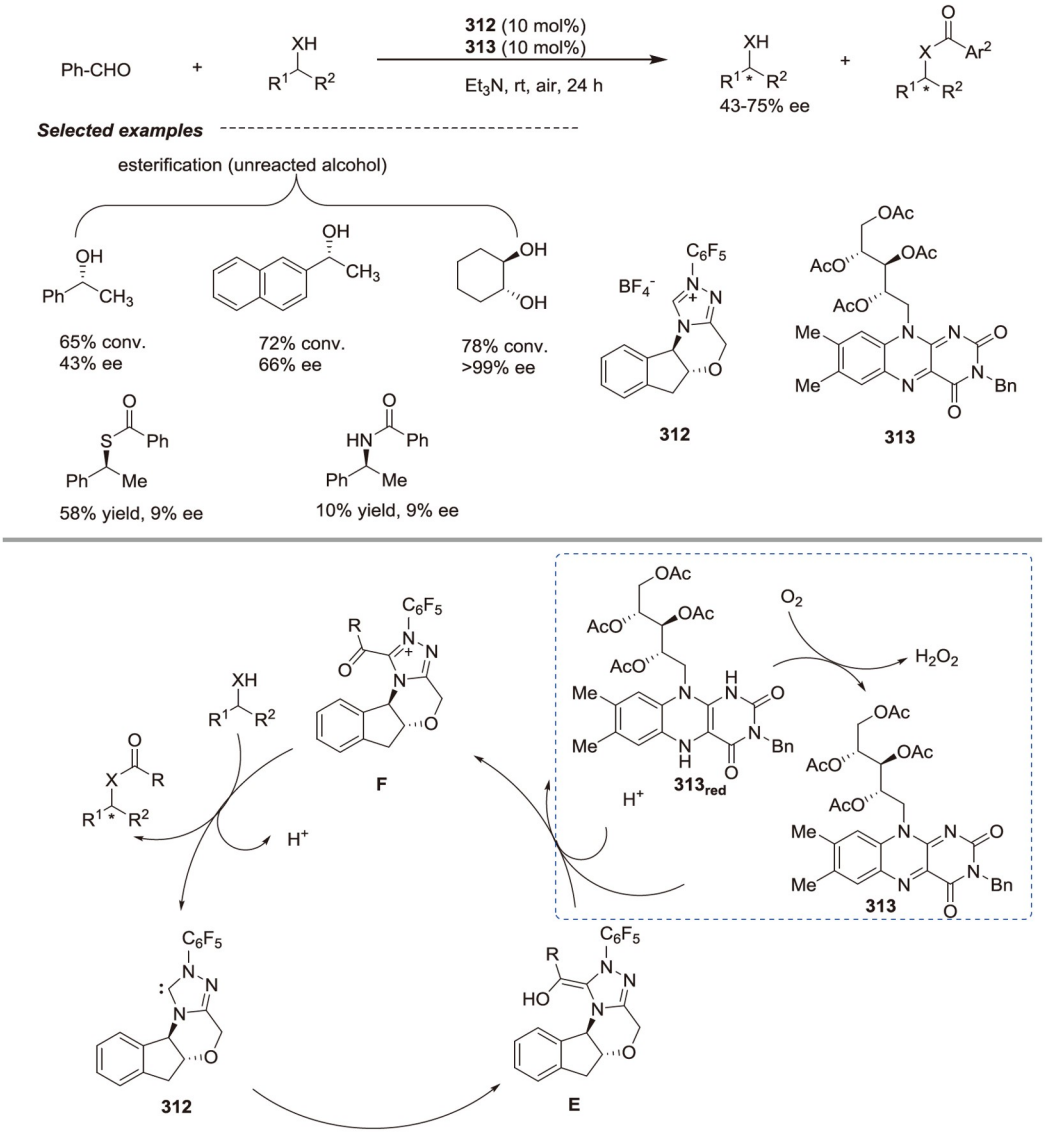

Scheme 102 Oxidative esterification, thioesterification, and amidation enabled by chiral NHC **312**/riboflavin **313** synergistic catalysis (color online).

electron transfer process from molecular oxygen for the next redox cycle. Nucleophilic replacement of thiazolium in **F** by secondary alcohols, thioalcohols, and amines provides optically active esters, thioesters, and amides and unreacted nucleophiles.

6.4 Summary and perspectives of flavin-based biomimetic asymmetric oxidation

Flavin-based biomimetic organocatalysts have been successfully used in asymmetric sulfide oxidation, Baeyer-Villager oxidation, and oxidative esterification/thioesterification/amidation using environmentally benign oxidants hydrogen peroxide and molecule oxygen under mild conditions. However, the reaction types and substrate scopes are still very narrow, and chiral induction is in a moderate level. Thus, this field is still on the horizon, which is mainly due to the lack of flavins with competent privileged scaffolds that could provide proper chiral pockets and suitable secondary interaction with substrates. The development of novel chiral flavin catalysts will certainly open a new avenue in this area. We also believe that flavin-involved synergistic catalysis will lead to the development of further unique and more efficient tandem reactions promoted by multi-catalyst systems as observed in the cell [312,313].

7 Hydrogenase-based biomimetic asymmetric catalysis

Hydrogenases are highly efficient redox enzymes for H_2. On the one hand, hydrogenases can efficiently catalyze the reduction of protons to hydrogen to achieve a pollution-free hydrogen evolution. On the other hand, they can also cata-

lyze the reversible cleavage of hydrogen and promote the reduction of a variety of unsaturated bonds [314].

Hydrogenases consist of two parts: the protein shell as reaction pocket and the coenzyme as the active site. Accordng to the central metals of the active sites, hydrogenases can be classified into three categories: [Fe]-hydrogenases, [FeFe]-hydrogenases, and [NiFe]-hydrogenases. The active centers of the latter two types of enzymes are binuclear organometallic complexes [315]. The protein structures of all these three types of enzymes contain gas channels that facilitate the diffusion of hydrogen into the active sites. In addition, the structures of hydrogenases generally contain ionized amino acid residues that promote proton transfer and iron-sulfur clusters that promote single electron transfer. Both of them play key roles in the heterolytic cleavage of hydrogen.

Biomimetic chemistry of hydrogenases has been a frontier topic. The researchers expect to utilize hydrogen under mild conditions like nature. Meanwhile, since hydrogen is a very clean energy source, the researchers also try to develop efficient biomimetic hydrogen evolution catalysts under electrocatalytic or photocatalytic conditions by mimicking hydrogenase, so as to alleviate the increasingly tight energy problem [316].

Some progress has been made in field of biomimetic catalysis for all of the three hydrogenases, especially of [FeFe]-hydrogenase (Figure 17). Researchers designed and synthesized a series of chiral catalysts by combining core structure of hydrogenases with asymmetric catalysis, and realized numerous efficient asymmetric hydrogenation reactions [317].

7.1 Biomimetic hydrogenation catalysts based on [FeFe]-hydrogenases

Among the three hydrogenases, [FeFe]-hydrogenases catalyze hydrogen evolution from protons with the highest catalytic efficiency [318]. The [FeFe]-hydrogenases isolated from Desulfovibrio desulfurican and Clostridium pasteurianum can catalyze the reduction of protons to hydrogen at rate of 9,000 and 6,000 mol s^{-1}, respectively [319,320]. Moreover, the [FeFe]-hydrogenase can also catalyze the oxidation of hydrogen reversely.

The active site of [FeFe]-hydrogenase is a [2Fe2S] subcluster [321], in which the two Fe centers are bridged by a bis(thiol) anion ligand and a carbonyl group. The linking group of two S atoms can be N–H group, which plays an important role in assisting the Fe center to activate H_2. While the Fe center activating hydrogen gas through heterolysis cleavage, N–H group acts as an internal base to bind the

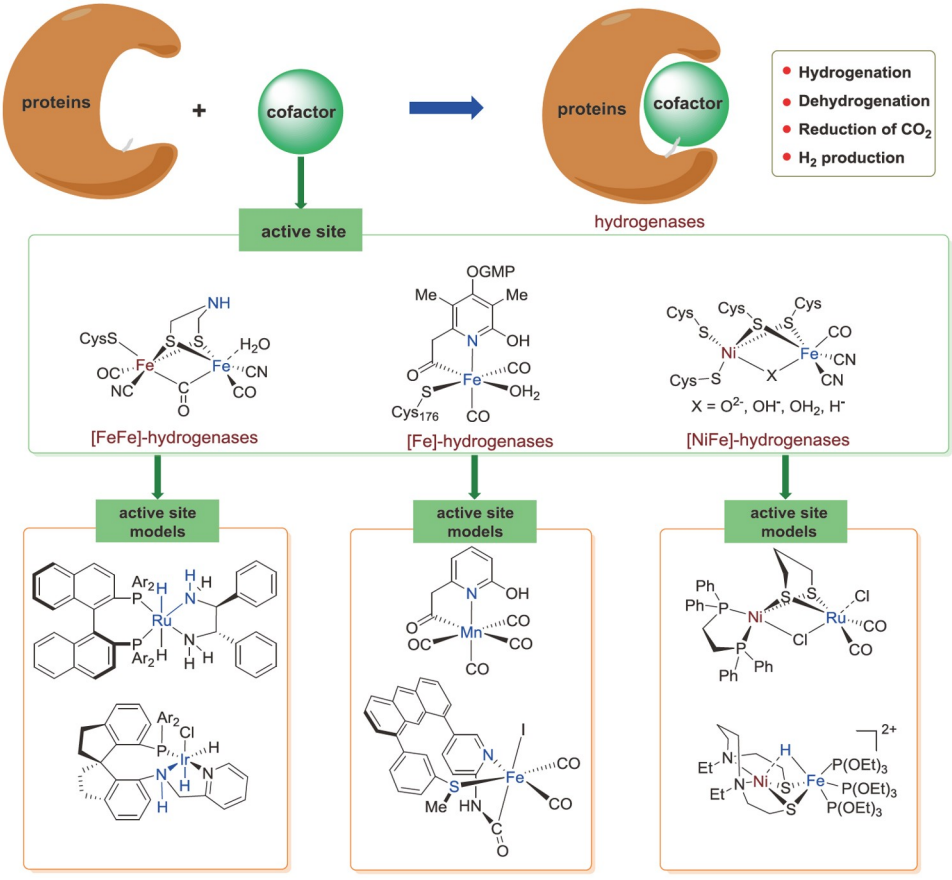

Figure 17 Structure of hydrogenases and representative biomimetic catalysts (color online).

proton. In addition, [FeFe]-hydrogenase has a [4Fe4S] cluster attached to the cysteine, which promotes the electron transfer during the hydrogen transfer (Scheme 103) [322].

Coincidentally, the mode of N–H ligand assisted hydrogen activation in [FeFe]-hydrogenase has long been demonstrated in a series of efficient and highly selective artificial hydrogenation catalysts. The metal centers of these artificial catalysts are generally coordinated to more than three heteroatoms (N, P, O, S, *etc*.), and these coordination sites contain more than one N–H group (Scheme 104a). At the beginning of the catalytic cycle, the proton on the N–H group and the anionic ligand (*e.g*., –Cl) on the metal center of the catalyst precursor are removed by base, and then the nitrogen obtains the proton after H_2 heterolytic cleavage, while forming the active M–H species. Mechanistic studies reveal that alcohols can assist this process to complete the activation of hydrogen through a six-membered ring transition state, which is more favorable than the direct activation of hydrogen through a four-membered ring transition state (Scheme 104b) [323].

The hydride on the metal and the proton on the nitrogen in the active catalyst can be matched electrically with a polar double bond and achieve the transfer of hydrogen from the catalyst to the substrate through a transition state of a six-membered ring. Computational and experimental results indicate that alkali metal ions can also assist this process instead of protons (Scheme 104c) [324]. Besides, compared with the real hydrogenases, these artificial catalysts can be easily synthesized and modified due to their simpler structure. Therefore, it's feasible to introduce chiral structures into the ligands to achieve stereoselective control in the hydrogen transfer process so as to achieve asymmetric hydrogenation (Scheme 104d). In recent years, asymmetric hydrogenation and transfer hydrogenation based on this mode have been rapidly developed, and a large number of catalysts have been designed and synthesized to be successfully used for the asymmetric reduction of polar double bonds (typically, C=O and C=N).

As early as 1986 (Scheme 105), Shov *et al*. [325] disclosed that cyclopentadienone anion Ru complex **314** reversibly catalyzed the reduction of cyclohexanone in the presence of H_2. The mechanism of this hydrogenation reaction involves the critical process of synergitic hydride transfer from the metal and proton transfer from the oxygen to polar double bonds [326]. In 2007, Casey and Guan [327a] found that the cyclopentadienone anion coordinated iron complex **315**, known as Knölker complex, could hydrogenate aromatic aldehydes, aryl alkyl ketones, arylalkyl imines, and C=C of α,β-unsaturated ketone at a hydrogen pressure of 3 atm. Subsequently, Wills and Gennari [327b–e] made some chiral modifications for Knölker complex but failed to achieve good enantioselectivity in hydrogenation of ketones. In 2011, Beller *et al*. [328] used chiral phosphoric acid and Knölker complexes together to achieve highly enantioselective asymmetric hydrogenation of imines with up to 98% ee.

In 1995, Noyori's group [329] developed the chiral ruthenium-bisphosphine/diamine complex **316** [$RuCl_2$(BINAP)(diamine)]. In the asymmetric hydrogenation of acetophenone catalyzed by **316**, turnover number (TON) could be more than one million. This catalyst and its ana-

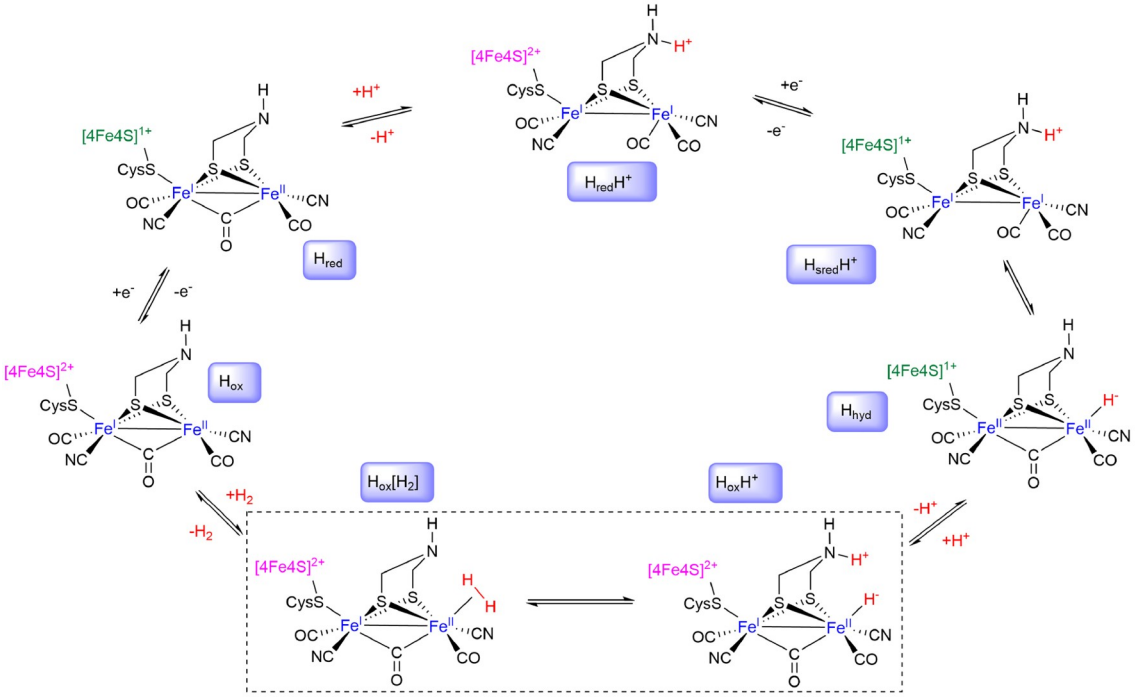

Scheme 103 Mechanism for hydrogen activation catalyzed by [FeFe]-hydrogenase (color online).

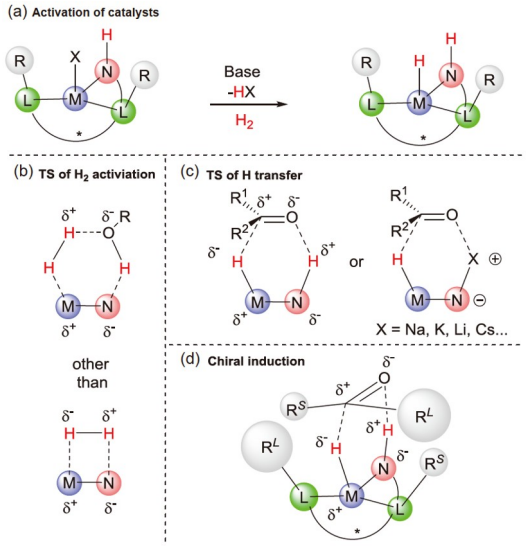

Scheme 104 Mechanism of asymmetric hydrogenation for artificial catalysts (color online).

logues are also highly efficient catalysts for the hydrogenation of various ketones with up to 99% ee. In the same year, the group reported the chiral ruthenium-diamine complex **317** [Ru-TsDPEN], which effectively catalyzed the asymmetric transfer hydrogenation of aryl alkyl ketones with an enantioselectivity of up to 98% ee [330]. Wills *et al*. [331] and Ikariya *et al*. [332] modified the scaffold of this complex later by using linkers to connect the benzene ring with the chiral diamine to further increase the stability of the catalyst. The chiral ruthenium-diamine complex **318** developed by Ikariya achieved up to 30,000 TON and 99% ee in the asymmetric transfer hydrogenation of aryl alkyl ketones.

Zhang and coworkers [333] performed extensive and excellent work on asymmetric hydrogenation. In 1998, they developed the Ru-ambox complex **319** with a tridentate N ligand. This complex exhibited enantioselectivity (up to 98% ee) comparable to Noyori's Ru-TsDPEN catalyst in transfer hydrogenation, and catalyst **319** was more active when the reaction was carried out at higher temperature, while the enantioselectivity was maintained [333e].

In 2008, Baratta and coworkers [334] developed a chiral Os complex **320** modified by a non-chiral CNN tridentate ligand and a chiral bisphosphine ligand (Josiphos) to achieve asymmetric transfer hydrogenation of aryl alkyl ketones. The chiral Os catalyst exhibited very high activity with turnover frequency (TOF) up to 111 s^{-1} and with 97% ee as well. Direct asymmetric hydrogenation of aryl alkyl ketones also was achieved in methanol solvent and at 5 atm hydrogen pressure.

Zhou's group [335] did remarkable work in the field of asymmetric hydrogenation. Their chiral spiro PNN-type ligand modified Ir complex **321** developed in 2011 is a superhighly efficient catalyst for asymmetric hydrogenation. In the asymmetric hydrogenation of simple ketones, up to 99.9% ee and up to 4,550,000 TON (the enantioselectivity still remains 98% ee at this point) were achieved. It is indicated that this chiral catalyst is extremely stable and does not undergo decomposition during the entire reaction process [335a]. This spiro catalyst is the most efficient chiral molecular catalyst to date. In 2020, they developed a spiro PNP-type ligand modified Ir complex **322** with more crowded chiral pocket, which achieved the most challenging asymmetric hydrogenation of bis-alkyl ketones and gave more than 90% ee in most cases [335c].

Morris and coworkers [336] made in-depth studies in the field of iron-catalyzed asymmetric hydrogenation and transfer hydrogenation. In 2013, they developed a tetradentate bisphosphine/bisamine-iron complex **323**, which exhibited very high activity (TOF up to 200 s^{-1}) in transfer hydrogenation reactions of ketones and imines, and high enantioselectivity in the hydrogenation of aryl alkyl ketones and arylalkyl imines [336c].

In 2014, Gao and coworkers [337] developed a ligand **324a** with structure of 22-membered ring. Using this macrocycle ligand and Fe_3CO_{12} together could catalyze the asymmetric hydrogenation of aryl alkyl ketones. At a catalyst-loading of 0.5 mol%, more than 90% ee were achieved for most substrates. This catalyst could also hydrogenate the carbonyl groups of β-ketoester with up to 99% ee. In 2015, Mezzetti's group [338] reported a bisphosphine/bisamine-iron complex **324b** with a structure of 14-membered ring. The stability of the metal center was enhanced by the introduction of two isonitrile ligands. The complex showed good enantioselectivity and substrate scope in the transfer hydrogenation of arylalkyl ketones. For various types of arylalkyl ketones, more than 90% ee were achieved.

In 2014, Morris and coworkers [336d] prepared a chiral PNP-Fe complex **325**. At 0.1 mol% catalyst-loading and low hydrogen pressure, the asymmetric hydrogenation of acetophenone catalyzed by **325** was accomplished with 80% ee. In 2017, Beller and coworkers [339] developed a chiral PNP-Mn complex **326**, which afforded up to 84% ee in the hydrogenation of arylalkyl ketones and bis-alkyl ketones. Notably, the analogous PNP-Ru complex can also be used in CO_2 reduction and fixation [340].

A number of tridentate ligands based on the ferrocene scaffold were successfully applied in the asymmetric hydrogenation reactions [341,333f–g]. Zhang's group [333f] designed a ferrocene based PNN tridentate ligand **327** containing a chiral oxazoline moiety, and used it in a highly efficient Ir-catalyzed hydrogenation with up to 1,000,000 TON and high enantioselectivities. Clarke and coworkers [341c] reported a PNN tridentate ligand modified manganese complex **328**, which was used as a catalyst in the asymmetric hydrogenation of aryl alkyl ketones with up to 97% ee.

Ding's group [342] also made very important contributions

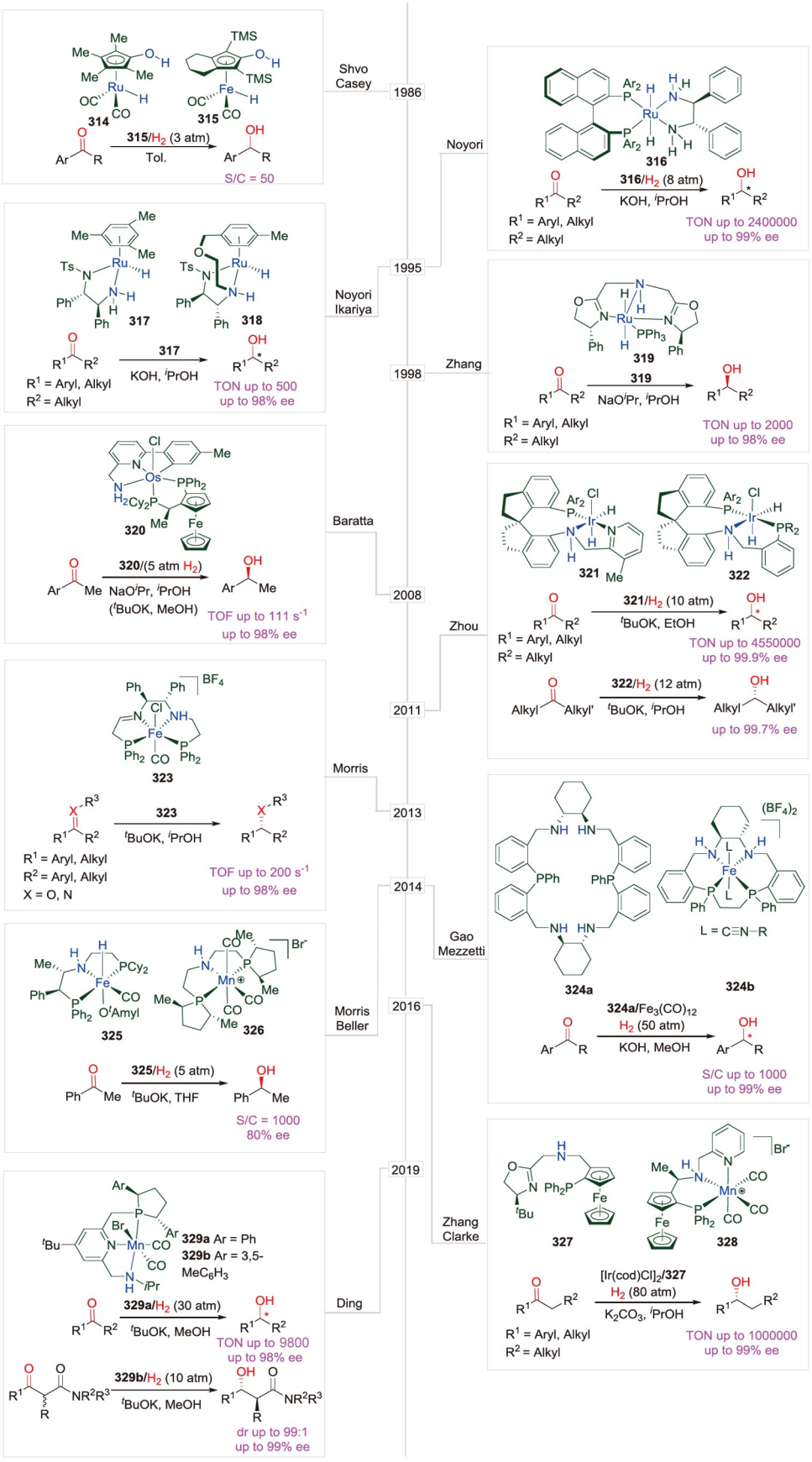

Scheme 105 Development of biomimetic asymmetric hydrogenation catalyst based on [FeFe]-hydrogenase (color online).

in this field. This group developed a chiral PNN-Mn complex **329a** based on the pyridine backbone [342d]. In the asymmetric hydrogenation of ketones, **329a** exhibited good catalytic activity, up to 9,800 TON, and 85%–98% ee. Soon later, they also found that an analogous chiral manganese complex **329b** could also achieve dynamic kinetic resolution [343] of β-carbonyl amides by asymmetric hydrogenation with up to 99:1 dr and up to 99% ee [342e].

7.2 Biomimetic hydrogenation catalysts based on [Fe]-hydrogenases

[Fe]-hydrogenase was first discovered in the hydrogenotrophic methanogenic archaea [344], which is not only a good catalyst for hydrogen production but also can catalyze hydrogen oxidation. In the presence of hydrogen, [Fe]-hydrogenase can reversibly catalyze the reduction of methenyl-H_4 MPT^+ to produce methene-H_4 MPT and proton, which is a key step in the microbial conversion of carbon dioxide to methane [345].

FeGP coenzyme is the active site of [Fe]-hydrogenase. The center of coenzyme has only one unsaturated five-coordinated Fe atom and there is no iron-sulfur cluster but a special "2-pyridinol methylene acyl" ligand [346]. For [Fe]-hydrogenase, besides the Fe's Lewis acidity can promote the heterolytic cleavage of the H–H bond, the sulfur atom on the cysteine or the hydroxyl on the pyridine ring can also play a proton-binding role in the process of hydrogen activation. DFT calculations revealed that during the cleavage of H_2, the transition state TS1 that O ligand assists to bind proton is more favorable than the transition state TS1′ that S ligand binds proton. Then more stable intermediate Fe-$H^{\delta-}$—$H^{\delta+}$-O is derived, followed by the transfer of hydride to MPT^+ (Scheme 106) [347]. Notably, this hydrogenase also requires the assistance of O or S ligands for hydrogen activation (TS1 & TS1′), which is similar to [FeFe]-hydrogenase, but its hydride transfer and proton transfer are not concerted, which is significantly different from [FeFe]-hydrogenase.

Since the X-ray crystal structure of [Fe]-hydrogenase was determined by Shima *et al*. [346] in 2008, a number of active-site models of [Fe]-hydrogenase have been synthesized. These analogs synthesized early showed only structural similarity but did not display the ability of activating the hydrogen [348]. In 2016 (Scheme 107), Hu's group [349] replaced the two COs on the iron center with a bisphosphine ligand to obtain complex **330**. At the presence of hydrogen, complex **330** was able to reduce aryl aldehydes stoichiometrically. Then the complex would decompose into 2-methoxy-6-methylpyridine and iron salt coordinated by CO and bisphosphine.

In 2017, Rose and coworkers [350] reported a [Fe]-hydrogenase based mimic **331a** containing anthracene scaffold. When I^- was exchanged by $[BAr_F]^-$, the complex can activate H_2 under mild conditions or grab hydrogen from the active C–H bond of imidazolidine to generate Fe-H species **331b**. Fe-H species can react with 2,6-di-*tert*-butyl-4-methoxyphenol to evolution hydrogen. A year later, the same group [351] developed a monoiron complex **332** by modifying the mimetic complex **331a**. At the present of D_2, complex **332** can catalyze the reduction of imidazoline that is a simulation of reducing methenyl-H_4 MPT^+ to methene-H_4 HMPT by [Fe]-hydrogenases.

In the field of [Fe]-hydrogenase-based biomimetic chemistry, another important breakthrough is the functional model complex **333** reported by Hu's group [352] in 2019. This complex, with manganese as the metal center, enables catalytic hydrogenation of C=C, C=N, and C=C. In addition, after reconstituting this manganese complex and apoenzyme, the "artificial hydrogenase" is also biologically active and can catalyze the reduction of methenyl-H_4 MPT^+ under H_2 reversibly [353]. In 2020, they synthesized analogous acyl-manganese complex **334**, whose ability of reducing polar double bonds was further enhanced. Combined with NAD(P)H analogue, this catalyst could also be used for the asymmetric reduction of C=N of benzoxazinones [354]. However, no example of [Fe]-hydrogenase-based mimics with H_2 to achieve asymmetric hydrogenation has been reported until now.

7.3 Biomimetic hydrogenation catalysts based on [NiFe]-hydrogenases

The active site of [NiFe]-hydrogenase is a Ni-Fe heterodinuclear structure with four cysteines coordinated to Ni through the S atom, two of which serve as the terminal groups and the others are also connected to Fe through the S atom. The Fe center is also surrounded by a CO and two CN^-s. In the oxidized state of [NiFe]-hydrogenase (Ni-A or Ni-B), there is also a bridging oxygen ligand (generally H_2O, OH^-, or O^{2-}) between Fe and Ni. After getting electrons and protons, the oxidative [NiFe]-hydrogenase will lose a H_2O and be reduced to Ni-SI state. Then the hydrogen goes through the heterolytic cleavage in the Ni center to get the Ni-R state. There is a H^- bridge attached to the Ni and Fe, while the proton is transferred to the sulfur atom of the cysteine. Ni-R state gives proton and electron to produce the Ni-C state, which further gives proton and electron back to the Ni-SI state [355]. Similar to the models of the other two hydrogenases, [NiFe]-hydrogenase also facilitates hydrogen cleavage by assisting the metal through the sulfhydryl group of cysteine. But it is different from the other two hydrogenases wherein the hydride is coordinated to both metals at the same time (Scheme 108).

There are relatively fewer studies on [NiFe]-hydrogenases mimics, and most of them developed have low hydrogen evolution efficiency, probably due to the complex structure

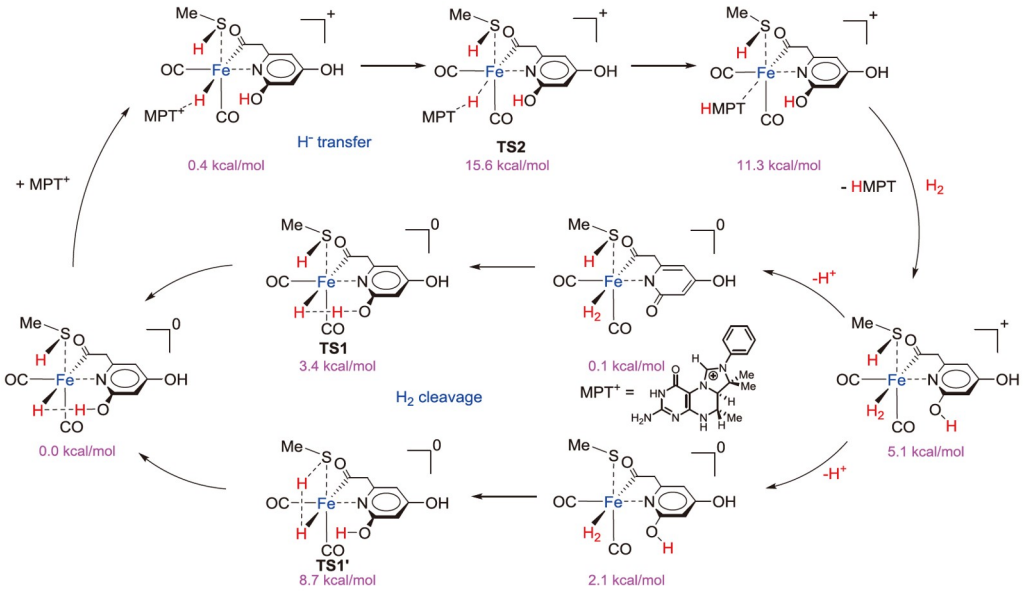

Scheme 106 Mechanism for hydrogen activation catalyzed by [Fe]-hydrogenase (color online).

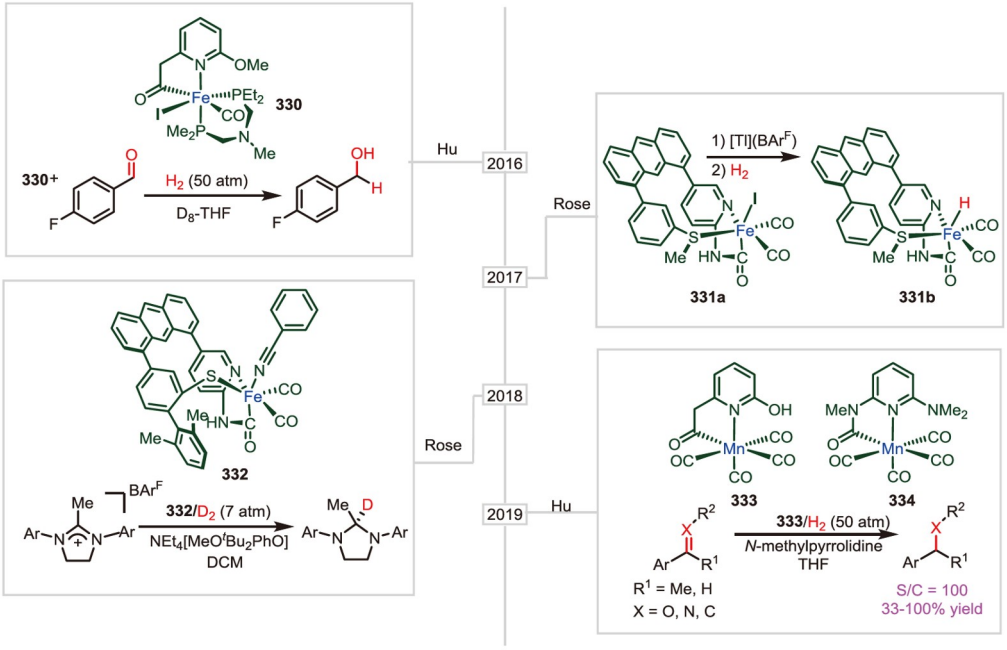

Scheme 107 Development of biomimetic catalyst based on [Fe]-hydrogenases (color online).

of the heterodinuclear metallic center [356]. At present, [NiFe]-hydrogenases-based biomimetic chemistry has made progress mainly in the field of developing efficient artificial hydrogen evolution catalysts, but examples of catalytic hydrogenation using [NiFe]-hydrogenases mimics have not been achieved yet.

In 2007 (Scheme 109), Ogo's group [357] reported that the Ni-Ru dinuclear metal complex **335** can activate hydrogen in the aqueous phase to give Ru-H species. In 2013, the same group reported that the Ni-Fe complex **336** could activate hydrogen under alkaline conditions to produce Fe-H species [358]. Under acidic conditions, Fe-H species can bind protons to produce hydrogen and regenerate **336**. Rauchfuss and coworkers synthesized [NiFe]-binuclear complexes **337a** [359] and borane-protected [NiFe] complexes **337b** [360], both of which could activate H_2 under mild conditions.

Based on the scaffold of bipyridine, Duboc *et al.* [361] synthesized [NiFe]-hydrogenase active-site models **338**, which could reduce protons to produce H_2 on a Hg-pool cathode. Foot-of-the-wave analysis disclosed a second-order

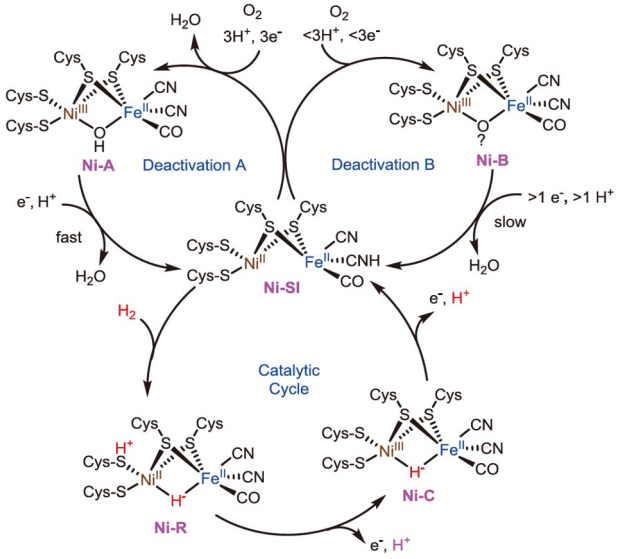

Scheme 108 Deactivation/reactivation mechanism for [NiFe]-hydrogenases (color online).

rate constant k_{cat}=2.5±0.3×10^4 M^{-1} s^{-1} and a TOF of 250 s^{-1}.

In recent years, the researchers developed numberous simple and stable photocatalysts for hydrogen evolution. Wu's group [362] made remarkable contribution in mimicking hydrogenases to achieve visible photocatalytic hydrogen evolution. They developed [NiFe]-hydrogenase-based mimetic catalyst of (dppe)Ni(μ-pdt)(μ-Cl)Ru(CO)$_2$Cl (**339**), which could catalyze hydrogen precipitation by proton reduction efficiently through both photocatalytic and electrocatalytic methods. The benchmark TOF of hydrogen production in the photocatalytic system is as high as 0.54 s^{-1}, and the mechanistic study in the electrocatalytic system shows that dimer of compound **339** is the real active catalytic species [362c].

7.4 Summary and perspctives of hydrogenase-based biomimetic asymmetric catalysis

Important progress has been made in biomimetic chemistry based on [FeFe], [Fe] and [NiFe] hydrogenases, demonstrating the great value and potential of hydrogenase-based biomimetic catalysts for applications in asymmetric hydrogenation, CO_2 reduction and fixation, and photolysis for hydrogen evolution. It should be noted that many artificial catalysts are not deliberately designed to mimic hydrogenases, but mechanistic studies have shown that they have similarities in the way of activating hydrogen and transferring hydrogen. Some of the highly efficient artificial hydrogenation catalysts have approached or even surpassed the enzyme catalysts in terms of activity. But the central metals of these super-highly active hydrogenation catalysts are generally based on 4d or 5d noble metals, such as Ru, Rh, Ir. Although there have been many successful examples of using abundant 3d metal catalysts in asymmetric hydrogenation reactions, the efficiency of most 3d metal catalysts is still much lower than that of noble metal catalysts.

On the contrary, hydrogenases show high catalytic activity with 3d central metals like Ni and Fe. The protein shell of the enzyme acts as a multi-dentate ligand around the catalytic center, not only stabilizing the structure of the active site, but also cunningly concealing it in the protein molecules, which effectively prevent the deactivation of the catalyst. It is difficult to directly replicate the effect of these complex protein structures in artificial catalysts by chemical synthesis. But based on the understanding of the enzymatic catalytic mechanism, we can expect to use more economical, sustainable and biocompatible 3d metals to achieve high catalytic activity and selectivity under mild reaction conditions. Therefore, understanding the reaction mechanism of enzyme

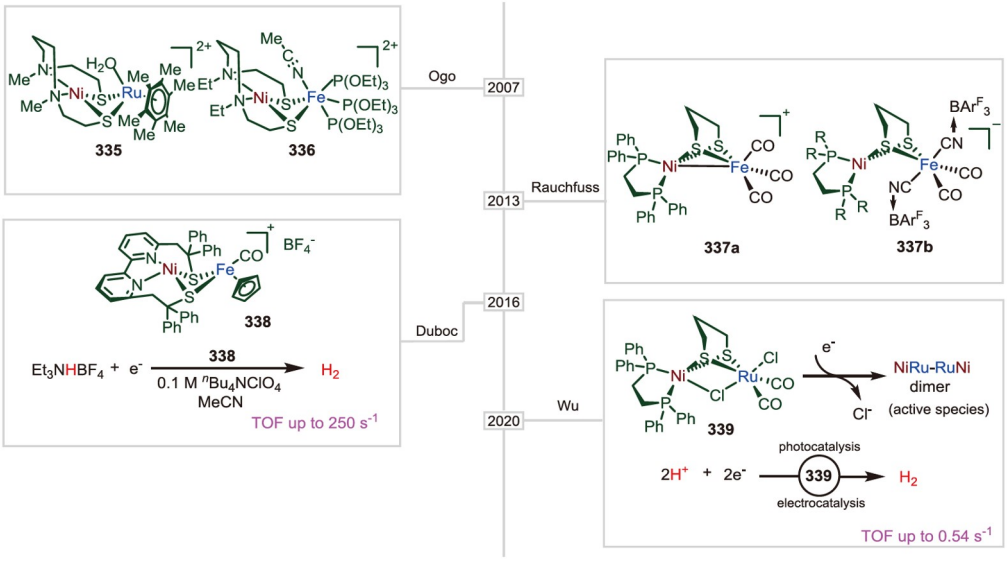

Scheme 109 Development of biomimetic catalysts based on [NiFe]-hydrogenase (color online).

catalysis, mimicking the key structure of enzymes, and performing biomimetic design of catalysts are the future directions to further improve the activity and selectivity of artificial catalysts.

8 Heme oxygenase-based biomimetic asymmetric catalysis

Heme oxygenase is an enzyme with iron porphyrin (or heme) as its auxiliary group (Figure 18). It is widely involved in the redox reactions in animals, plants, yeast, aerobic bacteria and anaerobic photosynthetic bacteria [363–365]. In 1958, Klingenberg [366] and Garfinkel [367] found that a pigment in the cell microsome had an absorption peak at 450 nm, named P450, after being reduced by carbon monoxide. In 1964, Omura and Sato [368,369] confirmed that P450 is indeed a protein. Heme oxygenase plays an important role in biological oxidation. In the currently known heme enzymes, there are more than 1,000 kinds of cytochrome P450 enzymes. Heme oxygenase has a strong catalytic function and can catalyze the directional oxidation of various foreign compounds, supporting reactions such as C–H bonds hydroxylation, double bond epoxidation, heteroatom oxidation, aromatic hydrocarbon oxidation and aldehyde and alcohol oxidation [25,370].

In the catalytic oxidation of alkanes by cytochrome P450 [371–373], the alkanes first bind to Fe(III) species (**A**) to obtain the ferric intermediate (**B**). This intermediate (**B**) is then reduced to Fe(II) ferrous species (**C**), which is then oxidized by oxygen to generate ferric-superoxo species (**D**). Subsequently, a second electron and a proton are transferred to the ferric-superoxo species (**D**) to produce a ferric(hydro) peroxo intermediate (**F**), which then combines with protons to release a molecule of H_2O to form a Fe(IV)=O species **G**, which is the real oxidative intermediate. Finally, alkanes are oxidized by this intermediate (**G**) by C–H bond cleavage and C–O bond formation. This last process may be cooperative or stepwise, involving hydrogen grabbing and oxygen rebound (Scheme 110).

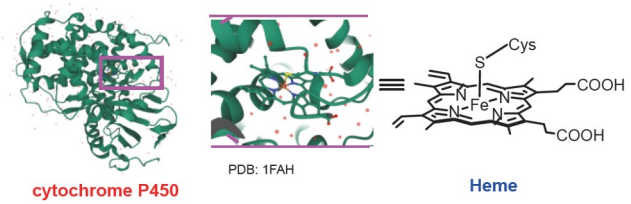

Figure 18 Cytochrome P450 enzymes: structure and function (color online).

Heme oxygenase is an oxidase with an iron porphyrin complex as its core, which is the key site in which catalytic functions are performed. Metalloporphyrin complexes can be used to simulate the catalytic function of heme oxygenase. Asymmetric catalytic simulations can also be achieved if chiral groups are introduced into porphyrin ligands. Similar to heme oxidase, metalloporphyrin complexes can form active catalytic species by activating molecular oxygen to undergo various reactions such as alkane C–H oxidation and alkene epoxidation.

This section mainly focuses on biomimetic asymmetric catalytic reactions based on heme oxygenase, and the most recent progress in the asymmetric epoxidation of olefins, asymmetric sulfoxylation of sulfides and asymmetric C–H bonds activation.

8.1 Metalloporphyrin-catalyzed asymmetric cyclization of alkenes

8.1.1 Asymmetric epoxidation of alkenes

The first example of asymmetric epoxidation of olefins

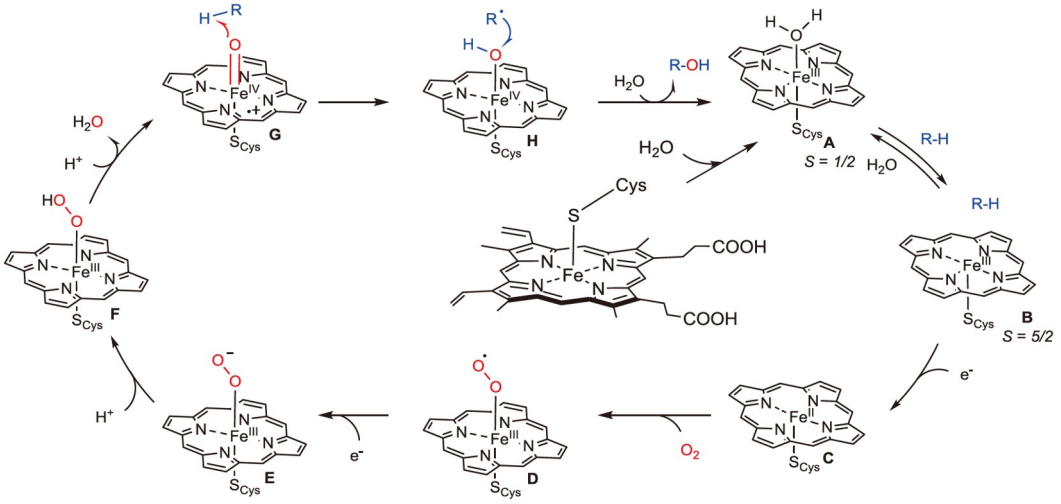

Scheme 110 Mechanism of hydroxylation of alkanes catalyzed by cytochrome P450 enzyme (color online).

catalyzed by metalloporphyrin complexes was published in 1983 when Groves *et al*. [374] used αβαβ-tetrakis(*o*-(*R*)-hydratropamidophenyl)porphyrin (**340**) and αβαβ-tetrakis(*o*-[(*S*)-2′-carboxymethyl-1,1′-binaphthyl-2-carboxamido]phenyl)porphyrin (**341**) iron complexes in their exploration of the oxidation of various substituted styrene and aliphatic olefins-reactions with an ee value between 9% and 51%. Although the enantioselectivity of this reaction is only moderate, these findings promoted the development of a new field (Scheme 111).

Binaphthyl with axial chirality is a member of a class of privileged chiral ligands and have made outstanding contributions in the field of asymmetric catalysis. A series of chiral porphyrin metal complexes have been made by introducing binaphthyl structures into the porphyrin system (Figure 19).

In 1990, Grove *et al*. [375] synthesized vaulted metalloporphyrin (**342**). The roles of iron and manganese porphyrin complexes in the asymmetric epoxidation of olefins were studied and the enantiomeric excess of such reactions was found to be moderate (Figure 20, entry 1).

In 1991, Naruta *et al*. [376,377] designed and synthesized a novel C_2-symmetric "Twin-Coronet" porphyrin of chiral binaphthyls, connected by ether bonds on both sides. In the epoxidation of aryl olefins catalyzed by iron porphyrin (**343**, M=FeCl) and iodosobenzene, the ee of 2-nitrostyrene is as high as 89% (Figure 20, entry 2). In 1992, the same group investigated the effect of the central metal and oxidants on the epoxidation of olefins. The asymmetric epoxidation of *cis*-β-methylstyrene catalyzed by manganese complexes was found to have better ee values than that developed with iron catalysis [377].

In 1992, Collman *et al*. [378] connected two chiral binaphthyl groups with a macrocyclic ether structure, and introduced them into a porphyrin structure. The iron porphyrin

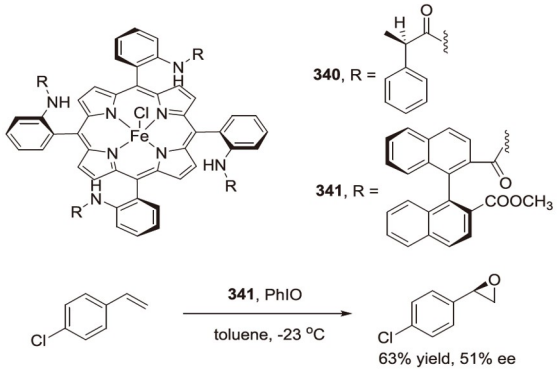

Scheme 111 Chiral iron-porphyrins for enantioselective epoxidation of olefins.

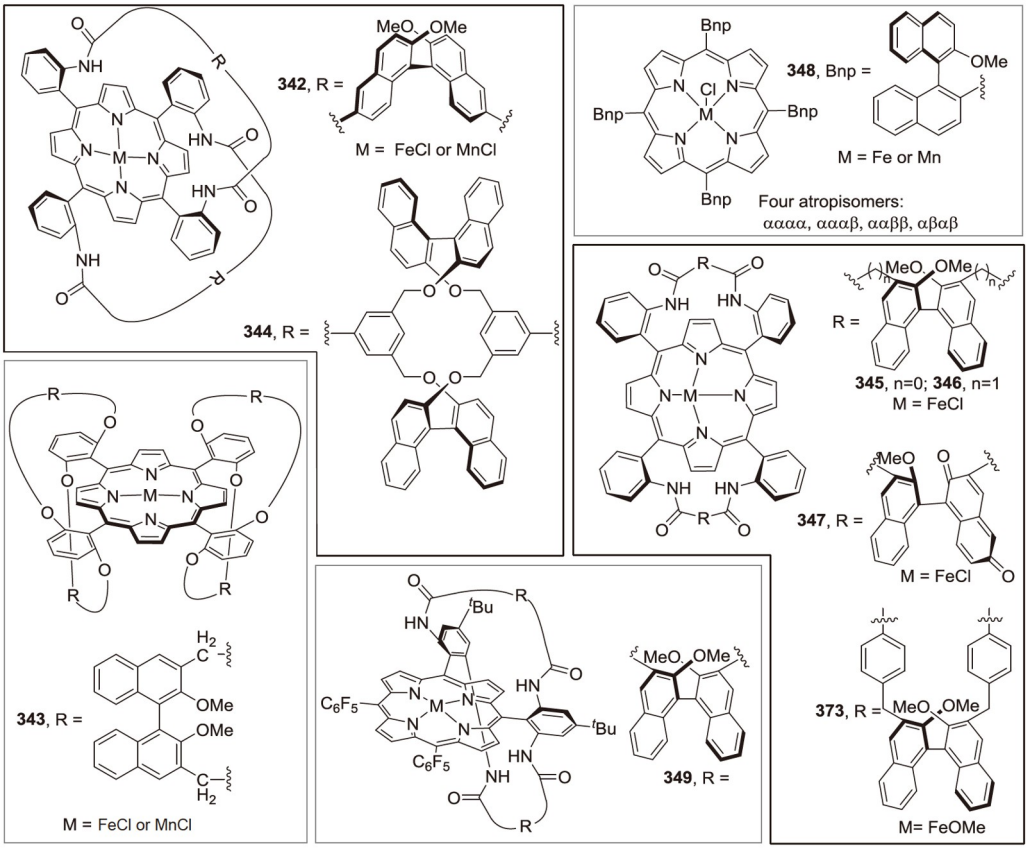

Figure 19 Porphyrin metal complexes containing chiral binaphthyl groups.

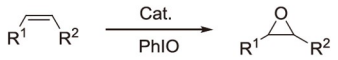

entry	alkenes	Cat.	yield (%)	ee (%)
1		**342** (M = FeCl) or **342** (M = MnCl)	9 to 73	6 to 72
2	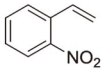	**343** (M = FeCl)	-	89
3		**344**	26 to 64	21 to 63
4		**345**	73 to 95	49 to 90
5		**348**	47	57
6	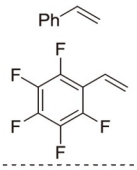	**349**	- -	59 85
7		**346**	75-96	81-97

Figure 20 Asymmetric epoxidation of alkenes.

complex (**344**) obtained from "binap capped" porphyrin has the same behavior as other metalloporphyrin complexes in the epoxidation of terminal olefins (Figure 20, entry 3).

Collman *et al*. [379] prepared, C_2-symmetric chiral porphyrin compounds (**345**) with binaphthyl handles in 1998. Using the iron porphyrin complexes (**345**), the corresponding epoxides can be obtained with excellent enantioselectivity under the oxidation of iodoylbenzene, $C_6H_5IO_2$ (Figure 20, entry 4). A naphthalene ring on metalloporphyrin could be oxidized to a quinone structure (**347**) during the reaction, and this may greatly improve the enantioselectivity of the reaction.

In 2000, Salvadori *et al*. [380] introduced a binaphthalene group to the *meso*-position of a porphyrin and obtained four atropisomers. Among these, the reaction of ααββ-isomer iron complexes (**348**) was the best, and produced (*S*)-phenylethylene oxide in 47% yield and 57% ee (Figure 20, entry 5).

In 2000, Rose *et al*. [381] prepared a C_2-symmetric chiral iron-porphyrin complex (**349**) containing binaphthalene and pentafluorophenyl, which was named "Seat" iron-porphyrin. The asymmetric epoxidation of styrene and pentafluorostyrene by the catalyst reached 59% and 85% ee, respectively (Figure 20, entry 6).

In 2004, Rose *et al*. [382] also developed a C_2-symmetric bis(binaphthyl)porphyrin that differs structurally by only two CH_2 groups from their previously published structures. The metal complex (**346**) gave 75%–96% yields and 81%–97% ee in the asymmetric epoxidation of olefins such as styrene (Figure 20, entry 7).

Chiral alcohols and amino acids are cheap and readily available chiral sources. In 1985, Mansuy *et al*. [383] introduced chiral phenylalanine into porphyrin compounds containing amino groups, and prepared "basket handle" iron porphyrin complexes (**350**) with L-phenylalanine, and "picket" iron porphyrins (**351** and **352**) (Figure 21). The "basket handle" iron porphyrin complexes could catalyze the epoxidation of *p*-chlorostyrene up to 50% ee, while "picket" iron porphyrins **351** and **352** delivered only 12% and 21% ee, respectively (Figure 22, entry 1).

In 1991, Momenteau *et al*. [384] introduced the acetyl-protected chiral glucose group into tetraphenylporphyrin through a covalent bond, and synthesized the corresponding iron porphyrin and manganese porphyrin complexes (**353**). However, the enantioselective control exerted by these catalysts is less than ideal (Figure 22, entry 2).

In 1997, Gross *et al*. [385] synthesized iron porphyrin complexes (**354, 355**) of a ketal-protected threitol derivative, and studied the complex catalyzed asymmetric epoxidation of alkenes under different conditions (Figure 22, entry 3).

In 2001, Smith *et al*. [386,387] introduced (*R*,*R*)-2,6-bis(1-phenylbutoxy)phenyl and pentafluorophenyl into porphyrins and synthesized four iron porphyrins and a manganese porphyrin complex. The iron porphyrin complex (**356**) with four dialkoxyphenyl units is a poor catalyst for epoxidation. The activity, stability and selectivity of the catalyst were improved by introducing the smaller penta-fluorophenyl group in place of the 2,6-di(1-phenylbutoxy)phenyl group (Figure 22, entry 4).

In 2003, Boitrel [388] reported the synthesis of picket-fence iron porphyrin complexes with L-prolinoyl as a chiral source. Four atropisomers were obtained, and the αβαβ-atropisomer (**361**) had the best ee (34%) for the epoxidation of 1,2-dihydronaphthalene (Figure 22, entry 5). In addition, they also obtained bis-strapped iron porphyrin complexes by linking L-proline groups through amides, but unfortunately these bis-strapped iron porphyrin complexes did not work well in the asymmetric epoxidation of olefins [389].

In 2004, Higuchi *et al*. [390,391] described a novel method for the efficient synthesis of D_4-symmetric chiral porphyrins using commercially available C_2-symmetric diols as the chiral source. The epoxidation reaction of styrene catalyzed by **362** showed the moderate enantioselectivity. The ee value was significantly increased by introduction of electron-withdrawing groups on the styrene ring. They also examined the electronic effect of the styrene substituents on the porphyrin catalyst and found that the electron-deficient groups decreased the enantioselectivity and electron-donating groups increased the enantioselectivity.

In 1997, Halterman's group [392] prepared the D_4-symmetric catalytic activity of their manganese complexes in the

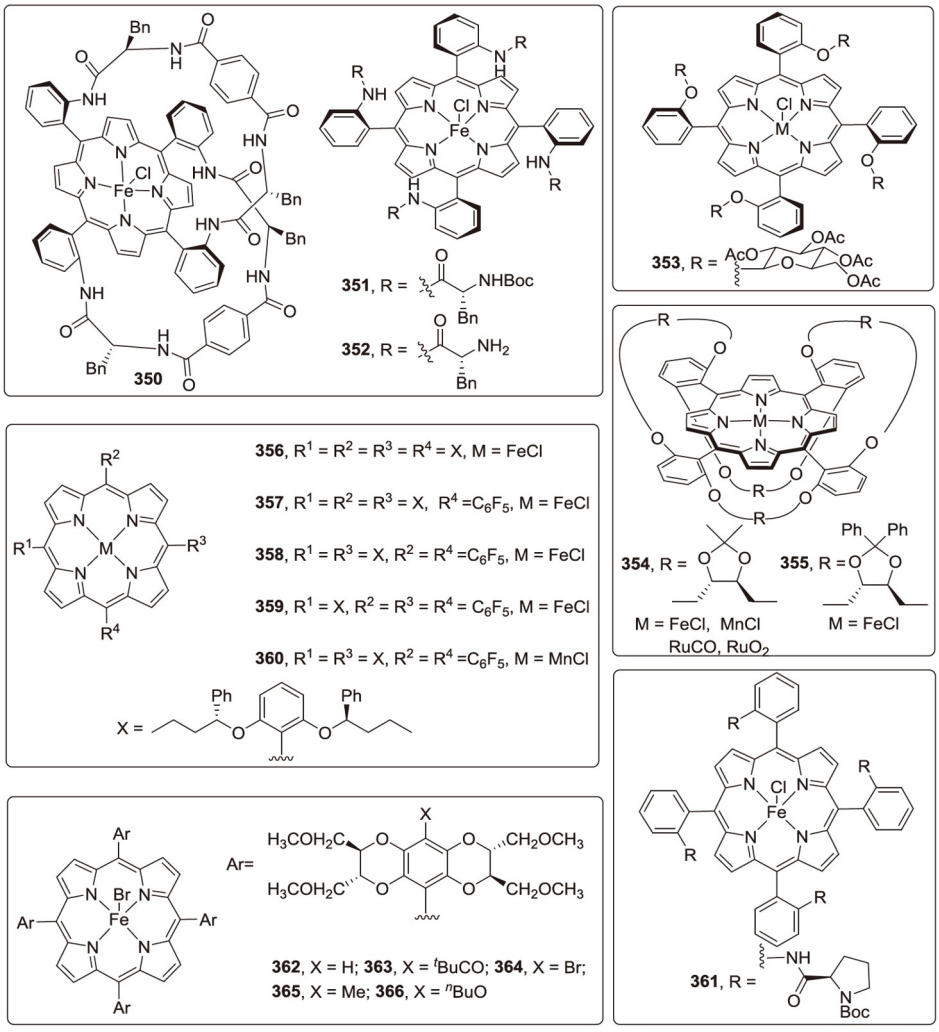

Figure 21 Metalloporphyrin complexes containing chiral alcohols and amino acids.

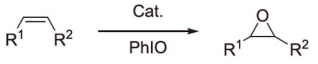

entry	alkenes	Cat.	yield (%)	ee (%)
1	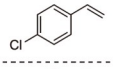	**350**	35	50
		351	50	12
		352	45	21
2	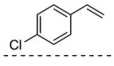	**353** (M = FeCl)	60	33
		353 (M = MnCl)	53	28
3	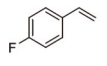	**354** (M = FeCl)	68	56
		355 (M = FeCl)	70	65
		354 (M = RuCO)	39	51
		354 (M = RuO_2)	9	53
4		**356**	48.5	16.3
		357	79.5	7.7
		358	91.6	16.6
		359	94.6	6.8
		360	87.0	7.3
5		**361** (αβαβ)	-	34
6		**362**	61	78
		363	68	71
		364	70	74
		365	70	78
		366	63	79

Figure 22 Metalloporphyrin-catalyzed asymmetric epoxidation of olefins.

epoxydation of aryl olefins (Figure 23). In the epoxidation of *cis*-β-methylstyrene, the methoxy-substituted manganese porphyrin metal complex (**369**) gave the best result (up to 83% ee).

In 2002, Yeung *et al*. [393] studied the effects of various organic bases on the asymmetric epoxidation of olefins catalyzed by Halterman's manganese porphyrin complexes (**368**). For the epoxidation of *cis*-β-methylstyrene, $KHSO_5$ was used as an oxidant. In the absence of an amine as an additive, the ee value was 43% and when DMAP was used as an additive, the ee value could be increased to 81%.

In 2006, Simonneaux *et al*. [394] used chiral metalloporphyrin (Fe, Ru) complexes functionalized with four vinyl groups to polymerize with styrene and divinylbenzene (or ethylene glycol) to obtain supported iron and ruthenium complexes (**370**). The heterogeneous asymmetric epoxidation styrene derivatives were carried out by using these polymers as catalysts, the ee was up to 75%.

In 2010, Bach *et al*. [395,396] introduced the concept of

hydrogen bond-directed reactions into the reactions catalyzed by ruthenium porphyrins (**372**). Rigid bulky sterically hindered chiral amide skeletons were introduced into porphyrin ligands with a Sonogashira reaction (Scheme 112a), and successfully achieved asymmetric epoxidation of alkenes with the ruthenium-porphyrin complexes. The catalytic epoxidation reaction uses 2,6-dichloropyridine-N-oxide as the oxidant, and the hydrogen bonding brings the substrate and the ruthenium-porphyrin complex into closer proximity, resulting in a highly enantioselective and regioselective reaction (Scheme 112b). The epoxidation reaction of 3-vinylquinolone reached up to 95% ee and 71% yield (Scheme 112c).

8.1.2 Asymmetric cyclopropanation of alkenes

Many drugs, natural products and important intermediates in organic synthesis contain a cyclopropane ring motif. The asymmetric cyclopropanation of alkenes with diazonium compounds and metalloporphyrin catalysis is significant.

In 1999, the Gross's group [397] used porphyrin with a ketal-protected chiral diol, and examined the reaction of styrene and ethyl diazoacetate catalyzed by different metalloporphyrin complexes (Scheme 113a). When using the ruthenium porphyrin complex (**354**), they obtained an ee value of 58%.

In 2006, Che and coworkers [398] used Halterman's iron porphyrin chiral complexes (**368**) as catalysts to realize the insertion reaction of ethyl diazoacetate to styrene compounds. In this way, they synthesized a series of cyclopropane compounds with high diastereo- and enantioselectivity (Scheme 113b).

Simonneaux *et al*. [399] converted a Halterman porphyrin complex into a polymer, using the chiral porphyrin iron and ruthenium (**370**) as heterogeneous catalysts, and achieved the insertion of 2,2,2-trifluorodiazoethane to styrene, producing the optically active trifluoromethylphenylcyclopropane (Scheme 113c). In 2008, the same group used chiral Halterman porphyrin compounds (**368**) with sulfuric acid to obtain a water-soluble tetrasulfonated porphyrin complex

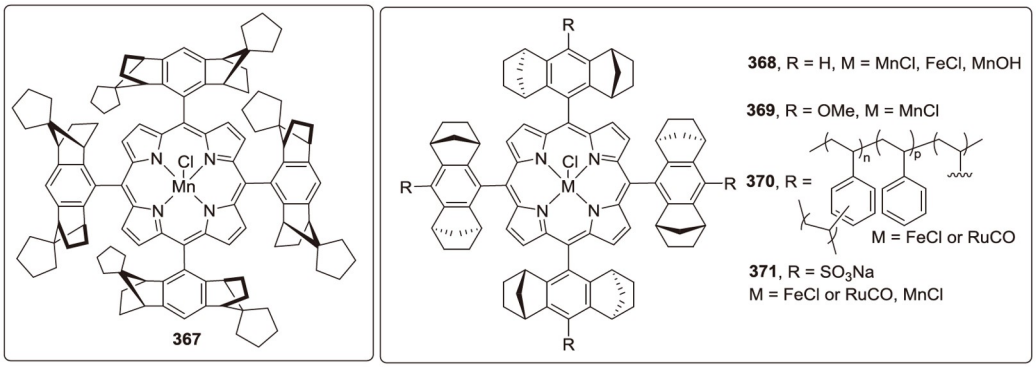

Figure 23 Halterman's porphyrin metal complexes.

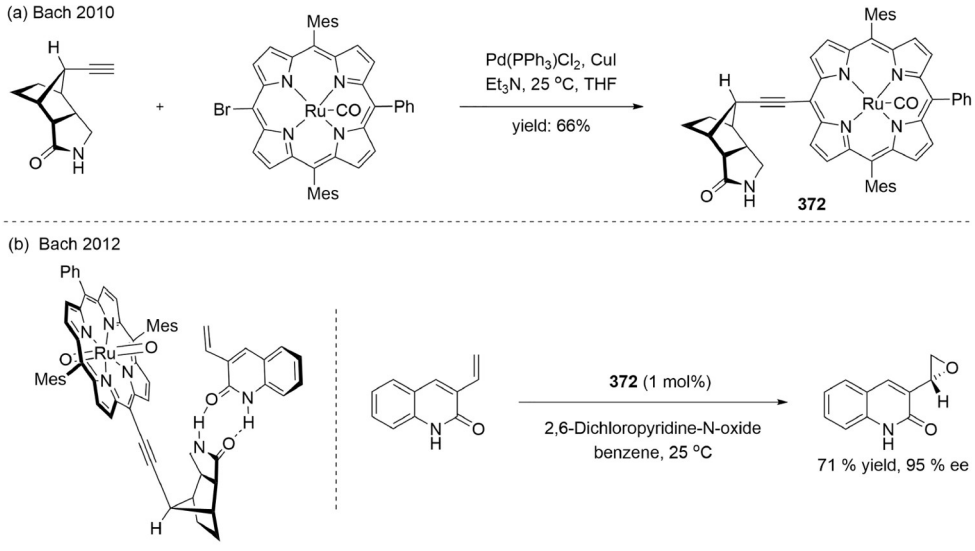

Scheme 112 Synthesis of ruthenium porphyrin complexes with amine directing groups.

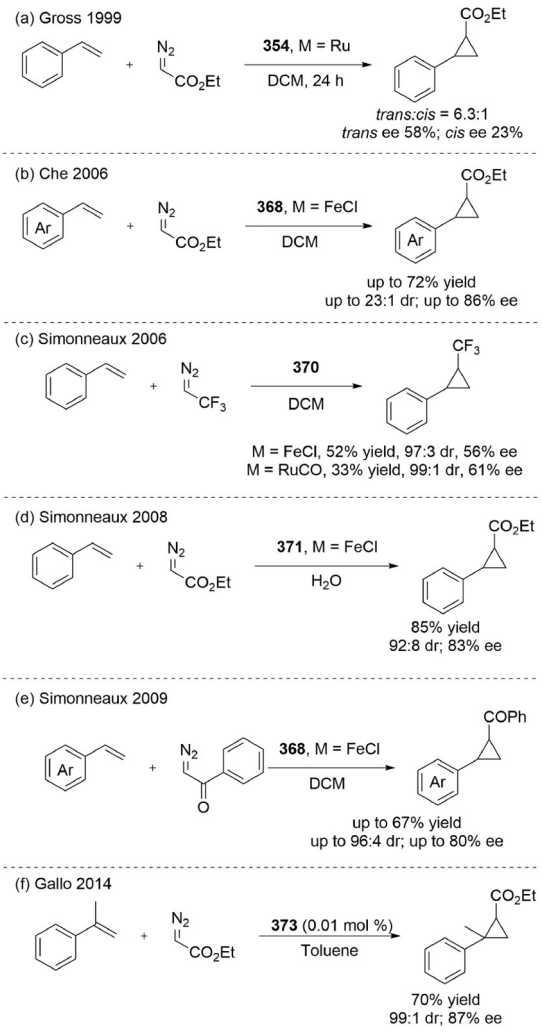

Scheme 113 Metalloporphyrins catalyze asymmetric cyclopropanation.

(**371**) [400]. Using this water-soluble chiral porphyrin iron or ruthenium in water for the asymmetric addition of ethyl diazoacetate to styrene, optically active *trans*-cyclopropyl ester compounds can be obtained (Scheme 113d). In 2009, Simonneaux *et al*. [401] also used chiral Halterman chiral iron porphyrin (**368**) (M=FeCl) as a homogeneous catalyst to asymmetrically add diazoacetophenone to styrene derivatives to obtain chiral cyclopropyl ketones (Scheme 113e). In 2014, Gallo *et al*. [402] synthesized a novel C_2-symmetric binap-bis-strappedironporphyrin complex (**373**) (Scheme 113f). This complex (**373**) catalyzed the stereoselective cyclopropanation of α-methylstyrene with good reactivity, enantio- and diastereoselectivity (up to 99:1 dr), producing the trans structure with up to 87% ee.

In 2003, Zhang *et al*. [403] found that tetraphenylporphyrin cobalt could efficiently catalyze the cyclopropanation of arylalkenes with ethyl diazoacetate. Two chiral porphyrin cobalt complexes (**374** and **375**) were synthesized, and the asymmetrically catalytic reaction was realized, but the diastereoselectivity and enantioselectivity of the reaction were only moderate (Figure 24). It was found that in the asymmetric cyclopropanation of alkenes, cobalt porphyrins have better catalytic efficiency than iron porphyrin complexes [404]. Subsequently, a 5,10-bis(2′,6′-dibromophenyl) porphyrin was developed as a general synthon, which can modularly construct chiral porphyrins by palladium-catalyzed multiple amidation of chiral amides [405,406]. A series of porphyrin-cobalt complexes were synthesized in this way (Figure 25). This chiral porphyrin cobalt family can efficiently catalyze asymmetric cyclopropanation of alkenes, asymmetric aziridination of alkenes, and asymmetric C–H bond activation of alkanes. The asymmetric cyclopropanation of styrene with diazoacetate is highly efficient (84% yield) and stereospecific (up to 99:1 dr, up to 98% ee) with the chiral porphyrin cobalt complex (**377**) as the catalyst [405]. Studies of the mechanism reveal that the cobalt porphyrin complex undergoes a cobalt-based metalloradical process [407–411]. There are many other diazo compounds that can participate in the asymmetric cyclopropanation of olefins to obtain the corresponding chiral cyclopropane compounds in good yields and with excellent stereoselectivity (Scheme 114a) [412–419]. The cobalt porphyrin catalyst can also catalyze the insertion of diazo compounds into alkynes to produce cyclopropene compounds (Scheme 114b) [420].

As diazo compounds, especially donor-substituted diazo compounds are unstable, Zhang *et al*. [421] used sulfonyl hydrazone, a precursor of diazo compounds in the presence

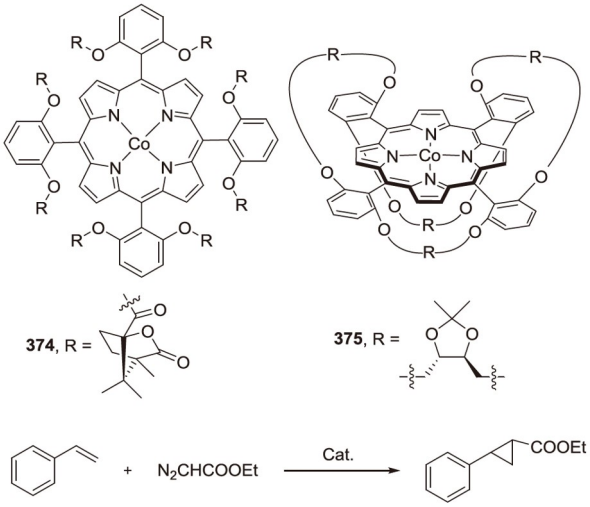

entry	Cat.	yield (%)	cis:trans	% ee	
				cis	trans
1	**374**	73	64:36	77	62
2	**375**	84	48:52	31	10

Reactions were carried out at 80 °C in toluene for 12 h under N_2 with 1.0 equiv of styrene , 1.2 equiv of EDA, and 2 mol % Cat..

Figure 24 Cobalt-porphyrins catalyze asymmetric cyclopropanation.

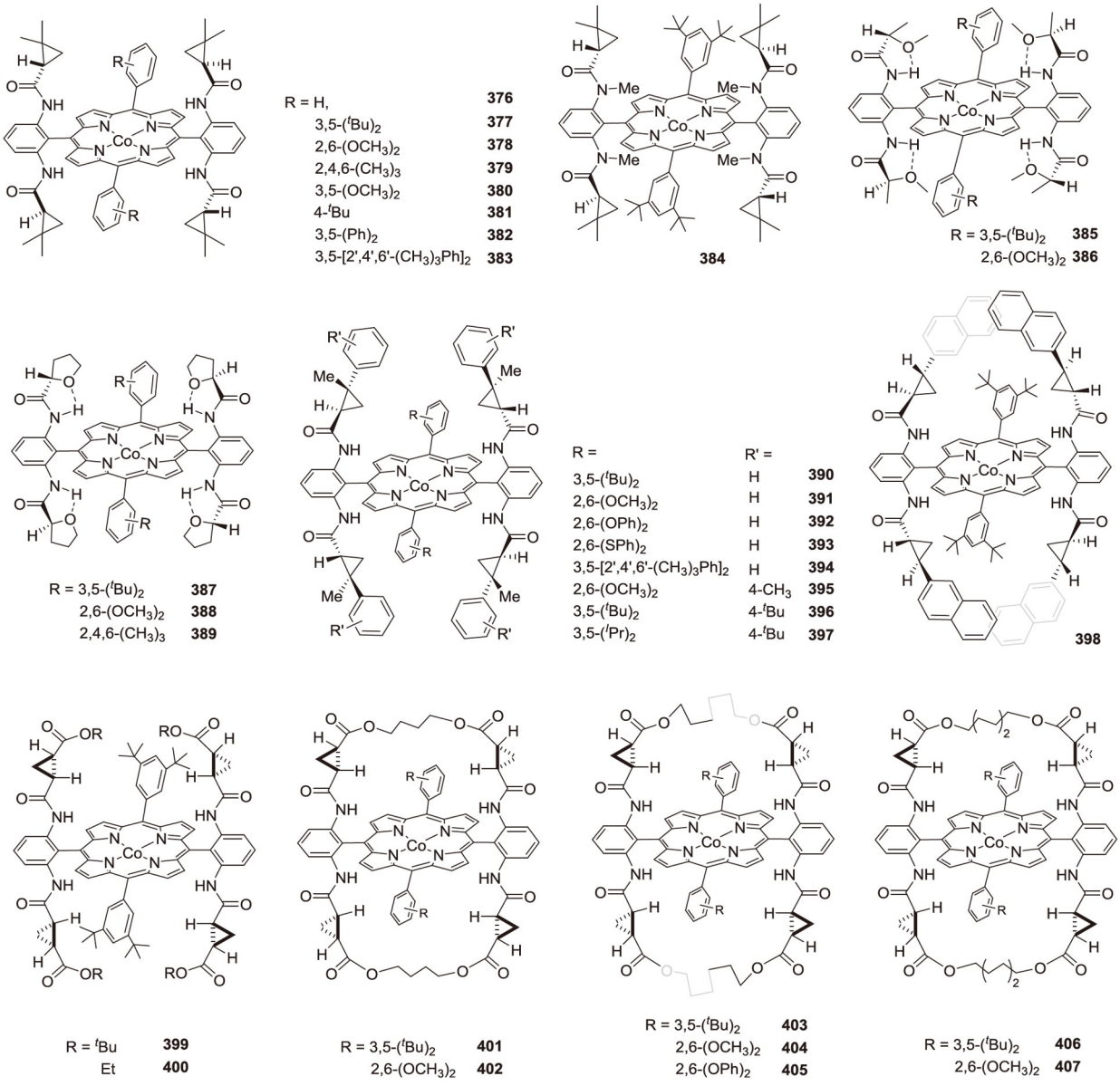

Figure 25 Zhang's cobalt porphyrin metal complexes.

of base, and achieved the radical asymmetric cyclopropanation of olefins. When the cobalt porphyrin complex (**398**) is used, the corresponding cyclopropanation products can be obtained in high yield, and the diastereo- and enantioselectivity of the reaction can be effectively controlled (Scheme 115a). Zhang *et al*. [422] also realized the asymmetric radical cyclopropanation of dehydroaminocarboxylates, and obtained a series of amino acid derivatives with chiral cyclopropane skeletons (Scheme 115b). By fine-tuning the cavity environment, they also synthesized a series of new D_2-chiral porphyrin complexes (**401**–**408**) [406]. The optimized Co porphyrin metal radical system can be widely applied to α-pyridyl and other α-heterocyclic substituted diazomethanes, and can be used for asymmetric cyclopropanation of other olefins (Scheme 115c) [423]. They also realized the asymmetric cyclopropanation reaction between α-alkynyl diazomethane and olefins, catalyzed by a cobalt porphyrin metal complex (**391**) using the corresponding sulfonyl hydrazone generated *in situ* under basic conditions (Scheme 115d) [424].

Compared with intermolecular reactions, the intramolecular insertion reaction of diazo compounds to alkenes has been studied less. Zhang *et al*. [425,426] realized the intramolecular asymmetric cyclopropanation of alkenes, providing a powerful strategy for the stereoselective construction of complex [3.0.1] bicyclic systems (Scheme 116a). They also applied their cobalt-based metalloradical catalytic system to the stereoselective radical cascade reaction of 1,6-enynes with diazonium compounds. By using a cobalt porphyrin metal complex (**383**) as a catalyst, the radical cascade reaction of 1,6-enyne

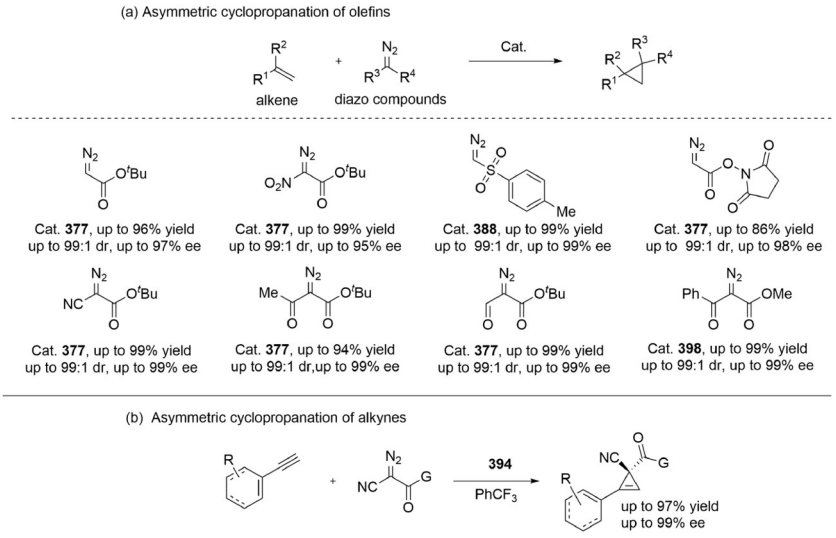

Scheme 114 Cobalt-based metalloradicals catalyze asymmetric cyclopropanation of alkene.

with diazo compounds can be realized, and a series of cyclopropane-fused tetrahydrofuran compounds can be obtained with good yield and excellent stereoselectivity (Scheme 116b) [427].

8.1.3 Asymmetric aziridination of alkenes

Chiral aziridine derivatives play an important role in chemistry and biology and consequently, the enantioselective synthesis of aziridine and its derivatives is significant. The synthesis of aziridines by metal-catalyzed insertion of nitrenes into alkenes has received extensive attention due to the abundance and variety of alkenes. In 1997, Che *et al*. [428] used D_4-symmetric Halterman manganese metalloporphyrin complexes (M=MnOH) (**368**) to catalyze the aziridination of styrene-type substrates, obtaining an enantiomeric excess of 43 - 68%. In 1999, Marchon *et al*. [429] used manganese and iron metalloporphyrin complexes (**408**) as catalysts to realize the asymmetric aziridine reaction of PhI=NTs with styrene (Figure 26). It is interesting that two different metals in this reaction have opposite stereoscopic configurations.

In 2008, Zhang's group [430,431] used the D_2-symmetric chiral porphyrin cobalt complex (**377**) that they had developed to realize the asymmetric aziridination of aryl alkenes using diphenylphosphonoazide as a source of the nitrene (Figure 27a, entry 1). This reaction affords the desired *N*-phosphine substituted aziridine compounds in moderate to high yields with good enantioselectivity. Other azide compounds including trichloroethoxysulfonyl azide (Figure 27a, entry 2) [432], fluorine substituted aryl azide (entry 3) [433], and trichloroethoxyformyl azide (entry 4) [434] can smoothly participate in the aziridination of alkenes, in the presence of a suitable cobalt porphyrin catalyst to give the corresponding product in high yield and with excellent stereoselectivity. In addition to the intermolecular aziridiation

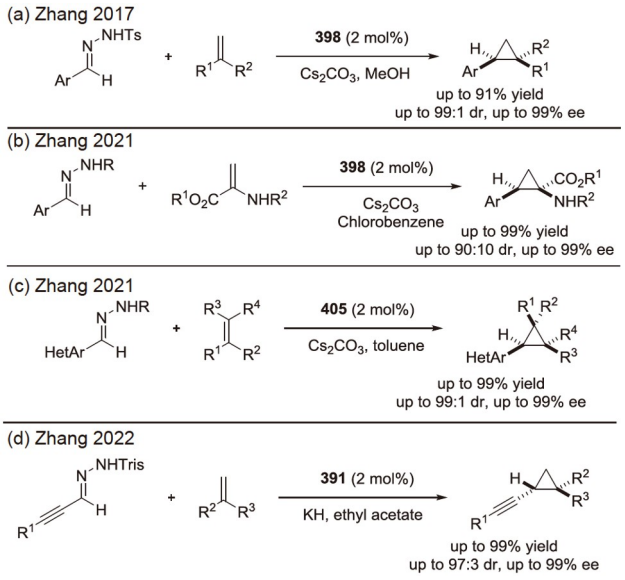

Scheme 115 Asymmetric cyclopropanation of sulfonyl hydrazone with alkenes.

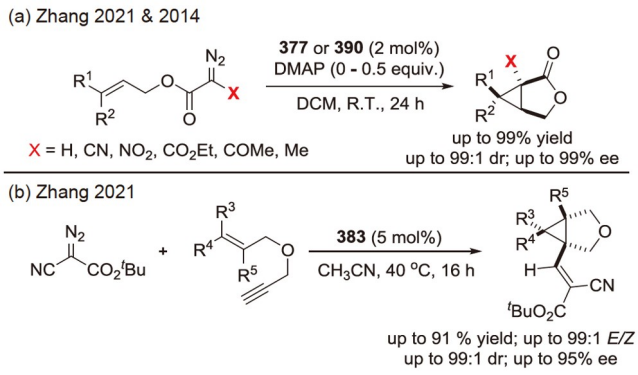

Scheme 116 Intramolecular insertion reaction of diazo compounds to alkenes (color online).

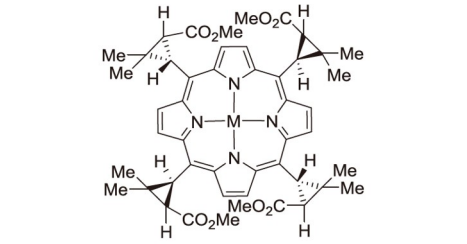

Entry	M	yield	ee
1	Fe	27	28(+)
2	Mn	34	57(-)

Figure 26 Manganese and iron porphyrins catalyzed asymmetric aziridination of styrene.

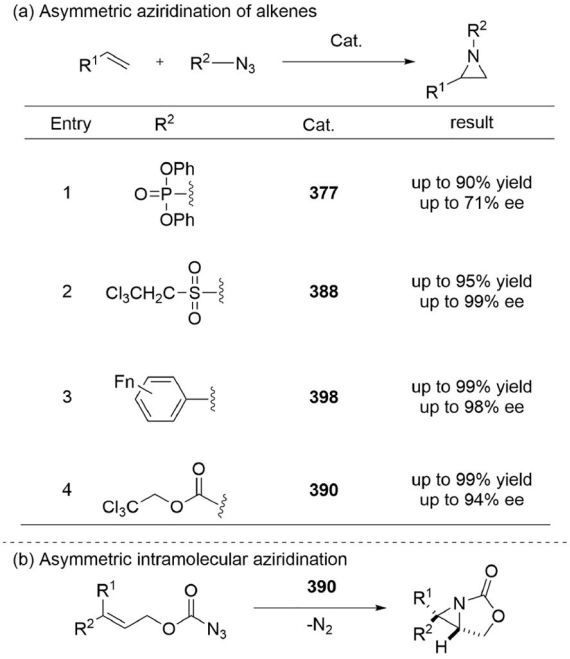

Figure 27 Cobalt-based metalloradicals catalyze asymmetric aziridination of alkenes.

of alkenes, Zhang's group [435] also realized the insertion reaction of intramolecular nitrenes into alkenes and efficiently constructed chiral [3.1.0]-bicyclic aziridines with high diastereo- and enantioselectivity (Figure 27b).

8.2 Metalloporphyrin-catalyzed asymmetric C–H bond activation

8.2.1 Asymmetric hydroxylation of C–H bonds

In 1989, Grove *et al*. [436] also used the synthesized vaulted metalloporphyrins (**342**) to catalyze the hydroxylation of C–H bonds. Using a chiral porphyrin iron complex (M=FeCl) (**342**) as catalyst and iodoylbenzene ($PhIO_2$) as oxidant, a hydroxylation product of ethyl benzene was obtained in 40% yield and with 41% ee value. In 1990, they synthesized the corresponding manganese porphyrin catalyst (M=MnCl) (**345**) and compared it with the iron porphyrin catalyst (M=FeCl) (**345**) in the benzylic C–H bond hydroxylation reaction (Figure 28) [375].

In 1999, Gross *et al*. [437] introduced a ketal-protected chiral diol into the porphyrin skeleton, and synthesized a class of D_2-symmetric chiral ruthenium porphyrin complexes (**409**). With ruthenium porphyrin (**409**) as the catalyst and 2,6-dichloropyridine nitrogen oxide as an oxidant, an asymmetric oxidation of a C–H bond on a tertiary carbon was achieved in 38% ee. The ruthenium porphyrin complex can also realize the kinetic resolution of secondary alcohols (Scheme 117).

Che *et al*. [438] reported the hydroxylation of C–H bonds in aromatic benzyl positions using 2,6-dichloropyridine nitrogen oxides as oxidants in the reaction catalyzed by ruthenium porphyrin catalysts with chiral norbornanes in the *meso*-position. In 2012, Simonneaux *et al*. [439] introduced four sulfonate groups into this chiral porphyrin compound and synthesized a water-soluble manganese porphyrin catalyst (**371**). The water-soluble manganese porphyrin catalyst can achieve asymmetric hydroxylation of alkanes in a water/methanol system with ee values up to 57% (Figure 29).

In 2015, Bach and coworkers [440] introduced a rigid and large hindered chiral amide skeleton into porphyrin ligands, and the resulting porphyrin ruthenium complex successfully realized the C–H bond oxidative desymmetrization of an oxidized spiro-indole (Figure 30a). The hydroxyl intermediates obtained in this reaction are unstable and are further oxidized to ketones under the conditions of Swern oxidation or PCC oxidation to give chiral spiro-dicarbonyl compounds with ee up to 96%. In 2018 and 2020, Bach's group realized the asymmetric hydroxylation of 3-dimethyl-3-dimethyl-3-dihydroquinolone using a similar strategy (Figure 30b) [441] and 3-benzylidene quinolone (Figure 30c) [442] with a manganese porphyrin as the catalyst in the presence of iodosobenzene, as oxidant, with a diastereoselectivity of up to 99%.

8.2.2 Asymmetric carbon-hydrogen bond alkylation

In 2012, Che's group [443] used Halterman's porphyrin iridium complex (**413**) to realize the asymmetric insertion reaction of diazonium compounds into 1,4-cyclohexadiene and tetrahydrofuran, which afforded the corresponding products with high yield and excellent enantioselectivity (Scheme 118a). Using the same catalytic system, they also realized the asymmetric intramolecular insertion reaction of diazo compounds into C–H bonds, obtaining the corresponding *cis*-β-lactone compounds (Scheme 118b) [444]. The reaction has high yield and excellent diastereoselec-

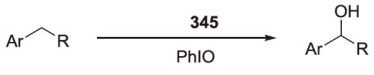

substrate	**345**-FeCl		**345**-MnCl	
	ee (%)	yield (%)	ee (%)	yield (%)
	40	40	26	77
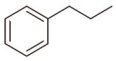	44	32	16	98
	54	72	18	82
	72	47	12	46

Reaction conditions: catalyst/iodosylbenzene/substrate = 1:100:1000, CH_2Cl_2 at 0 °C in the absence of oxygen.

Figure 28 Hydroxylations catalyzed by **345**-FeCl and **345**-MnCl.

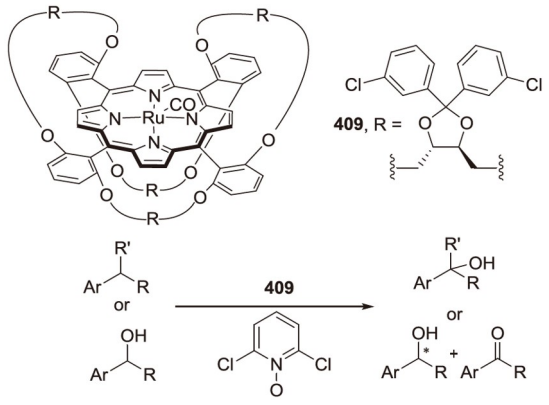

Scheme 117 Hydroxylation of C–H bonds and kinetic resolution of alcohols.

tivity.

In 2014, Zhang *et al*. [445] used a Co-based metalloradical catalyst system for the asymmetric intramolecular C–H alkylation of acceptor or acceptor-substituted diazo reagents (Scheme 119a). Using the cobalt porphyrin metal catalyst, 1,5-C–H alkylation can be achieved to give 5-membered sulfolane derivatives with high yield and excellent enantioselectivity and diastereoselectivity. Through chiral ligand judicious modulation using bridged D_2-symmetric chiral cobalt porphyrins as optimal supporting ligands, Zhang *et al*. [446] demonstrated the first Co-based metalloradical 1,4-C–H alkylation catalytic system, which involves the usually challenging 1,4-hydrogen atom abstraction (Scheme 119b). The reaction can be carried out under mild conditions with the support of optimal ligands to construct α,β-disubstituted cyclobutanones with high yield and excellent diastereo- and enantioselectivity. Using the strategy of cobalt-based metalloradical catalysis, Zhang's group [447,448] also realized the 1,5-C–H alkylation reaction using sulfonyl hydrazone as the precursor of the diazo compound (Scheme 119c, d). A series of five-membered

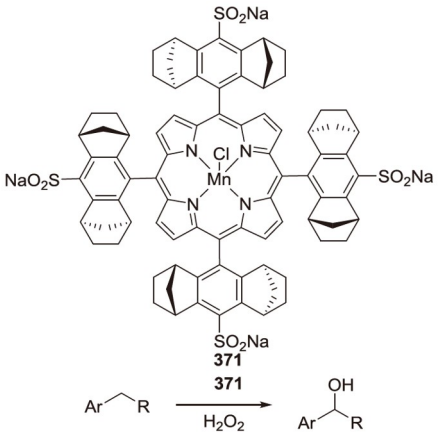

Substrate	conversion	alcohol/ketone ratio (%)	ee (%)
ethyl benzene	88	57/43	38
indane	88	77/23	32
tetralin	90	62/38	43
4-ethyltoluene	97	93/7	57
3-ethyltoluene	98	84/16	50
2-ethyltoluene	88	87/13	52
1-bromo-4-ethylbenzene	100	80/20	49

Reaction conditions: the reaction was conducted with syringe-pump addition of 5 equiv (relative to arylalkane) of H_2O_2 (30% in H_2O, diluted 5 times in MeOH) and imidazole (20 equiv relative to Mn) over 1 h at 25 °C to a solution of arylalkane/imidazole/**32** (40:4:1) in 0.4 mL of MeOH/PBS (pH 7) (1/1).

Figure 29 Water-soluble manganese porphyrins.

heterocyclic compounds were synthesized with high yield and excellent enantioselectivity.

8.2.3 Asymmetric amination of C–H bonds

In 1999, Che *et al*. [449] used chiral ruthenium (**414**) and manganese (**415**) porphyrins to catalyze the asymmetric amination of saturated C–H bonds in ethylbenzene and ethylnaphthalene, with 85% yield and 45%–58% ee (Scheme 120a). When using $PhI(OAc)_2$ as the oxidant, with the ruthenium porphyrin catalyst (**414**), the intramolecular asymmetric amination reaction can also be achieved, and the ee value was up to 87% (Scheme 120b) [450,451].

In 2019, Zhang *et al*. [452] activated sulfonyl azide with D_2-symmetric chiral cobalt porphyrin complexes for enantioselective radical 1,5-C–H amination which stereoselectively constructed 5-membered cyclic sulfonic acid amides (Scheme 121a). Interestingly, the absolute configuration of the 1,5-C–H amination product of sulfamic acid azide can be controlled by tuning the length of the bridge and other remote nonchiral elements of the cobalt catalysts (Scheme 121b) [453]. In 2020, the same group successfully used the cobalt-based metalloradical catalytic system for the enantioconvergent radical amination of a racemic tertiary C(sp^3)–H bond and constructed a chiral molecule with a quaternary stereocenter (Scheme 121c) [454]. Recently, they

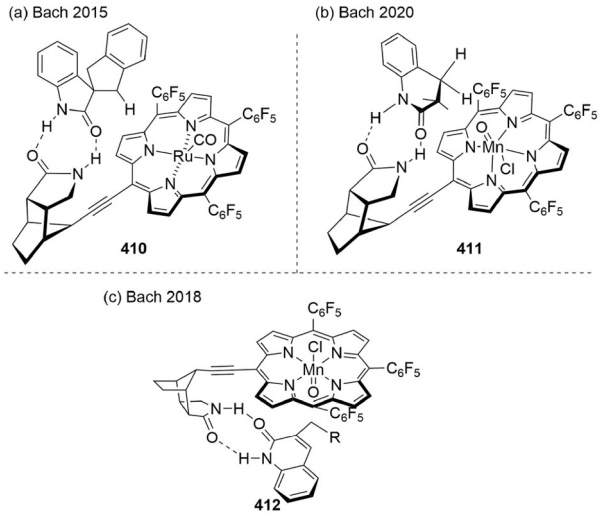

Figure 30 Hydrogen bond-directed asymmetric carbon-hydrogen bond oxidation.

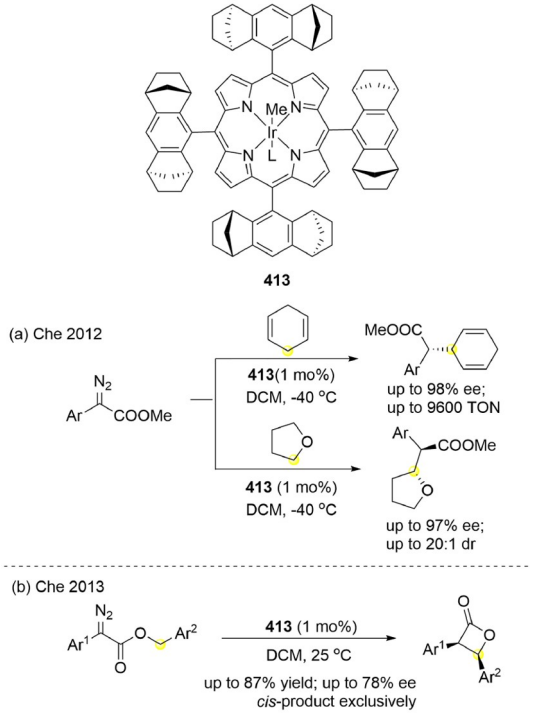

Scheme 118 Halterman porphyrin iridium-catalyzed asymmetric alkylation of C–H bonds (color online).

used alkoxysulfonyl azide derivatives derived from alcohols to perform asymmetric 1,5-C–H amination of alkoxysulfonyl azides with cobalt-based metalloradical catalysis to obtain five-membered chiral sulfamidates (Scheme 121d) [455], which can be used to deliver the corresponding chiral amino compound through the ring-opening reaction of the nucleophile.

Although significant progress has been made recently in intramolecular radical asymmetric C–H amination, intermolecular reactions remain a challenging problem. In 2020,

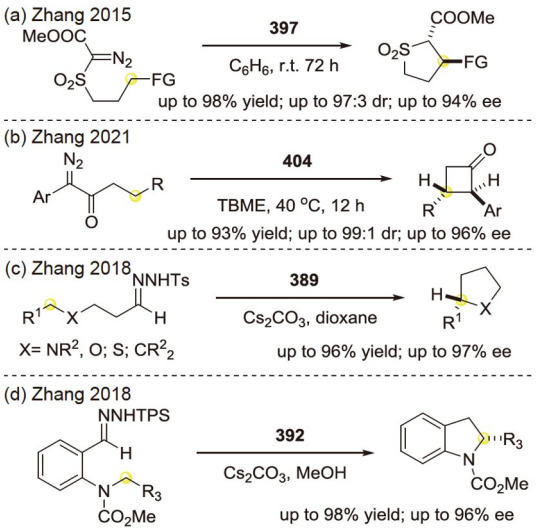

Scheme 119 Cobalt-based metalloradicals catalyze asymmetric C–H bond alkylation (color online).

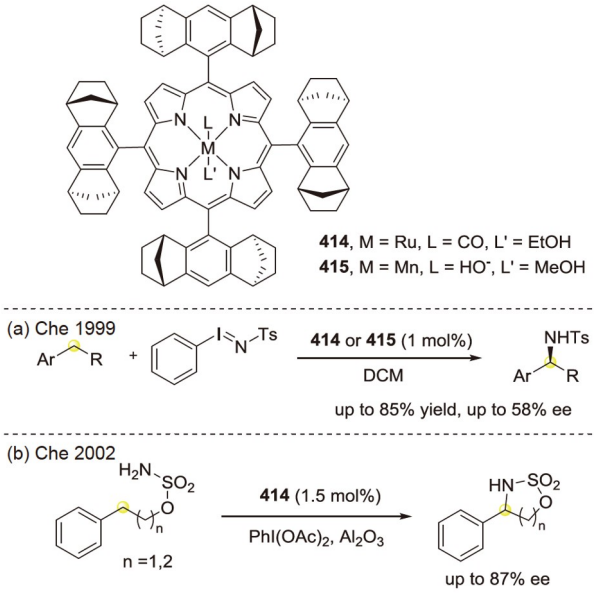

Scheme 120 Halterman's metal-porphyrin catalyzed asymmetric C–H bonds amination (color online).

Zhang *et al.* [456] used the cobalt-based metalloradical catalytic system to realize the intermolecular asymmetric C–H amination reaction of carboxylic and fluoroaryl azides (Scheme 122). The reaction can be carried out under mild conditions and provides an efficient way to obtain valuable chiral amino acid derivatives with high enantioselectivity.

8.3 Metalloporphyrin-catalyzed asymmetric sulfoxidation

In 1990, Grove *et al.* [375] used the vaulted iron porphyrin complexes (**342**) developed by their research group to catalyze the oxidation of sulfur compounds. The reaction can

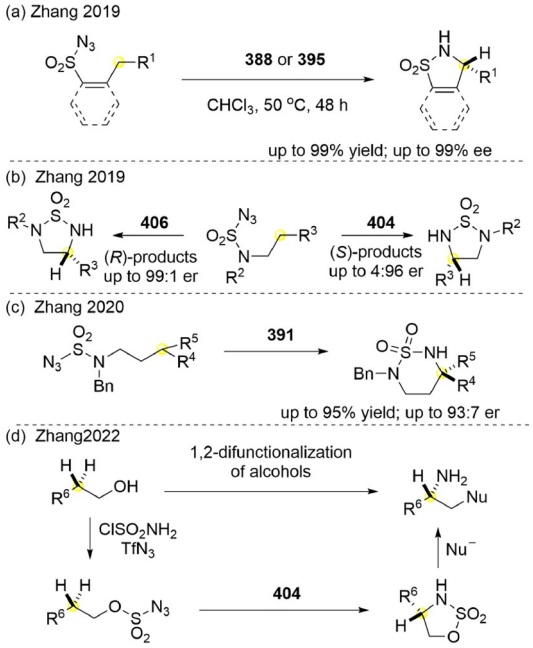

Scheme 121 Cobalt-based metalloradicals catalyze intramolecular asymmetric C–H bond amination (color online).

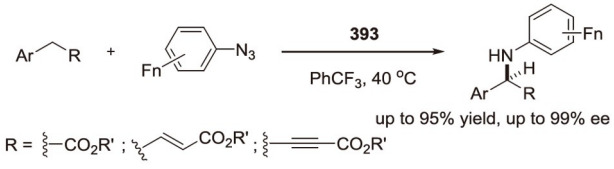

Scheme 122 Cobalt-based metalloradicals catalyze intermolecular asymmetric C–H bond amination.

produce the corresponding sulfoxide compounds in good yield, but its enantioselectivity is poor and the maximum ee value does not exceed 50% (Figure 31).

Naruta and Maruyama *et al.* [457,458] used their "twin crown" iron porphyrin (**343**) as a catalyst and iodoylbenzene as an oxidant to realize the asymmetric oxidation of sulfur-containing compounds in the presence of 1-methylimidazole. The reaction showed good enantioselectivity and catalyst turnover (Figure 32).

In 2006 and 2011, Simonneaux's group used Halterman's metalloporphyrin catalysts (**370**) [394] and Halterman's water-soluble metalloporphyrin catalysts (**371**) [459] to achieve asymmetric oxidation of sulfides. Protonic solvents such as methanol and hydrogen peroxide can be used as oxidants when using water-soluble iron porphyrin catalysts, and the ee value of the reaction can reach up to 87% (Figure 33).

8.4 Summary and perspectives of heme-oxygenase-based biomimetic asymmetric catalysis

Although the catalytic chemistry that mimics heme oxidase began many years ago, the research progress in this field has

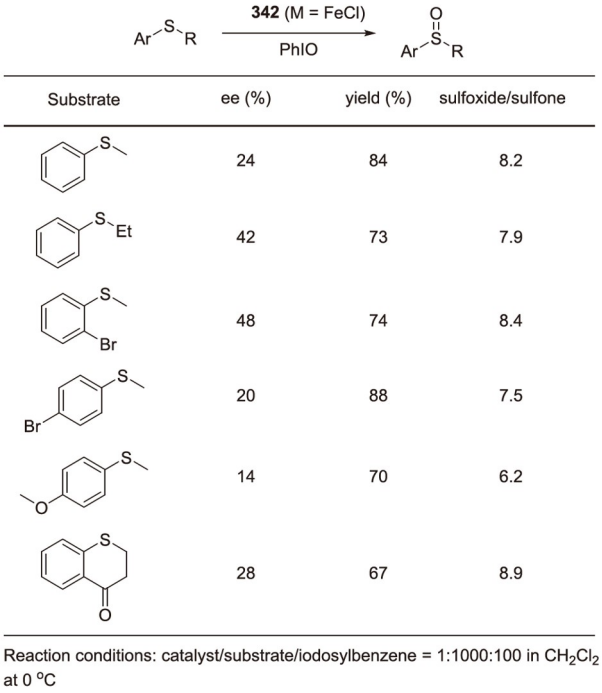

Figure 31 Asymmetric oxidation of sulfides catalyzed by vaulted iron porphyrin (**342**).

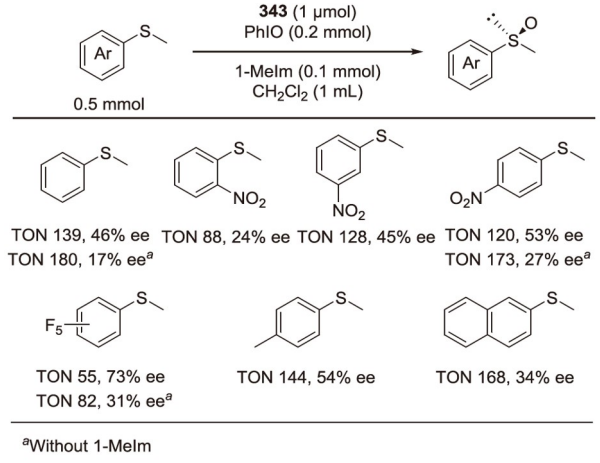

Figure 32 Asymmetric oxidation of sulfides catalyzed by "twin crown" iron porphyrin (**343**).

been relatively slow and has been hindered by the difficulty in the synthesis of chiral porphyrin compounds. The structure and mechanism of such enzymes remain to be further understood to facilitate the design and the development of catalysts, but due to the inertness of C–H bonds and the small difference in the reactivity of different C–H bonds, the asymmetric oxidation of C–H bonds is extremely challenging. Therefore, it is urgent to develop a chiral biomimetic catalytic system with higher activity and better selectivity to solve the oxidation problems. There are very few catalytic

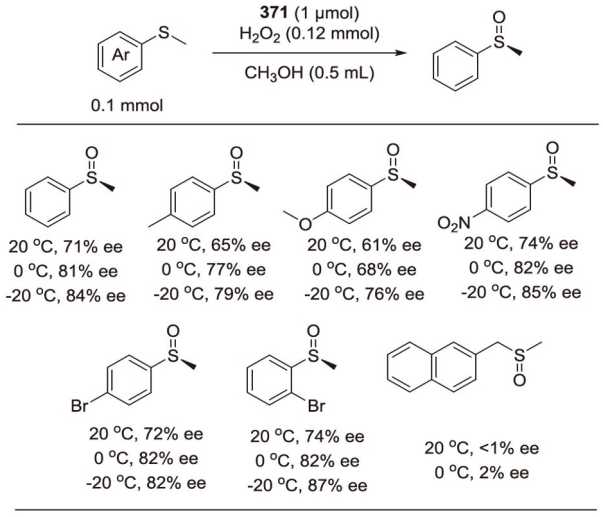

Figure 33 Asymmetric oxidation of sulfides with water-soluble metalloporphyrin catalysts (**371**).

systems that can effectively use O_2 as an oxidant. Therefore, the use of biomimetic strategies to achieve air oxidation of alkanes and alkenes will make the oxidation process more environmentally friendly and will have better industrial application value.

9 Nonheme oxygenase-based biomimetic asymmetric catalysis

There has been continued interest in the development of efficient catalysts for the enantioselective oxidation of organic molecules, since the resulting oxygenated motifs are prevalently found in pharmaceuticals and biologically active compounds [460–464]. In nature, nonheme iron enzymes that have iron active sites with a 2-His-1-carboxylate facial triad motif can carry out the highly selective O_2-dependent C–H and C=C oxidation reactions in the important metabolic processes [465,466]. As shown in Scheme 123a, these enzymes activate O_2 to generate high-valent iron(IV)-oxo species, thereby performing chemo- or enantioselective oxidation of various substrates. Actually, replicating the enzymatic reactivity with small artificial catalysts has been long recognized as an attractive strategy in oxidation chemistry [467]. Since the first crystal structure of a synthetic nonheme iron(IV)-oxo complex bearing a TMC ligand was reported in 2003 (Scheme 123b) [468], a great number of nonheme iron-oxo complexes, as well as other metal analogues, have been prepared, characterized, and investigated in various oxidation reactions [26]. These studies not only provided important insights into enzymatic pathways, but also offered valuable guidelines for the development of efficient oxidation catalysts. In addition to these characterizations of nonheme models, the use of nonheme iron complexes for catalytic oxidations has increasingly drawn much attention. In the past several decades, a plethora of nonheme metal complexes supporting with chiral linear tetradentate nitrogen (N4) ligands have been proven powerful catalysts for asymmetric oxidation reactions [469–472]. In this section, we describe these advances in the chemical evolution of the catalysts as well as the biomimetic oxidation reactions.

9.1 Asymmetric epoxidation of olefins with nonheme metal complexes

Asymmetric epoxidation (AE) of olefins is one of the most important organic transformations, since the resulting enantiomerically pure epoxides are highly useful building blocks in organic synthesis [460,461]. Not surprisingly, numerous efforts have been dedicated to development of the efficient catalysts. Impressively, the groups of Jacobsen [473] and Katsuki [474] independently developed the salen-Mn(III) complexes for the AE of a variety of unfunctionalized alkenes. However, regarding the catalytic efficiency and the involvement of environmentally harmful oxidants, the current catalytic methods for AE of olefins mismatch the requirements for the green chemistry [471]. Definitively, hydrogen peroxide and dioxygen are the ideal oxidant choice owing to the production of water as a sole byproduct. In 1999, Jacobsen *et al*. [475] reported an iron-based system *in-situ* generated from $FeCl_2$ and the polystyrene supported nitrogen ligands to perform the AE of olefins with hydrogen peroxide as the oxidant. A library of 5,760 ligand-metal complexes was rapidly screened by virtue of combinatorial chemistry (Scheme 124a). This pioneering work represented a significant step to emulate the reactivity of nonheme enzymes, although the level of enantiocontrol was still low. In 2001, Jacobsen and coworkers [476] demonstrated an iron (II)-mep complex for catalyzing epoxidation of olefins with H_2O_2 as the oxidant and acetic acid as a co-catalyst (Scheme 124b). This section will briefly introduce the well-defined iron and manganese complexes with chiral N4 ligands for the AE of olefins.

In 2003, Stack and coworkers [477] demonstrated that the manganese complex Mn(*R*,*R*-mcp)$(OTf)_2$ could efficiently catalyze the epoxidation of olefins with peracetic acid as the oxidant. However, they only examined the AE of vinyl cyclohexane to provide 10% ee (Figure 34, mcp). Along this vein, Costas and coworkers [478] modified the mcp ligand by fusing pinene rings at the pyridine moieties to afford a novel pinene-derived manganese complex. This complex provided a modest but remarkable enantioselectivity in olefin epoxidation (46% ee in the styrene epoxidation with peracetic acid). In 2009, Sun and coworkers [479] introduced aromatic groups into the framework of (*R*,*R*)-mcp to build a series of chiral N4 ligands (Figure 34, pmcp and bpmcp) and

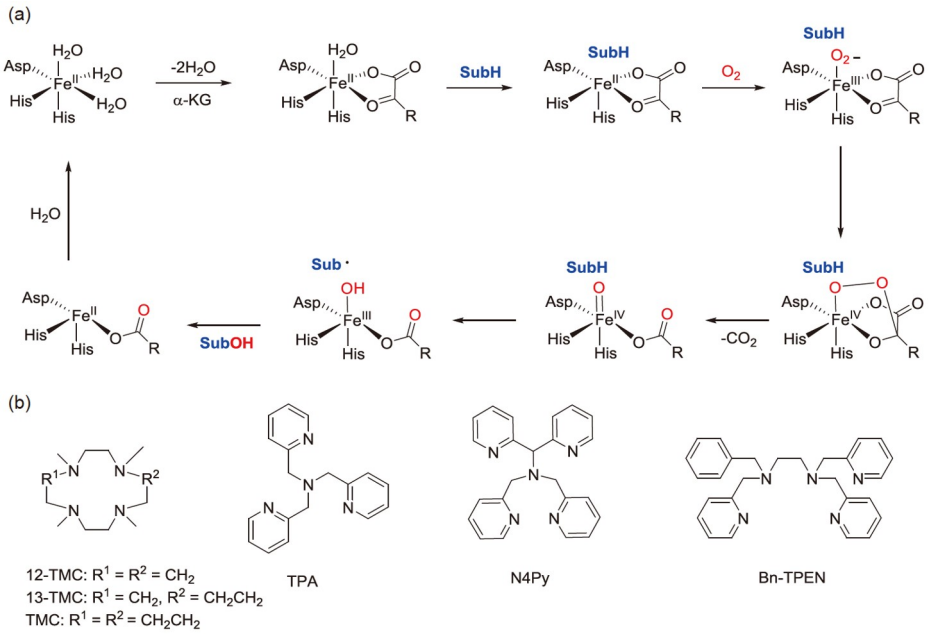

Scheme 123 (a) The catalytic cycle of α-KG-dependent enzymes. (b) Several examples of N4 or N5 ligands (color online).

these manganese complexes epoxidized various electron-deficient olefins in excellent yields with high enantioselectivities (up to 89% ee). This method employed hydrogen peroxide as the terminal oxidant and 5 equiv. of acetic acid (AA) as an additive. Additionally, the corresponding iron complexes could promote the AE of α,β-unsaturated ketones with up to 87% ee [480]. Since White's group [481] reported the (*S*,*S*-pdp)-Fe complex for the selective oxidation of aliphatic C–H bonds in 2007, Bryliakov *et al*. [482] and Costas *et al*. [483] examined the manganese complexes of pdp and bpbpp ligands for AE of olefins (Figure 34, pdp and bpbpp). Indeed, these complexes bearing a rigid bipyrrolidine backbone showed improved enantioselectivity than that of chiral mcp-Mn complex. In order to improve stereo-induction and catalytic efficiency, in 2012, Sun and coworkers [484] further prepared a C_1-symmetric *S*-peb ligand derived from *L*-proline and benzimidazole (Figure 34, *S*-peb). The *S*-peb-Mn complex could work well in the AE of olefins even at 0.01 mol% of catalyst loading, providing up to turnover numbers (TONs) of 9,600 and up to 95% ee. They also tested the application for the synthesis of important intermediate epoxyketone of Carfilzomib. Subsequently, Sun's group [485] achieved the AE of olefins with up to 98% ee using *S*-peb-Fe complex as the catalyst.

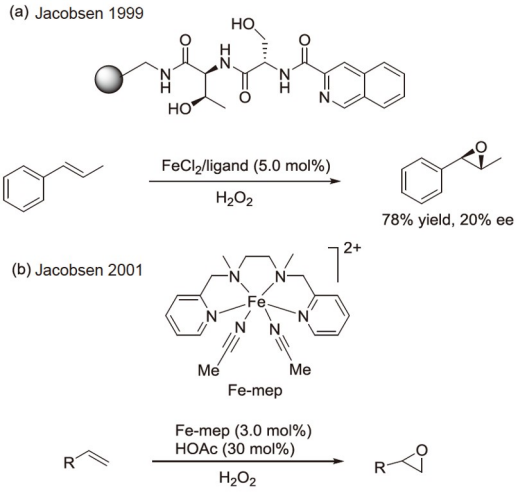

Scheme 124 Pioneering work for iron-catalyzed epoxidation of olefins with H_2O_2 as the oxidant.

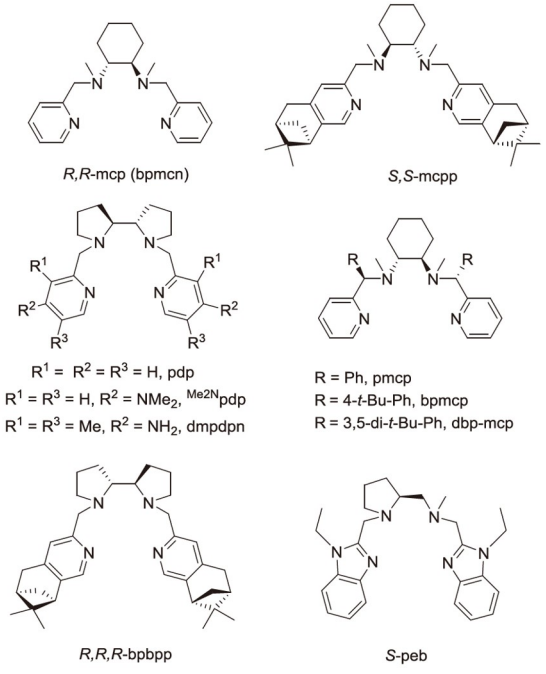

Figure 34 Typical chiral N4 ligands used in the AE of olefins.

More importantly, in 2012, Bryliakov, Talsi, and coworkers [486] described that the steric bulk of the carboxylic acid additive could affect the enantioselectivity of the epoxidation. Among the examined carboxylic acids, 2-ethylhexanoic acid (2-eha) led to the best stereocontrol. Therefore, they proposed that the carboxylic acid acted as a coligand coordinated to the possible Mn-oxo *via* an acid-assisted mechanism (Scheme 125). After evaluation of substituents on the γ-pyridine at the pdp ligand, in 2013, Costas and coworkers [487] identified that Fe(^{Me2N}pdp) provided the best activity and enantioselectivity in the AE of olefins. Incorporation with suitable carboxylic acid, such as 2-eha and *S*-ibuprofen, a variety of olefins could be converted to the epoxides with high enantioselectivities (up to 99% ee). It should be noted that the electron-rich Fe(^{Me2N}pdp) catalyst allowed for the use of catalytic amount of carboxylic acid (3 mol%) in this AE process. Moreover, using the same iron catalyst and with *N*-protected amino acid as an acid partner, they realized the AE of challenging α-alkyl-substituted styrenes (Scheme 126, up to 97% ee) [488]. Bryliakov with coworkers [489] also investigated the effect of steric and electronic properties of bipyrrolidine-derived N4 ligands, and an electron-rich Mn(dmpdpn) complex facilitated the AE of olefins with high efficiency and enantiocontrol (TON up to 8,500, and up to 99% ee; Figure 34, dmpdpn). After further elaboration of chiral N4 ligand in combination with a benzimidazole and a bulky pyridine, Costas's group [490] realized the AE of cyclic aliphatic enones in high yields and up to 99% ee using (*R*,*R*)^{Bz,TIPS}pdp-Fe catalyst (Scheme 127).

Apart from the use of carboxylic acid as the additive, Sun, Nam and coworkers [491] demonstrated that catalytic amount of sulfuric acid was suitable as the additive in the Mn-catalyzed asymmetric epoxidation. By employing aryl-substituted mcp-Mn complexes as the catalyst, typically (dbp-mcp)Mn(OTf)$_2$, the asymmetric epoxidation attained higher yields and enantioselectivities than those of catalytic systems using carboxylic acids. Computational mechanistic studies by density functional theory (DFT) suggested that a high-valent manganese(V)-oxo species can be generated as an epoxidizing intermediate *via* acid-promoted O–O bond heterolysis of a postulated Mn-OOH species (Scheme 128) [492].

The success of using the above chiral N4 metal catalysts in the asymmetric olefin epoxidations can be attributed to the reliable chiral N4 ligands and the key synergy of the carboxylic acid. Also, the structure of these iron and manganese catalysts is crucial to active oxidant. In principle, the linear N4 ligands in an octahedral coordination environment may exhibit *cis*-α, *cis*-β or *trans* topologies (Figure 35a) [493]. It is noteworthy that these above metal complexes exhibit a *cis*-α topology in which two potential *cis*-labile sites for the binding of both H_2O_2 and carboxylic acid facilitate the heterolytic O–O bond cleavage. Due to the lack of direct evidence, Sun, Nam and coworkers [494] further investigated the mechanism by employing nonheme manganese catalysts with a chiral N4 (ProBn2Py) ligand and a N5 (Pro3Py) ligand (Figure 35b). Actually, the use of Mn-N5 catalyst cannot promote the epoxidation under the same reaction conditions as that of Mn-N4 catalyst.

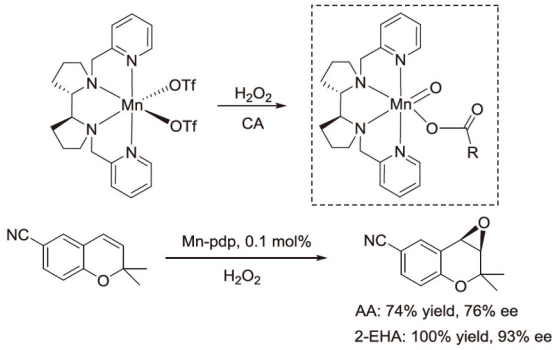

Scheme 125 Bulky carboxylic acid assisted AE of olefins with pdp-Mn complex.

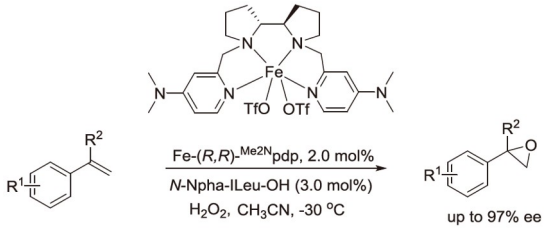

Scheme 126 Synergistic interplay of a nonheme iron catalyst and N-protected amino acid for AE of α-alkyl-substituted styrene.

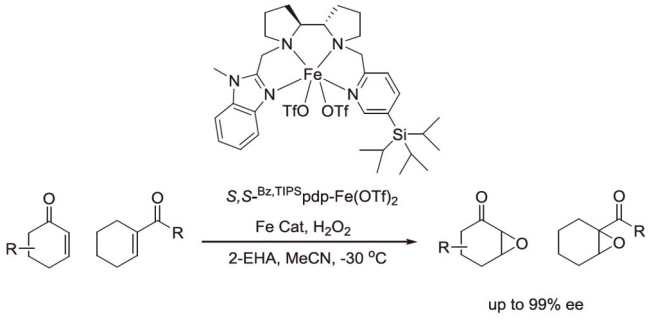

Scheme 127 AE of cyclic enones catalyzed by nonheme iron catalyst with H_2O_2.

Understanding the relationship between the ligand topologies and the reactivity of this class of metal complexes are important for the design of efficient bioinspired catalysts. More recently, Sun *et al.* [495] prepared a class of manganese complexes with 4-*tert*-Bu-phenyl-substituted mcp ligands, and the single-crystal X-ray analysis revealed these complexes adopted a special quasi-*trans* topology irrespective of the different groups on the pyridine donors and the coordinated anions. These quasi-*trans* topology manganese

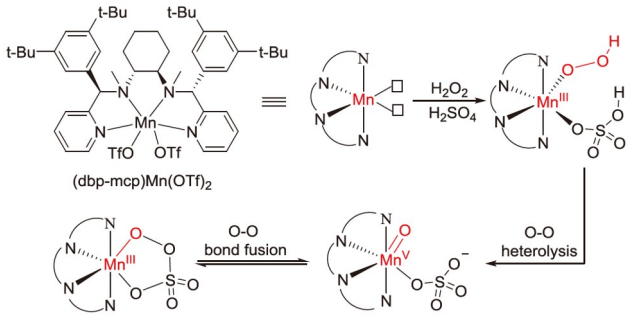

Scheme 128 Possible intermediates for the (dbp-mcp)Mn(OTf)$_2$ with H_2O_2 in the presence of sulfuric acid (color online).

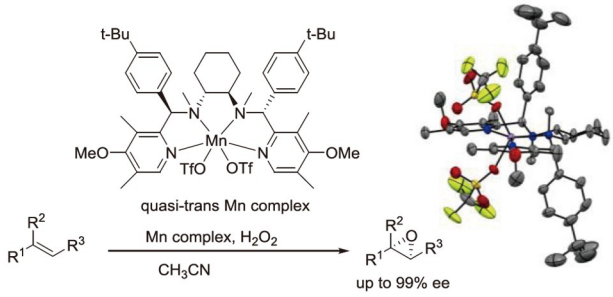

Scheme 129 AE of olefins catalyzed by a quasi-trans Mn-N4 complex (color online).

complexes could catalyze AE of olefins with H_2O_2. Possibly, interconversion between quasi-*trans* and *cis*-α topologies could occur in the solutions (Scheme 129).

Despite these significant advances, these bioinspired catalysts still suffer from catalyst decomposition under oxidizing conditions. Gebbink and coworkers [496] disclosed a typical decomposition pathway *via* C–H oxidation on the 2-pyridinylmethylene sites of the complexes by the active oxidants generated *in situ*. In this context, Sun and coworkers [497] prepared a series of porous organic polymer-supported Mn-N4 catalysts in which the single-site catalytic units were dispersed in the skeleton of porous organic polymers. As expected, these porous single-site Mn-N4 catalysts demonstrated excellent activity and recyclability in both C–H oxidation and AE reactions. Considering the enantioinduction, efficiency, and substrate scope, these above achievements represent the state-of-the-art progress in the field of asymmetric olefin epoxidation. Encouragingly, on the basis of AE catalytic system by Sun's group [484,498], Walker *et al.* recently accomplished the kilogram-scale synthesis of the epoxyketone of carfilzomib with a 0.04 mol% loading of chiral Mn-N4 catalyst [499].

9.2 Asymmetric *cis*-dihydroxylation of olefins with nonheme metal complexes

Among the methods for functionalization of olefins, asymmetric *cis*-dihydroxylation of olefins is a powerful tool to introduce both stereo- and enantiospecific diol units into organic molecules. Sharpless asymmetric dihydroxylation of olefins using OsO_4 and chiral phthalazine ligands has proven the most successful approach [500]. The environmentally

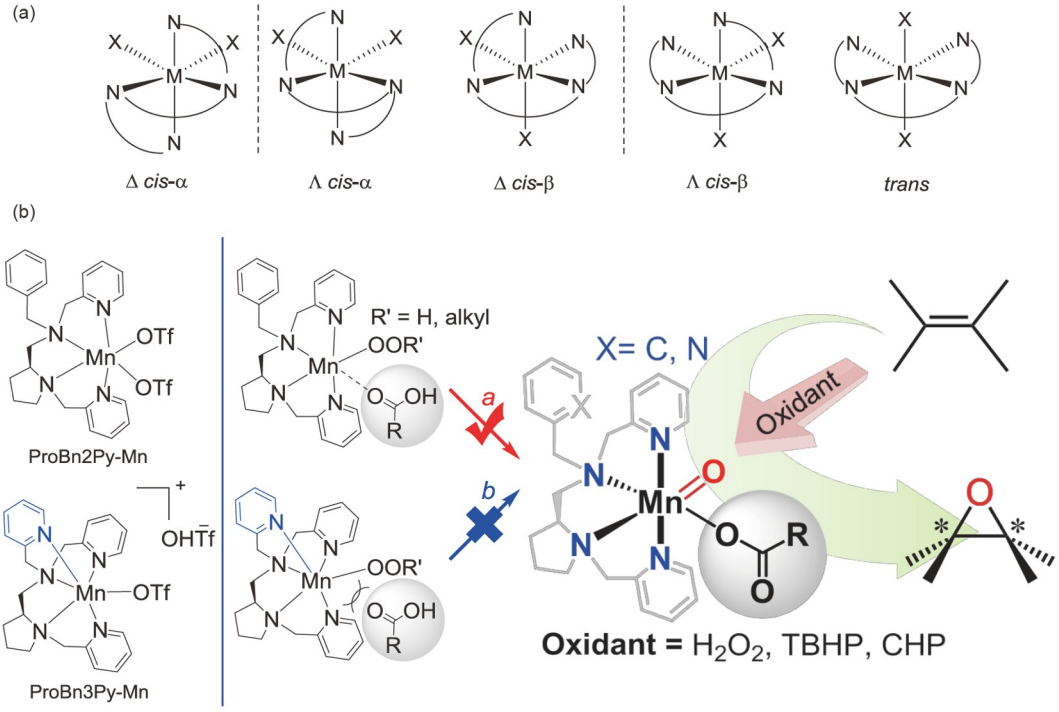

Figure 35 (a) Possible topologies for octahedral metal complexes with linear N4 ligands. (b) Mechanistic studies with N4/N5 manganese complexes (color online).

benign metal catalyst is still demanding due to the toxicity and cost of osmium reagent. In this context, Rieske dioxygenases, having a mononuclear iron center to a 2-His-1-carboxylate motif, can perform the *cis*-dihydroxylation of C=C bonds in the biodegradation of arenes [501,502]. Inspired by these unique property, in 2001, Que and coworkers [503] demonstrated the first example of an Fe-catalyzed asymmetric *cis*-dihydroxylation of olefins with Fe(*S*,*S*-6-Me_2-BPMCN)$(OTf)_2$ as the catalyst and H_2O_2 as the oxidant (Figure 36). In the case of asymmetric *cis*-dihydroxylation of *trans*-2-octene, 82% ee was obtained. However, olefin should be used in a 50-fold excess with respect to the oxidant. In 2008, they realized the asymmetric *cis*-dihydroxylation of olefins in up to 97% ee using Fe^{II}(*R*,*R*-6-Me_2-BPBP)$(OTf)_2$ catalyst, wherein a rigid bipyrrolidine was involved in the chiral N4 ligand (Figure 36) [504]. In 2011, a more practical method for asymmetric *cis*-dihydroxylation of electron-deficient olefins was developed by Che and coworkers [505]. This method employed a Mn-(*S*,*S*-BQCN) complex as the catalyst and Oxone as the oxidant to provide the chiral diols with up to 96% ee.

Along the same line, in 2016, Che and coworkers [506] investigated a variety of substituted *R*,*R*-BQCN-Fe$(OTf)_2$ complexes for the asymmetric *cis*-dihydroxylation of olefins. Among these complexes, Fe-(*R*,*R*-2-Me_2-BQCN)$(OTf)_2$ complex showed outstanding performance in the asymmetric *cis*-dihydroxylation of olefins under substrate-limiting conditions (Figure 36, up to 99.8% ee). Notably, various simple olefins could be well tolerated, for example, the reaction of *trans*-4-octene afforded the desired product in 99% ee. In a subsequent study, they modified this BQCN-type ligands with classic 1,2-diphenylethane-1,2-diamine backbone instead of cyclohexane-1,2-diamine to get several novel substituted BQPN ligands. A variety of trisubstituted electron-deficient olefins could be efficiently oxidized to chiral *cis*-diols with high yields and enantioselectivities using Fe-(*R*,*R*-2-Me_2-BQPN)$(OTf)_2$ as the catalyst (Figure 36, up to 99.9% ee) [507]. More recently, Wang, Nam and coworker [508] reported the asymmetric *cis*-dihydroxylation of substituted aliphatic acrylates to produce a diverse set of *cis*-2,3-dihydroxy esters by using the [Fe-(*R*,*R*-2-Me_2-BQCN)$(MeCN)_2$]$(ClO_4)_2$ (Figure 36). In these reactions, the iron complex with perchlorate counteranions is more reliable than that of Fe-(*R*,*R*-2-Me_2-BQCN)$(OTf)_2$. This above asymmetric *cis*-dihydroxylation method based on the nonheme iron catalysts and H_2O_2 represent a green and practical approach. The success strongly depends on the elaboration of the chiral N4 ligands.

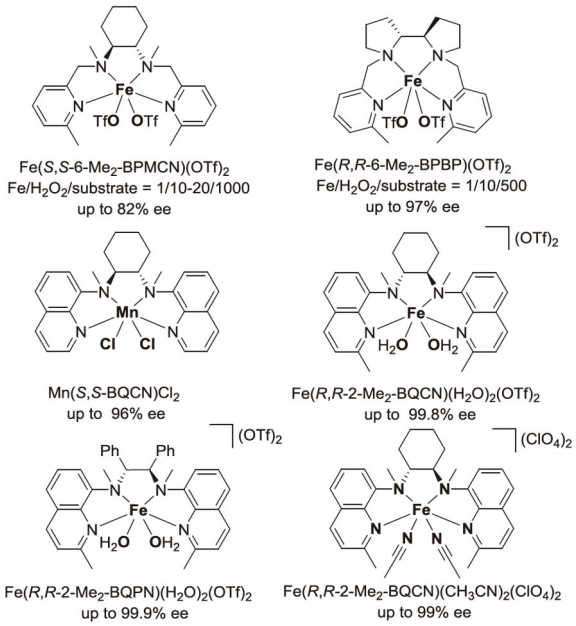

Figure 36 Chiral N4-Fe catalysts used in the asymmetric *cis*-dihydroxylation.

9.3 Asymmetric C–H oxidation catalyzed by nonheme metal complexes

The enantioselective oxidation of C–H bonds offers a direct yet challenging tool for the transformation of organic molecules into chiral oxygen-containing compounds [509,510]. In nature, heme and nonheme enzymes that oxygenate a variety of organic compounds with high efficiency and specificity have thus inspired the intensive biomimetic studies over the several past decades. In 1989, Groves and coworkers [436] demonstrated the first example of asymmetric hydroxylation of ethylbenzenes by a chiral iron-porphyrin. According to the C–H bond hydroxylation by high-valent metal-oxo complexes, it follows the H-atom abstraction and subsequent oxygen-rebound mechanism that has been well-established in heme systems [511]. However, the enantioselective oxidation of C–H bonds has long been a formidable challenge, especially in the unactivated C–H bond oxidation. In this regard, more reliable chiral catalysts are highly desirable. The intensive studies of chiral N4 ligands and their oxidation catalysis indeed provide the opportunities to accomplish the enantioselective oxidation of C–H bonds in some types of substrates. Since the selective oxidation of aliphatic C–H bonds with (*S*,*S*-pdp)-Fe complex was reported by White *et al*. [481] in 2007, surprisingly, no further investigation on the enantioselective oxidation of aliphatic C–H bonds was attempted for a long time. In 2012, Bryliakov and coworkers [512] investigated the stereospecific oxidation of aliphatic C–H with mcp-Mn or pdp-Mn (typically, with 0.1 mol% loading) and H_2O_2 in the presence of acetic acid. Later, Sun and coworkers [513] reported the efficient benzylic and aliphatic C–H oxidation in methylenic sites with proline-derived pmb-Mn complex and H_2O_2. To a large extent, these studies trigger the subsequent enantioselective oxidation of C–H bonds due to the attractive reactivity of these manganese complexes.

In 2017, Costas, Bietti and coworkers [514] achieved the enantioselective aliphatic C–H oxidation with a Mn(*S*,*S*-^{TIPS}ecp) complex to prepare a series of monosubstituted *N*-cyclohexylalkanamides. After a systematic survey of iron, manganese complexes as well as carboxylic acid partners, they identified the catalytic system with Mn(*S*,*S*-^{TIPS}ecp) complex and cycloproanecarboxylic acid to achieve high level of site- and enantioselective C–H oxidation (Scheme 130). In the same year, Sun and Nam [515] reported the kinetic resolution of racemic secondary alcohols with previous (*R*,*R*-dbp-mcp) $Mn(OTf)_2/H_2O_2/H_2SO_4$ catalytic system. Actually, the oxidation of racemic secondary alcohols also involved the enantioselective C–H oxidation. DFT calculations revealed that the energy barriers for the α–C–H bond activation of 1-phenylethanol (*R*- and *S*-enantiomers) by a high-valent manganese-oxo species are significantly different. Bryliakov and coworkers [516] also explored the enantioselective benzylic hydroxylation of arylalkanes with a trifluoroethoxy-substituted Mn(^{TFE,Me}pdp) complex as the catalyst and *N*-Boc-(*S*)-proline as the acid additive, affording 1-arylalkanols in up to 86% ee. In 2018, Sun, Nam and coworkers [517] established a useful method for the enantioselective oxidation of benzylic methylene in spirocyclic precursors to produce chiral spirocyclic β,β′-diketones with high yields and enantioselectivities, wherein *S*-peb-Mn complex was proved to be a suitable catalyst (Scheme 131). This catalytic system was also applicable to the enantioselective oxidation of spirocyclic oxindoles and quinolinones. According to the asymmetric oxidation of spirocyclic quinolinones, the corresponding alcohols could be obtained in up to 99% ee [518]. In 2019, Costas, Bietti and coworkers [519] reported the enantioselective lactonization of unactivated methylenes in up to 99% ee *via* a Mn-catalyzed C–H oxidation directed by carboxylic acids (Scheme 132a). More recently, they further expanded this strategy to modify α-amino acids and α,α-disubstituted α-amino acids. In the cases of α,α-disubstituted α-amino acids, lactonization of γ-methylenic site provided the desired products with outstanding diastereo- and enantioselectivity (up to 97% ee) [520]. In these approaches, fluorinated alcohol, such as 2,2,2-trifluoroethanol (TFE), was selected as the solvent, and it might assist H_2O_2 activation as well as the subsequent lactonization of the resulting hydroxy acid because of its mild acidity and high polarity. They also showed that TFE as reaction solvent enhanced the aliphatic hydroxylation selectivity in the Mn-catalyzed aliphatic C–H bond oxidation [521]. Bryliakov and coworkers [522] further examined the benzylic hydroxylation of arylalkanes in fluorinated alcohols, and up to 89% ee was observed with 2,2-difluoroethanol as the reaction solvent. Subsequently, they established a one-pot sequential asymmetric hydroxylation/oxidative kinetic resolution approach for the synthesis of chiral alcohols, where hexafluoroisopropanol was used as a solvent (Scheme 132b) [523]. Prompted by these achievements, Sun and coworkers [524] recently reported the diastereo- and enantioselective hydroxylation of benzylic methylene C–H bonds of indane-derived ketones catalyzed by the *S*-peb-Mn complex. By employing TFE as the reaction solvent, the benzylic alcohols were furnished in high levels of diastereoselectivities (up to >95:5) and enantioselectivities (up to 95% ee) (Scheme 133).

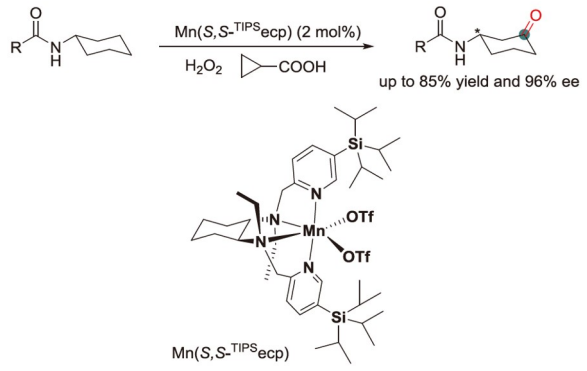

Scheme 130 Enantioselective C–H oxidation of N-cyclohexylamides with a nonheme manganese complex (color online).

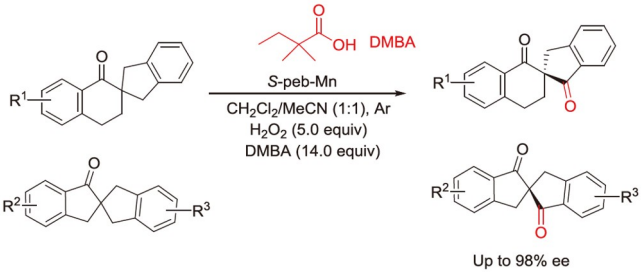

Scheme 131 Enantioselective benzylic C–H oxidation catalyzed by *S*-peb-Mn complex (color online).

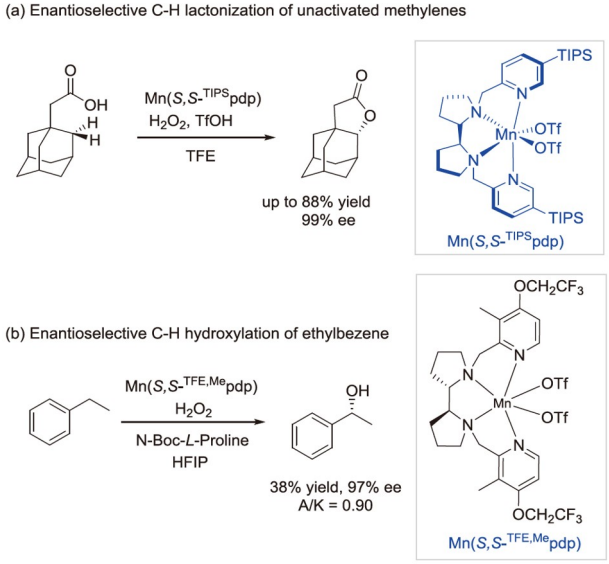

Scheme 132 Enantioselective C–H oxidation catalyzed by pdp-Mn catalysts (color online).

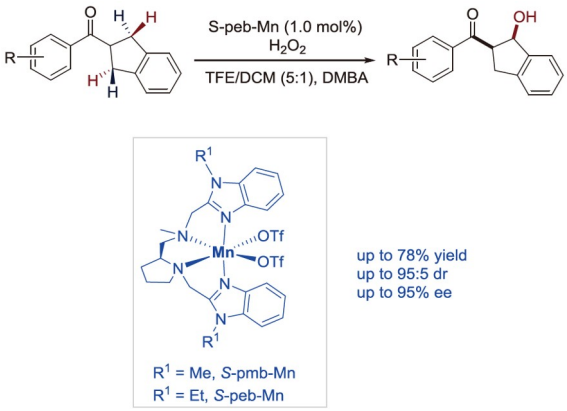

Scheme 133 Diastereo- and enantioselective benzylic C–H oxidation with proline-derived manganese complexes (color online).

9.4 Summary and perspectives of nonheme oxygenase-based biomimetic asymmetric catalysis

Nature has evolved unique ability to perform an array of metabolically vital oxidative transformations by using iron-containing enzymes, thereby offering a strong basis for developing efficient oxidation catalysts. In the past two decades, we have witnessed the rapid growth in the field of asymmetric oxidation reactions with chiral nonheme iron and manganese complexes. Remarkably, a great number of chiral linear N4 ligands have been designed and prepared, and their metal complexes such as Fe and Mn have shown versatile and unprecedented performance in asymmetric olefin epoxidation, *cis*-dihydroxylation, and enantioselective C–H oxidation reactions. The success was strongly inspired by the introduction of chiral linear N4 ligands that feature facile structural modification in both electronic and steric properties. Despite significant advances, we cannot neglect the catalyst decomposition because of the generation of highly active oxidants under oxidizing conditions. Therefore, how to address this paradox existing in the oxidation catalysis remains a demanding task. It is anticipated that there will be a solution for the access of more efficient oxidation catalysis.

10 Biomimetic asymmetric catalysis mediated by dinuclear & multinuclear metal complexes

Conventionally, the metal-based catalysts used in asymmetric transformations consist of a single metal center supported by a chiral ligand. Despite tremendous progress in this area, there are still a number of important asymmetric reactions that lack of efficient chiral catalysts. As an important source of inspiration for the development of artificial chiral catalysts, Nature has already developed some specific and highly selective catalysts for reactions that are difficult to achieve in organic chemistry, namely, metalloenzymes containing two or more metal ions in proximity as their active sites (Figure 37) [525]. The metal centers in these metalloenzymes usually demonstrate cooperative effects by synergistic interaction with the reactants, thus achieving amazing efficiency and outstanding selectivity in the catalysis. For example, the urease was known to catalyze the conversion of urea to ammonia and carbon dioxide *via* the cooperative action of the two nickel(II) centers in the process. Imitating the dinuclear active sites of biocatalysts, the development of chiral dinuclear/multinuclear metal complexes for asymmetric catalysis has attracted great attention, owing to the potential synergistic effects between the metal centers for the activation of reagents in a chiral environment, and thus may achieve enhanced catalytic activities and selectivities compared with the traditional approach based on mononuclear systems. Herein, some representative applications of (bio-inspired) chiral bi- or multi-metallic catalysts in the area of asymmetric catalysis are highlighted.

10.1 Chiral multimetallic self-assembled complexes developed by Shibasaki group

Shibasaki's group pioneered the use of multifunctional homo- and hetero-metallic catalysts in asymmetric transformations. In 1992, Shibasaki and coworkers [526] reported a groundbreaking study using a BINOL-based polymetallic complex as the catalyst for asymmetric nitroaldol reaction, which generally contains one rare metal, three alkali metals and three chiral BINOL units (Scheme 134a). The bifunctional nature of this type of catalysts, *i.e.*, the Lewis acidity at the lanthanide center and Brønsted basicity at the alkoxide sites counterbalanced by the proximal alkali metal cations, was believed to be crucial for the catalysis, enabling a high yield (91%) and excellent enantioselectivity (90% ee) of the reaction. Soon after, the same group disclosed an asymmetric conjugate addition of malonates to α, β-unsaturated ketones using similar multimetallic catalyst, with Na^+ ions as the alkali metal cations in this case (Scheme 134b), giving the corresponding products in high yields (89%–98%) with good to excellent enantioselectivities (72%–92% ee) [527]. Since then, a series of multimetallic complexes self-assembled *in situ* from various rare earth-and alkali metals with BINOLs, linked-BINOLs, and dinucleating Schiff bases have been developed by Shibasaki's group and successfully applied as catalysts in a variety of enantioselective transformations, including nitroaldol reaction, direct aldol reaction, Michael reaction, epoxidation of enones, epoxide opening reaction, Diels-Alder reaction, nitro-Mannich reaction, cyanosilylation of aldehydes and ketones, Strecker reaction, and Reissert reaction, and these achievements have been well summarized in several excellent reviews (Scheme 134c) [528].

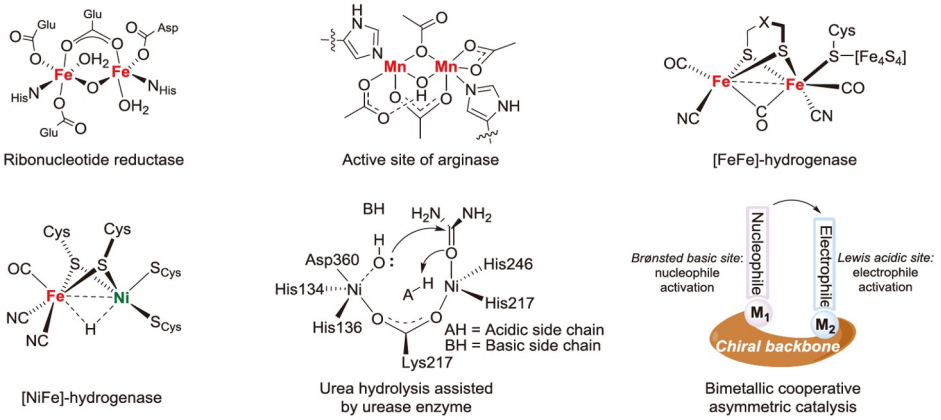

Figure 37 Selected examples of the metalloenzymes containing binuclear sites (color online).

10.2 Chiral metallosalen-type bimetallic systems

Chiral metallosalen complexes have been widely used as a class of privileged catalysts in asymmetric catalysis [529]. Interestingly, cooperative bimetallic reaction mechanisms, in which both the electrophile and the nucleophile are activated simultaneously by two catalyst molecules, have been established in several transformations catalyzed by metallosalens [530]. Jacobsen's group have made seminal contributions to the studies on asymmetric catalysis using bimetallic salen metal complexes, typically comprising of two or more metallosalen moieties tethered together in the catalyst skeleton by a linker unit, which demonstrated greatly enhanced reactivity as compared with monomeric catalysts and often with improved enantioselectivity. The first example reported by Jacobsen's group [531] in 1998 was a series of dinuclear Cr(salen) complexes of covalently linked dimeric salen ligand used for the asymmetric ring opening of epoxides by trimethylsilly azide (Scheme 135a). Besides the asymmetric epoxide ring-opening reactions, oligomeric metallosalen catalysts have also displayed enhanced efficiency in asymmetric conjugate addition of trimethylsilyl cyanide to α,β-unsaturated carbonyl derivatives and enantioselective intramolecular ring-opening reaction of oxetanes [532]. In 2010, Ding and coworkers [533] reported a dimeric titanium complex in which the two salen units were connected through a covalent tether, which was demonstrated to be one of the best catalysts developed so far for the enantioselective cyanation of aldehydes in terms of catalytic efficiency, enantioselectivity and substrate adaptability (Scheme 135b).

Chiral metallosalen-type bimetallic systems have also been successfully applied in the enantioselective polymerization of epoxides. In 2010, Coates and coworkers [534] reported an asymmetric catalytic ring-opening polymerization of a variety of monosubstituted epoxides using an enantiopure bis(salencobalt) complex as a highly active catalyst, leading to the formation of enantiopure epoxides and isotactic polyethers from racemic epoxides (Scheme 136a). In this case, a covalently tethered bimetallic complex featuring a chiral binaphthol linker was proved to be highly active and selective in this reaction. In 2013, Lu and coworkers [535] reported a chiral catalyst system based on enantiopure dinuclear Salen-Co(III) complexes, which exhibited excellent activity and high enantioselectivity in desymmetrization copolymerization of meso-epoxides with CO_2 to give optically active polycarbonates (Scheme 136b). Later, Lu's group [536] also developed the synthesis of stereoregular polyesters by the asymmetric copolymerization of meso-epoxides and cyclic anhydrides using catalyst systems based on enantiopure bimetallic Salen complexes.

10.3 Chiral dinuclear ProPhenol/Zn catalysts

In 2000, Trost and coworkers [537] developed a chiral ProPhenol/Zn catalyst (Scheme 137a) for enantioselective direct aldol reactions between aryl methyl ketones and aldehydes, affording the chiral aldol adducts in good yields with high enantioselectivities (Scheme 137b). As a member of the chiral aza-crown family, the ProPhenol ligand can spontaneously form a bimetallic complex upon treatment with an alkyl metal reagent such as Et_2Zn. The resulting complex features Lewis acidic and Brønsted basic sites, thus both nucleophile and electrophile can be simultaneous activated in the same chiral environment, allowing for new bond formation in a highly effective and stereoselective manner. Upon treatment of the *in situ* prepared catalyst solution with *p*-nitrophenol, Ding and coworkers [538] successfully elucidated the dinuclear structure of a chiral ProPhenol/Zn-type catalyst *via* X-ray analysis in 2005. After Trost's seminal work, this type of prominent dinuclear metal-ProPhenol catalysts have been successfully used in a variety of enantioselective reactions such as desymmetrization of meso-diol, alkynylation, Mannich, Henry and Friedel-Crafts re-

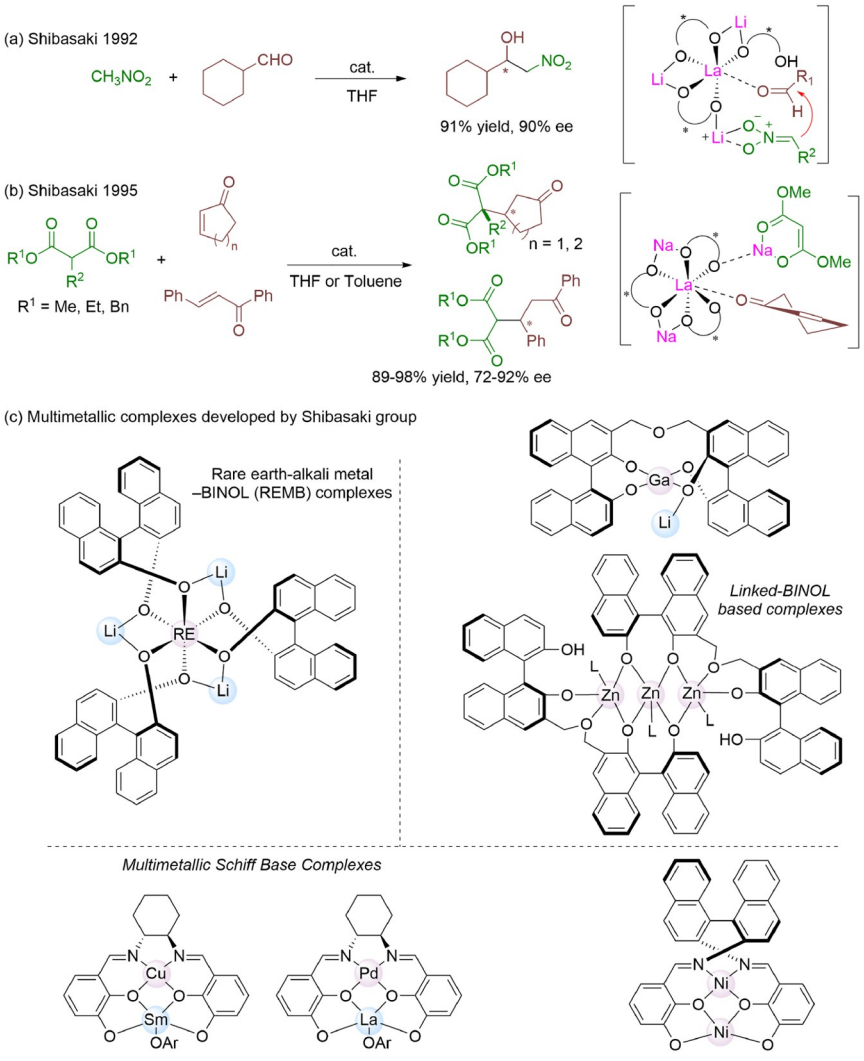

Scheme 134 Chiral homo- and hetero-metallic catalysis developed by Shibasaki group (color online).

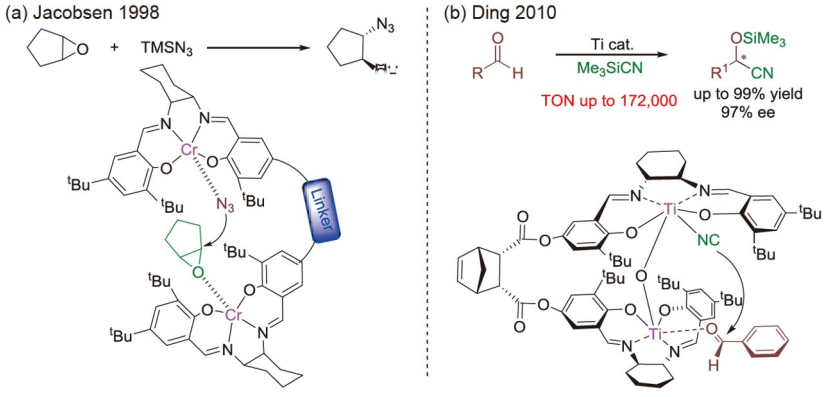

Scheme 135 Selected examples of asymmetric catalytic reactions with chiral bimetallic salen complexes (color online).

actions, and much of the progress has been well summarized in an excellent review by Trost and coworkers [539]. In 2021, Huang and coworkers [540,541] reported an elegant reductive desymmetrization of malonic esters catalyzed by a dinuclear zinc complex with an unsymmetrical tetradentate chiral ligand (Scheme 137c). The reduction features excellent enantiocontrol that can differentiate sterically similar substituents and high chemoselectivity towards the diester

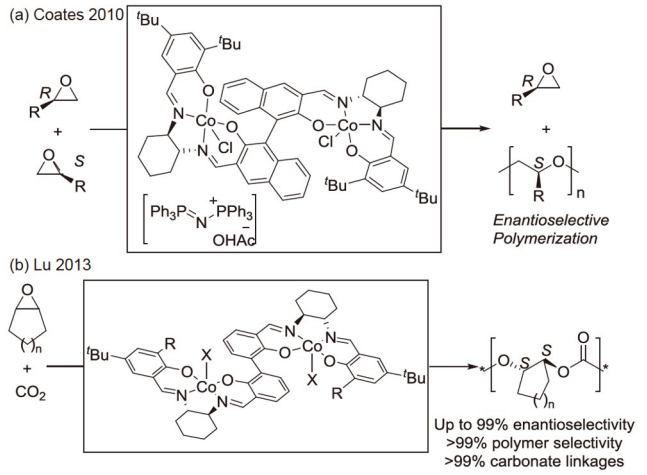

Scheme 136 Chiral bimetallic salen catalysis in enantioselective polymerization.

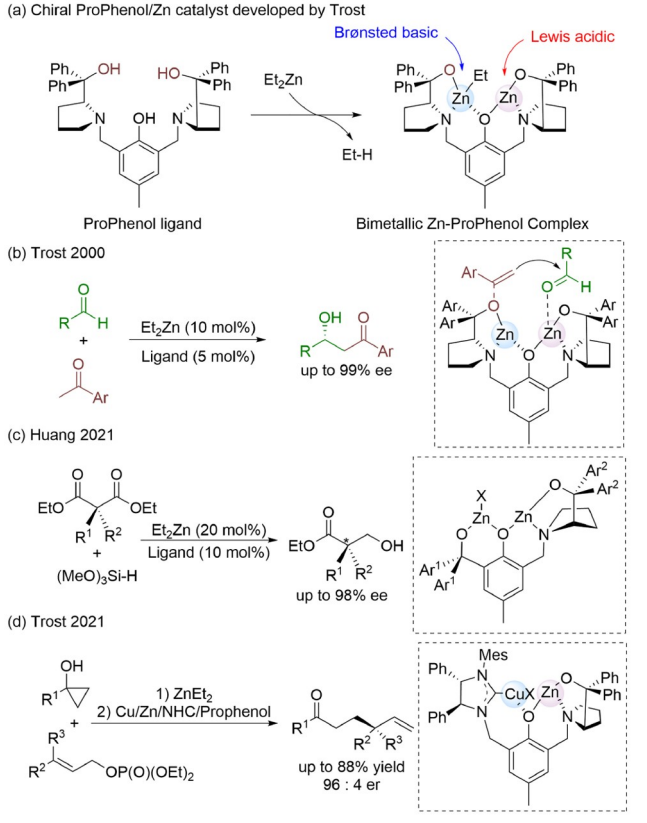

Scheme 137 Chiral ProPhenol/Zn catalysts in asymmetric synthesis (color online).

motif, giving α-quaternary β-hydroxyesters in good yields with excellent ee values. In 2021, Trost *et al*. [542] reported the development of a modified ProPhenol ligand by replacing one of the chiral prolinol arms with a chiral NHC moiety, the so-called NHC-ProPhenol ligand, which was found to facilitate the formation of the hetero-bimetallic Zn-Cu catalyst (Scheme 137d). This chiral Cu/Zn heterobimetallic complex has been successfully applied in the asymmetricallylic alkylation reactions of allyl phosphates with zinc keto-homoenolates, leading to the formation of various γ-vinyl ketones in good regio- and enantioselectivities.

10.4 Other selected chiral dinuclear metal catalysts

In 2002, Gong and coworkers [543] reported an enantioselective oxidative coupling of 2-naphthol derivatives, using oxovanadium complexes derived from chiral biphenol or binaphthol as the catalysts and air or oxygen as the terminal oxidant (Scheme 138). An intramolecular radical-radical coupling pathway involving catalytic species bearing two vanadium metal centers was suggested as the key step in this reaction. A closely related homodinuclear vanadium-Schiff base complex for oxidative coupling reactions was also reported by Sasai and coworkers [544].

In 2003, Martell and coworkers [545] reported the use of a structurally defined chiral dinuclear Cu complex as the precatalyst for the asymmetric oxidative coupling of 2-naphthol, leading to the formation of binaphthol in good yield and good enantioselectivity (Scheme 139). In this catalyst structure, two Cu metal centers are bound by two N_2O_2 moiety in the cavity formed in the fused chiral polyamino macrocycle ligand.

In 2008, Peters and Jautze [546] reported the use of a planar-chiral ferrocenyl bispalladacycle for the catalytic enantioselective Michael addition of trisubstituted α-cyanoacetates to enones, affording the corresponding Michael adducts with excellent yields (TONs up to 2450) and high enantioselectivities (Scheme 140). It was proposed that the α-cyanoacetate can be activated by coordination of the nitrile moiety to one Pd^{II} center, while the enone might be simultaneously activated by coordination of the olefinic double bond to the carbophilic Lewis acid Pd^{II}, thus leading to superior catalytic activity and a high level of stereocontrol.

Zhang and coworkers [547] reported in 2012 the development of a chiral bimetallic Ru catalyst based on a ruthenocenyl phosphino-oxazoline ligand (RuPHOX), which showed good activity and high enantioselectivity in asymmetric hydrogenation of various C=O and/or C=C substrates. It should be highlighted that this bimetallic Ru catalyst has been applied in the synthesis of dihydroartemisinic (DHAA) in 98% yield with 99.7:0.3 er, a key intermediate for the synthesis of artemisinin (Scheme 141) [548]. Under otherwise identical conditions, the corresponding *mono*-RuPHOX/Ru complex gave lower reaction activity and inferior enantioselectivity compared with the binuclear catalyst, suggesting that the both Ru atoms of the RuPHOX-Ru act as catalytic sites and are essential for the excellent catalytic behavior, which is proposed to improve the catalytic activity and to establish a bulkier steric hindrance.

In 2015, Bhadra, Yamamoto and coworkers [549] reported

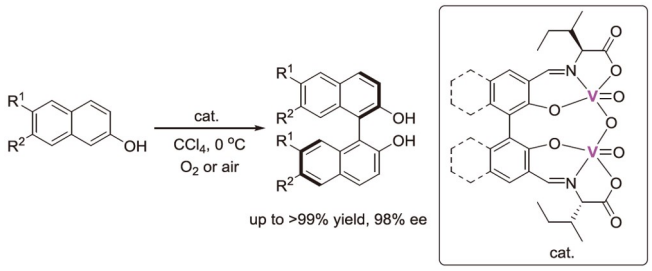

Scheme 138 Enantioselective oxidative coupling reactions catalyzed by chiral binuclear oxovanadium complexes (color online).

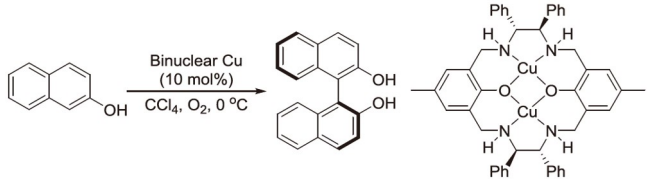

Scheme 139 Chiral binuclear Cu catalyzed asymmetric oxidative coupling.

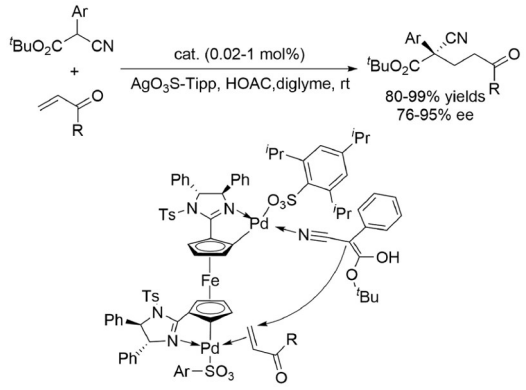

Scheme 140 The asymmetric Michael addition reaction catalyzed by a planar-chiral ferrocenyl bispalladacycle.

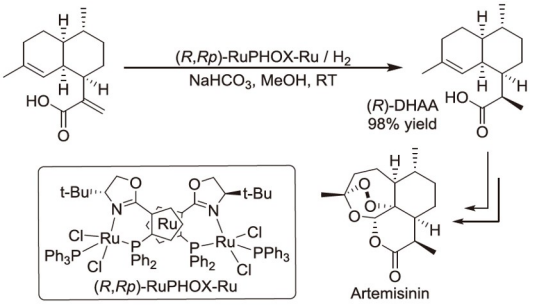

Scheme 141 RuPHOX-Ru catalyzed asymmetric hydrogenation as a key step for the synthesis of DHAA.

a highly regio- and stereoselective epoxidation of homoallylic alcohols catalyzed by a binuclear titanium complex, formed with a chiral ligand featuring two 8-quinolinol moieties tethered on a BINOL backbone (Scheme 142). It was proposed that one of the metal centers can act as a Lewis acid to bind with the hydroxy moiety of the alkenol substrate, while the other metal center can draw the electrophilic oxidant in proximity to the olefin site, and thus may facilitate the reaction to occur.

In 2020, Stoltz, Hong and coworkers [550] reported the use of a salen nickel catalyst, featured by the presence of polyether functionalities that may act as crown-ether-like cation-binding site for alkali ions, for the enantioselective alkynylation of trifluoromethyl ketones (Scheme 143), leading to the formation of chiral trifluoromethyl substituted tertiary alcohols in high yields (up to 99%) with high enantioselectivities (up to 97% ee). It was proposed that the salen ligand framework with a pendant crown ether can interact with an alkali metal cation to form a Ni^{II}/K^{+} heterobimetallic catalyst, which can facilitate the cooperative catalysis, as the Lewis acid and Brønsted base moieties could be held in close proximity by a rigid structure.

10.5 Chiral binuclear complexes containing metal-metal bonds

Besides the examples shown above, several chiral binuclear metal complexes with metal-metal bonds have also been reported to be useful in asymmetric catalysis [551]. A representative example is the well-established class of chiral dirhodium(II) paddlewheel complexes, which have been demonstrated as exceptionally versatile catalysts for a wide range of transformations, including fascinating C–H bond functionalization and cycloaddition such as aziridination and cyclopropanation *via* Rh(II) nitrenoid and carbenoid intermediates [552].

Other types of metal-metal bond based chiral binuclear complexes have also been developed, showing unique catalytic activities and good chiral induction in asymmetric catalysis. Nishibayashi and Hidai *et al*. [553] reported catalytic propargylic substitution reactions with various nucleophiles using alkanethiolate-bridged diruthenium complexes $[Cp^{*}RuCl(SR)]_2$. The chiral thiolate bridged diruthenium complexes bearing a phenethyl alcohol derivative were reported by the Nishibayashi group's in 2005, demonstrating good enantioselectivities (up to 82% ee) in the catalytic propargylic substitution reactions of propargylic alcohols with acetone (Scheme 144) [554]. The attractive C–H/π interaction between the C–H bond of the terminal phenyl group in the thiolate ligand and the π-system of the benzene ring on the allenylidene complex was proposed to play a key role to control the stereoselectivity. These chiral thiolate-bridged diruthenium complexes have also been successfully used in other asymmetric intermolecular and intramolecular propargylation reactions by Nishibayashi and coworkers [555].

In 2014, Uyeda's group [556] reported the synthesis of

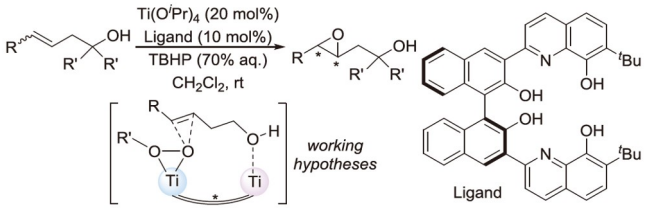

Scheme 142 Asymmetric epoxidation of homoallylic alcohols catalyzed by a titanium complex of a binucleating chiral multidentate ligand (color online).

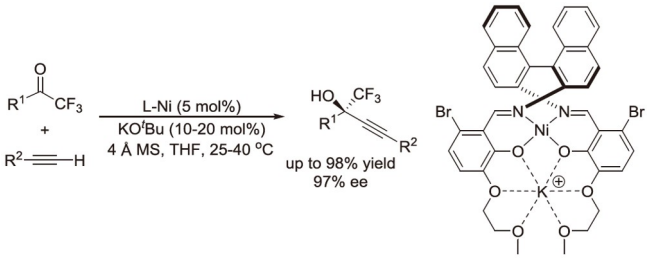

Scheme 143 Enantioselective alkynylation of trifluoromethyl ketones enabled by a Ni^{II}/K^{+} heterobimetallic catalyst.

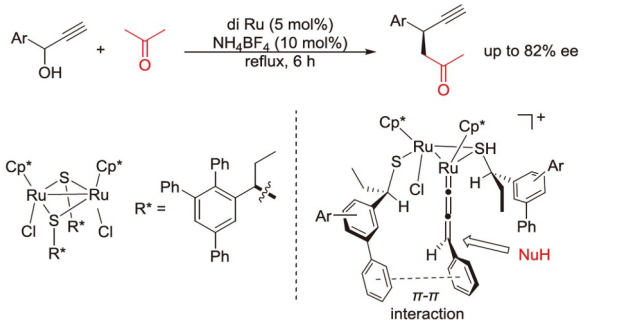

Scheme 144 Asymmetric propargylic substitution reactions catalyzed by chiral alkanethiolate-bridged diruthenium complexes (color online).

dinuclear Ni(I) complexes of a naphthyridine diamine (NDI) ligand, and metal-metal bonding interaction was found to exist in the resulting structures. These dinickel complexes were employed as catalysts for [4+1]-cycloaddition reactions of 1,3-dienes and 1,1-dichloroalkenes [557]. Ni(I)–Ni(I) bonds can be retained in the catalytic process due to the redox activity of the NDI ligands. In 2020, Uyeda's group [558] synthesized a new class of dinickel complexes of NDI ligands, containing two chiral oxazolyl units anchored on a naphthyridyl skeleton, which were used as catalysts in enantioselective intermolecular [4+1]-cycloadditions reaction of vinylidene equivalents and 1,3-dienes, providing the corresponding cycloadducts with ee values of up to 98% (Scheme 145a). In the same year, Cramer and co-workers [559] reported a novel class of chiral naphthyridyl diimine ligands readily accessible from the chiral C_2-symmetric 2,6-di-(1-arylethyl) anilines. These ligands were used in a reductive $[Ni]_2$-catalyzed enantioselective alkylidene transfer reaction from 1,1-dichloroalkenes to olefins, giving a broad range of synthetically valuable alkylidenecyclopropanes in high yields and enantioselectivities (up to 96:4 er) (Scheme 145b).

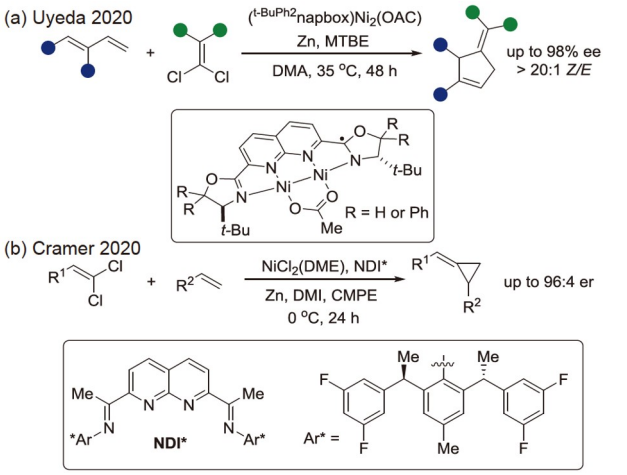

Scheme 145 Asymmetric cycloaddition reactions catalyzed by chiral dinickel complexes (color online).

10.6 Summary and perspectives of biomimetic asymmetric catalysis mediated by dinuclear & multinuclear metal complexes

Inspired by the salient catalytic performance of some multinuclear metalloenzymes in nature, the development of chiral catalysts containing two or more metal sites have attracted significant attention in the field of asymmetric catalysis. Some successful examples of asymmetric catalysis featured by the use of bi- or multi-metallic complexes as catalysts have been reported so far and have demonstrated substantially enhanced catalytic efficiencies and/or higher selectivities than their mono-nuclear counterpart complexes in some types of reactions. Despite the huge potential in this area, progress in the field of asymmetric catalysis by dinuclear/multinuclear metal complexes lags far behind the prominent position of mono-nuclear transition metal complexes, probably as a result of difficulties in effective construction of well-defined chiral multinuclear complexes, and the lacking of mechanistic understanding of the potential synergistic cooperations.

11 Conclusions and outlooks

Over the past several decades, much progress has been made in the area of biomimetic asymmetric catalysis. By mimicking various significant enzymes, many biomimetic catalysts, including organo and metallic categories, have been developed. Although biomimetic catalysts are much

smaller than the corresponding enzymes, many of them have displayed impressive enzyme-like features, such as high catalytic activity, excellent diastereo- and enantiocontrol, and environmentally friendly reaction conditions. Biomimetic asymmetric catalysis has been grown into unique and powerful tools for the construction of chiral C–C, C–O, C–N and C–X bonds and it has been widely utilized in the synthesis of complicated bioactive compounds.

Despite much remarkable progress achieved, biomimetic asymmetric catalysis is still at the early stage of development. Many grand challenges await further studies to address. First of all, as compared to thousands of natural enzymes, the enzymes well-mimicked are still very limited so far. Many significant enzymes are still waiting for biomimetic studies to develop new chemistry of asymmetric catalysis. Secondly, in terms of catalytic activity, most of the biomimetic catalysts are far below the level of the corresponding enzymes. Improvement of the catalytic efficiency to the level of enzymes needs more efforts. In addition, currently, biomimetic asymmetric catalysis was developed mainly by mimicking of the catalytic centers of enzymes, sometimes together with the imitation of the cooperative catalytic functions of amino acid residues. Actually, the catalytic cavity constructed by protein skeletons also plays an important role in substrate recognition, reaction activation, and chiral induction for enzymatic catalysis. Thus, introducing a suitable chiral pocket should be a highly promising startegy for the enhancement of the performance of biomimetic catalysts; however, it remains to be one of the most formidable challenges in the area of biomimetic chemistry. Finally, up to now, the development of efficient biomimetic catalysts still mainly depends on trial-and-error screening. Rational design has contributed little to this area so far. It would play an increasingly important role in the future along with more mechanistic understanding of the relationship between the structure and function of chiral biomimetic catalysts.

Opportunities always coexist with challenges. These problems also represent future directions of development in the field of biomimetic asymmetric catalysis. Considering the huge diversity and the extraordinary catalytic power of enzymes, chemists may get inexhaustible inspirations from enzymes and they would have unlimited motivations to continue to contribute their wisdom and efforts for developing more efficient new biomimetic catalysts. Undoubtedly, biomimetic asymmetric catalysis is growing into a powerful and green platform for the synthesis of chiral molecules with biological and chemical significance.

Acknowledgements This work was supported by the National Natural Science Foundation of China (22231011, 22221002, 22031006, 21831008, 22271192, 92256301, 92256303, 91956116), the NSFC Distinguished Young Scholars (22225107) and the Major Program of the Lanzhou Institute of Chemical Physics, Chinese Academy of Sciences (ZYFZFX-9).

Conflict of interest The authors declare no conflict of interest.

1 (a) Lwao O. *Catalytic Asymmetric Synthesis*. 3rd Ed. Hoboken: John Wiley & Sons, 2010; (b) Krupadanam GLD. *Fundamentals of Asymmetric Synthesis*. London: CRC Press, 2014; (c) Mandal DK. *Stereochemistry and Organic Reactions: Conformation, Configuration, Stereoelectronic Effects and Asymmetric Synthesis*. London: Elsevier, 2021
2 (a) Blaser H, Federsel HE. *Asymmetric Catalysis on Industrial Scale: Challenges, Approaches, and Solutions*. Weinheim: Wiley-VCH, 2010; (b) Hughes DL. *Comprehensive Chirality*. Volume 9: Industrial Applications of Asymmetric Synthesis. Amsterdam: Elsevier B.V., 2012
3 (a) Gotor V, Alfonso I, García-Urdiales E. *Asymmetric Organic Synthesis with Enzymes*. Weinheim: Wiley-VCH, 2008; (b) Chen K, Arnold FH. *Nat Catal*, 2020, 3: 203–213
4 (a) Sandoval CA, Noyori R. An Overview of Recent Developments in Metal-Catalyzed Asymmetric Transformations. In: Ding K, Dai LX, Eds. *Organic Chemistry-Breakthroughs and Perspectives*. Weinheim: Wiley-VCH Verlag GmbH & Co. KGaA, 2012. 335–366; (b) Zhang L, Meggers E. *Chem Asian J*, 2017, 12: 2335–2342
5 (a) Dalko PI. *Comprehensive Enantioselective Organocatalysis: Catalysts, Reactions, and Applications*. Weinheim: Wiley-VCH, 2013; (b) Xiang SH, Tan B. *Nat Commun*, 2020, 11: 3786
6 Chen DF, Gong LZ. *J Am Chem Soc*, 2022, 144: 2415–2437
7 Wu S, Snajdrova R, Moore JC, Baldenius K, Bornscheuer UT. *Angew Chem Int Ed*, 2021, 60: 88–119
8 (a) Antenucci A, Dughera S, Renzi P. *ChemSusChem*, 2021, 14: 2785–2853; (b) Ayad T, Phansavath P, Ratovelomanana-Vidal V. *Chem Record*, 2016, 16: 2754–2771
9 Das A, Hessin C, Ren Y, Desage-El Murr M. *Chem Soc Rev*, 2020, 49: 8840–8867
10 (a) Liu F. *Chirality*, 2013, 25: 675–683; (b) Xie Y, Pan H, Liu M, Xiao X, Shi Y. *Chem Soc Rev*, 2015, 44: 1740–1748; (c) Sun W, Sun Q. *Acc Chem Res*, 2019, 52: 2370–2381; (d) Costas M. *Chem Record*, 2021, 21: 4000–4014; (e) Radhika S, Aneeja T, Philip RM, Anilkumar G. *Appl Organomet Chem*, 2021, 35: 6217
11 Umile TP. *Catalysis for Sustainability: Goals, Challenges, and Impacts*. Boca Raton: CRC Press, 2016
12 (a) Li S, Cao S, Piletsky SA, Turner APF. *Molecularly Imprinted Catalysts: Principles, Syntheses, and Applications*. Amsterdam: Elsevier B.V., 2016; (b) Metrano AJ, Chinn AJ, Shugrue CR, Stone EA, Kim B, Miller SJ. *Chem Rev*, 2020, 120: 11479–11615
13 (a) Pedersen KJ. *J Phys Chem*, 1934, 38: 559–571; (b) Westheimer FH, Cohen H. *J Am Chem Soc*, 1938, 60: 90–94
14 (a) Breslow R. *Chem Soc Rev*, 1972, 1: 553–580; (b) Breslow R. *Artificial Enzymes*. Weinheim: Wiley-VCH Verlag GmbH & Co. KGaA, 2005; (c) Breslow R. *J Biol Chem*, 2009, 284: 1337–1342
15 Breslow R. *J Am Chem Soc*, 1958, 80: 3719–3726
16 Breslow R, Dong SD. *Chem Rev*, 1998, 98: 1997–2012
17 Bernardi L, Fochi M, Comes Franchini M, Ricci A. *Org Biomol Chem*, 2012, 10: 2911–2922
18 Zhao M, Wang HB, Ji LN, Mao ZW. *Chem Soc Rev*, 2013, 42: 8360–8375
19 Erkkilä A, Majander I, Pihko PM. *Chem Rev*, 2007, 107: 5416–5470
20 (a) Mukherjee S, Yang JW, Hoffmann S, List B. *Chem Rev*, 2007, 107: 5471–5569; (b) Chen Z, Du W, Chen Y. *Chin J Chem*, 2021, 39: 1775–1786; (c) Enders D, Niemeier O, Henseler A. *Chem Rev*, 2007, 107: 5606–5655; (d) Bugaut X, Glorius F. *Chem Soc Rev*, 2012, 41: 3511–3522; (e) Ryan SJ, Candish L, Lupton DW. *Chem Soc Rev*, 2013, 42: 4906–4917; (f) Hopkinson MN, Richter C, Schedler M, Glorius F. *Nature*, 2014, 510: 485–496; (g) Mahatthananchai J, Bode JW. *Acc Chem Res*, 2014, 47: 696–707; (h) Flanigan DM, Romanov-Michailidis F, White NA, Rovis T. *Chem Rev*, 2015, 115: 9307–

9387; (i) Mondal S, Yetra SR, Mukherjee S, Biju AT. *Acc Chem Res*, 2019, 52: 425–436; (j) Chen XY, Gao ZH, Ye S. *Acc Chem Res*, 2020, 53: 690–702; (k) Bellotti P, Koy M, Hopkinson MN, Glorius F. *Nat Rev Chem*, 2021, 5: 711–725
21 (a) Murakami Y, Kikuchi J, Hisaeda Y, Hayashida O. *Chem Rev*, 1996, 96: 721–758; (b) Chen J, Liu YE, Gong X, Shi L, Zhao B. *Chin J Chem* 2019, 37: 103–112
22 (a) Paul CE, Arends IWCE, Hollmann F. *ACS Catal*, 2014, 4: 788–797; (b) Zheng C, You SL. *Chem Soc Rev*, 2012, 41: 2498–2518
23 (a) Imada Y, Naota T. *Chem Record*, 2007, 7: 354–361; (b) Gelalcha FG. *Chem Rev*, 2007, 107: 3338–3361; (c) Bäckvall JE. *Modern Oxidation Methods*. *2nd Ed*. Weinheim: Wiley-VCH, 2010; (d) de Gonzalo G, Fraaije MW. *ChemCatChem*, 2013, 5: 403–415; (e) Cibulka R. *Eur J Org Chem*, 2015, 2015: 915–932
24 (a) Noyori R. *Angew Chem Int Ed*, 2002, 41: 2008–2022; (b) Wang H, Wen J, Zhang X. *Chem Rev*, 2021, 121: 7530–7567
25 Cook DJ, Finnigan JD, Cook K, Black GW, Charnock SJ, Cytochromes P450: history, classes, catalytic mechanism, and industrial application. In: *Advances in Protein Chemistry and Structural Biology*. Amsterdam: Elsevier Ltd., 2016. 105–126
26 (a) Guo M, Corona T, Ray K, Nam W. *ACS Cent Sci*, 2019, 5: 13–28; (b) Nam W. *Acc Chem Res*, 2015, 48: 2415–2423
27 (a) Li G, Zhu D, Wang X, Su Z, Bryce MR. *Chem Soc Rev*, 2020, 49: 765–838; (b) El Amouri H, Gruselle M. *Chem Rev*, 1996, 96: 1077–1104
28 Trost BM, Brindle CS. *Chem Soc Rev*, 2010, 39: 1600–1632
29 Wakagi T. *TIGG*, 2013, 25: 71–81
30 Clapes P, Joglar J, Edited by Mahrwald R. *Modern Methods in Stereoselective Aldol Reactions*. Weinheim: Wiley-VCH, 2013. 475–527
31 Clapes P, Fessner WD. *Sci Synth Stere Syn*, 2011, 2: 677–734
32 Marsh JJ, Lebherz HG. *Trends Biochem Sci*, 1992, 17: 110–113
33 Lai CY, Nakai N, Chang D. *Science*, 1974, 183: 1204–1206
34 Hine J. *Acc Chem Res*, 1978, 11: 1–7
35 Hamilton GA, Westheimer FH. *J Am Chem Soc*, 1959, 81: 6332–6333
36 Heine A, DeSantis G, Luz JG, Mitchell M, Wong CH, Wilson IA. *Science*, 2001, 294: 369–374
37 Hajos ZG, Parrish DR. German patent DE, 2102623, 1971
38 Eder U, Sauer G, Wiechert R. *Angew Chem Int Ed Engl*, 1971, 10: 496–497
39 Whitesides GM, Wong CH. *Angew Chem Int Ed Engl*, 1985, 24: 617–638
40 Greenberg WA, Varvak A, Hanson SR, Wong K, Huang H, Chen P, Burk MJ. *Proc Natl Acad Sci USA*, 2004, 101: 5788–5793
41 Wagner J, Lerner RA, Barbas Carlos F. I. *Science*, 1995, 270: 1797–1800
42 Jiang L, Althoff EA, Clemente FR, Doyle L, Rothlisberger D, Zanghellini A, Gallaher JL, Betker JL, Tanaka F, Barbas Iii CF, Hilvert D, Houk KN, Stoddard BL, Baker D. *Science*, 2008, 319: 1387–1391
43 List B, Lerner RA, Barbas CF. *J Am Chem Soc*, 2000, 122: 2395–2396
44 Ahrendt KA, Borths CJ, MacMillan DWC. *J Am Chem Soc*, 2000, 122: 4243–4244
45 Hayashi Y, Gotoh H, Hayashi T, Shoji M. *Angew Chem Int Ed*, 2005, 44: 4212–4215
46 Marigo M, Wabnitz TC, Fielenbach D, Jørgensen KA. *Angew Chem Int Ed*, 2005, 44: 794–797
47 Chen XH, Yu J, Gong LZ. *Chem Commun*, 2010, 46: 6437–6448
48 Luo S, Mi X, Zhang L, Liu S, Xu H, Cheng JP. *Angew Chem Int Ed*, 2006, 45: 3093–3097
49 Lelais G, MacMillan DWC. *Aldrichim Acta*, 2006, 39: 79–87
50 (a) Zhang L, Fu N, Luo S. *Acc Chem Res*, 2015, 48: 986–997; (b) Cai M, Zhang R, Yang C, Luo S. *Chin J Chem*, 2023, 41: 548–559
51 Liu K, Cui HF, Nie J, Dong KY, Li XJ, Ma JA. *Org Lett*, 2007, 9: 923–925
52 McCooey SH, Connon SJ. *Org Lett*, 2007, 9: 599–602
53 Zhang L, Luo S. *Synlett*, 2012, 23: 1575–1589
54 Jiang H, Albrecht Ł, Jørgensen KA. *Chem Sci*, 2013, 4: 2287–2300
55 Bertelsen S, Jørgensen KA. *Chem Soc Rev*, 2009, 38: 2178–2189
56 Bertelsen S, Marigo M, Brandes S, Dinér P, Jørgensen KA. *J Am Chem Soc*, 2006, 128: 12973–12980
57 Jia ZJ, Jiang H, Li JL, Gschwend B, Li QZ, Yin X, Grouleff J, Chen YC, Jørgensen KA. *J Am Chem Soc*, 2011, 133: 5053–5061
58 Chen Z, Du W, Chen Y. *Chin J Chem*, 2021, 39: 1775–1786
59 Enders D, Hüttl MRM, Grondal C, Raabe G. *Nature*, 2006, 441: 861–863
60 Tian J, Zhong J, Li Y, Ma D. *Angew Chem Int Ed*, 2014, 53: 13885–13888
61 Zhu S, Yu S, Wang Y, Ma D. *Angew Chem Int Ed*, 2010, 49: 4656–4660
62 Zi W, Xie W, Ma D. *J Am Chem Soc*, 2012, 134: 9126–9129
63 Song J, Guo C, Adele A, Yin H, Gong L. *Chem Eur J*, 2013, 19: 3319–3323
64 Zhang Q, Zhang FM, Zhang CS, Liu SZ, Tian JM, Wang SH, Zhang XM, Tu YQ. *Nat Commun*, 2019, 10: 2507
65 Umemiya S, Sakamoto D, Kawauchi G, Hayashi Y. *Org Lett*, 2017, 19: 1112–1115
66 Brandau S, Landa A, Franzén J, Marigo M, Jørgensen KA. *Angew Chem Int Ed*, 2006, 45: 4305–4309
67 Hong BC, Kotame P, Tsai CW, Liao JH. *Org Lett*, 2010, 12: 776–779
68 You L, Liang XT, Xu LM, Wang YF, Zhang JJ, Su Q, Li YH, Zhang B, Yang SL, Chen JH, Yang Z. *J Am Chem Soc*, 2015, 137: 10120–10123
69 Beeson TD, Mastracchio A, Hong JB, Ashton K, MacMillan DWC. *Science*, 2007, 316: 582–585
70 Pirnot MT, Rankic DA, Martin DBC, MacMillan DWC. *Science*, 2013, 339: 1593–1596
71 Bui NN, Ho XH, Mho S, Jang HY. *Eur J Org Chem*, 2009, 2009: 5309–5312
72 Wang D, Zhang L, Luo S. *Org Lett*, 2017, 19: 4924–4927
73 Arceo E, Jurberg ID, Álvarez-Fernández A, Melchiorre P. *Nat Chem*, 2013, 5: 750–756
74 Hörmann FM, Kerzig C, Chung TS, Bauer A, Wenger OS, Bach T. *Angew Chem Int Ed*, 2020, 59: 9659–9668
75 Huang M, Zhang L, Pan T, Luo S. *Science*, 2022, 375: 869–874
76 Sibi MP, Hasegawa M. *J Am Chem Soc*, 2007, 129: 4124–4125
77 Jia Z, Zhang L, Luo S. *J Am Chem Soc*, 2022, 144: 10705–10710
78 Xu C, Zhang L, Luo S. *Angew Chem Int Ed*, 2014, 53: 4149–4153
79 Ikeda M, Miyake Y, Nishibayashi Y. *Angew Chem Int Ed*, 2010, 49: 7289–7293
80 Zhang J, Wang Y, You C, Shi M, Mi X, Luo S. *Org Lett*, 2022, 24: 1186–1189
81 Ibrahem I, Córdova A. *Angew Chem Int Ed*, 2006, 45: 1952–1956
82 Ding Q, Wu J. *Org Lett*, 2007, 9: 4959–4962
83 Ibrahem I, Santoro S, Himo F, Córdova A. *Adv Synth Catal*, 2011, 353: 245–252
84 Krautwald S, Sarlah D, Schafroth MA, Carreira EM. *Science*, 2013, 340: 1065–1068
85 Binder JT, Crone B, Haug TT, Menz H, Kirsch SF. *Org Lett*, 2008, 10: 1025–1028
86 Zhang Q, Li Y, Zhang L, Luo S. *Angew Chem Int Ed*, 2021, 60: 10971–10976
87 Capacci AG, Malinowski JT, McAlpine NJ, Kuhne J, MacMillan DWC. *Nat Chem*, 2017, 9: 1073–1077
88 Cai M, Xu K, Li Y, Nie Z, Zhang L, Luo S. *J Am Chem Soc*, 2021, 143: 1078–1087
89 Yang Q, Zhang L, Ye C, Luo S, Wu L, Tung C. *Angew Chem Int Ed*, 2017, 56: 3694–3698
90 Fu N, Li L, Yang Q, Luo S. *Org Lett*, 2017, 19: 2122–2125
91 Li L, Li Y, Fu N, Zhang L, Luo S. *Angew Chem Int Ed*, 2020, 59: 14347–14351
92 Luo S, Xu H, Li J, Zhang L, Cheng JP. *J Am Chem Soc*, 2007, 129: 3074–3075
93 Fu N, Zhang L, Li J, Luo S, Cheng JP. *Angew Chem Int Ed*, 2011, 50:

11451–11455
94 Hu S, Li J, Xiang J, Pan J, Luo S, Cheng JP. *J Am Chem Soc*, 2010, 132: 7216–7228
95 Wang Y, Chai J, You C, Zhang J, Mi X, Zhang L, Luo S. *J Am Chem Soc*, 2020, 142: 3184–3195
96 (a) Williams RR. *J Am Chem Soc*, 1935, 57: 229–230; (b) Williams RR, Waterman RE, Keresztesy JC, Buchman ER. *J Am Chem Soc*, 1935, 57: 536–537; (c) Williams RR. *J Am Chem Soc*, 1936, 58: 1063–1064; (d) Williams RR, Cline JK. *J Am Chem Soc*, 1936, 58: 1504–1505; (e) Cline JK, Williams RR, Ruehle AE, Waterman RE. *J Am Chem Soc*, 1937, 59: 530–533
97 Lohmann K, Schuster P. *Naturwissenschaften*, 1937, 25: 26–27
98 Ukai T, Tanaka R, Dokawa T. *J Pharm Soc Jpn*, 1943, 63: 296–300
99 Mizuhara S, Handler P. *J Am Chem Soc*, 1954, 76: 571–573
100 Lapworth A. *J Chem Soc Trans*, 1903, 83: 995–1005
101 Lapworth A. *J Chem Soc Trans*, 1904, 85: 1206–1214
102 Igau A, Grutzmacher H, Baceiredo A, Bertrand G. *J Am Chem Soc*, 1988, 110: 6463–6466
103 Arduengo AJ III, Harlow RL, Kline M. *J Am Chem Soc*, 1991, 113: 361–363
104 Sheehan JC, Hunneman DH. *J Am Chem Soc*, 1966, 88: 3666–3667
105 (a) Enders D, Breuer K, Teles JH. *Helv Chim Acta*, 1996, 79: 1217–1221; (b) Teles JH, Breuer K, Enders D, Gielen H. *Synth Commun*, 1999, 29: 1–9
106 Berkessel A, Elfert S, Etzenbach-Effers K, Teles JH. *Angew Chem Int Ed*, 2010, 49: 7120–7124
107 DiRocco DA, Oberg KM, Rovis T. *J Am Chem Soc*, 2012, 134: 6143–6145
108 Maji B, Mayr H. *Angew Chem Int Ed*, 2012, 51: 10408–10412
109 Paul M, Sudkaow P, Wessels A, Schlörer NE, Neudörfl J, Berkessel A. *Angew Chem Int Ed*, 2018, 57: 8310–8315
110 (a) Sheehan JC, Hara T. *J Org Chem*, 1974, 39: 1196–1199; (b) Knight RL, Leeper FJ. *Tetrahedron Lett*, 1997, 38: 3611–3614; (c) Enders D, Kallfass U. *Angew Chem Int Ed*, 2002, 41: 1743–1745; (d) Ma Y, Wei S, Wu J, Yang F, Liu B, Lan J, Yang S, You J. *Adv Synth Catal*, 2008, 350: 2645–2651; (e) Brand J, Siles J, Waser J. *Synlett*, 2010, 2010(6): 881–884; (f) O'Toole SE, Connon SJ. *Org Biomol Chem*, 2009, 7: 3584; (g) Baragwanath L, Rose CA, Zeitler K, Connon SJ. *J Org Chem*, 2009, 74: 9214–9217
111 Huang XL, Ye S. *Chin Sci Bull*, 2010, 55: 1753–1757
112 Enders D, Niemeier O, Balensiefer T. *Angew Chem Int Ed*, 2006, 45: 1463–1467
113 Takikawa H, Hachisu Y, Bode JW, Suzuki K. *Angew Chem Int Ed*, 2006, 45: 3492–3494
114 Kerr MS, Read de Alaniz J, Rovis T. *J Am Chem Soc*, 2002, 124: 10298–10299
115 Jia MQ, You SL. *ACS Catal*, 2013, 3: 622–624
116 Mennen SM, Gipson JD, Kim YR, Miller SJ. *J Am Chem Soc*, 2005, 127: 1654–1655
117 DiRocco DA, Rovis T. *Angew Chem Int Ed*, 2012, 51: 5904–5906
118 Sun LH, Liang ZQ, Jia WQ, Ye S. *Angew Chem Int Ed*, 2013, 52: 5803–5806
119 Stetter H. *Angew Chem Int Ed*, 1976, 15: 639–647
120 Enders D, Balensiefer T. *Acc Chem Res*, 2004, 37: 534–541
121 Enders D, Han J, Henseler A. *Chem Commun*, 2008, 3989
122 Liu Q, Perreault S, Rovis T. *J Am Chem Soc*, 2008, 130: 14066–14067
123 Ciganek E. *Synthesis*, 1995, 1311–1314
124 Enders D, Breuer K, Runsink J, Teles JH. *Helv Chim Acta*, 1996, 79: 1899–1902
125 (a) Pesch J, Harms K, Bach T. *Eur J Org Chem*, 2004, 2004: 2025–2035; (b) Read de Alaniz J, Rovis T. *J Am Chem Soc*, 2005, 127: 6284–6289; (c) Mennen SM, Blank JT, Tran-Dubé MB, Imbriglio JE, Miller SJ. *Chem Commun*, 2005, 195–197; (d) Matsumoto Y, Tomioka K. *Tetrahedron Lett*, 2006, 47: 5843–5846; (e) Rong ZQ, Li Y, Yang GQ, You SL. *Synlett*, 2011, 2011: 1033–1037; (f) Jia MQ, Li Y, Rong ZQ, You SL. *Org Biomol Chem*, 2011, 9: 2072–2074; (g) Rafiński Z, Kozakiewicz A, Rafińska K. *ACS Catal*, 2014, 4: 1404–1408
126 Han R, He L, Liu L, Xie X, She X. *Chem Asian J*, 2016, 11: 193–197
127 Piel I, Steinmetz M, Hirano K, Fröhlich R, Grimme S, Glorius F. *Angew Chem Int Ed*, 2011, 50: 4983–4987
128 Liu F, Bugaut X, Schedler M, Fröhlich R, Glorius F. *Angew Chem Int Ed*, 2011, 50: 12626–12630
129 Das TK, Biju AT. *Chem Commun*, 2020, 56: 8537–8552
130 (a) He M, Bode JW. *Org Lett*, 2005, 7: 3131–3134; (b) He L, Jian TY, Ye S. *J Org Chem*, 2007, 72: 7466–7468
131 (a) Patra A, Mukherjee S, Das TK, Jain S, Gonnade RG, Biju AT. *Angew Chem Int Ed*, 2017, 56: 2730–2734; (b) Harish B, Subbireddy M, Suresh S. *Chem Commun*, 2017, 53: 3338–3341
132 Fernando JEM, Nakano Y, Zhang C, Lupton DW. *Angew Chem Int Ed*, 2019, 58: 4007–4011
133 Das TK, Ghosh A, Balanna K, Behera P, Gonnade RG, Marelli UK, Das AK, Biju AT. *ACS Catal*, 2019, 9: 4065–4071
134 Suzuki Y, Yamauchi K, Muramatsu K, Sato M. *Chem Commun*, 2004, 40: 2770–2771
135 Kano T, Sasaki K, Maruoka K. *Org Lett*, 2005, 7: 1347–1349
136 Kuwano S, Harada S, Kang B, Oriez R, Yamaoka Y, Takasu K, Yamada K. *J Am Chem Soc*, 2013, 135: 11485–11488
137 He M, Struble JR, Bode JW. *J Am Chem Soc*, 2006, 128: 8418–8420
138 He M, Uc GJ, Bode JW. *J Am Chem Soc*, 2006, 128: 15088–15089
139 (a) Duguet N, Campbell CD, Slawin AMZ, Smith AD. *Org Biomol Chem*, 2008, 6: 1108–1113; (b) Zhang YR, He L, Wu X, Shao PL, Ye S. *Org Lett*, 2008, 10: 277–280
140 Hao L, Du Y, Lv H, Chen X, Jiang H, Shao Y, Chi YR. *Org Lett*, 2012, 14: 2154–2157
141 (a) Burstein C, Glorius F. *Angew Chem Int Ed*, 2004, 43: 6205–6208; (b) Sohn SS, Rosen EL, Bode JW. *J Am Chem Soc*, 2004, 126: 14370–14371
142 Menon RS, Biju AT, Nair V. *Chem Soc Rev*, 2015, 44: 5040–5052
143 Chiang PC, Kaeobamrung J, Bode JW. *J Am Chem Soc*, 2007, 129: 3520–3521
144 Cardinal-David B, Raup DEA, Scheidt KA. *J Am Chem Soc*, 2010, 132: 5345–5347
145 Sun LH, Shen LT, Ye S. *Chem Commun*, 2011, 47: 10136–10138
146 Check CT, Jang KP, Schwamb CB, Wong AS, Wang MH, Scheidt KA. *Angew Chem Int Ed*, 2015, 54: 4264–4268
147 Phillips EM, Reynolds TE, Scheidt KA. *J Am Chem Soc*, 2008, 130: 2416–2417
148 (a) Izquierdo J, Orue A, Scheidt KA. *J Am Chem Soc*, 2013, 135: 10634–10637; (b) Lv H, Jia WQ, Sun LH, Ye S. *Angew Chem Int Ed*, 2013, 52: 8607–8610
149 Chiang PC, Rommel M, Bode JW. *J Am Chem Soc*, 2009, 131: 8714–8718
150 Fu Z, Xu J, Zhu T, Leong WWY, Chi YR. *Nat Chem*, 2013, 5: 835–839
151 Merski M, Townsend CA. *J Am Chem Soc*, 2007, 129: 15750–15751
152 Zeitler K. *Org Lett*, 2006, 8: 637–640
153 Kaeobamrung J, Mahatthananchai J, Zheng P, Bode JW. *J Am Chem Soc*, 2010, 132: 8810–8812
154 Zhu ZQ, Zheng XL, Jiang NF, Wan X, Xiao JC. *Chem Commun*, 2011, 47: 8670–8672
155 Candish L, Forsyth CM, Lupton DW. *Angew Chem Int Ed*, 2013, 52: 9149–9152
156 Sun FG, Sun LH, Ye S. *Adv Synth Catal*, 2011, 353: 3134–3138
157 Cheng J, Huang Z, Chi YR. *Angew Chem Int Ed*, 2013, 52: 8592–8596
158 De Sarkar S, Grimme S, Studer A. *J Am Chem Soc*, 2010, 132: 1190–1191
159 De Sarkar S, Studer A. *Angew Chem Int Ed*, 2010, 49: 9266–9269
160 Rong ZQ, Jia MQ, You SL. *Org Lett*, 2011, 13: 4080–4083
161 Chen XY, Gao ZH, Song CY, Zhang CL, Wang ZX, Ye S. *Angew Chem Int Ed*, 2014, 53: 11611–11615
162 Wu X, Hao L, Zhang Y, Rakesh M, Reddi RN, Yang S, Song BA,

Chi YR. *Angew Chem Int Ed*, 2017, 56: 4201–4205
163 Shen LT, Shao PL, Ye S. *Adv Synth Catal*, 2011, 353: 1943–1948
164 Mo J, Chen X, Chi YR. *J Am Chem Soc*, 2012, 134: 8810–8813
165 Chen XY, Xia F, Cheng JT, Ye S. *Angew Chem Int Ed*, 2013, 52: 10644–10647
166 Li BS, Wang Y, Jin Z, Zheng P, Ganguly R, Chi YR. *Nat Commun*, 2015, 6: 6207
167 Zhu T, Mou C, Li B, Smetankova M, Song BA, Chi YR. *J Am Chem Soc*, 2015, 137: 5658–5661
168 Xu K, Li W, Zhu S, Zhu T. *Angew Chem Int Ed*, 2019, 58: 17625–17630
169 Gillard RM, Fernando JEM, Lupton DW. *Angew Chem Int Ed*, 2018, 57: 4712–4716
170 (a) Dai L, Ye S. *ACS Catal*, 2020, 10: 994–998; (b) Dai L, Qiu Y, Xu YY, Ye S. *Cell Rep Phys Sci*, 2020, 1: 100071
171 DiRocco DA, Rovis T. *J Am Chem Soc*, 2012, 134: 8094–8097
172 Bay AV, Fitzpatrick KP, Betori RC, Scheidt KA. *Angew Chem Int Ed*, 2020, 59: 9143–9148
173 Ren SC, Lv WX, Yang X, Yan JL, Xu J, Wang FX, Hao L, Chai H, Jin Z, Chi YR. *ACS Catal*, 2021, 11: 2925–2934
174 Yu X, Meng QY, Daniliuc CG, Studer A. *J Am Chem Soc*, 2022, 144: 7072–7079
175 Yang W, Hu W, Dong X, Li X, Sun J. *Angew Chem Int Ed*, 2016, 55: 15783–15786
176 Dai L, Xia Z, Gao Y, Gao Z, Ye S. *Angew Chem Int Ed*, 2019, 58: 18124–18130
177 (a) Guo C, Fleige M, Janssen-Müller D, Daniliuc CG, Glorius F. *J Am Chem Soc*, 2016, 138: 7840–7843; (b) Guo C, Janssen-Müller D, Fleige M, Lerchen A, Daniliuc CG, Glorius F. *J Am Chem Soc*, 2017, 139: 4443–4451
178 Singha S, Patra T, Daniliuc CG, Glorius F. *J Am Chem Soc*, 2018, 140: 3551–3554
179 Singha S, Serrano E, Mondal S, Daniliuc CG, Glorius F. *Nat Catal*, 2020, 3: 48–54
180 Zhang J, Gao YS, Gu BM, Yang WL, Tian BX, Deng WP. *ACS Catal*, 2021, 11: 3810–3821
181 Li YY, Li S, Fan T, Zhang ZJ, Song J, Gong LZ. *ACS Catal*, 2021, 11: 14388–14394
182 Zhang Z, Zhang L, Geng R, Song J, Chen X, Gong L. *Angew Chem Int Ed*, 2019, 58: 12190–12194
183 Liu H, Han YF, Gao ZH, Zhang CL, Wang C, Ye S. *ACS Catal*, 2022, 12: 1657–1663
184 Fan T, Song J, Gong L. *Angew Chem Int Ed*, 2022, 61: e202201678
185 (a) Namitharan K, Zhu T, Cheng J, Zheng P, Li X, Yang S, Song BA, Chi YR. *Nat Commun*, 2014, 5: 3982; (b) Han YF, Gao ZH, Zhang CL, Ye S. *Org Lett*, 2020, 22: 8396–8400
186 (a) Zhou L, Wu X, Yang X, Mou C, Song R, Yu S, Chai H, Pan L, Jin Z, Chi YR. *Angew Chem Int Ed*, 2020, 59: 1557–1561; (b) Jiang J, Wang X, Liu S, Zhang S, Yang B, Zhao Y, Lu S. *Angew Chem Int Ed*, 2022, 61: e202115464
187 He L, Zhang YR, Huang XL, Ye S. *Synthesis*, 2008, 2008: 2825–2829
188 Chen XY, Sun LH, Ye S. *Chem Eur J*, 2013, 19: 4441–4445
189 Bae S, Zhang C, Gillard RM, Lupton DW. *Angew Chem Int Ed*, 2019, 58: 13370–13374
190 Mozzarelli A, Bettati S. *Chem Record*, 2006, 6: 275–287
191 Steffen-Munsberg F, Vickers C, Kohls H, Land H, Mallin H, Nobili A, Skalden L, van den Bergh T, Joosten HJ, Berglund P, Höhne M, Bornscheuer UT. *Biotechnol Adv*, 2015, 33: 566–604
192 Phillips RS. *Biochim Biophys Acta*, 2015, 1854: 1167–1174
193 (a) Ayling J, Snell EE. *Biochemistry*, 1968, 7: 1616–1625; (b) Liao RZ, Ding WJ, Yu JG, Fang WH, Liu RZ. *J Comput Chem*, 2008, 29: 1919–1929
194 Mathew S, Yun H. *ACS Catal*, 2012, 2: 993–1001
195 (a) Nozaki H, Kuroda S, Watanabe K, Yokozeki K. *J Mol Catal B-Enzymatic*, 2009, 59: 237–242; (b) Dückers N, Baer K, Simon S, Gröger H, Hummel W. *Appl Microbiol Biotechnol*, 2010, 88: 409–424
196 Humble MS, Cassimjee KE, Håkansson M, Kimbung YR, Walse B, Abedi V, Federsel HJ, Berglund P, Logan DT. *FEBS J*, 2012, 279: 779–792
197 Malashkevich VN, Jaeger J, Ziak M, Sauder U, Gehring H, Christen P, Jansonius JN. *Biochemistry*, 1995, 34: 405–414
198 (a) Snell EE. *J Am Chem Soc*, 1945, 67: 194–197; (b) Metzler DE, Ikawa M, Snell EE. *J Am Chem Soc*, 1954, 76: 648–652
199 Kuzuhara H, Komatsu T, Emoto S. *Tetrahedron Lett*, 1978, 19: 3563–3566
200 (a) Tachibana Y, Ando M, Kuzuhara H. *Chem Lett*, 1982, 11: 1765–1768; (b) Ando M, Kuzuhara H. *Bull Chem Soc Jpn*, 1989, 62: 244–250
201 (a) Zimmerman SC, Czarnik AW, Breslow R. *J Am Chem Soc*, 1983, 105: 1694–1695; (b) Zimmerman SC, Breslow R. *J Am Chem Soc*, 1984, 106: 1490–1491; (c) Breslow R, Czarnik AW, Lauer M, Leppkes R, Winkler J, Zimmerman S. *J Am Chem Soc*, 1986, 108: 1969–1979
202 (a) Kuzuhara H, Watanabe N, Ando M. *J Chem Soc Chem Commun*, 1987, 63: 95–96; (b) Ando M, Watanabe J, Kuzuhara H. *Bull Chem Soc Jpn*, 1990, 63: 88–90
203 (a) Koh JT, Delaude L, Breslow R. *J Am Chem Soc*, 1994, 116: 11234–11240; (b) Liu L, Rozenman M, Breslow R. *Bioorg Med Chem*, 2002, 10: 3973–3979
204 Breslow R, Hammond M, Lauer M. *J Am Chem Soc*, 1980, 102: 421–422
205 (a) Zhou W, Yerkes N, Chruma JJ, Liu L, Breslow R. *Bioorg Med Chem Lett*, 2005, 15: 1351–1355; (b) Bandyopadhyay S, Zhou W, Breslow R. *Org Lett*, 2007, 9: 1009–1012; (c) Wei S, Wang J, Venhuizen S, Skouta R, Breslow R. *Bioorg Med Chem Lett*, 2009, 19: 5543–5546
206 Shi L, Tao C, Yang Q, Liu YE, Chen J, Chen J, Tian J, Liu F, Li B, Du Y, Zhao B. *Org Lett*, 2015, 17: 5784–5787
207 Lan X, Tao C, Liu X, Zhang A, Zhao B. *Org Lett*, 2016, 18: 3658–3661
208 (a) Kikuchi J, Zhang ZY, Murakami Y. *J Am Chem Soc*, 1995, 117: 5383–5384; (b) Kuang H, Brown ML, Davies RR, Young EC, Distefano MD. *J Am Chem Soc*, 1996, 118: 10702–10706; (c) Kuang H, Distefano MD. *J Am Chem Soc*, 1998, 120: 1072–1073; (d) Häring D, Distefano MD. *Bioconjugate Chem*, 2001, 12: 385–390
209 (a) Xiao X, Xie Y, Su C, Liu M, Shi Y. *J Am Chem Soc*, 2011, 133: 12914–12917; (b) Wu Y, Deng L. *J Am Chem Soc*, 2012, 134: 14334–14337; (c) Kang QK, Selvakumar S, Maruoka K. *Org Lett*, 2019, 21: 2294–2297
210 (a) Bernauer K, Deschenaux R, Taura T. *Helv Chim Acta*, 1983, 66: 2049–2058; (b) Knudsen KR, Bachmann S, Jørgensen KA. *Chem Commun*, 2003, 2602–2603
211 Liu YE, Lu Z, Li B, Tian J, Liu F, Zhao J, Hou C, Li Y, Niu L, Zhao B. *J Am Chem Soc*, 2016, 138: 10730–10733
212 Cai W, Qiao X, Zhang H, Li B, Guo J, Zhang L, Chen WW, Zhao B. *Nat Commun*, 2021, 12: 5174
213 Griswold WR, Toney MD. *J Am Chem Soc*, 2011, 133: 14823–14830
214 Crugeiras J, Rios A, Amyes TL, Richard JP. *Org Biomol Chem*, 2005, 3: 2145–2149
215 Juillerat-Jeanneret L. *J Med Chem*, 2014, 57: 2197–2212
216 (a) Li S, Chen XY, Enders D. *Chem*, 2018, 4: 2026–2028; (b) Wang Q, Gu Q, You S. *Angew Chem Int Ed*, 2019, 58: 6818–6825; (c) Gong LZ. *Sci China Chem*, 2019, 62: 3–4
217 Chen J, Gong X, Li J, Li Y, Ma J, Hou C, Zhao G, Yuan W, Zhao B. *Science*, 2018, 360: 1438–1442
218 Crugeiras J, Rios A, Riveiros E, Richard JP. *J Am Chem Soc*, 2011, 133: 3173–3183
219 (a) Liu JH, Wen W, Liao J, Shen QW, Lin Y, Wu ZL, Cai T, Guo QX. *Nat Commun*, 2022, 13: 2509; (b) Wen W, Luo MJ, Yuan Y, Liu JH, Wu ZL, Cai T, Wu ZW, Ouyang Q, Guo QX. *Nat Commun*, 2020, 11: 5372; (c) Chen L, Luo MJ, Zhu F, Wen W, Guo QX. *J Am Chem Soc*, 2019, 141: 5159–5163; (d) Wen W, Chen L, Luo MJ,

Zhang Y, Chen YC, Ouyang Q, Guo QX. *J Am Chem Soc*, 2018, 140: 9774–9780
220 Cheng A, Zhang L, Zhou Q, Liu T, Cao J, Zhao G, Zhang K, Song G, Zhao B. *Angew Chem Int Ed*, 2021, 60: 20166–20172
221 Ma J, Zhou Q, Song G, Song Y, Zhao G, Ding K, Zhao B. *Angew Chem Int Ed*, 2021, 60: 10588–10592
222 Ma J, Gao B, Song G, Zhang R, Wang Q, Ye Z, Chen W, Zhao B. *Angew Chem Int Ed*, 2022, 61: e202200850
223 (a) Campos KR. *Chem Soc Rev*, 2007, 36: 1069–1084; (b) Mitchell EA, Peschiulli A, Lefevre N, Meerpoel L, Maes BUW. *Chem Eur J*, 2012, 18: 10092–10142; (c) Seidel D. *Acc Chem Res*, 2015, 48: 317–328; (d) Gonnard L, Guérinot A, Cossy J. *Tetrahedron*, 2019, 75: 145–163
224 (a) Daniel PE, Weber AE, Malcolmson SJ. *Org Lett*, 2017, 19: 3490–3493; (b) Sechi ML, Andrade M, Foy H, Pilkington M, Dudding T, Metallinos C. *Adv Synth Catal*, 2020, 362: 4397–4408; (c) Maamer BC, Mpawenayo PC, Lecachey B, Alouane N, Mangeney P, van der Lee A, Marrot J, Bouaouli S, Guillaumont M, Besbes R, Gerard H, Vrancken E, Campagne JM. *Org Lett*, 2021, 23: 6305–6310
225 Ji P, Liu X, Xu J, Zhang X, Guo J, Chen W, Zhao B. *Angew Chem Int Ed*, 2022, 61: e202206111
226 Hou C, Peng B, Ye S, Yin Z, Cao J, Xiao X, Zhao B. *Nat Catal*, 2022, 5: 1061–1068
227 Gonzalez AZ, Eksterowicz J, Bartberger MD, Beck HP, Canon J, Chen A, Chow D, Duquette J, Fox BM, Fu J, Huang X, Houze JB, Jin L, Li Y, Li Z, Ling Y, Lo MC, Long AM, McGee LR, McIntosh J, McMinn DL, Oliner JD, Osgood T, Rew Y, Saiki AY, Shaffer P, Wortman S, Yakowec P, Yan X, Ye Q, Yu D, Zhao X, Zhou J, Olson SH, Medina JC, Sun D. *J Med Chem*, 2014, 57: 2472–2488
228 (a) Huang H, Degnan AP, Balakrishnan A, Easton A, Gulianello M, Huang Y, Matchett M, Mattson G, Miller R, Santone KS, Senapati A, Shields EE, Sivarao DV, Snyder LB, Westphal R, Whiterock VJ, Yang F, Bronson JJ, Macor JE. *Bioorg Med Chem Lett*, 2016, 26: 4165–4169; (b) Degnan AP, Huang H, Snyder LB, Yang F, Gillman KW, Parker MF. Oxazolidinones as Modulators of mGluR5. USA Patent, WO 2012064603, 2012-5-18
229 Wallar BJ, Lipscomb JD. *Chem Rev*, 1996, 96: 2625–2658
230 Walsh CT, Tu BP, Tang Y. *Chem Rev*, 2018, 118: 1460–1494
231 Zehani S, Gelbard G. *J Chem Soc Chem Commun*, 1985, 17: 1162–1163
232 Yang JW, Hechavarria Fonseca MT, List B. *Angew Chem Int Ed*, 2004, 43: 6660–6662
233 Rueping M, Sugiono E, Azap C, Theissmann T, Bolte M. *Org Lett*, 2005, 7: 3781–3783
234 Hoffmann S, Seayad AM, List B. *Angew Chem Int Ed*, 2005, 44: 7424–7427
235 Akiyama T. *Chem Rev*, 2007, 107: 5744–5758
236 Rueping M, Kuenkel A, Atodiresei I. *Chem Soc Rev*, 2011, 40: 4539–4549
237 Rueping M, Nachtsheim BJ, Ieawsuwan W, Atodiresei I. *Angew Chem Int Ed*, 2011, 50: 6706–6720
238 You SL. *Chem Asian J*, 2007, 2: 820–827
239 Rueping M, Dufour J, Schoepke FR. *Green Chem*, 2011, 13: 1084–1105
240 Ouellet SG, Walji AM, Macmillan DWC. *Acc Chem Res*, 2007, 40: 1327–1339
241 Connon SJ. *Org Biomol Chem*, 2007, 5: 3407–3417
242 Zhu C, Akiyama T. *Org Lett*, 2009, 11: 4180–4183
243 Ohnishi Y, Kagami M, Ohno A. *J Am Chem Soc*, 1975, 97: 4766–4768
244 Burgess VA, Davies SG, Skerlj RT. *J Chem Soc Chem Commun*, 1990, 0: 1759–1762
245 Imanishi T, Hamano Y, Yoshikawa H, Iwata C. *J Chem Soc Chem Commun*, 1988, 7: 473–475
246 Gaillard S, Papamicaël C, Marsais F, Dupas G, Levacher V. *Synlett*, 2005, 441–444
247 Aizpurua JM, Palomo C, Fratila RM, Ferrón P, Benito A, Gómez-Bengoa E, Miranda JI, Santos JI. *J Org Chem*, 2009, 74: 6691–6702
248 Hoshide F, Banba N, Oda J', Inouye Y. *Agric Biol Chem*, 1983, 47: 2141–2143
249 Ohno A, Ikeguchi M, Kimura T, Oka S. *J Am Chem Soc*, 1979, 101: 7036–7040
250 De Kok PMT, Bastiaansen LAM, Van Lier PM, Vekemans JAJM, Buck HM. *J Org Chem*, 1989, 54: 1313–1320
251 Mikata Y, Hayashi K, Mizukami K, Matsumoto S, Yano S, Yamazaki N, Ohno A. *Tetrahedron Lett*, 2000, 41: 1035–1038
252 Meyers AI, Oppenlaender T. *J Am Chem Soc*, 1986, 108: 1989–1996
253 Combret Y, Torche JJ, Binay P, Dupas G, Bourguignon J, Queguiner G. *Chem Lett*, 1991, 20: 125–128
254 Bédat J, Levacher V, Dupas G, Quéguiner G, Bourguignon J. *Chem Lett*, 1995, 24: 327–328
255 Vasse JL, Dupas G, Duflos J, Quéguiner G, Bourguignon J, Levacher V. *Tetrahedron Lett*, 2001, 42: 4613–4616
256 Leroy C, Levacher V, Dupas G, Quéguiner G, Bourguignon J. *Tetrahedron-Asymmetry*, 1997, 8: 3309–3318
257 Kanomata N, Nakata T. *Angew Chem Int Ed*, 1997, 36: 1207–1211
258 Jouin P, Troostwijk CB, Kellogg RM. *J Am Chem Soc*, 1981, 103: 2091–2093
259 Lo HC, Fish RH. *Angew Chem Int Ed*, 2002, 41: 478–481
260 Procuranti B, Connon SJ. *Chem Commun*, 2007, 1421
261 Chen QA, Chen MW, Yu CB, Shi L, Wang DS, Yang Y, Zhou YG. *J Am Chem Soc*, 2011, 133: 16432–16435
262 Chen QA, Gao K, Duan Y, Ye ZS, Shi L, Yang Y, Zhou YG. *J Am Chem Soc*, 2012, 134: 2442–2448
263 Chen ZP, Chen MW, Guo RN, Zhou YG. *Org Lett*, 2014, 16: 1406–1409
264 Lu LQ, Li Y, Junge K, Beller M. *Angew Chem Int Ed*, 2013, 52: 8382–8386
265 Lu LQ, Li Y, Junge K, Beller M. *J Am Chem Soc*, 2015, 137: 2763–2768
266 Wang J, Zhu Z, Chen M, Chen Q, Zhou Y. *Angew Chem Int Ed*, 2019, 58: 1813–1817
267 Wang J, Zhao ZB, Zhao Y, Luo G, Zhu ZH, Luo Y, Zhou YG. *J Org Chem*, 2020, 85: 2355–2368
268 Zhao Z, Li X, Wu B, Zhou Y. *Chin J Chem*, 2020, 38: 714–718
269 Zhao ZB, Li X, Chen MW, Zhao ZK, Zhou YG. *Chem Commun*, 2020, 56: 7309–7312
270 Zhu ZH, Ding YX, Zhou YG. *Tetrahedron*, 2021, 83: 131968–131974
271 Zhu ZH, Ding YX, Wu B, Zhou YG. *Chem Sci*, 2020, 11: 10220–10224
272 Zhu ZH, Ding YX, Wu B, Zhou YG. *Org Lett*, 2021, 23: 7166–7170
273 Zhu ZH, Ding YX, Zhou YG. *Chem Commun*, 2022, 58: 3973–3976
274 Bryliakov KP. *Environmentally Sustainable Catalytic Asymmetric Oxidations*. Boca Raton: CRC Press, 2015
275 Murahashi SI. *Angew Chem Int Ed*, 1995, 34: 2443–2465
276 Murahashi SI, Zhang D. *Chem Soc Rev*, 2008, 37: 1490–1501
277 Meunier B. *Biomimetic Oxidations Catalyzed by Transition Metal Complexes*. London: Imperial Collge Press, 2000
278 Bruice TC. *Acc Chem Res*, 1980, 13: 256–262
279 Walsh C. *Acc Chem Res*, 1980, 13: 148–155
280 Breslow R. *Acc Chem Res*, 1995, 28: 146–153
281 Kamerbeek N, Janssen D, van Berkel W, Fraaije M. *Adv Synth Catal*, 2003, 345: 667–678
282 Schmid RD, Urlancher-Kursif VB. *Modern Biooxidation-Enzymes, Reactions, and Applications*. Weinheim: Wiley-VCH, 2007
283 Weber S, Schleicher E. *Flavins and Flavoproteins: Methods and Protocols*. Heidelberg: Springer, 2014
284 Muller F. *Chemistry and Biochemistry of Flavoenzymes: Volume II*. Boca Raton: CRC Press, 2018
285 Massey V. *J Biol Chem*, 1994, 269: 22459–22462
286 Kemal C, Chan TW, Bruice TC. *J Am Chem Soc*, 1977, 99: 7272–7286
287 Ball S, Bruice TC. *J Am Chem Soc*, 1979, 101: 4017–4019

288 Kemal C, Bruice TC. *Proc Natl Acad Sci USA*, 1976, 73: 995–999
289 Bruice TC, Noar JB, Ball SS, Venkataram UV. *J Am Chem Soc*, 1983, 105: 2452–2463
290 Spencer CM, Faulds D. *Drugs*, 2000, 60: 321–329
291 Tembe DV, Dhavale A, Desai H, Mane DN, Raut SK, Dhingra G, Sardesai U, Saoji S, Rohra M, Shinde VG, Padsalge M, Paliwal A, Abbasi K, Devnani P, Papinwar S, Phadke S, Mehta H, Bhailume V. *Neurol Res Int*, 2011, 2011: 1–6
292 Han J, Soloshonok VA, Klika KD, Drabowicz J, Wzorek A. *Chem Soc Rev*, 2018, 47: 1307–1350
293 Shinkai S, Yamaguchi T, Manabe O, Toda F. *J Chem Soc, Chem Commun*, 1988, 1399-1401
294 Jurok R, Cibulka R, Dvořáková H, Hampl F, Hodačová J. *Eur J Org Chem*, 2010, 2010: 5217–5224
295 Jurok R, Hodačová J, Eigner V, Dvořáková H, Setnička V, Cibulka R. *Eur J Org Chem*, 2013, 2013: 7724–7738
296 Iida H, Iwahana S, Mizoguchi T, Yashima E. *J Am Chem Soc*, 2012, 134: 15103–15113
297 Mojr V, Herzig V, Buděšínský M, Cibulka R, Kraus T. *Chem Commun*, 2010, 46: 7599–7601
298 Mojr V, Buděšínský M, Cibulka R, Kraus T. *Org Biomol Chem*, 2011, 9: 7318–7326
299 Hartman T, Herzig V, Buděšínský M, Jindřich J, Cibulka R, Kraus T. *Tetrahedron-Asymmetry*, 2012, 23: 1571–1583
300 Tomanová P, Šturala J, Buděšínský M, Cibulka R. *Molecules*, 2015, 20: 19837–19848
301 Renz M, Meunier B. *Eur J Org Chem*, 1999, 1999: 737–750
302 ten Brink GJ, Arends IWCE, Sheldon RA. *Chem Rev*, 2004, 104: 4105–4124
303 Murahashi SI, Ono S, Imada Y. *Angew Chem Int Ed*, 2002, 41: 2366–2368
304 Xu S, Wang Z, Zhang X, Zhang X, Ding K. *Angew Chem Int Ed*, 2008, 47: 2840–2843
305 Xu S, Wang Z, Zhang X, Ding K. *Chin J Chem*, 2010, 28: 1731–1735
306 Shinkai S, Nakao H, Manabe O. *Tetrahedron Lett*, 1985, 26: 5183–5186
307 Shinkai S, Kawanabe S, Kawase A, Yamaguchi T, Manabe O, Harada S, Nakamura H, Kasai N. *Bull Chem Soc Jpn*, 1988, 61: 2095–2102
308 Shinkai S, Nakao H, Tsuno T, Manabe O, Ohno A. *J Chem Soc Chem Commun*, 1984, 13: 849–850
309 Poudel PP, Arimitsu K, Yamamoto K. *Chem Commun*, 2016, 52: 4163–4166
310 Mo J, Shen L, Chi YR. *Angew Chem Int Ed*, 2013, 52: 8588–8591
311 Iwahana S, Iida H, Yashima E. *Chem Eur J*, 2011, 17: 8009–8013
312 Wasilke JC, Obrey SJ, Baker RT, Bazan GC. *Chem Rev*, 2005, 105: 1001–1020
313 Zhou J. *Chem Asian J*, 2010, 5: 422–434
314 (a) Alper J. *Science*, 2003, 299: 1686–1687; (b) Vincent KA, Parkin A, Armstrong FA. *Chem Rev*, 2007, 107: 4366–4413; (c) Lubitz W, Reijerse EJ, Messinger J. *Energy Environ Sci*, 2008, 1: 15–31; (d) Cracknell JA, Vincent KA, Armstrong FA. *Chem Rev*, 2008, 108: 2439–2461; (e) Yang J, Wang D, Han H, Li C. *Acc Chem Res*, 2013, 46: 1900–1909; (f) Willkomm J, Orchard KL, Reynal A, Pastor E, Durrant JR, Reisner E. *Chem Soc Rev*, 2016, 45: 9–23; (g) Evans RM, Siritanaratkul B, Megarity CF, Pandey K, Esterle TF, Badiani S, Armstrong FA. *Chem Soc Rev*, 2019, 48: 2039–2052
315 Vignais PM, Billoud B. *Chem Rev*, 2007, 107: 4206–4272
316 (a) Lubitz W, Reijerse EJ, Messinger J. *Energy Environ Sci*, 2008, 1: 15–31; (b) Wang M, Chen L, Sun L. *Energy Environ Sci*, 2012, 5: 6763–6778
317 (a) Noyori R, Ohkuma T. *Angew Chem Int Ed*, 2001, 40: 40–73; (b) Ikariya T, Blacker AJ. *Acc Chem Res*, 2007, 40: 1300–1308; (c) Li YY, Yu SL, Shen WY, Gao JX. *Acc Chem Res*, 2015, 48: 2587–2598; (d) Xie JH, Bao DH, Zhou QL. *Synthesis*, 2015, 47: 460–471
318 Patil DS, Moura JJ, He SH, Teixeira M, Prickril BC, DerVartanian DV, Peck Jr HD, LeGall J, Huynh BH. *J Biol Chem*, 1988, 263: 18732–18738
319 Hatchikian EC, Forget N, Fernandez VM, Williams R, Cammack R. *Eur J Biochem*, 1992, 209: 357–365
320 Adams MWW. *Biochim Biophys Acta*, 1990, 1020: 115–145
321 De Lacey AL, Stadler C, Cavazza C, Hatchikian EC, Fernandez VM. *J Am Chem Soc*, 2000, 122: 11232–11233
322 (a) Adamska A, Silakov A, Lambertz C, Rüdiger O, Happe T, Reijerse E, Lubitz W. *Angew Chem Int Ed*, 2012, 51: 11458–11462; (b) Amaro-Gahete J, Pavliuk MV, Tian H, Esquivel D, Romero-Salguero FJ, Ott S. *Coord Chem Rev*, 2021, 448: 214172; (c) Camara JM, Rauchfuss TB. *Nat Chem*, 2012, 4: 26–30
323 Sandoval CA, Ohkuma T, Muñiz K, Noyori R. *J Am Chem Soc*, 2003, 125: 13490–13503
324 (a) Yamakawa M, Ito H, Noyori R. *J Am Chem Soc*, 2000, 122: 1466–1478; (b) Dub PA, Henson NJ, Martin RL, Gordon JC. *J Am Chem Soc*, 2014, 136: 3505–3521; (c) Liang Z, Yang T, Gu G, Dang L, Zhang X. *Chin J Chem*, 2018, 36: 851–856; (d) Hartmann R, Chen P. *Angew Chem Int Ed*, 2001, 40: 3581–3585
325 Shvo Y, Czarkie D, Rahamim Y, Chodosh DF. *J Am Chem Soc*, 1986, 108: 7400–7402
326 Casey CP, Singer SW, Powell DR, Hayashi RK, Kavana M. *J Am Chem Soc*, 2001, 123: 1090–1100
327 (a) Casey CP, Guan H. *J Am Chem Soc*, 2007, 129: 5816–5817; (b) Johnson TC, Clarkson GJ, Wills M. *Organometallics*, 2011, 30: 1859–1868; (c) Hodgkinson R, Del Grosso A, Clarkson G, Wills M. *Dalton Trans*, 2016, 45: 3992–4005; (d) Del Grosso A, Chamberlain AE, Clarkson GJ, Wills M. *Dalton Trans*, 2018, 47: 1451–1470; (e) Gajewski P, Renom-Carrasco M, Facchini SV, Pignataro L, Lefort L, de Vries JG, Ferraccioli R, Forni A, Piarulli U, Gennari C. *Eur J Org Chem*, 2015, 2015: 1887–1893
328 Zhou S, Fleischer S, Junge K, Beller M. *Angew Chem Int Ed*, 2011, 50: 5120–5124
329 Ohkuma T, Ooka H, Hashiguchi S, Ikariya T, Noyori R. *J Am Chem Soc*, 1995, 117: 2675–2676
330 Hashiguchi S, Fujii A, Takehara J, Ikariya T, Noyori R. *J Am Chem Soc*, 1995, 117: 7562–7563
331 Hannedouche J, Clarkson GJ, Wills M. *J Am Chem Soc*, 2004, 126: 986–987
332 Touge T, Hakamata T, Nara H, Kobayashi T, Sayo N, Saito T, Kayaki Y, Ikariya T. *J Am Chem Soc*, 2011, 133: 14960–14963
333 (a) Wen J, Wang F, Zhang X. *Chem Soc Rev*, 2021, 50: 3211–3237; (b) Wan F, Tang W. *Chin J Chem*, 2021, 39: 954–968; (c) Zhang W, Chi Y, Zhang X. *Acc Chem Res*, 2007, 40: 1278–1290; (d) Li W, Hou GH, Wang CJ, Jiang YT, Zhang XM. *Chem Commun*, 2010: 46, 3979-3981; (e) Jiang Y, Jiang Q, Zhang X. *J Am Chem Soc*, 1998, 120: 3817–3818; (f) Wu W, Liu S, Duan M, Tan X, Chen C, Xie Y, Lan Y, Dong XQ, Zhang X. *Org Lett*, 2016, 18: 2938–2941; (g) Yu J, Long J, Yang Y, Wu W, Xue P, Chung LW, Dong XQ, Zhang X. *Org Lett*, 2017, 19: 690–693; (h) Yu J, Duan M, Wu W, Qi X, Xue P, Lan Y, Dong XQ, Zhang X. *Chem Eur J*, 2017, 23: 970–975
334 Baratta W, Ballico M, Chelucci G, Siega K, Rigo P. *Angew Chem Int Ed*, 2008, 47: 4362–4365
335 (a) Xie JH, Liu XY, Xie JB, Wang LX, Zhou QL. *Angew Chem Int Ed*, 2011, 50: 7329–7332; (b) Zhu SF, Zhou QL. *Acc Chem Res*, 2017, 50: 988–1001; (c) Zhang FH, Zhang FJ, Li ML, Xie JH, Zhou QL. *Nat Catal*, 2020, 3: 621–627
336 (a) Morris RH. *Chem Soc Rev*, 2009, 38: 2282–2291; (b) Morris RH. *Acc Chem Res*, 2015, 48: 1494–1502; (c) Zuo W, Lough AJ, Li YF, Morris RH. *Science*, 2013, 342: 1080–1083; (d) Lagaditis PO, Sues PE, Sonnenberg JF, Wan KY, Lough AJ, Morris RH. *J Am Chem Soc*, 2014, 136: 1367–1380
337 Li Y, Yu S, Wu X, Xiao J, Shen W, Dong Z, Gao J. *J Am Chem Soc*, 2014, 136: 4031–4039
338 Bigler R, Huber R, Mezzetti A. *Angew Chem Int Ed*, 2015, 54: 5171–5174
339 Garbe M, Junge K, Walker S, Wei Z, Jiao H, Spannenberg A, Bachmann S, Scalone M, Beller M. *Angew Chem Int Ed*, 2017, 56:

11237–11241
340 Zhang L, Han Z, Zhao X, Wang Z, Ding K. *Angew Chem Int Ed*, 2015, 54: 6186–6189
341 (a) Widegren MB, Clarke ML. *Catal Sci Technol*, 2019, 9: 6047–6058; (b) Ling F, Nian S, Chen J, Luo W, Wang Z, Lv Y, Zhong W. *J Org Chem*, 2018, 83: 10749–10761; (c) Widegren MB, Harkness GJ, Slawin AMZ, Cordes DB, Clarke ML. *Angew Chem Int Ed*, 2017, 56: 5825–5828
342 (a) Wang X, Han Z, Wang Z, Ding K. *Acc Chem Res*, 2021, 54: 668–684; (b) Wang X, Ding K. *Chin J Chem*, 2018, 36: 899–903; (c) Han Z, Rong L, Wu J, Zhang L, Wang Z, Ding K. *Angew Chem Int Ed*, 2012, 51: 13041–13045; (d) Zhang L, Tang Y, Han Z, Ding K. *Angew Chem Int Ed*, 2019, 58: 4973–4977; (e) Zhang L, Wang Z, Han Z, Ding K. *Angew Chem Int Ed*, 2020, 59: 15565–15569
343 (a) Huerta FF, Minidis ABE, Bäckvall JE. *Chem Soc Rev*, 2001, 30: 321–331; (b) Junge K, Wendt B, Addis D, Zhou S, Das S, Fleischer S, Beller M. *Chem Eur J*, 2011, 17: 101–105; (c) Bao DH, Gu XS, Xie JH, Zhou QL. *Org Lett*, 2017, 19: 118–121
344 Thauer RK, Kaster AK, Goenrich M, Schick M, Hiromoto T, Shima S. *Annu Rev Biochem*, 2010, 79: 507–536
345 Shima S, Thauer RK. *Chem Record*, 2007, 7: 37–46
346 Shima S, Pilak O, Vogt S, Schick M, Stagni MS, Meyer-Klaucke W, Warkentin E, Thauer RK, Ermler U. *Science*, 2008, 321: 572–575
347 Yang X, Hall MB. *J Am Chem Soc*, 2009, 131: 10901–10908
348 (a) Royer AM, Rauchfuss TB, Gray DL. *Organometallics*, 2009, 28: 3618–3620; (b) Obrist BV, Chen D, Ahrens A, Schünemann V, Scopelliti R, Hu X. *Inorg Chem*, 2009, 48: 3514–3516; (c) Chen D, Scopelliti R, Hu X. *Angew Chem Int Ed*, 2010, 49: 7512–7515; (d) Song LC, Hu FQ, Wang MM, Xie ZJ, Xu KK, Song HB. *Dalton Trans*, 2014, 43: 8062–8071
349 Xu T, Yin CJM, Wodrich MD, Mazza S, Schultz KM, Scopelliti R, Hu X. *J Am Chem Soc*, 2016, 138: 3270–3273
350 Seo J, Manes TA, Rose MJ. *Nat Chem*, 2017, 9: 552–557
351 Kerns SA, Magtaan AC, Vong PR, Rose MJ. *Angew Chem Int Ed*, 2018, 57: 2855–2858
352 Pan HJ, Huang G, Wodrich MD, Tirani FF, Ataka K, Shima S, Hu X. *Nat Chem*, 2019, 11: 669–675
353 Shima S, Chen D, Xu T, Wodrich MD, Fujishiro T, Schultz KM, Kahnt J, Ataka K, Hu X. *Nat Chem*, 2015, 7: 995–1002
354 Pan H, Hu X. *Angew Chem Int Ed*, 2020, 59: 4942–4946
355 (a) Lubitz W, Ogata H, Rüdiger O, Reijerse E. *Chem Rev*, 2014, 114: 4081–4148; (b) Yagi T, Ogo S, Higuchi Y. *Int J Hydrogen Energy*, 2014, 39: 18543–18550; (c) Goris T, Wait AF, Saggu M, Fritsch J, Heidary N, Stein M, Zebger I, Lendzian F, Armstrong FA, Friedrich B, Lenz O. *Nat Chem Biol*, 2011, 7: 310–318; (d) Hamdan AA, Burlat B, Gutiérrez-Sanz O, Liebgott PP, Baffert C, De Lacey AL, Rousset M, Guigliarelli B, Léger C, Dementin S. *Nat Chem Biol*, 2013, 9: 15–17
356 (a) Ogo S. *Chem Commun*, 2009, 3317; (b) Tard C, Pickett CJ. *Chem Rev*, 2009, 109: 2245–2274; (c) Kaur-Ghumaan S, Stein M. *Dalton Trans*, 2014, 43: 9392–9405; (d) Simmons TR, Berggren G, Bacchi M, Fontecave M, Artero V. *Coord Chem Rev*, 2014, 270-271: 127–150; (e) Schilter D, Camara JM, Huynh MT, Hammes-Schiffer S, Rauchfuss TB. *Chem Rev*, 2016, 116: 8693–8749
357 Ogo S, Kabe R, Uehara K, Kure B, Nishimura T, Menon SC, Harada R, Fukuzumi S, Higuchi Y, Ohhara T, Tamada T, Kuroki R. *Science*, 2007, 316: 585–587
358 Ogo S, Ichikawa K, Kishima T, Matsumoto T, Nakai H, Kusaka K, Ohhara T. *Science*, 2013, 339: 682–684
359 Barton BE, Rauchfuss TB. *J Am Chem Soc*, 2010, 132: 14877–14885
360 Manor BC, Rauchfuss TB. *J Am Chem Soc*, 2013, 135: 11895–11900
361 Brazzolotto D, Gennari M, Queyriaux N, Simmons TR, Pécaut J, Demeshko S, Meyer F, Orio M, Artero V, Duboc C. *Nat Chem*, 2016, 8: 1054–1060
362 (a) Chen B, Wu LZ, Tung CH. *Acc Chem Res*, 2018, 51: 2512–2523; (b) Wu LZ, Chen B, Li ZJ, Tung CH. *Acc Chem Res*, 2014, 47: 2177–2185; (c) Wang X, Meng S, Xiao H, Feng K, Wang Y, Jian J, Li X, Tung C, Wu L. *Angew Chem Int Ed*, 2020, 59: 18400–18404
363 de Montellano PRO. *Acc Chem Res*, 1998, 31: 543–549
364 De Montellano PRO, Wilks A. *Adv Inorg Chem*, 2000, 50: 359–407
365 Poulos TL. *Chem Rev*, 2014, 114: 3919–3962
366 Klingenberg M. *Arch Biochem Biophys*, 1958, 75: 376–386
367 Garfinkel D. *Arch Biochem Biophys*, 1958, 77: 493–509
368 Omura T, Sato R. *J Biol Chem*, 1964, 239: 2370–2378
369 Omura T, Sato R. *J Biol Chem*, 1964, 239: 2379–2385
370 Vaz ADN. *Curr Drug Metab*, 2001, 2: 1–16
371 Schlichting I, Berendzen J, Chu K, Stock AM, Maves SA, Benson DE, Sweet RM, Ringe D, Petsko GA, Sligar SG. *Science*, 2000, 287: 1615–1622
372 Jiang Y, Li S. *Chin J Org Chem*, 2018, 38: 2307–2323
373 Meunier B, de Visser SP, Shaik S. *Chem Rev*, 2004, 104: 3947–3980
374 Groves JT, Myers RS. *J Am Chem Soc*, 1983, 105: 5791–5796
375 Groves JT, Viski P. *J Org Chem*, 1990, 55: 3628–3634
376 Naruta Y, Tani F, Ishihara N, Maruyama K. *J Am Chem Soc*, 1991, 113: 6865–6872
377 Naruta Y, Tani F, Maruyama K. *Tetrahedron Lett*, 1992, 33: 6323–6326
378 Collman JP, Zhang X, Lee VJ, Brauman JI. *J Chem Soc Chem Commun*, 1992, 1647–1649
379 Collman JP, Wang Z, Straumanis A, Quelquejeu M, Rose E. *J Am Chem Soc*, 1999, 121: 460–461
380 Reginato G, Bari LD, Salvadori P, Guilard R. *Eur J Org Chem*, 2000, 2000: 1165–1171
381 Rose E, Quelquejeu M, Pandian RP, Lecas-Nawrocka A, Vilar A, Ricart G, Collman JP, Wang Z, Straumanis A. *Polyhedron*, 2000, 19: 581–586
382 Rose E, Ren QZ, Andrioletti B. *Chem Eur J*, 2004, 10: 224–230
383 Mansuy D, Battioni P, Renaud JP, Guerin P. *J Chem Soc Chem Commun*, 1985, 155–156
384 Maillard P, Guerquin-Kern JL, Momenteau M. *Tetrahedron Lett*, 1991, 32: 4901–4904
385 Gross Z, Ini S. *J Org Chem*, 1997, 62: 5514–5521
386 Smith JRL, Reginato G. *Org Biomol Chem*, 2003, 1: 2543–2549
387 Foxon SP, Lindsay Smith JR, O'Brien P, Reginato G. *J Chem Soc Perkin Trans 2*, 2001, 1145–1153
388 Boitrel B, Baveux-Chambenoît V. *New J Chem*, 2003, 27: 942–947
389 Boitrel B, Baveux-Chambenoît V, Richard P. *HCA*, 2004, 87: 2447–2464
390 Nakagawa H, Sei Y, Yamaguchi K, Nagano T, Higuchi T. *J Mol Catal A-Chem*, 2004, 219: 221–226
391 Nakagawa H, Sei Y, Yamaguchi K, Nagano T, Higuchi T. *Tetrahedron-Asymmetry*, 2004, 15: 3861–3867
392 Halterman RL, Jan ST, Abdulwali AH, Standlee DJ. *Tetrahedron*, 1997, 53: 11277–11296
393 Lai TS, Ng KH, Liu HY, Chang CK, Yeung LL. *Synlett*, 2002, 2002 (9): 1475–1478
394 Ferrand Y, Daviaud R, Le Maux P, Simonneaux G. *Tetrahedron-Asymmetry*, 2006, 17: 952–960
395 Fackler P, Berthold C, Voss F, Bach T. *J Am Chem Soc*, 2010, 132: 15911–15913
396 Fackler P, Huber SM, Bach T. *J Am Chem Soc*, 2012, 134: 12869–12878
397 Gross Z, Galili N, Simkhovich L. *Tetrahedron Lett*, 1999, 40: 1571–1574
398 Lai TS, Chan FY, So PK, Ma DL, Wong KY, Che CM. *Dalton Trans*, 2006, 40: 4845–4851
399 Maux PL, Juillard S, Simonneaux G. *Synthesis*, 2006, 2006: 1701–1704
400 Nicolas I, Maux PL, Simonneaux G. *Tetrahedron Lett*, 2008, 49: 5793–5795
401 Nicolas I, Roisnel T, Maux PL, Simonneaux G. *Tetrahedron Lett*, 2009, 50: 5149–5151
402 Intrieri D, Le Gac S, Caselli A, Rose E, Boitrel B, Gallo E. *Chem Commun*, 2014, 50: 1811–1813

403 Huang L, Chen Y, Gao GY, Zhang XP. *J Org Chem*, 2003, 68: 8179–8184
404 Chen Y, Zhang XP. *J Org Chem*, 2007, 72: 5931–5934
405 Chen Y, Fields KB, Zhang XP. *J Am Chem Soc*, 2004, 126: 14718–14719
406 Hu Y, Lang K, Tao J, Marshall MKK, Cheng Q, Cui X, Wojtas L, Zhang XP. *Angew Chem Int Ed*, 2019, 58: 2670–2674
407 Dzik WI, Xu X, Zhang XP, Reek JNH, de Bruin B. *J Am Chem Soc*, 2010, 132: 10891–10902
408 Dzik WI, Zhang XP, de Bruin B. *Inorg Chem*, 2011, 50: 9896–9903
409 Lu H, Dzik WI, Xu X, Wojtas L, de Bruin B, Zhang XP. *J Am Chem Soc*, 2011, 133: 8518–8521
410 Lyaskovskyy V, Suarez AIO, Lu H, Jiang H, Zhang XP, de Bruin B. *J Am Chem Soc*, 2011, 133: 12264–12273
411 Goswami M, Lyaskovskyy V, Domingos SR, Buma WJ, Woutersen S, Troeppner O, Ivanović-Burmazović I, Lu H, Cui X, Zhang XP, Reijerse EJ, DeBeer S, van Schooneveld MM, Pfaff FF, Ray K, de Bruin B. *J Am Chem Soc*, 2015, 137: 5468–5479
412 Chen Y, Ruppel JV, Zhang XP. *J Am Chem Soc*, 2007, 129: 12074–12075
413 Zhu S, Perman J, Zhang X. *Angew Chem Int Ed*, 2008, 47: 8460–8463
414 Zhu S, Ruppel JV, Lu H, Wojtas L, Zhang XP. *J Am Chem Soc*, 2008, 130: 5042–5043
415 Ruppel JV, Gauthier TJ, Snyder NL, Perman JA, Zhang XP. *Org Lett*, 2009, 11: 2273–2276
416 Zhu S, Xu X, Perman JA, Zhang XP. *J Am Chem Soc*, 2010, 132: 12796–12799
417 Xu X, Zhu S, Cui X, Wojtas L, Zhang XP. *Angew Chem Int Ed*, 2013, 52: 11857–11861
418 Xu X, Wang Y, Cui X, Wojtas L, Zhang XP. *Chem Sci*, 2017, 8: 4347–4351
419 Wang J, Xie J, Lee WCC, Wang DS, Zhang XP. *Chem Catal*, 2022, 2: 330–344
420 Cui X, Xu X, Lu H, Zhu S, Wojtas L, Zhang XP. *J Am Chem Soc*, 2011, 133: 3304–3307
421 Wang Y, Wen X, Cui X, Wojtas L, Zhang XP. *J Am Chem Soc*, 2017, 139: 1049–1052
422 Lee WCC, Wang DS, Zhang C, Xie J, Li B, Zhang XP. *Chem*, 2021, 7: 1588–1601
423 Wang X, Ke J, Zhu Y, Deb A, Xu Y, Zhang XP. *J Am Chem Soc*, 2021, 143: 11121–11129
424 Ke J, Lee WCC, Wang X, Wang Y, Wen X, Zhang XP. *J Am Chem Soc*, 2022, 144: 2368–2378
425 Xu X, Lu H, Ruppel JV, Cui X, Lopez de Mesa S, Wojtas L, Zhang XP. *J Am Chem Soc*, 2011, 133: 15292–15295
426 Ruppel JV, Cui X, Xu X, Zhang XP. *Org Chem Front*, 2014, 1: 515–520
427 Zhang C, Wang DS, Lee WCC, McKillop AM, Zhang XP. *J Am Chem Soc*, 2021, 143: 11130–11140
428 Lai TS, Che CM, Kwong HL, Peng SM. *Chem Commun*, 1997, 2373–2374
429 Simonato JP, Pécaut J, Marchon JC, Robert Scheidt W. *Chem Commun*, 1999, 989–990
430 Jones JE, Ruppel JV, Gao GY, Moore TM, Zhang XP. *J Org Chem*, 2008, 73: 7260–7265
431 Tao J, Jin LM, Zhang XP. *Beilstein J Org Chem*, 2014, 10: 1282–1289
432 Subbarayan V, Ruppel JV, Zhu S, Perman JA, Zhang XP. *Chem Commun*, 2009, 4266–4268
433 Jin LM, Xu X, Lu H, Cui X, Wojtas L, Zhang XP. *Angew Chem Int Ed*, 2013, 52: 5309–5313
434 Riart-Ferrer X, Sang P, Tao J, Xu H, Jin LM, Lu H, Cui X, Wojtas L, Zhang XP. *Chem*, 2021, 7: 1120–1134
435 Jiang H, Lang K, Lu H, Wojtas L, Zhang XP. *J Am Chem Soc*, 2017, 139: 9164–9167
436 Groves JT, Viski P. *J Am Chem Soc*, 1989, 111: 8537–8538
437 Gross Z, Ini S. *Org Lett*, 1999, 1: 2077–2080
438 Zhang R, Yu WY, Lai TS, Che CM. *Chem Commun*, 1999, 1791–1792
439 Srour H, Maux PL, Simonneaux G. *Inorg Chem*, 2012, 51: 5850–5856
440 Frost JR, Huber SM, Breitenlechner S, Bannwarth C, Bach T. *Angew Chem Int Ed*, 2014, 54: 691–695
441 Burg F, Breitenlechner S, Jandl C, Bach T. *Chem Sci*, 2020, 11: 2121–2129
442 Burg F, Gicquel M, Breitenlechner S, Pöthig A, Bach T. *Angew Chem Int Ed*, 2018, 57: 2953–2957
443 Wang JC, Xu ZJ, Guo Z, Deng QH, Zhou CY, Wan XL, Che CM. *Chem Commun*, 2012, 48: 4299–4301
444 Wang JC, Zhang Y, Xu ZJ, Lo VKY, Che CM. *ACS Catal*, 2013, 3: 1144–1148
445 Cui X, Xu X, Jin LM, Wojtas L, Zhang XP. *Chem Sci*, 2015, 6: 1219–1224
446 Xie J, Xu P, Zhu Y, Wang J, Lee WCC, Zhang XP. *J Am Chem Soc*, 2021, 143: 11670–11678
447 Wang Y, Wen X, Cui X, Zhang XP. *J Am Chem Soc*, 2018, 140: 4792–4796
448 Wen X, Wang Y, Zhang XP. *Chem Sci*, 2018, 9: 5082–5086
449 Zhou XG, Yu XQ, Huang JS, Che CM. *Chem Commun*, 1999, 2377–2378
450 Liang JL, Yuan SX, Huang JS, Yu WY, Che CM. *Angew Chem Int Ed*, 2002, 41: 3465–3468
451 Liang JL, Yuan SX, Huang JS, Che CM. *J Org Chem*, 2004, 69: 3610–3619
452 Hu Y, Lang K, Li C, Gill JB, Kim I, Lu H, Fields KB, Marshall MK, Cheng Q, Cui X, Wojtas L, Zhang XP. *J Am Chem Soc*, 2019, 141: 18160–18169
453 Lang K, Torker S, Wojtas L, Zhang XP. *J Am Chem Soc*, 2019, 141: 12388–12396
454 Lang K, Li C, Kim I, Zhang XP. *J Am Chem Soc*, 2020, 142: 20902–20911
455 Lang K, Hu Y, Lee WCC, Zhang XP. *Nat Synth*, 2022, 1: 548–557
456 Jin LM, Xu P, Xie J, Zhang XP. *J Am Chem Soc*, 2020, 142: 20828–20836
457 Naruta Y, Tani F, Maruyama K. *J Chem Soc Chem Commun*, 1990, 1378–1380
458 Naruta Y, Tani F, Maruyama K. *Tetrahedron-Asymmetry*, 1991, 2: 533–542
459 Le Maux P, Simonneaux G. *Chem Commun*, 2011, 47: 6957–6959
460 Wong OA, Shi Y. *Chem Rev*, 2008, 108: 3958–3987
461 Zhu Y, Wang Q, Cornwall RG, Shi Y. *Chem Rev*, 2014, 114: 8199–8256
462 Milan M, Bietti M, Costas M. *Chem Commun*, 2018, 54: 9559–9570
463 Herrmann P, Bach T. *Chem Soc Rev*, 2011, 40: 2022–2038
464 Sun Q, Sun W. *Chin J Org Chem*, 2020, 40: 3686–3696
465 Que L Jr., Tolman WB. *Nature*, 2008, 455: 333–340
466 Ray K, Pfaff FF, Wang B, Nam W. *J Am Chem Soc*, 2014, 136: 13942–13958
467 Price JC, Barr EW, Tirupati B, Bollinger, JM, Krebs C. *Biochemistry*, 2003, 42: 7497–7508
468 Rohde JU, In JH, Lim MH, Brennessel WW, Bukowski MR, Stubna A, Munck E, Nam W, Que Jr. L. *Science*, 2003, 299: 1037–1039
469 Sun W, Sun Q. *Acc Chem Res*, 2019, 52: 2370–2381
470 Vicens L, Olivo G, Costas M. *ACS Catal*, 2020, 10: 8611–8631
471 Bryliakov KP. *Chem Rev*, 2017, 117: 11406–11459
472 Bryliakov KP, Talsi EP. *Coord Chem Rev*, 2014, 276: 73–96
473 Zhang W, Loebach JL, Wilson SR, Jacobsen EN. *J Am Chem Soc*, 1990, 112: 2801–2803
474 Irie R, Noda K, Ito Y, Matsumoto N, Katsuki T. *Tetrahedron Lett*, 1990, 31: 7345–7348
475 Francis MB, Jacobsen EN. *Angew Chem Int Ed*, 1999, 38: 937–941
476 White MC, Doyle AG, Jacobsen EN. *J Am Chem Soc*, 2001, 123: 7194–7195

477 Murphy A, Dubois G, Stack TDP. *J Am Chem Soc*, 2003, 125: 5250–5251
478 Gómez L, Garcia-Bosch I, Company A, Sala X, Fontrodona X, Ribas X, Costas M. *Dalton Trans*, 2007, 5539–5545
479 Wu M, Wang B, Wang S, Xia C, Sun W. *Org Lett*, 2009, 11: 3622–3625
480 Wu M, Miao CX, Wang S, Hu X, Xia C, Kühn FE, Sun W. *Adv Synth Catal*, 2011, 353: 3014–3022
481 Chen MS, White MC. *Science*, 2007, 318: 783–787
482 Ottenbacher RV, Bryliakov KP, Talsi EP. *Adv Synth Catal*, 2011, 353: 885–889
483 Garcia-Bosch I, Gómez L, Polo A, Ribas X, Costas M. *Adv Synth Catal*, 2012, 354: 65–70
484 Wang B, Miao C, Wang S, Xia C, Sun W. *Chem Eur J*, 2012, 18: 6750–6753
485 Wang B, Wang S, Xia C, Sun W. *Chem Eur J*, 2012, 18: 7332–7335
486 Lyakin OY, Ottenbacher RV, Bryliakov KP, Talsi EP. *ACS Catal*, 2012, 2: 1196–1202
487 Cussó O, Garcia-Bosch I, Ribas X, Lloret-Fillol J, Costas M. *J Am Chem Soc*, 2013, 135: 14871–14878
488 Cussó O, Ribas X, Lloret-Fillol J, Costas M. *Angew Chem Int Ed*, 2015, 54: 2729–2733
489 Ottenbacher RV, Samsonenko DG, Talsi EP, Bryliakov KP. *ACS Catal*, 2014, 4: 1599–1606
490 Cussó O, Cianfanelli M, Ribas X, Klein Gebbink RJM, Costas M. *J Am Chem Soc*, 2016, 138: 2732–2738
491 Miao C, Wang B, Wang Y, Xia C, Lee YM, Nam W, Sun W. *J Am Chem Soc*, 2016, 138: 936–943
492 Lin J, Wang F, Tian J, Zhang J, Wang Y, Sun W. *Chin Chem Lett*, 2022, 33: 1515–1518
493 Aldrich-Wright JR, Vagg RS, Williams PA. *Coord Chem Rev*, 1997, 166: 361–389
494 Du J, Miao C, Xia C, Lee YM, Nam W, Sun W. *ACS Catal*, 2018, 8: 4528–4538
495 Lin J, Miao C, Wang F, Yang P, Sun Q, Sun W. *ACS Catal*, 2020, 10: 11857–11863
496 Chen J, Klein Gebbink RJM. *ACS Catal*, 2019, 9: 3564–3575
497 Wang B, Lin J, Sun Q, Xia C, Sun W. *ACS Catal*, 2021, 11: 10964–10973
498 Qiu B, Xia C, Sun W. *Chin Chem Lett*, 2019, 30: 698–701
499 Beaver MG, Shi X, Riedel J, Patel P, Zeng A, Corbett MT, Robinson JA, Parsons AT, Cui S, Baucom K, Lovette MA, Içten E, Brown DB, Allian A, Flick TG, Chen W, Yang N, Walker SD. *Org Process Res Dev*, 2020, 24: 490–499
500 Kolb HC, VanNieuwenhze MS, Sharpless KB. *Chem Rev*, 1994, 94: 2483–2547
501 Costas M, Mehn MP, Jensen MP, Que L. *Chem Rev*, 2004, 104: 939–986
502 Wolfe MD, Lipscomb JD. *J Biol Chem*, 2003, 278: 829–835
503 Costas M, Tipton AK, Chen K, Jo DH, Que L. *J Am Chem Soc*, 2001, 123: 6722–6723
504 Suzuki K, Oldenburg P , Que L. *Angew Chem Int Ed*, 2008, 47: 1887–1889
505 Chow TWS, Liu Y, Che CM. *Chem Commun*, 2011, 47: 11204–11206
506 Zang C, Liu Y, Xu ZJ, Tse CW, Guan X, Wei J, Huang JS, Che CM. *Angew Chem Int Ed*, 2016, 55: 10253–10257
507 Wei J, Wu L, Wang H, Zhang X, Tse C, Zhou C, Huang J, Che C. *Angew Chem Int Ed*, 2020, 59: 16561–16571
508 Chen J, Luo X, Sun Y, Si S, Xu Y, Lee YM, Nam W, Wang B. *CCS Chem*, 2022, 4: 2369–2381
509 Che CM, Lo VKY, Zhou CY, Huang JS. *Chem Soc Rev*, 2011, 40: 1950–1975
510 Costas M. *Chem Record*, 2021, 21: 4000–4014
511 Cho KB, Hirao H, Shaik S, Nam W. *Chem Soc Rev*, 2016, 45: 1197–1210
512 Ottenbacher RV, Samsonenko DG, Talsi EP, Bryliakov KP. *Org Lett*, 2012, 14: 4310–4313
513 Shen D, Miao C, Wang S, Xia C, Sun W. *Org Lett*, 2014, 16: 1108–1111
514 Milan M, Bietti M, Costas M. *ACS Cent Sci*, 2017, 3: 196–204
515 Miao C, Li XX, Lee YM, Xia C, Wang Y, Nam W, Sun W. *Chem Sci*, 2017, 8: 7476–7482
516 Talsi EP, Samsonenko DG, Ottenbacher RV, Bryliakov KP. *ChemCatChem*, 2017, 9: 4580–4586
517 Qiu B, Xu D, Sun Q, Miao C, Lee YM, Li XX, Nam W, Sun W. *ACS Catal*, 2018, 8: 2479–2487
518 Qiu B, Xu D, Sun Q, Lin J, Sun W. *Org Lett*, 2019, 21: 618–622
519 Cianfanelli M, Olivo G, Milan M, Klein Gebbink RJM, Ribas X, Bietti M, Costas M. *J Am Chem Soc*, 2020, 142: 1584–1593
520 Vicens L, Bietti M, Costas M. *Angew Chem Int Ed*, 2021, 60: 4740–4746
521 Dantignana V, Milan M, Cussó O, Company A, Bietti M, Costas M. *ACS Cent Sci*, 2017, 3: 1350–1358
522 Ottenbacher RV, Talsi EP, Rybalova TV, Bryliakov KP. *ChemCatChem*, 2018, 10: 5323–5330
523 Ottenbacher RV, Talsi EP, Bryliakov KP. *J Catal*, 2020, 390: 170–177
524 Sun Q, Sun W. *Org Lett*, 2020, 22: 9529–9533
525 (a) Holm RH, Kennepohl P, Solomon EI. *Chem Rev*, 1996, 96: 2239–2314; (b) Lindahl PA. *J Inorg Biochem*, 2012, 106: 172–178
526 Sasai H, Suzuki T, Arai S, Arai T, Shibasaki M. *J Am Chem Soc*, 1992, 114: 4418–4420
527 Sasai H, Arai T, Satow Y, Houk KN, Shibasaki M. *J Am Chem Soc*, 1995, 117: 6194–6198
528 (a) Shibasaki M, Yoshikawa N. *Chem Rev*, 2002, 102: 2187–2210; (b) Matsunaga S, Ohshima T, Shibasaki M. *Adv Synthesis Catal*, 2002, 344: 3–15; (c) Shibasaki M, Matsunaga S. *Chem Soc Rev*, 2006, 35: 269–279; (d) Shibasaki M, Kanai M, Matsunaga S, Kumagai N. *Acc Chem Res*, 2009, 42: 1117–1127; (e) Matsunaga S, Shibasaki M. *Synthesis*, 2013, 45: 421–437; (f) Matsunaga S, Shibasaki M. *Chem Commun*, 2014, 50: 1044–1057
529 Haak RM, Wezenberg SJ, Kleij AW. *Chem Commun*, 2010, 46: 2713–2723
530 Lidskog A, Li Y, Wärnmark K. *Catalysts*, 2020, 10: 705
531 Konsler RG, Karl J, Jacobsen EN. *J Am Chem Soc*, 1998, 120: 10780–10781
532 Mazet C, Jacobsen E . *Angew Chem Int Ed*, 2008, 47: 1762–1765
533 Zhang Z, Wang Z, Zhang R, Ding K. *Angew Chem Int Ed*, 2010, 49: 6746–6750
534 Thomas RM, Widger PCB, Ahmed SM, Jeske RC, Hirahata W, Lobkovsky EB, Coates GW. *J Am Chem Soc*, 2010, 132: 16520–16525
535 Liu Y, Ren WM, Liu J, Lu XB. *Angew Chem Int Ed*, 2013, 52: 11594–11598
536 Li J, Liu Y, Ren WM, Lu XB. *J Am Chem Soc*, 2016, 138: 11493–11496
537 Trost BM, Ito H. *J Am Chem Soc*, 2000, 122: 12003–12004
538 Xiao Y, Wang Z, Ding K. *Chem Eur J*, 2005, 11: 3668–3678
539 Trost BM, Hung C-J, Mata G. *Angew Chem Int Ed*, 2020, 59: 4240–4261
540 Xu P, Huang Z. *Nat Chem*, 2021, 13: 634–642
541 Xu P, Liu S, Huang Z. *J Am Chem Soc*, 2022, 144: 6918–6927
542 Trost BM, Zhang G, Xu M, Qi X. *Chem Eur J*, 2022, 28: e202104268
543 (a) Luo Z, Liu Q, Gong L, Cui X, Mi A, Jiang Y. *Angew Chem Int Ed*, 2002, 41: 4532–4535; (b) Guo QX, Wu ZJ, Luo ZB, Liu QZ, Ye JL, Luo SW, Cun LF, Gong LZ. *J Am Chem Soc*, 2007, 129: 13927–13938
544 Takizawa S, Katayama T, Somei H, Asano Y, Yoshida T, Kameyama C, Rajesh D, Onitsuka K, Suzuki T, Mikami M, Yamataka H, Jayaprakash D, Sasai H. *Tetrahedron*, 2008, 64: 3361–3371
545 Gao J, Reibenspies JH, Martell AE. *Angew Chem Int Ed*, 2003, 42: 6008–6012

546 Jautze S, Peters R. *Angew Chem Int Ed*, 2008, 47: 9284–9288
547 (a) Guo H, Liu D, Butt NA, Liu Y, Zhang W. *Tetrahedron*, 2012, 68: 3295–3299; (b) Wang J, Liu D, Liu Y, Zhang W. *Org Biomol Chem*, 2013, 11: 3855–3861
548 Li J, Shen J, Xia C, Wang Y, Liu D, Zhang W. *Org Lett*, 2016, 18: 2122–2125
549 Bhadra S, Akakura M, Yamamoto H. *J Am Chem Soc*, 2015, 137: 15612–15615
550 Park D, Jette CI, Kim J, Jung W, Lee Y, Park J, Kang S, Han MS, Stoltz BM, Hong S. *Angew Chem Int Ed*, 2020, 59: 775–779
551 (a) Powers IG, Uyeda C. *ACS Catal*, 2017, 7: 936–958; (b) Wang Q, Brooks SH, Liu T, Tomson NC. *Chem Commun*, 2021, 57: 2839–2853; (c) Xu W, Li M, Qiao L, Xie J. *Chem Commun*, 2020, 56: 8524–8536; (d) Xiong N, Zhang G, Sun X, Zeng R. *Chin J Chem*, 2020, 38: 185–201
552 (a) Müller P, Fruit C. *Chem Rev*, 2003, 103: 2905–2920; (b) Doyle MP. *J Org Chem*, 2006, 71: 9253–9260; (c) Hansen J, Davies HML. *Coord Chem Rev*, 2008, 252: 545–555; (d) Dequirez G, Pons V, Dauban P. *Angew Chem Int Ed*, 2012, 51: 7384–7395; (e) Roizen JL, Harvey ME, Du Bois J. *Acc Chem Res*, 2012, 45: 911–922
553 (a) Nishibayashi Y, Wakiji I, Hidai M. *J Am Chem Soc*, 2000, 122: 11019–11020; (b) Nishibayashi Y, Milton MD, Inada Y, Yoshikawa M, Wakiji I, Hidai M, Uemura S. *Chem Eur J*, 2005, 11: 1433–1451; (c) Sakata K, Nishibayashi Y. *Catal Sci Technol*, 2018, 8: 12–25
554 Inada Y, Nishibayashi Y, Uemura S. *Angew Chem Int Ed*, 2005, 44: 7715–7717
555 (a) Miyake Y, Uemura S, Nishibayashi Y. *ChemCatChem*, 2009, 1: 342–356; (b) Sakata K, Goto Y, Yoshikawa T, Nishibayashi Y. *Chem Asian J*, 2021, 16: 3760–3766
556 Zhou YY, Hartline DR, Steiman TJ, Fanwick PE, Uyeda C. *Inorg Chem*, 2014, 53: 11770–11777
557 Zhou YY, Uyeda C. *Science*, 2019, 363: 857–862
558 Behlen MJ, Uyeda C. *J Am Chem Soc*, 2020, 142: 17294–17300
559 Braconi E, Cramer N. *Angew Chem Int Ed*, 2020, 59: 16425–16429